# New Diagnostic Features from Multilead ECG Signal for Detection of Cardiac Ailments

*A*

*Thesis submitted*

*for the award of the degree of*

**DOCTOR OF PHILOSOPHY**

By

**Rajesh Kumar Tripathy**

DEPARTMENT OF ELECTRONICS AND ELECTRICAL ENGINEERING
INDIAN INSTITUTE OF TECHNOLOGY GUWAHATI
GUWAHATI - 781039, INDIA

JULY 2016

*Dedicated to my*

*God and Parents*

# Declaration

I hereby declare that the work which is being presented in the thesis entitled, "**New Diagnostic Features from Multilead ECG Signal for Detection of Cardiac Ailments**", in partial fulfillment of the requirements for the award of the degree of **Doctor of Philosophy** at *Indian Institute of Technology Guwahati*, is an authentic record of my own work carried out under the supervision of Prof. S. Dandapat and refers other researchers works which are duly listed in the reference section. The contents of this thesis, in full or in parts, have not been submitted to any other Institute or University for the award of any degree or diploma.

Rajesh Kumar Tripathy.
Department of Electronics and Electrical Engineering,
Indian Institute of Technology Guwahati,
Guwahati - 781039, India.

Dated:

Place: IIT Guwahati

# Certificate

This is to certify that the thesis entitled "**New Diagnostic Features from Multilead ECG Signal for Detection of Cardiac Ailments**", submitted by **Rajesh Kumar Tripathy** (136102010), a research scholar in the *Department of Electronics and Electrical Engineering, Indian Institute of Technology Guwahati*, for the award of the degree of **Doctor of Philosophy**, is a record of an original research work carried out by him under my supervision and guidance. The thesis has fulfilled all requirements as per the regulations of the Institute and in my opinion, it has reached the standard needed for submission. The results embodied in this thesis have not been submitted to any other University or Institute for the award of any degree or diploma.

Dr. S. Dandapat, Professor.
Department of Electronics and Electrical Engineering,
Indian Institute of Technology Guwahati,
Guwahati - 781039, India.

Dated:

Place: IIT Guwahati

# Acknowledgements

This work was carried out at the department of electronics and electrical engineering (EEE), Indian Institute of Technology (IIT) Guwahati, India under the supervision of Prof. S. Dandapat.

I would like to express my sincere gratitude to Prof. S. Dandapat for his guidance and support throughout my work. Without him, I will never be able to complete my thesis work with this ease. He was very patient to hear my problems that I am facing during research work and finding the solutions. I am very much thankful to him for giving his valuable time for me.

I would like to express my sincere thanks to my doctoral committee members, Prof. S. R Mahadeva Prasanna, Prof. Rohit Sinha, Prof. Harshal B. Nemade and Dr. Prithwijit Guha for their support, encouragement and suggestions during evaluation of my research work. I sincerely acknowledge and thank the faculties, Prof. P. K. Bora, Dr. T. Jacob, Dr S. Sundaram and Dr. M. K. Bhuyan, in this regard. I would like to thank other faculty members of EEE department who helped directly or indirectly during my research work. My special thanks to Dr. L. N. Sharma for encouragement and guidance.

I would like to acknowledge the support shown by my friends Mr. Abhishek Sharma, Mr. Suman Deb, Mr. Rajib Sharma, Mr. Balaji Rao Katika, Mr. Ramesh Rathore, Mr. Prateek Rathore, Mr. Nagraj Adiga, Mr. K. T. Deepak, Mr. Rohan Kumar Das, Mr. Biswajit Dev Sharma, Mr. Anurag Singh, Mr. Jiss J. Nalikuzy, Mr. Alex Paul kamson, Mr. Sishir Kalita and Mr. Akhilesh Dubey for their suggestions and encouragement. My sincere gratitude to all the research scholars of Signal and Informatics Lab, and Electromedical and Speech Technology Lab for encouragement and support during research work.

I thank God for giving me a chance to pursue my doctoral work in IIT Guwahati, India.

Finally, my hearty thanks to my family members for their sacrifice that encouraged me to proceed with the work.

***Rajesh Kumar Tripathy***

# Abstract

Electrocardiogram (ECG) provides the diagnostic information about the depolarization and the relaxation activities of heart chambers. This diagnostic information is captured using morphological features. The variations in the morphological features of ECG are the symptoms of particular heart pathology. It is a time-consuming task for medical experts to visually identify any subtle changes in the morphological features during 24 hours of ECG recording. Therefore, the automated analysis of ECG signal using various signal processing techniques is needed for accurate detection of cardiac ailments. This thesis documents our investigations on the diagnostic information of ECG signal for detection of various cardiac abnormalities. There are three major contributions. First, the multiscale approach is proposed and evaluated for detection and localization of myocardial infarction (MI) from multilead ECG. The discrete wavelet transform (DWT) grossly segments the diagnostic components of ECG such as the P-wave, the QRS-complex and the T-wave into different sub-bands. In MI pathology, the shape and the amplitude of the diagnostic components of multilead ECG are different from the normal sinus rhythm (NSR). These pathological changes may affect the characteristics of the wavelet coefficients of multilead ECG at different sub-bands. The features evaluated from the wavelet coefficients of multilead ECG will be helpful for detection and localization of MI. The proposed multiscale approach is based on the evaluation of multiscale energy and eigenspace (MEES) features of multilead ECG. The MEES features of multilead ECG and various classifiers are used for detection and localization of MI. The proposed multiscale approach shows improved performance over existing methods for MI detection.

Second, the complex wavelet magnitude and phase features are proposed for the detection and classification of three cardiac ailments namely bundle branch block (BBB), MI and heart muscle diseases (HMD) from multilead ECG. The dual tree complex wavelet

transform (DTCWT) of multilead ECG produces complex wavelet coefficients at different sub-bands. In addition to magnitude information, the DTCWT provides an additional (phase) information of multilead ECG in different wavelet scales. The phase captures the temporal information of a signal. In HMD and BBB pathologies, the duration, the amplitude and the shape parameters are different from the normal heart rhythm. It is expected that, the features evaluated from the complex wavelet coefficients will be helpful for detection of these cardiac ailments. In this work, the multiscale phase alternation (PA) features, and the complex wavelet sub-band bi-spectrum (CWSB) magnitude and phase features are proposed. The multiscale PA features are evaluated from the phase of the complex wavelet coefficients of multilead ECG. The CWSB of multilead ECG is evaluated using higher order complex wavelet analysis (HOCWA). The complex wavelet features of multilead ECG and different classifiers are used for classification of BBB, HMD and MI pathologies. Comparison with the existing techniques for detection of cardiac ailments using 12-lead ECG shows the advantage of the proposed method.

Third, the variational mode energy and entropy (VMEE) features are proposed for the detection and classification of shockable ventricular arrhythmia (rapid ventricular tachycardia and ventricular fibrillation) and non-shockable episodes (NSR, ventricular bigeminy, ventricular ectopic beats, and ventricular escape rhythm) from ECG. The abnormal patterns other than 'PQRST' morphologies appear in ECG due to shockable ventricular arrhythmia. The wavelet based methods require proper selection of basis function with morphology similar to ECG. During shockable ventricular arrhythmia (rapid ventricular tachycardia and ventricular fibrillation), the ECG signal doesn't have 'PQRST' morphologies. Therefore, a data-dependent multiresolution analysis method will be helpful to capture pathological changes in ECG during shockable ventricular arrhythmia. In this work, the variational mode decomposition (VMD) is used to decompose the ECG signal into number of modes or sub-signals. The energy, the Renyi entropy and the permutation entropy features are evaluated from the modes of ECG. The proposed VMEE features of ECG and the random forest classifier are used for detection of shockable ventricular arrhythmia. Comparison with the existing techniques reveals the effectiveness of the proposed method for detection

and classification of shockable ventricular arrhythmia and non-shockable ECG episodes.

The major contributions of the work reported in this thesis includes,

- MEES approach for detection and localization of MI from multilead ECG.
- Multiscale PA features for detection of cardiac abnormalities from multilead ECG.
- CWSB features for detection and classification of various cardiac ailments such as BBB, MI and HMD from multilead ECG.
- VMEE features for detection and classification of shockable ventricular arrhythmia and non-shockable episodes from ECG.

The other contributions are,

- Multiresolution inter-sample and inter-lead eigen error features for detection of cardiac ailments.
- Detection of cardiac ailments from multilead ECG using diagnostic eigen error features.
- Multiscale non-linear analysis for classification of cardiac ailments from multilead ECG.

**Keywords:** ECG, Multilead ECG, Diagnostic features, DWT, DTCWT, VMD, feature selection, classifiers, performance measures.

# Synopsis

## Abstract

Electrocardiogram (ECG) provides the diagnostic information about the depolarization and the relaxation activities of heart chambers. This diagnostic information is captured using morphological features (amplitude, duration and shape of P-wave, QRS-complex and T-wave of ECG). The variations in the morphological features of ECG are the symptoms of particular heart pathology. It is a time-consuming task for medical experts to visually identify any subtle changes in the morphological features during 24 hours of ECG recording. Therefore, the automated analysis of ECG signal using various signal processing techniques is required for accurate detection of cardiac ailments. This thesis documents our investigations on the diagnostic information of ECG signal for detection of various cardiac abnormalities. There are three major contributions. First, the multiscale energy and eigenspace (MEES) features are proposed for detection and localization of myocardial infarction (MI) from multilead ECG. Second, the complex wavelet magnitude and phase features are evaluated for detection of bundle branch block (BBB), heart muscle diseases (HMD) and MI. Third, the variational mode energy and entropy (VMEE) features are tested for detection of shockable ventricular arrhythmia. Comparison with the existing methods for detection of cardiac abnormalities shows the effectiveness of the performance of the proposed diagnostic features of ECG signal.

## Introduction

The aim of cardiac signal processing is to extract significant diagnostic information from ECG signal for diagnosis, therapy and monitoring [3, 10]. In clinical practice, the ECG is used as a gold standard for diagnosis of heart pathologies [2]. The cardiologist examines the clinical components of ECG for diagnosis. For ambulatory or holter monitoring applications, one or two ECG leads are commonly

used. The standard 12-lead or multilead ECG is typically used for detection of life-threatening cardiac ailments such as conduction defect, muscle defect and MI [1]. In multilead ECG, each lead views the heart at a different angle and provides both spatial and temporal information of cardiac activities. During continuous recording of ECG from a patient, large amount of data are generated. It is a time-consuming task for the cardiologist to visually inspect all the ECG data for diagnosis of cardiac ailments. In such a scenario, the automated diagnostic system (ADS) is useful to assist the cardiologist in diagnosing the cardiac ailments [2, 3]. The ADS consists of preprocessing of ECG data, diagnostic information extraction and classification of cardiac abnormalities [3]. The quantification of diagnostic information is the crucial stage in ADS. The diagnostic information of ECG signal is captured using features. The diagnostic features of ECG are evaluated using signal processing techniques. Although various signal processing techniques have been proposed for evaluation of diagnostic features of ECG, these features are not sufficient to capture the pathological variations during cardiac arrhythmia. Therefore, new way of quantifying diagnostic information from ECG signal is required for accurate detection of cardiac abnormalities. In this thesis, three new methods are proposed for evaluation of the diagnostic features of ECG signal. These diagnostic features are used for detection of cardiac abnormalities such as MI, BBB, HMD and shockable ventricular arrhythmia (rapid ventricular tachycardia and ventricular fibrillation). The first part of the work is based on the detection and localization of MI from multilead ECG using MEES features. In the second part, the detection of BBB, HMD and MI pathologies from multilead ECG using complex wavelets is proposed. Third, the detection of shockable ventricular arrhythmia from ECG using variational mode decomposition (VMD) is proposed and evaluated.

**Detection and Localization of MI**

MI is a life-threatening cardiac ailment and it occurs due the occlusion in one of the coronary arteries of heart [1]. The pathological symptoms of MI in ECG are T-wave inversion, ST-segment elevation and abnormal Q-wave [1, 12]. Detection and localization of MI from multilead ECG is a challenging problem. The state-of-art methods use only few ECG leads for detection of MI. Instead of entire ECG segments, the methods are based on the analysis of the clinical components such as the ST-

segment, T-wave and QRS-complex. This demands for an accurate detection of fiducial points (P, Q, R, S and T) of ECG. The prior information about the presence of disease in selected ECG leads are also required for MI detection and localization. In recent years, the multiscale analysis using discrete wavelet transform (DWT) is found to be an effective method for various ECG signal processing applications [14, 25, 50]. The 'PQRST' morphologies of ECG signal are grossly captured in different sub-bands using multiscale analysis. When all the channels of multilead ECG are subjected to multiscale analysis with identical mother wavelet and same decomposition levels, it helps formulate the multivariate multiscale matrices. These sub-band matrices capture the inter-sample and inter-lead correlations of multilead ECG at different wavelet scales. The inter-lead correlation can be higher for multilead ECG at different scales. The multiscale analysis of multilead ECG for detection and localization of MI has not been used. It is expected that, the multiscale analysis of multilead ECG can provide discriminative diagnostic information, which are more sensitive to capture the pathological variations during MI. This motivates us to use the multiscale features of multilead ECG for detection and localization of MI.

In this work, the multiscale approach is proposed for detection and localization of MI from multilead ECG. The approach is based on the evaluation of MEES features of multilead ECG. The statistical significance of MEES features is shown for MI detection. The support vector machine (SVM) and the K-nearest neighbor (KNN) classifiers are used for detection of MI from the MEES features of multilead ECG. The SVM classifier with RBF kernel has better performance with accuracy, sensitivity and specificity values of 96%, 93% and 99%, respectively. For MI localization, the MEES features are evaluated from the multilead ECG beats. The statistical significance of MEES features for MI localization is analyzed. The multiclass SVM classifier is used to classify the MEES features of multilead ECG beat into anterior MI (AMI), anterio-lateral MI (ALMI), anterio-septal MI (ASMI), inferior MI (IMI), inferio-lateral MI (ILMI) and inferio-posterio-lateral MI (IPLMI). The multiclass SVM with RBF kernel has better performance for MI localization with an average accuracy value of 99.58%. Comparison with the existing techniques reveals that, the proposed method has advantages for detection and localization of MI from 12-lead or multilead ECG.

**Complex Wavelets for Detection of BBB, HMD and MI**

The life-debilitating cardiac ailments HMD (cardiomyopathy and hypertrophy), MI and BBB occur due to abnormal heart muscle, obstruction in one of the coronary arteries and improper conduction [1, 16, 12]. Detection and classification of BBB, HMD and MI from multilead ECG are challenging tasks in clinical practice. The existing methods for detection of BBB, MI, HMD and cardiac dysrhythmia are beat-specific and few ECG leads are used for evaluation of diagnostic features. In clinical practice, the serial recording of ECG data with multiple electrodes are used for accurate detection of MI, HMD and BBB pathologies [12]. Some of the reported methods have used various morphological features of multilead ECG. For evaluation of these features, it is required to detect the P, Q, R, S, T points of each ECG lead [41, 42]. The multiscale analysis using dual tree complex wavelet transform (DTCWT) has the advantage that, it provides both magnitude and phase information of the ECG signal. The phase captures the temporal information of an ECG signal [178]. The duration parameters of ECG show significant variations during MI, BBB and HMD pathologies. It is expected that, the features evaluated from the phase of complex wavelet coefficients of multilead ECG at different scales will be helpful to capture the pathologies. The DTCWT also overcomes the drawbacks of DWT with its important properties such as the shift invariant, substantial reduction in aliasing effect and the non-oscillating characteristics of the wavelet coefficients [67]. The magnitude and the phase features of 12-lead or multilead ECG in wavelet domain have not been used for detection of cardiac abnormalities. The complex wavelet magnitude and phase features of multilead ECG can be used for detection and classification of muscle defects (HMD), conduction defect (BBB) and MI.

In this work, two new methods are proposed for detection and of MI, HMD and BBB pathologies. The first method is based on the evaluation of multiscale phase alternation (PA) features of multilead ECG. The multiscale PA features are evaluated from the complex wavelet coefficients of multilead ECG. The KNN and the fuzzy KNN classifiers are used for classification of cardiac ailments from multiscale PA features. The accuracy values of 94.31%, 80.90% and 78.12% for MI, HMD and BBB classes are found using Fuzzy KNN classifier and selected multiscale PA features. In the second method, the complex wavelet sub-band bi-spectrum (CWSB) magnitude and phase features are proposed. The CWSB of multilead ECG is evaluated using higher order complex wavelet analysis.

The magnitude and the phase features of CWSB are analyzed for normal sinus rhythm (NSR) and pathological cases. A feature selection technique based on symmetrical uncertainty score is used for choosing relevant CWSB features of multilead ECG. The extreme learning machine (ELM) and the SVM classifiers are used to evaluate the performance of CWSB features. The overall accuracy values of ELM and SVM classifiers are obtained as 97.17% and 97.55%, respectively. The individual class accuracy values of 98.37%, 97.39% and 96.40% are found for MI, HMD and BBB classes using selected CWSB features and SVM classifier. Comparison with the existing 12-lead ECG based cardiac disease classification techniques shows the superiority of the proposed methods.

**Variational Mode Decomposition for Detection of Shockable Ventricular Arrhythmia**

The rapid ventricular tachycardia (VT) and the ventricular fibrillation (VF) are two types of shockable ventricular arrhythmia that can lead to sudden cardiac death; however, they can be stopped with a shock delivered by a defibrillator and regular cardiac activity could be restored [2, 19, 20]. Detection of these cardiac abnormalities is one of the important steps in automated external defibrillator (AED) and implantable cardioverter defibrillator (ICD) therapy [20]. The existing diagnostic features are not sufficient to capture the pathological changes of ECG during shockable ventricular arrhythmia. The wavelet based methods for detection of shockable ventricular arrhythmia require proper selection of basis function. During VT and VF, the ECG signal doesn't have 'PQRST' morphologies. Therefore, a data-dependent multiresolution analysis method for evaluation of the diagnostic features of ECG will be helpful for detection of shockable ventricular arrhythmia. The VMD is a data-dependent and iterative method to decompose ECG signal into modes or sub-signals [68]. The center frequency and bandwidth of each mode are different. The pathological changes in the clinical components of ECG during shockable ventricular arrhythmia can be effectively captured using these modes. The non-linear analysis techniques such as the Renyi entropy and the permutation entropy (PE) provide a great opportunity to better understand the cardiac activities and explore the hidden patterns in ECG and heart rate (HR) signals [149, 179]. It is expected that, the time-domain features (energy and PE) and the frequency-domain features (Renyi entropy) evaluated from the modes of ECG will be helpful for detection and classification of shockable ventricular arrhythmia and non-shockable ECG episodes.

This motivates us to use the time-domain and the frequency-domain features of ECG for detection of shockable ventricular arrhythmia.

In this work, a new method is proposed for detection and classification of shockable ventricular arrhythmia and non-shockable episodes from ECG. This method is based on the evaluation of variational mode energy and entropy (VMEE) features from ECG signal. The modes of ECG are evaluated using VMD. The statistical significance and the within-class variations of VMEE features are analyzed. The VMEE features of the ECG episodes and the random forest classifier are used for detection and classification of shockable ventricular arrhythmia and non-shockable ECG episodes. The proposed method has better performance with accuracy, sensitivity and specificity values of 97.23%, 96.54% and 97.97% using random forest classifier and selected VMEE features. The VMEE features correctly capture the diagnostic information of ECG for classification of non-shockable ECG episodes and shockable ventricular arrhythmia. The important finding of this method is that, the energy and the PE of each mode are significant for detection of shockable ventricular arrhythmia. The beat-to-beat variation in a NSR (healthy heart) is higher than that of VT/VF cases. The PE shows a lower mean value for shockable ventricular arrhythmia class. Similarly, the mean value of energy feature is higher for shockable ventricular arrhythmia class compared to non-shockable ECG class. The method can be further improved by evaluating more features such as sample entropy, detrend fluctuation coefficients, Hurst exponent from each mode of ECG to capture the pathological variations.

The major contributions of the work reported in this thesis includes,

- MEES approach for detection and localization of MI from multilead ECG.
- Multiscale PA features for detection of cardiac abnormalities from multilead ECG.
- CWSB features for detection and classification of various cardiac ailments such as BBB, MI and HMD from multilead ECG.
- VMEE features for detection and classification of shockable ventricular arrhythmia and non-shockable episodes from ECG.

The other contributions are,

- Multiresolution inter-sample and inter-lead eigen error features for detection of cardiac ailments.
- Detection of cardiac ailments from multilead ECG using diagnostic eigen error features.
- Multiscale non-linear analysis for classification of cardiac ailments from multilead ECG.

## Organization of the Thesis

The contents of the thesis are organized as:

- In **Chapter 1**, the introduction to ECG, the cardiac ailments diagnosed using ECG, the ADS for detection of cardiac ailments and the diagnostic features of ECG are discussed. The scope for the proposed work is also described in this chapter.
- The related reviews on existing diagnostic feature extraction methods for detection of various cardiac ailments from ECG, and the processing of ECG signal using DWT, DTCWT and VMD are discussed in **Chapter 2**. The feature selection methods and the classifiers are also discussed in this chapter. The motivation of this thesis work is written in the same chapter.
- In **Chapter 3**, the multiscale approach is proposed for detection and the localization of MI from multilead ECG. This approach is based on the evaluation of MEES features from multilead ECG.
- In **Chapter 4**, the complex wavelet magnitude and phase features are proposed and analyzed for detection of various cardiac ailments such as BBB, HMD and MI from multilead ECG.
- A new feature extraction method of ECG is proposed for detection and classification of shockable ventricular arrhythmia and non-shockable ECG episodes in **Chapter 5**. This method is based on the evaluation of VMEE features from ECG.
- The conclusion of this thesis work is drawn in **Chapter 6** with major contributions from this thesis and the scope for further research.

# Contents

भारतीय प्रौद्योगिकी संस्थान गुवाहाटी
Indian Institute of Technology Guwahati

# List of Figures

# List of Tables

# List of Abbreviations

| | |
|---|---|
| ADS | Automated Diagnostic System |
| ANN | Artificial Neural Networks |
| ANOVA | Analysis of Variance |
| AV | Atrioventricular |
| APC | Atrial Premature Contraction |
| AMI | Anterior MI |
| ALMI | Antero-lateral MI |
| ASMI | Antero-septal MI |
| ANFIS | Adaptive Neuro-Fuzzy Inference System |
| AROC | Area Under ROC Curve |
| BBB | Bundle Branch Block |
| CWT | Continuous Wavelet Transform |
| CUDB | Creighton University Ventricular Tachyarrhythmia Database |
| CFS | Correlation Based Feature Selection |
| CWD | Choi-Williams Distribution |
| CKD | Cone Kernel Distribution |
| CD | Correlation Dimension |
| CAD | Coronary Artery Disease |
| CWSB | Complex Wavelet Sub-band Bi-spectrum |
| DCT | Discrete Cosine Transform |
| DFT | Discrete Fourier Transform |
| DWT | Discrete Wavelet Transform |
| DTCWT | Dual Tree Complex wavelet Transform |

| | |
|---|---|
| DFA | Detrend Fluctuation Analysis |
| ECG | Electrocardiogram |
| ELM | Extreme Learning Machine |
| EMD | Empirical Mode Decomposition |
| FFT | Fast Fourier Transform |
| FIR | Finite Impulse Response |
| FD | Fractal Dimension |
| GMM | Gaussian Mixture Models |
| GDA | Gaussian Discriminant Analysis |
| GLM | Generalized Linear Model |
| HMD | Heart Muscle diseases |
| HOS | Higher Order spectra |
| HRV | Heart rate Variability |
| HE | Hurst Exponent |
| HC | Healthy Control |
| ICA | Independent Component Analysis |
| IIR | Infinite Impulse Response |
| IDWT | Inverse Discrete Wavelet Transform transform |
| IDTCWT | Inverse Dual Tree Complex Wavelet Transform |
| IC | Independent Component |
| IMI | Inferior MI |
| ILMI | Infero-lateral MI |
| IPLMI | Infero-posterio-lateral MI |
| IIR | Infinite impulse response |
| IMF | Intrinsic Mode Function |
| IG | Information Gain |
| KNN | K-nearest Neighbor |
| LAH | Left Atrial Hypertrophy |
| LVH | Left Ventricular Hypertrophy |

| | |
|---|---|
| LP | Linear Prediction |
| LDA | Linear Discriminant Analysis |
| LE | Lyapunov Exponent |
| MI | Myocardial Infarction |
| MEES | Multiscale Energy and Eigenspace |
| MITDB | MIT-BIH Arrhythmia Database |
| MLPNN | Multilayer Perceptron Neural Network |
| MMSE | Multivariate Multiscale Sample Entropy |
| MIL | Multi Instance Learning |
| PVC | Premature Ventricular Complex |
| PDF | Probability Density Function |
| PC | Principal Component |
| PCA | Principal Component Analysis |
| PTB | Physikalisch Technische Bundesanstalt |
| PMMSE | Principal Component Multivariate Multiscale Sample Entropy |
| PWVD | Pseudo Wigner-Ville Distribution |
| PE | Permutation Entropy |
| PA | Phase Alternation |
| QDA | Quadratic Discriminant Analysis |
| RAH | Right Atrial Hypertrophy |
| RVH | Right Ventricular Hypertrophy |
| ROC | Receiver Operating Characteristics |
| RQA | Recurrence Quantification Analysis |
| RF | Random Forest |
| RBFNN | Radial Basis Function Neural Network |
| SVM | Support Vector Machines |
| SA | Sinoatrial |
| SD | Statistical Dependency |
| SU | Symmetrical Uncertainty |

| | |
|---|---|
| SVD | Singular Value Decomposition |
| SVEB | Supra-ventricular ectopic beats |
| SE | Sample Entropy |
| VT | Ventricular Tachycardia |
| VF | Ventricular Fibrillation |
| VEB | Ventricular Ectopic Beats |
| VB | Ventricular Bigeminy |
| VER | Ventricular Escape Rhythm |
| VMD | Variational Mode Decomposition |
| VFDB | MIT-BIH Malignant Ventricular Arrhythmia Database |
| VPC | Ventricular Premature Contraction |
| VCG | Vectorcardiogram |
| WT | Wavelet Transform |

# List of Symbols

| | |
|---|---|
| $\alpha$ | Quadratic penalty factor or balancing parameter of the data-fidelity constraint |
| $a$ | Scaling parameter |
| $Acc$ | Accuracy |
| $AWGN$ | Additive white Gaussian noise |
| $\mathbf{A}_L$ | Multivariate approximation sub-band matrix |
| $\beta$ | Lagrangian multiplier |
| $b$ | Translation parameter |
| $\mathbf{B}(f1, f2)$ | Bi-spectrum of a signal |
| $\mathbf{B}(f1, f2, f3)$ | Tri-spectrum of a signal |
| $Bi$ | Total number of bins |
| $b_h$ | Bias value for $h^{\text{th}}$ hidden neuron |
| $BW_t$ | Bandwidth of t$^{\text{th}}$ mode |
| $cA_L(k)$ | Approximation Subband wavelet coefficients |
| $cD_l(k)$ | $l^{\text{th}}$ detail sub-band wavelet coefficients |
| $\tilde{cA}_L(k)$ | Real part of the approximation sub-band wavelet coefficients |
| $\tilde{cD}_l(k)$ | Real part of the $l^{\text{th}}$ detail sub-band wavelet coefficients |
| $\overline{cA}_L(k)$ | Imaginary part of the approximation sub-band wavelet coefficients |
| $\overline{cD}_l(k)$ | Imaginary part of the $l^{\text{th}}$ detail sub-band wavelet coefficients |
| $\mathbf{C}_{\mathbf{A}_L}$ | Covariance Matrix of approximation Scale |
| $\mathbf{C}_{\mathbf{D}_l}$ | Covariance Matrix of $j^{th}$ detail Scale |
| $\mathbf{C}$ | Covariance matrix |
| $C$ | Regularization parameter of SVM |

| | |
|---|---|
| $c$ | Degree of the polynomial kernel function |
| $\tilde{C}$ | Total number of classes |
| $dist_i$ | Distance for $i^{\text{th}}$ instance |
| $d$ | Attribute or feature number |
| $\overline{d}$ | Embedding dimension |
| $\mathbf{D}_l$ | Multivariate $l^{\text{th}}$ detail sub-band matrix |
| $\mathbf{d}$ | Significant sub-bands of ECG |
| $E_t$ | Energy of $t^{\text{th}}$ mode |
| $FP$ | False positive |
| $FN$ | False negative |
| $F_s$ | Sampling frequency |
| $\mathbf{F}$ | Hidden layer matrix of ELM |
| $\mathbf{g}$ | Impulse response of high-pass filter |
| $\gamma$ | Regularization parameter for ELM classifier |
| $\tilde{\mathbf{g}}$ | High-pass filter for tree A in DTCWT |
| $\overline{\mathbf{g}}$ | High-pass filter for tree B in DTCWT |
| $\mathbf{h}$ | Impulse response of low-pass filter |
| $H_{\mathbf{Z}^d}$ | marginal entropy of $d^{\text{th}}$ feature |
| $H_{\mathbf{y}}$ | Marginal entropy of class labels |
| $\mathbf{h}$ | Low-pass filter for DWT |
| $\tilde{\mathbf{h}}$ | Low-pass filter for tree A in DTCWT |
| $\overline{\mathbf{h}}$ | Low-pass filter for tree B in DTCWT |
| $h$ | Number of hidden neurons for ELM |
| $IG^d$ | Mutual information score of $d^{\text{th}}$ feature |
| $IA_i$ | Individual class accuracy of $i^{\text{th}}$ class |
| $I$ | Identity matrix |
| $j$ | Complex number notation |
| $\mathbf{J}_{Primal}$ | Primal Optimization problem of SVM |
| $\mathbf{J}_{Dual}$ | Dual optimization problem of SVM |

| | |
|---|---|
| $\tilde{k}$ | Number of nearest neighbors |
| $\tilde{K}$ | Number of folds |
| $K(\mathbf{z}_i, \mathbf{z}_r)$ | Kernel function |
| $L$ | Number of Wavelet Decomposition Level |
| $\mathbf{\Lambda}_{\mathbf{A}_L}$ | Eigenvalue matrix at approximation scale |
| $\mathbf{\Lambda}_{\mathbf{D}_l}$ | Eigenvalue matrices at $l$ $^{\text{th}}$ detail Scale |
| $\mathbf{\Lambda}$ | Eigenvalue matrix |
| $\lambda$ | Eigenvalues |
| $\mathcal{L}$ | Lagrangian |
| $\bar{l}$ | Lag for each mode |
| $\mathbf{m}$ | Number of leads |
| $\mu$ | Mean value |
| $\mathbf{n}$ | Number of ECG samples |
| $\omega_t$ | $t^{\text{th}}$ mode center frequency of VMD |
| $OA$ | Overall accuracy |
| $\psi^*(t)$ | Mother wavelet |
| $\phi_{l,k}(n)$ | Scaling function |
| $\psi_{l,k}(n)$ | Wavelet function |
| $p$ | Number of Instances |
| $P$ | Probability |
| $P(\mathbf{Z}_b^d, \mathbf{y}_b)$ | Joint histogram or PDF of the $d^{\text{th}}$ feature and class labels |
| $P(\mathbf{y}_b)$ | Histogram of the class labels |
| $P(\mathbf{Z}_b^d)$ | Histogram of the $d^{\text{th}}$ feature |
| $\pi_t(i)$ | $i^{\text{th}}$ permutation pattern for $t^{\text{th}}$ mode |
| $PE_t$ | Permutation entropy of $t^{\text{th}}$ mode |
| $q$ | Number of features |
| $\tilde{q}$ | Number of selected features |
| $\overline{r}_{CF}$ | Mean feature-class correlation |
| $\overline{r}_{FF}$ | Mean feature-feature inter-correlation |

| | |
|---|---|
| $RE_t$ | Renyi entropy of $t^{\text{th}}$ mode |
| $r$ | Number of output neurons |
| $\psi(x)$ | Mother Wavelet |
| $SU^d$ | Symmetrical uncertainty score of $d^{\text{th}}$ feature |
| $\mathbf{s}_t(n)$ | Signal at $t^{\text{th}}$ mode |
| $\mathbf{s}_t(f)$ | Spectrum of $t^{\text{th}}$ mode |
| $Score_A$ | Score of the feature subset $A$ using CFS |
| $\sigma$ | Standard deviation |
| $SE$ | Sensitivity |
| $SP$ | Specificity |
| $SV$ | Support Vectors |
| $T$ | Number of Modes |
| $tol$ | Tolerance of convergence criterion |
| $TP$ | True positive |
| $TN$ | True negative |
| $\theta$ | Order of renyi entropy measure |
| $\mathbf{V_{A_L}}$ | Eigenvector Matrix at $L^{\text{th}}$ Approximation scale |
| $\mathbf{V_{D_l}}$ | Eigenvector Matrix at $l^{\text{th}}$ Detail Scale |
| $\mathbf{w}_h$ | Weight vector for $h^{\text{th}}$ hidden neuron |
| $\mathbf{W}(a,b)$ | Scalogram Matrix |
| $\tilde{W}$ | Weight between hidden layer and output layer in ELM |
| $\mathbf{x}(n)$ | ECG signal |
| $\mathbf{x}_{A_L}$ | Approximation Sub-band Signal |
| $\mathbf{x}_{D_l}$ | $l^{\text{th}}$ detail sub-band signal |
| $\mathbf{X}$ | Multilead ECG $n \times m$ data matrix |
| $\mathbf{Y}$ | Projected Matrix obtained after PCA of multilead ECG |
| $\mathbf{y}(f)$ | Fourier transform of the ECG signal |
| $\mathbf{y}$ | Class label vector |
| $y_i$ | Class Label for $i^{\text{th}}$ instance |

| | |
|---|---|
| $y_{test}$ | Class label for a test instance |
| $\tilde{\mathbf{y}}_t(\overline{d})$ | Embedding vector for $t^{\text{th}}$ mode |
| $\mathbf{Z}$ | Feature matrix with dimension $p \times q$ |
| $\mathbf{z}_i$ | Feature vector for $i^{\text{th}}$ instance |
| $\mathbf{z}_{te}$ | Feature vector for a test instance |

# 1

# Introduction

## Contents

## 1. Introduction

This thesis work is an investigation on the cardiac diagnostic information of electrocardiogram (ECG) signal. In clinical practice, the ECG is commonly used for diagnosis of heart pathologies. The cardiologist examines the clinical components of ECG for diagnosis [1]. For ambulatory or holter monitoring applications, one or two ECG leads are commonly used. The standard 12-lead or multilead ECG is typically used for detection of life-threatening cardiac ailments such as conduction defect, muscle defect and myocardial infarction. In multilead ECG, each lead views the heart from a different angle and provides both spatial and temporal information about the cardiac activities. Large amount of data are generated during continuous recording of ECG from a patient. It is a tedious task for the cardiologist to visually inspect all the ECG data for diagnosis of cardiac ailments. Therefore, an automated diagnostic system (ADS) is useful to assist the cardiologist in diagnosing the cardiac ailments [2]. The ADS consists of preprocessing of ECG data, diagnostic information extraction and classification [3]. The preprocessing stage involves the filtering of ECG data and segmentation. The final stage of ADS is the detection and classification of cardiac ailments from the diagnostic information of ECG. The quantification of diagnostic information is the crucial stage in ADS. This stage involves the evaluation of diagnostic features of ECG signal. The diagnostic features are evaluated using signal processing techniques. Although various signal processing techniques have been proposed for evaluation of diagnostic features of ECG, these features are not sufficient to capture the pathological variations during cardiac arrhythmia. This motivates us to develop new feature extraction methods for detection of different cardiac abnormalities.

In this work, three new feature extraction methods are proposed for quantifying diagnostic information from ECG signal. These diagnostic features are used for automated detection of various cardiac abnormalities. The first method deals with the multiscale approach for detection and localization of myocardial infarction (MI) from multilead ECG. The wavelet decomposition of multilead ECG grossly segregates the clinical components at different scales or sub-bands. In MI, the characteristics of the clinical components of multilead ECG are different than those from the normal sinus rhythm (NSR). These pathological changes can be captured using the multivariate sub-band matrices of multilead ECG. The sub-band matrices are formulated using the wavelet coefficients of each ECG lead. The multiscale energy and eigenspace (MEES) features are evaluated from the significant sub-band matrices of multilead ECG. The performance of MEES features of multilead ECG is evaluated using

various classifiers for detection and localization of MI. The second method deals with the complex wavelet magnitude and phase features of multilead ECG for detection of three cardiac ailments such as bundle branch block (BBB), heart muscle diseases (HMD) and MI. The dual tree complex wavelet transform of multilead ECG produces complex wavelet coefficients at different sub-bands. The complex wavelet coefficients at different sub-bands can capture the pathological symptoms of multilead ECG during MI, HMD and BBB. In this work, the multiscale phase alternation (PA) features, and the complex wavelet sub-band bi-spectrum (CWSB) magnitude and phase features are evaluated. The performance of complex wavelet magnitude and phase features is assessed using different classifiers for detection of HMD, MI and BBB pathologies. The third method deals with the variational mode energy and entropy (VMEE) features for detection and classification of shockable ventricular arrhythmia and non-shockable ECG episodes. The ECG signal is decomposed into number of modes or sub-signals using variational mode decomposition (VMD). These modes capture the grossly segmented clinical components of ECG. The time domain features (energy and permutation entropy) and the frequency domain features (Renyi entropy) are evaluated from each mode. The random forest classifier is used to classify the VMEE features of ECG signal into shockable ventricular arrhythmia and non-shockable episodes.

The ECG signals used in this work are taken from four publicly available databases. These are Physikalisch Technische Bundesanstalt (PTB) diagnostic multilead ECG database, Creighton university ventricular tachyarrhythmia database (CUDB), MIT-BIH arrhythmia database (MITDB) and MIT-BIH malignant ventricular arrhythmia database (VFDB) [4] [5] [6]. The multilead ECG signals from PTB database are used for detection of MI, BBB and HMD. The ECG signals from CUDB, MITDB and VFDB databases are used for detection and classification of shockable ventricular arrhythmia and non-shockable episodes. The descriptions of each of the databases are given in chapter-2. The following section briefly discusses the bio-electrical activity of heart and the morphological features of ECG.

## 1.1 Electrical Activity of the Heart and the Electrocardiogram

The heart is an autonomous organ and it provides oxygenated blood to the whole body. The cross-sectional view of the heart is depicted in Fig. 1.1. It consists of four chambers (Left atrium, right

atrium, left ventricle and right ventricle) and four valves (Tricuspid valve, mitral valve, semilunar valve and aortic valve) [1]. The left atrium and the right atrium are separated by a thin membranous wall called as the inter-atrial septum. Similarly, the left ventricle and the right ventricle are separated by a thick muscular wall called as inter-ventricular septum. The blood circulation inside the heart is described as follows. In the heart, the blood flows in a unidirectional manner. First, the de-oxygenated blood is received by the right atrium through large veins called as superior vena cava and inferior vena cava [7]. Then, the blood is transferred from the right atrium (RA) to the right ventricle (RV) through the tricuspid valve. The function of the tricuspid valve is to prevent back flow of blood from RV to RA. The right ventricle pumps the blood to lungs through semilunar valve for oxygenation. The oxygen-rich blood is collected by the left atrium. The blood is then passed to the left ventricle through the mitral valve. The left ventricle pumps the oxygenated blood to the aorta through the aortic valve. Then, the aorta transfers the oxygenated blood to the whole body. The entire heart activity is coordinated by an electrical conduction path or system [1]. This electrical conduction path is established using four specialized cardiac myocytes or pacemaker cells namely, sino-atrial (SA) node, atrio-ventricular (AV) node, HIS bundle and purkinje fibers [7]. Firstly, the left atrium and the right atrium are depolarized due to the firing of SA node. The firing rate of SA node varies from 60 to 100 beats per minute. Then, the firing of AV node transfers the heart electrical activity from atria to ventricles. The AV node has a firing rate varying from 40 to 60 beats per minute. The depolarization of the septum and the ventricles are due to the firing of HIS bundle and purkinje fibers [1]. The intrinsic peaks of these two pacemaker cells vary from 25 to 45 beats per minute. The re-polarization of cardiomyocytes occurs in the reverse order of depolarization.

The electrocardiogram (ECG) is a non-invasive way of measuring the entire electrical activity of heart. Each ECG cycle contains number of time-varying local waves, such as P-wave, QRS-complex and T-wave. The morphological features of ECG are the amplitude, the duration and the shape of the local waves [8]. Cardiologists use these features for detection of cardiac ailments. The descriptions of each of the morphological feature of ECG signal are given below.

***P-wave***: P-wave represents the depolarization of the right atrium and the left atrium of heart [1]. For NSR, the amplitude and the duration of the P-wave are 0.25 mV, and 80 ms to 100 ms, respectively. A tall P-wave with amplitude greater than 0.25 mV and a wide P-wave with duration more than 100

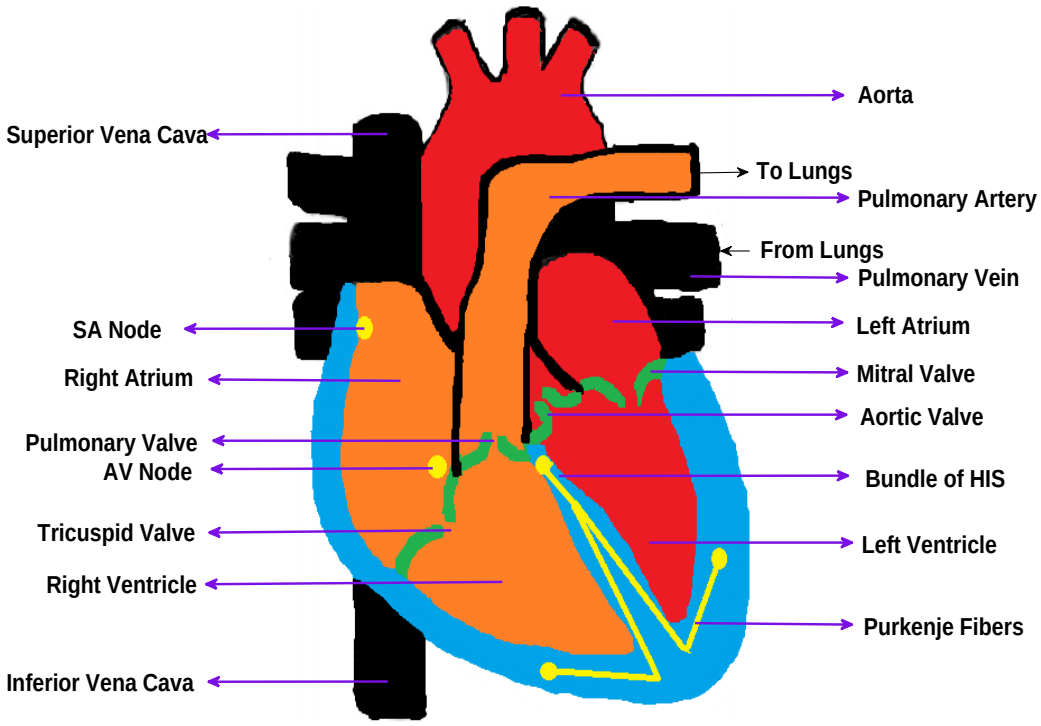


**Fig. 1.1:** Cross-sectional view of human heart. SA- Sino atrial, AV-Atrio ventricular.

ms are the pathological symptoms of atrial hypertrophy. The unordered nature of P-wave with a very high rate is the pathological signature for atrial fibrillation and atrial flutter types of cardiac ailments.

***PR-Interval***: The PR-interval is the time duration between the end of atrial depolarization and the beginning of ventricular depolarization [9]. This time interval is also termed as the delay in the transfer of electrical activity from atria to ventricles. For NSR, the PR-interval varies from 120 ms to 200 ms. The PR-interval increases during 1st degree AV block, second degree AV block and rheumatic cardiac diseases. During pheochromocytoma and Wolfe-Parkinson-White Syndrome, the short PR-interval are observed in ECG signal.

***Q-wave***: Q-wave manifests the depolarization of intra-ventricular septum [1]. It is the first downward deflection of the QRS-complex. For NSR, the duration of Q-wave is less than 40 ms. The amplitude of Q-wave in ECG is 25% of the R-wave amplitude. The deep or abnormal Q-wave is the pathological symptom for MI.

***R-wave***: R-wave is the part of QRS-complex and it represents the part of ventricular depolarization

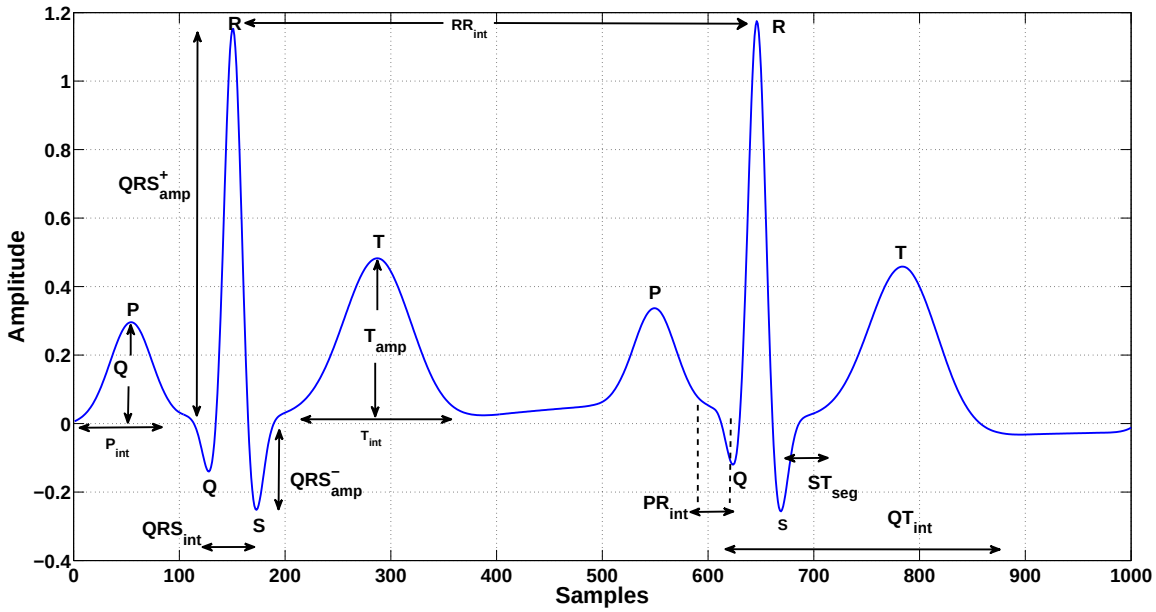


**Fig. 1.2:** The amplitude (mV) and the duration parameters of a synthetic ECG signal. The sampling frequency of the ECG signal is 500 Hz.

cycle. The amplitude of R-wave is an important diagnostic feature for detection of left BBB and hypertrophy [9].

***S-wave***: S-wave represents the remaining part of the ventricular depolarization and in ECG, it is the first downward deflection after R-wave [1]. The shape of S-wave is different in left BBB and right ventricular hypertrophy pathologies.

***QRS-Complex***: QRS-complex represents the depolarization of left and right ventricles. For NSR, the duration of QRS-complex varies from 80 ms to 100 ms [1]. The duration of QRS-complex is greater than 100 ms in BBB pathology.

***RR-Interval***: RR-interval represents the ventricular rate. This time duration is evaluated based on the difference between the R-peak locations of the consecutive beats in the ECG signal. The RR-interval is an important diagnostic feature for detection of sleep apnea and respiratory disorders [9].

***ST-Segment***: In ECG, the ST-segment represents the duration between the end of ventricular depolarization and the beginning of ventricular repolarization. The slope of ST-segment is used as a diagnostic feature for detection of various cardiac ailments. The elevation and the depression in ST-segment are the pathological symptoms for MI and cardiomyopathy [3].

***T-wave***: The T-wave in ECG represents the repolarization of ventricles [1]. The amplitude of T-wave is less than 0.5 mV for NSR. The duration of T-wave varies from 100 ms to 250 ms. The abnormally shaped T-wave is the pathological symptom for MI, hyperkalemia, cardiomyopathy, hypokalemia and hypercalcemia [3].

***QT-Interval***: QT-interval represents the time duration between the beginning of ventricular depolarization and the end of ventricular repolarization. For NSR, the QT-interval varies from 350 ms to 450 ms. The QT-interval is prolonged during bradycardia and for tachycardia, the QT-interval shortens [9].

***U-wave***: The U-wave in ECG is due to the delayed repolarization of Purkinje fibers. The abnormal U-waves are seen during sinus bradycardia and severe hypokalaemia [3].

## 1.2 Multilead Electrocardiogram

The multilead or 12-lead ECG is commonly used in intensive care unit (ICU) or coronary care unit (CCU) for diagnosis of cardiac ailments [10] [11]. The 12-lead ECG signals are recorded by placing ten electrodes at the standardized positions [9]. The 12-lead ECG consists of bipolar leads (I, II, III), unipolar limb leads (aVR, aVL, aVF) and precordial leads (V1, V2, V3, V4, V5, V6). The bipolar leads and the unipolar limb leads are derived using the electrodes that are placed on the left leg (LL), the right leg (RL), the left arm (LA) and the right arm (RA), respectively [9]. The precordial leads are obtained from six standardized positions on the surface of chest or thorax. The lead V1 and the lead V2 are positioned at the fourth intercostal space just to right sternum and left sternum, respectively [9]. The lead V4 is placed on the fifth inter-coastal space at the midclavicular line. The lead V3 is positioned in between the lead V2 and lead V4. The lead V5 and lead V6 are positioned at the anterior auxiliary line and the midaxillary line, respectively. In clinical setting, the cardiologists use serial recording of ECG data from twelve electrodes for diagnosis of cardiac disorders [12]. This shows the importance of 12-lead ECG for accurate detection and localization of life-threatening cardiac abnormalities.

### 1.2.1 Different Views of Heart from Multilead ECG

The unipolar limb leads, the bipolar limb leads and the precordial leads of multilead ECG visualize the heart from different angles. The angles of orientations for lead I, lead II and lead III are $0°$, $60°$

and $120^{\circ}$, respectively. Similarly, $-30^{\circ}$, $-150^{\circ}$ and $90^{\circ}$ are the angles of orientations for lead aVL, lead aVR and lead aVF [9]. The left lateral, the inferior, the anterior, the posterior and the right lateral views of the heart are shown in Fig. 1.3. The left lateral view of heart is seen using the ECG signals of lead I, lead aVL, lead V5 and lead V6, respectively. Similarly, the lead II, the lead III and the lead aVF view the inferior portion of the heart. The lead V1, the lead V2, the lead V3 and the lead V4 are used for anterior view of the heart. The right lateral view of heart is seen using the lead aVR. The various types of MI are diagnosed by observing the pathological variations in different lead sets [12]. The inferior MI can be diagnosed using the pathological signatures of lead II, lead III and lead aVF. Similarly, the pathological variations in the ECG signals of lead I, lead aVL, lead V5 and lead V6 are the evidences for detection of lateral MI. The posterior MI is diagnosed using the reciprocal changes of the ECG signals of lead V1 and lead V2. The pathological changes in lead V1, lead V2, lead V3 and lead V4 ECG signals are used for detection of anterior MI [9].

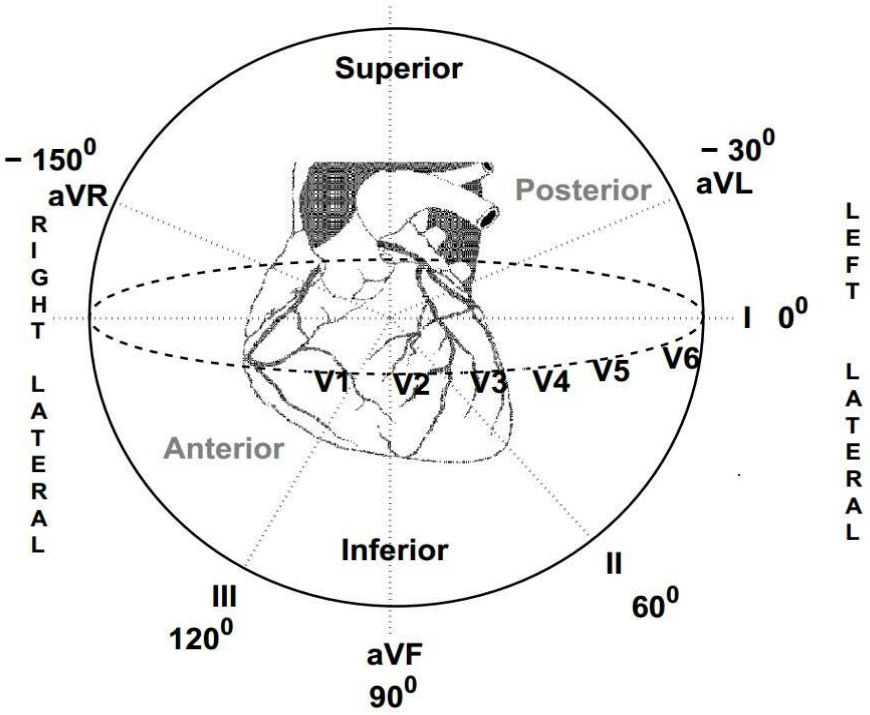


**Fig. 1.3:** Anterior, inferior, lateral and posterior view of heart from multilead ECG [1].

### 1.2.2 Clinical Components of ECG in Different Leads

The 12-lead ECG provides the three dimensional view of the depolarization and the repolarization of atria and ventricles. The clinical components of 12-lead or multilead ECG are P-wave, QRS-complex and T-wave along each lead [1]. The signal characteristics of limb leads and precordial leads are shown in Table 1.1 and Table 1.2, respectively. The P-wave manifests the depolarization of left and right atrium. The P-wave is upright in lead I, lead II, lead V3, lead V4, lead V5 and lead V6, respectively [11]. In lead aVR and lead aVL, the P-waves are inverted. The P-wave is either biphasic or upright in lead V1 and lead V2. In junctional rhythm, the P-waves are absent. The P-wave has opposite polarity in non-sinus atrial rhythm. The QRS-complex manifests the depolarization of inter-ventricular septum, right ventricle and left ventricle. The QRS-complex is upright in lead I, lead II, lead III, lead aVL, lead aVF, lead V4, lead V5 and lead V6, respectively. In lead V3, the QRS-complex is either upright or equiphasic [11] [1]. The lead V1 and the lead V2 have a different QRS morphology (appearance of rS-wave). In rapid ventricular tachycardia and ventricular fibrillation, the abnormal waves other than QRS-complexes are seen in ECG. The T-wave represents the relaxation of left and right ventricles of the heart. The amplitude of T-wave is negative in lead aVR and lead aVL. For other ECG leads, the T-waves are upright. The T-wave inversion is the pathological signature for MI and cardiomyopathy [1].

**Table 1.1:** Orientations of P-wave, QRS-complex and T-waves in unipolar and bipolar limb leads.

| Components | Lead I | Lead II | Lead III | Lead aVR | Lead aVL | Lead aVF |
|---|---|---|---|---|---|---|
| P-wave | upright | upright | negative/upright | negative | negative | upright |
| QRS-complex | upright | upright | upright | negative | upright | upright |
| T-wave | upright | upright | negative/upright | negative | upright | upright |

**Table 1.2:** Orientations of P-wave, QRS-complex and T-waves in precordial leads.

| Components | Lead V1 | Lead V2 | Lead V3 | Lead V4 | Lead V5 | Lead V6 |
|---|---|---|---|---|---|---|
| P-wave | upright/biphasic | upright/biphasic | upright | upright | upright | upright |
| QRS-complex | rS-wave | rS-wave | equiphasic/upright | upright | upright | upright |
| T-wave | upright | upright | upright | upright | upright | upright |

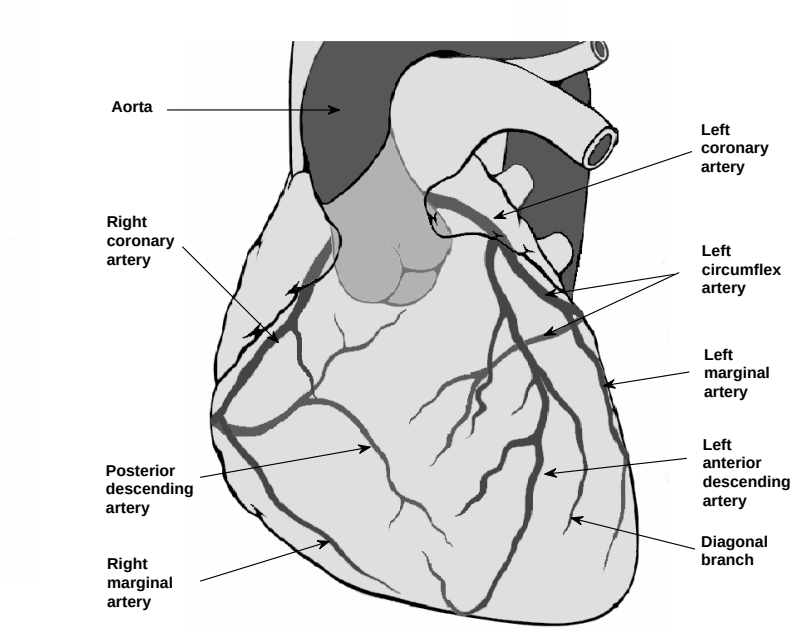


**Fig. 1.4:** Coronary arteries and the anatomical relations in heart [1].

## 1.3 Cardiac Ailments and Pathological Changes in ECG

In this section, the pathological variations in the ECG signal due to various cardiac ailments are discussed. Five kinds of cardiac ailments are considered in this work. These are MI, HMD, BBB, shockable ventricular arrhythmia and non-shockable ventricular arrhythmia.

***Myocardial Infarction***: Myocardial Infarction (MI) occurs due to the occlusion in one of the coronary arteries of the heart [13]. The coronary arteries and the anatomical relations in heart are depicted in Fig. 1.4. The left main coronary artery (LCA) splits into left anterior descending (LAD) and left circumflex (LCX) coronary arteries (Fig. 1.4). The anterior left ventricle (LV), the lateral and the posterior LV walls, the inter-ventricular septum and the apex get blood supply from these two arteries. The right coronary artery (RCA) supplies blood and other nutrients to right ventricle (RV), inferior wall of LV, part of the posterior wall of the LV through the posterior descending artery and posterior interventricular septum [7]. MI progresses in three phases such as ischemic phase, acute phase and necrosis phase [14]. In ischemic phase, the blood flow in one of the coronary arteries is reduced due to the formation of plaque by atherosclerosis. The second phase corresponds to the acuteness of the

ischemia and in third phase, the myocardial necrosis occur. The pathological symptoms of MI in ECG are the T-wave peaking followed by T-wave inversion, the ST-segment elevation and the appearance of pathological Q-wave (as shown in Fig. 1.5 (b)-(d)). The MI heart disease is categorized based on the location of infarction or the occlusions in the coronary arteries [1]. The 12-lead or multilead ECG is commonly used in clinical practice for localization of MI. The different types of myocardial infarction are anterior MI, anterio-septal MI, anterio-lateral MI, inferior MI, inferio-lateral MI and inferio-posterio-lateral MI.

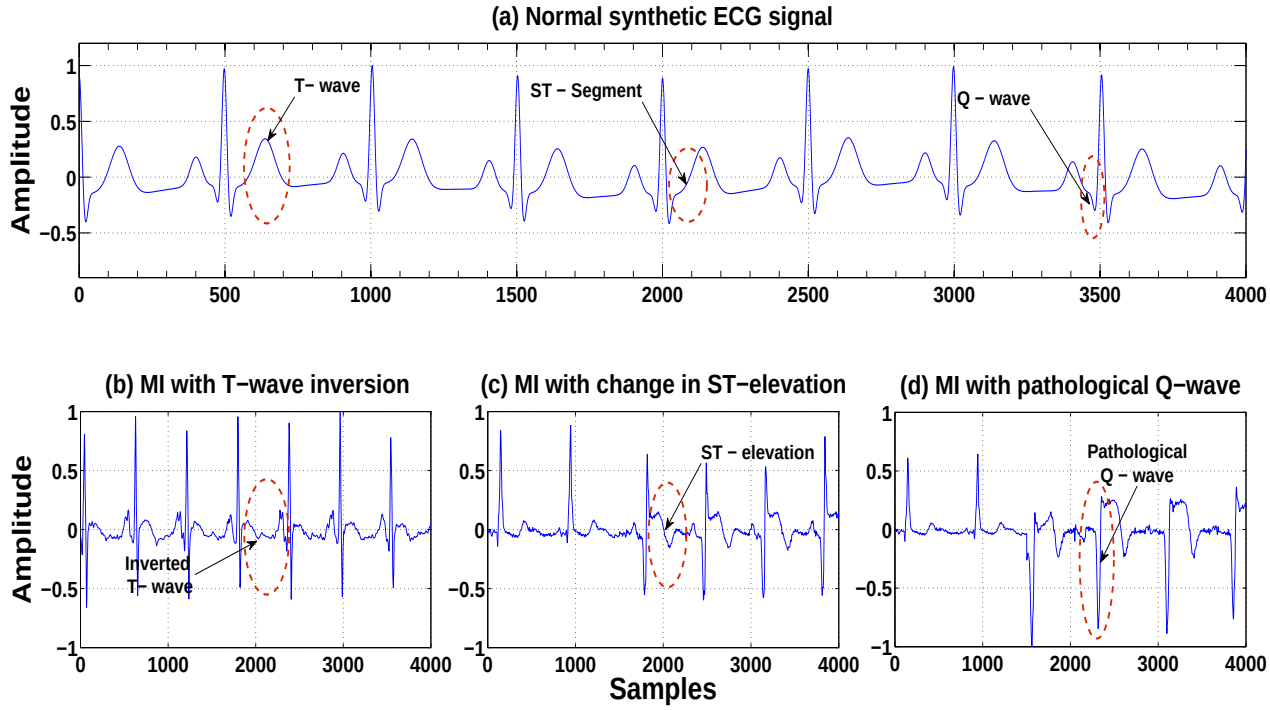


**Fig. 1.5:** Normal synthetic ECG with three stages of MI evolution. (a) Normal synthetic ECG signal for reference. (b) MI with T-wave peaking and inversion. (c) MI with change in ST elevation. (d) MI with pathological Q-wave formation. The amplitude of ECG signals with MI symptoms is in mV and the sampling frequency is 1000 Hz.

***Anterior MI***: The anterior MI (AMI) is due to the obstruction in the left anterior descending artery [12]. The pathological variations in multilead ECG include the T-wave inversions in lead I, lead aVL, lead V2, lead V3, lead V4 and lead V5, respectively. The ST-segment elevation is seen in lead I, lead V4 and lead V5, respectively. The QS-notch and the abnormal Q-wave are appeared in lead V2 and lead aVF, respectively [1].

***Anterio-lateral MI***: The Anterio-lateral MI (ALMI) is due to the combined obstructions in the left

anterior descending artery and the right coronary artery [12]. The pathological signatures of ALMI in multilead ECG are the ST-segment elevations in lead I, lead aVL, lead V3, lead V4 and lead V6, respectively. The loss of r-wave progression is seen in lead V2. The T-wave inversion is also observed in lead II, lead V3, lead V4, lead V5 and lead V6, respectively [9].

***Anterio-septal MI***: The anterio-septal MI (ASMI) is due to partial obstruction in one of the branches of the left anterior descending artery [12]. In this type of MI, the tissue damage is located around anterio-septal wall (region between the left and the right ventricles). The pathological changes in multilead ECG due to ASMI are the appearance of QS-complexes in lead V1, lead V2 and lead V3, respectively. The ST-segment elevation and T-wave inversion are seen in different ECG leads [9].

***Inferior MI***: The Inferior MI (IMI) is due to the occlusion in right coronary artery [12]. Due to this type of MI, the abnormal Q-waves appear in lead III and lead aVF, respectively. The ST-segment elevations are also seen in lead II, lead III and lead aVF, respectively. The ST-segment depression is observed in different precordial leads [1].

***Inferio-lateral MI***: The inferio-lateral MI (ILMI) is due to the combined occlusions in the right marginal artery and the left anterior descending artery [12]. The pathological signatures of the ILMI in multilead ECG are the presence of abnormal Q-wave in lead aVF, the ST-segment elevations in lead I and lead aVL, and the T-wave inversions in lead II and lead V6, respectively. The amplitude of r-wave in lead V1, lead V2 and lead V3 are higher than NSR [9].

***Inferio-posterio-lateral MI***: The Inferio-posterio-lateral MI (IPLMI) is due to the combined obstructions in the left circumflex artery and the right coronary artery [12]. The pathological variations in multilead ECG due to this type of MI are the tall R-waves and the peaked T-waves in lead V2 and lead V3, respectively. The ST-segment elevation and the T-wave inversion are seen in lead V5 and lead V6, respectively. The pathological Q-waves are also observed in lead III and lead aVF, respectively [1].

***Heart Muscle Diseases***: Hypertrophy and cardiomyopathy are heart muscle diseases (HMD) [15]. The pathological changes in ECG due to cardiomyopathy and hypertrophy are shown in Fig. 1.6 (a)-(c). In hypertrophy, the size of cardiomyocytes increase as a result, there are the increment in the size of heart chambers [9]. The hypertrophy pathology can be broadly classified as right atrial hypertrophy (RAH), left atrial hypertrophy (LAH), right ventricular hypertrophy (RVH) and left

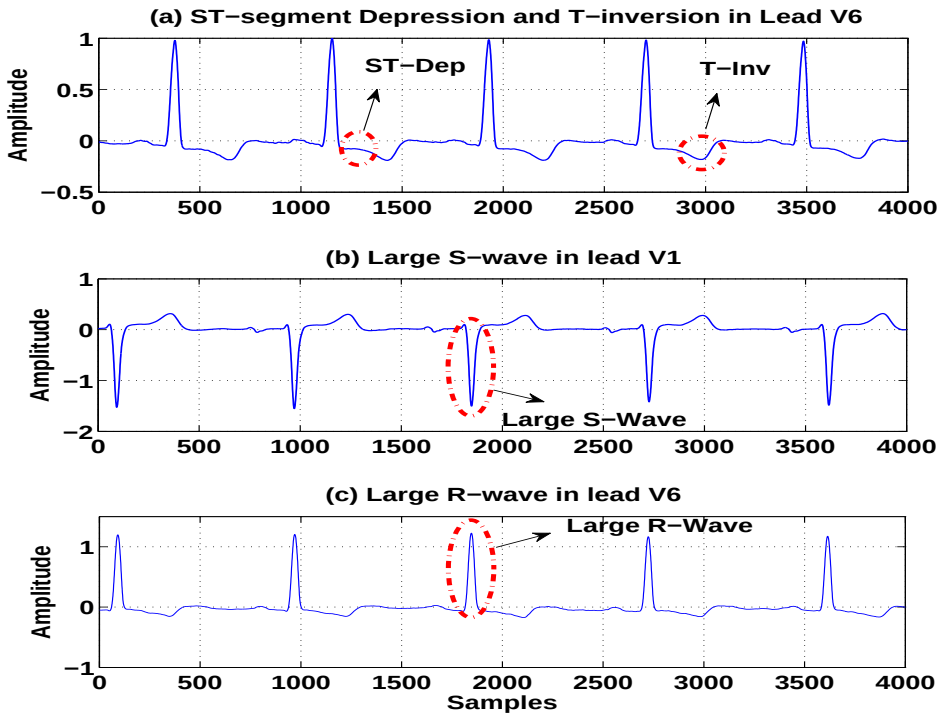


**Fig. 1.6:** (a) ST-segment depression and T-wave inversion in lead V6 due to cardiomyopathy. (b) S-wave with higher amplitude in lead V1 due to hypertrophy. (c) Higher R-wave amplitude in lead V6 due to hypertrophy. The amplitude of each ECG signal is in mV and the sampling frequency is 1000 Hz.

ventricular hypertrophy (LVH). RAH is a consequence of right atrial overload, tricuspid valve disease and pulmonary valve disease [9]. Due to RAH, the amplitude of P-wave is greater than 0.25 mV in lead II, lead III and lead aVF. Similarly, the LAH is the consequence of left atrial overload and mitral valve disease. The notched P-wave and the biphasic P-wave with negative amplitude greater than 0.1 mV are seen in lead II and lead V1, respectively [1]. RVH is the consequence of pulmonary valve stenosis and pulmonary hypertension. The tall R-waves with amplitude higher than 0.7 mV are seen in lead V1 and lead V2. The wide R-wave is also seen in lead V5 and lead V6. The LVH is the consequence of aortic valve disease and mitral valve disease [9]. The tall R-wave in lead I, lead V5 and lead V6, and the tall S-wave in lead III, lead V1 and lead V2 are the pathological symptoms of LVH. Cardiomyopathy is an inherited heart muscle disease and it is one of the leading cause of death in young athletes [16]. The pathological symptoms of cardiomyopathy in ECG are T-wave inversion, ST-segment depression, abnormal Q-waves and left atrial enlargement.

***Bundle Branch Block***: Bundle branch block (BBB) causes delay in the conduction process of the

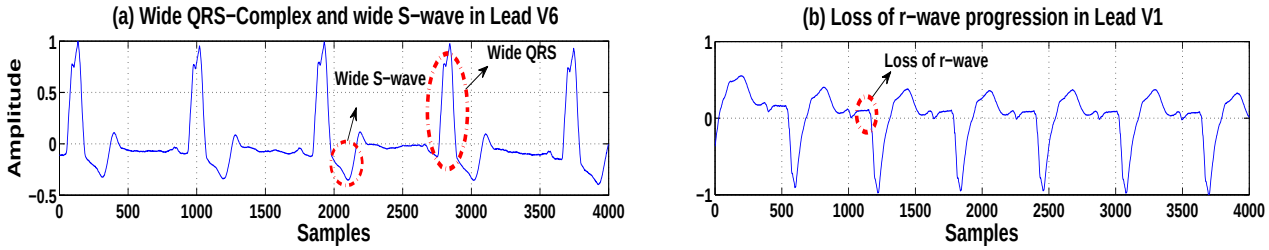


**Fig. 1.7:** (a) Wide QRS-complex and wide S-wave in lead V6 ECG signal due to left BBB. (b) Loss of septal r-wave progression in lead V1 ECG signal de to left BBB. Amplitude of each ECG signal is in mV and the sampling frequency is 1000 Hz.

heart. This delay may occur in the right and the left sides of the ventricles. Left BBB corresponds to the delay in the depolarization of left ventricle [1]. The pathological variations in left BBB are the absence of septal r-wave and septal Q-wave in lead V1 and lead V6 (as shown in Fig. 1.7 (a) and Fig. 1.7 (b)). The right BBB is the delay in the activation of right ventricle. The wide R-wave and the wide S-wave in lead V1 and the lead V6 are the pathological symptoms for right BBB. The QRS-complex duration and the R-wave amplitude are high in BBB pathology [1].

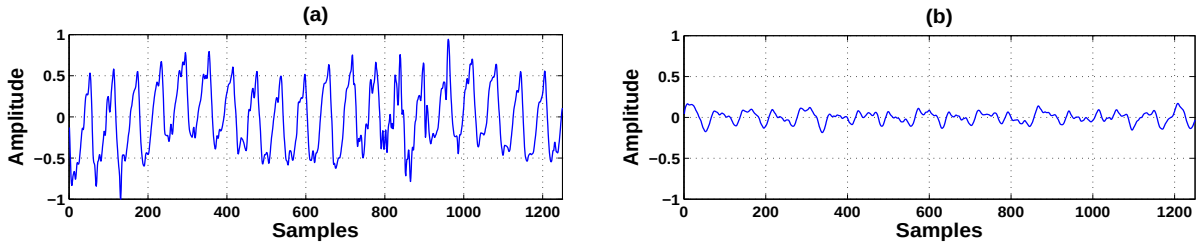


**Fig. 1.8:** (a) Rapid ventricular tachycardia episode in ECG. (b) Ventricular fibrillation episode in ECG. The amplitude of each ECG signal is in mV and the sampling frequency is 250 Hz.

***Shockable Ventricular Cardiac Ailments***: The shockable ventricular cardiac ailments are rapid ventricular tachycardia (VT) and ventricular fibrillation (VF) [17]. The major cause of rapid VT and VF are ischemic heart disease. The rapid VT and VF episodes in ECG are shown in Fig. 1.8 (a) and Fig. 1.8 (b), respectively. VT is a fast cardiac rhythm and it originates in the lower chambers (left and right ventricles) of the heart. In ECG, the abnormal or bizarre QRS-complexes with duration more than 0.14 sec appear [9]. During VT, the heart rate varies from 100 to 250 beats per minute. If the VT episodes sustain more than 30 sec, then it can turn into ventricular fibrillation, causing sudden cardiac death of the patient. VF occurs due to the firing of more than one ectopic pacemakers

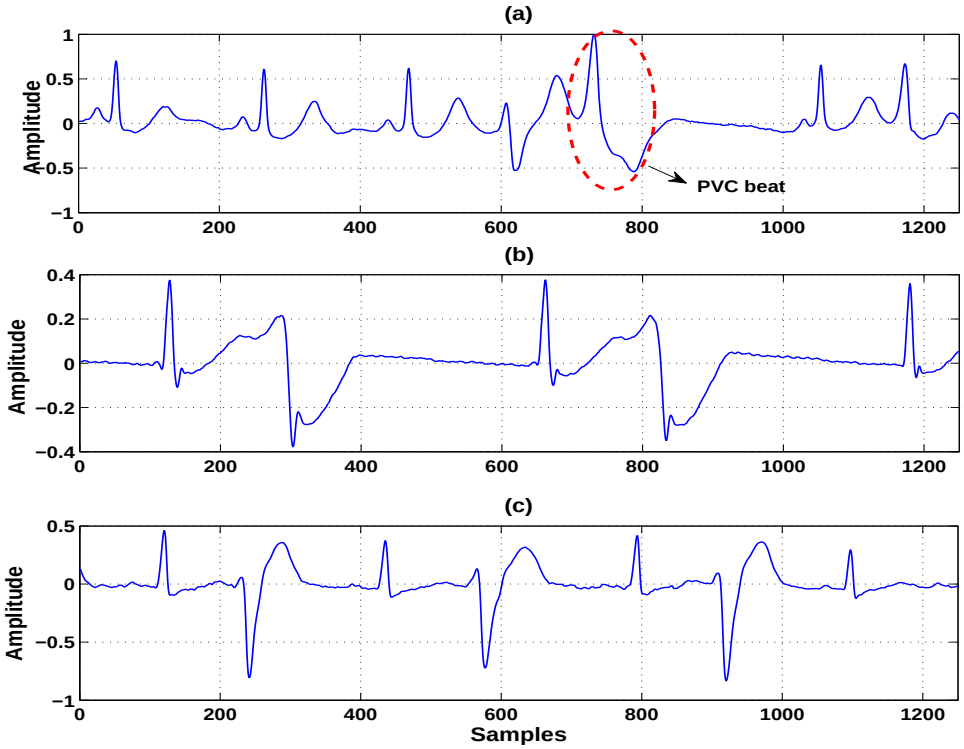


**Fig. 1.9:** (a) Premature ventricular contraction (PVC) beat. (b) Ventricular escape rhythm. (c) Ventricular bigeminy. The amplitude of each ECG signal is in mV and the sampling frequency is 250 Hz.

in the lower chambers of the heart [18]. The different parts of the myocardium contract in an unsynchronized manner at different times. The left and the right ventricles are unable to pump the blood into lungs and arteries, as a result, there is no or insignificant cardiac output. In ECG, the abnormal patterns appear due to VF. The automated external defibrillator (AED) and the implantable cardioverter defibrillator (ICD) are used for diagnosis of rapid VT and VF episodes.

***Non-shockable Ventricular Cardiac Ailments***: The non-shockable ventricular cardiac ailments are ventricular ectopic beats (VEB), ventricular escape rhythm (VER) and ventricular bigeminy (VB) [19], [20]. The pathological variations in ECG signals due to these cardiac ailments are shown in Fig. 1.9 (a), Fig. 1.9 (b) and Fig. 1.9 (c), respectively. VEB is an extra beat originating from the ventricles. In this condition, more than one pacemaker may be involved in the electrical conduction of heart. The site of pacemaker may be in purkenje fibers or bundle branches [9]. In ECG, the premature ventricular complex (bizarre shaped QRS-complex) is generated due to this arrhythmia. VER is a condition when the contraction of ventricles falls below the base heart rate and the pacemaker

activity of heart is initiated from the lower chambers. This type of rhythm indicates the failure in the conduction process of the heart [9]. In VER, the shape of QRS-complex is broader and there is a delay in the heart electrical activity. VB is the condition where the heart alternates one normal beat with other premature ventricular complex (PVC) beat.

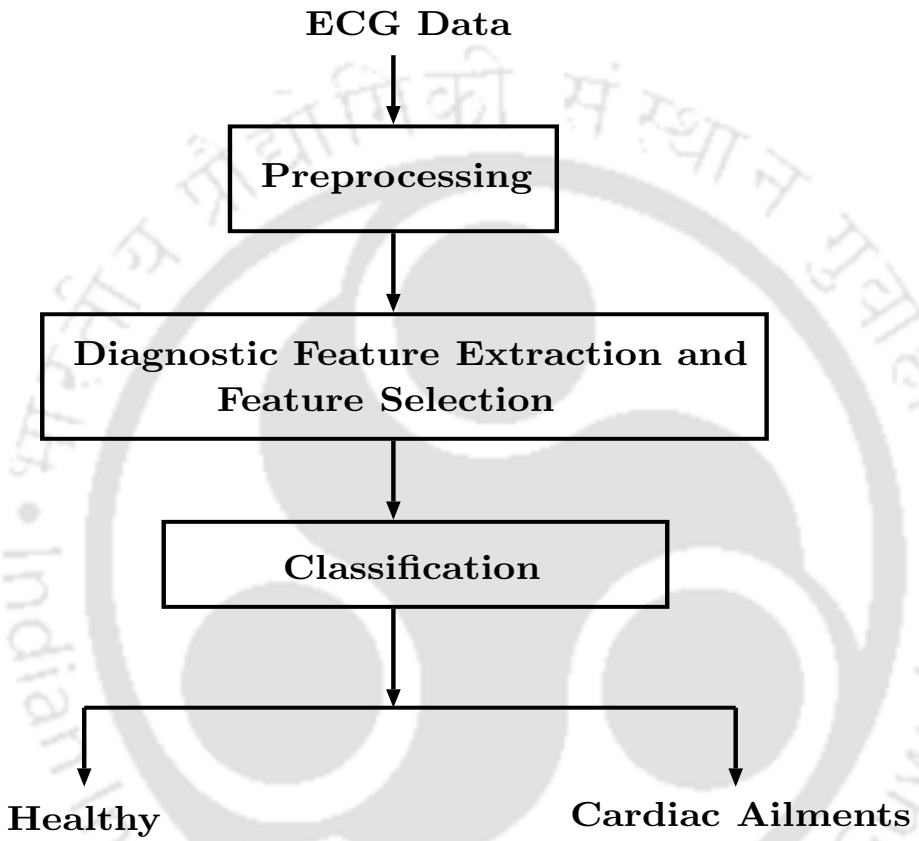


**Fig. 1.10:** Automated Diagnostic system for detection of cardiac ailments.

## 1.4 Automated Diagnostic System

ECG is the non-invasive way of recording the electrical activity of cardiomyocytes during a heart beat [1]. Trained medical experts and cardiologists detect and classify different group of cardiac abnormalities from the ECG recordings. In a 24 hour or 36 hour ECG recording, over 100,000 heart beats are generated [2] [21]. The minute variations in the clinical components of ECG depict a particular type of cardiac arrhythmia. It is a time consuming task for cardiologist to manually examine the entire ECG data for detection of cardiac abnormalities and he/she can overlook some vital informa-

tion during manual procedure. Therefore, an automatic diagnostic system (ADS) that characterizes cardiac activities from ECG signals is the universal need for clinical applications [3]. The flow-chart of ADS is shown in Fig. 1.10. It consists of preprocessing of ECG data, diagnostic feature extraction and feature selection, and classification of cardiac ailments from the diagnostic features of ECG [21]. The following subsections briefly discuss the different parts of the ADS.

### 1.4.1 Preprocessing

The preprocessing of ECG signal includes the filtering of various noises and segmentation. The ECG may contain artifacts or undesired signals during recording [22]. These artifacts are baseline drift or wander, powerline interference and high frequency slurs and noises [23]. Selection of suitable filters for filtering of the aforementioned noises are important task in ECG signal processing. **Baseline drift** is a low-frequency noise (below 1Hz) present in an ECG signal [3]. This kind of noise in ECG is due to poor electrode contact, body movement and respiration. The iso-electric line and the ST-segment of ECG signal are affected due to baseline drift. The detection of QRS-complex is difficult during the presence of this artifact. The baseline drift may be filtered out using non-linear filtering [24], zero-phase filters [25], wavelet transform [26], emperical mode decomposition (EMD) [27] and variational mode decomposition (VMD) methods [28]. **Electromyographic (EMG) noise** is due to the electrical activity of the skeletal muscles during contraction [22]. This kind of noise is commonly seen in ECG signal during ambulatory monitoring. The frequency content of this noise is below 100 Hz. The band-pass filters and the wavelet based techniques have been used for filtering of this noise [23] [29]. **Powerline noise** is the interference of nearby equipment during the recording of ECG data [30]. The frequency content of this noise is 60/50 Hz with harmonics. The powerline interference noise can be filtered out using adaptive filters [31] and infinite impulse response (IIR) filters [22].

The segmentation of ECG data is done based on the detection of R-peaks [32]. Two types of segmentation methods have been used in ADS. These are beat-by-beat segmentation [33] and frame-based segmentation [20]. There are three types of correlations present in an ECG signal. These are intra-beat correlation, inter-beat correlation and inter-lead correlation [34], [35]. The correlation between the adjacent samples within an ECG cycle is called as intra-beat or inter-sample correlation. The correlation between the adjacent beats of ECG data is termed as inter-beat correlation. The

correlation between the leads of multilead ECG is called as inter-lead correlation. The beat-by-beat segmentation of ECG data exploits the intra-beat correlation. The cardiac ailments like PVC beat, VB, VEB, localization of myocardial infarction and atrial premature beats are diagnosed based on the beat-by-beat segmentation of ECG data [36], [37]. Cardiologists suggest for serial recording of ECG data from 12-leads for detection of cardiac abnormalities [12]. To exploit both intra-beat and inter-beat correlations, the frame based processing is needed. In this thesis work, the frame based processing of ECG data is used for detection of various cardiac ailments. For multilead ECG case, the frame based processing has the advantage of capturing the inter-lead, the intra-beat and the inter-beat correlations.

### 1.4.2 Diagnostic Feature Extraction and Feature Selection

ECG signal contains the information about the contraction and the relaxation of heart chambers (atria and ventricles) [3]. This information is used by the cardiologist for diagnosis of various cardiac ailments such as MI, conduction defects, HMD, shockable ventricular arrhythmias and supra-ventricular arrhythmias. Analysis of ECG signal is one of the primary steps to measure the diagnostic information. The diagnostic information of ECG can be effectively captured using features. Diagnostic feature extraction is a key component in ADS for detection of cardiac abnormalities [37]. In this step, the most relevant information from the ECG signal is obtained and this information is represented in a lower dimensional space (feature vector). There are two type of methods used for evaluation of diagnostic features from ECG signal. These are direct and indirect methods. The direct method is based on the evaluation of morphological features such as P-wave amplitude, QRS maximum positive amplitude, QRS maximum negative amplitude, T-wave amplitude, RR-interval, QT-interval, PR-interval, QRS-interval, QRS-angle and ST-segment slope [8]. The cardiologist subjectively examines these features for detection and localization of various cardiac ailments. These morphological features have been used for detection of cardiac ailments such as MI, hypertrophic cardiomyopathy and cardiac dysrhythmia [38], [36], [39], [40]. The direct method requires accurate detection of fiducial points (P, Q, R, S, T points) along each ECG lead for evaluation of the diagnostic features [41], [42]. Though, it is possible to evaluate the fiducial points manually, automated detection using signal processing algorithms are not error free [43]. Therefore, the indirect methods have been widely used in ADS for

evaluation of diagnostic features from ECG signal [2]. The indirect method is based on various signal processing algorithms. After evaluating the relevant features of ECG signal, the diagnostic feature vector is formulated [3]. The effectiveness of ADS will depend on an efficient quantification of relevant diagnostic information. The feature selection is a method of choosing the relevant attributes from the diagnostic feature vector of ECG signal. The feature selection methods are based on either statistical measures or optimization algorithms [37].

### 1.4.3 Classification of Cardiac Ailments

Classification of cardiac ailments from the diagnostic features of ECG is the final stage of ADS. In this stage, the machine learning leaning techniques are used to perform this task. Two kinds of machine learning approaches have been used [3] [37]. These are supervised and unsupervised learning. In supervised learning, the input instances of the classifier is labeled whereas for unsupervised learning case, the class labels of the input instances are not given. The supervised learning techniques used for classification of cardiac ailments are Bayes classifier, Gaussian mixer model, Hidden Markov model, nearest neighbor classifier, neural networks, random forest classifier, support vector machine and extreme learning machine [3]. Similarly, the unsupervised learning techniques such as k-means clustering, hierarchical clustering and self organizing map have also been used [3]. For supervised learning case, the feature matrix (matrix formulated using the feature vectors of the ECG instances) is divided into training data matrix and test data matrix. The training instances are used to build the hypothesis for classifier. Then, the test instances are used for evaluation. The methods such as the hold-out cross validation and the K-fold cross-validation have been used for selection of training and test instances of classifier [44] [45]. In hold-out cross-validation, the training and the test instances of classifier are evaluated by dividing the feature matrix using certain percentage. Typically, 70% of the instances are used for training and the rest 30% instances are used for testing purpose. For 5-fold cross-validation case, the $\frac{4}{5}$th instances of each fold are used for training and the remaining $\frac{1}{5}$th instances are used for testing of classifier. The performance of classifier is evaluated using various measures such as sensitivity, specificity, accuracy, F-measure and area under receiver operating characteristics (ROC) curve [22].

## 1.5 Diagnostic Features for Automated Detection of Cardiac Ailments

In recent years, number of methods have been proposed for evaluation of the diagnostic features of ECG signal. These features are used for detection of different groups of cardiac abnormalities. The methods are based on discrete Fourier transform (DFT) [46], discrete cosine transform [47], discrete time continuous wavelet transform (CWT) [48] [49], discrete wavelet transform (DWT) [50], dual-tree complex wavelet transform (DTCWT) [51], auto-regressive model coefficients [52], time-delay methods [53], Non-linear Analysis [54], principal component analysis (PCA) [55], independent component analysis (ICA) [56], higher order spectral analysis [57], polynomial regression coefficients [2] and tensor based analysis [58]. The PCA and the linear prediction (LP) analysis methods have been used in [59], for classification of left BBB, right BBB, ventricular ectopic beats (VEB) and supra-ventricular ectopic beats (SVEB). The first twelve principal components (PCs) of LP residual have been used as diagnostic features for classification. Martis $et\ al.$ [47] have used DCT and PCA methods to evaluate features from the ECG signal. The first twelve PCs evaluated in DCT domain are used for classification of SVEB, VEB and fusion beats. Balasundaram $et\ al.$ [48] have used discrete time CWT and singular value decomposition (SVD) for detection of VT and VF episodes from ECG. The linear discriminant analysis (LDA) classifier is used to evaluate the performance of the eigenspace features of the scalogram matrix. Banerjee $et\ al.$ [49] have used the wavelet cross spectrum and wavelet coherence features of ECG for detection of MI. The wavelet cross spectrum and the wavelet coherence features are evaluated based on the discrete time CWT of reference ECG and analyzed ECG signals.

The DWT has been used for various ECG signal processing applications such as filtering, compression and feature extraction [60], [61], [62], [63]. The wavelet coefficients of ECG signal at different scale capture the grossly segmented diagnostic components. The low-frequency components are obtained using the inner product of ECG signal with the scaling function. Similarly, the inner product of ECG signal with wavelet function gives high-frequency components [64]. Recently, the multiscale analysis using DWT has been used for denoising and compression of multilead ECG data [65], [25]. Jayachandran $et\ al.$ [50] have evaluated the energy and the entropy features from the wavelet coefficients of single lead ECG. They have used threshold based classifier for detection of MI. The multiscale recurrent quantification analysis (RQA) of vectorcardiogram (VCG) has been proposed for

detection of MI [14]. The RQA is applied to the sub-band signals (signals reconstructed from the wavelet coefficients at different scales or sub-band) of VCG. The multiscale RQA features and the quadratic discriminant analysis (QDA) classifier are used for detection of MI. Acharya $et\ al.$ [66] have used DWT and eigenspace analysis methods for classification of arrhythmia beats from ECG. The wavelet coefficients of ECG are evaluated using DWT. The PCA, and the ICA have been used for dimension reduction. The first twelve components of wavelet coefficients in PCA, FDA and ICA domains are used as features for classification. The dual-tree complex wavelet transform (DTCWT) is the modifications of DWT and it uses pair of filter banks to compute the real and the imaginary components of the wavelet coefficients at different scales [67]. The DTCWT features have been used for classification left BBB, right BBB, PVC and ventricular paced beats from ECG [51]. The variational mode decomposition is a data-dependent technique for multiresolution analysis of non-stationary signals [68]. The center frequencies and the maximum phase difference features of the variational modes of ECG have been used for classification of supra-ventricular and ventricular arrhythmias [69].

## 1.6 Scope for the Present Work

Automated detection and localization of MI from multilead ECG is a challenging problem. In recent years, the multiscale decomposition using DWT is most preferred technique for analysis of ECG signal. The multiscale features of single lead ECG have been used for detection of MI. The multiscale analysis of multilead ECG for detection and localization of MI has not been addressed. There are scopes to use multiscale features of multilead ECG for detection and localization of MI.

The life-debilitating cardiac ailments are BBB, HMD and MI. Detection and classification of these cardiac ailments from multilead ECG are challenging tasks. The multiscale analysis using DTCWT has been used for detection and classification of various cardiac ailments from single lead ECG. The DTCWT of ECG signal produces complex wavelet coefficients at different scales. The magnitude and the phase features can be evaluated from these complex wavelet coefficients. The complex wavelet magnitude and the phase features have not been used for analysis of multilead ECG during various pathological conditions. There are scopes to use the complex wavelet magnitude and phase features of multilead ECG for detection of life-debilitating cardiac abnormalities.

Rapid VT and VF are shockable ventricular cardiac ailments. The initial step in both AED and

ICD devices is to detect rapid VT and VF episodes. After successful detection, electric shock is given to bring back the heart activity to NSR. The detection and classification of shockable ventricular arrhythmia and non-shockable episodes from ECG is a challenging problem. The VMD is recently proposed in the signal processing literature for analysis of non-linear and non-stationary signals. This method has been applied for denoising of ECG signal and detection of various cardiac ailments from ECG. The ECG signal is decomposed into modes or sub-signals using VMD. There are the scopes to evaluate diagnostic features from the modes of ECG for detection of shockable ventricular arrhythmia.

## 1.7 Organization of the Thesis

The contents of this thesis are organized as follows. In **Chapter 1**, the introduction to ECG, the cardiac ailments diagnosed using ECG, the ADS for detection of cardiac ailments and the diagnostic features of ECG are discussed. The scope for the proposed work is also described in this chapter. In **Chapter 2**, the related reviews on existing diagnostic feature extraction methods for detection of various cardiac ailments from ECG, and the processing of ECG signal using DWT, DTCWT and VMD are discussed. The feature selection methods and the classifiers are also discussed in this chapter. The motivation of this thesis work is written in the same chapter. In **Chapter 3**, the multiscale approach is proposed for detection and the localization of MI from multilead ECG. In **Chapter 4**, the complex wavelet magnitude and phase features are proposed and analyzed for detection of various cardiac ailments such as BBB, HMD and MI from multilead ECG. In **Chapter 5**, a new feature extraction method based on the VMD of ECG is proposed for detection and classification of shockable ventricular arrhythmia and non-shockable episodes. The conclusion of this thesis work is drawn in **Chapter 6** with major contributions from this thesis and the scope for further research.

# 2

# Analysis of Diagnostic Information for Detection of Cardiac Ailments: A review

## Contents

The electrocardiogram (ECG) signal provides the diagnostic information about the electrical conduction process of the heart [1]. This information is captured as features or parameters of ECG signal. The effectiveness of automated diagnostic system (ADS) depends on an efficient quantification of diagnostic information. The relevant diagnostic information can be evaluated through proper selection of features. The key motivation for researchers is to use various signal processing algorithms to evaluate the diagnostic features of ECG. The performance of the diagnostic features of ECG is evaluated using classifiers for detection of cardiac abnormalities. Various signal processing techniques have been used to estimate the diagnostic information of ECG signal. These techniques are based on heart rate variability (HRV) analysis, linear prediction (LP) analysis, higher order spectra (HOS), independent component analysis (ICA), principal component analysis (PCA), non-linear analysis, discrete wavelet transform (DWT), dual tree complex wavelet transform (DTCWT) and variational mode decomposition (VMD). The feature selection techniques such as the mutual information based feature ranking, symmetrical uncertainty based feature scoring and correlation based feature selection (CFS) have been used for choosing relevant diagnostic information. The classifiers such as K-nearest neighbor (KNN) and fuzzy KNN, random forest (RF), support vector machine (SVM) and extreme learning machine (ELM) have been used for classification of cardiac ailments from the diagnostic features of ECG. This chapter reviews the existing diagnostic feature extraction methods of ECG, the feature selection methods and the classifiers for detection of cardiac ailments. The rest of this chapter is arranged as follows. The databases used for evaluation of the proposed work are described in Section 2.1. The ECG diagnostic features for detection of myocardial infarction (MI), shockable ventricular arrhythmia and other groups of cardiac ailments are briefly discussed in Section 2.2. The wavelet transform and the VMD based processing of ECG signal are described in Section 2.3 and Section 2.4, respectively. The diagnostic features based on the PCA, the HOS and the nonlinear analysis of ECG are discussed in Section 2.5, Section 2.6 and Section 2.7, respectively. In Section 2.8, the feature selection methods such as the correlation based technique, the mutual information and the statistical uncertainty are described. The machine learning techniques such as KNN and fuzzy KNN, RF, SVM and ELM classifiers are discussed in Section 2.9. The performance measures of the classifiers such as accuracy, sensitivity, specificity and area under receiver operating characteristics (ROC) curve are also discussed in the same section. The motivation of the proposed

work is written in the last section (Section 2.10) of this chapter.

## 2.1 Database

In this work, the algorithms developed for evaluation of ECG diagnostic features and detection of cardiac ailments are tested using four standard publicly available databases. These are Physikalisch Technische Bundesanstalt (PTB) diagnostic multilead ECG database [4], Creighton university ventricular tachy-arrhythmia database (CUDB) [5], MIT-BIH arrhythmia database (MITDB) [6] and MIT-BIH malignant ventricular arrhythmia database (VFDB) [5]. The PTB diagnostic database is a collection of digitized 12-lead ECG records from healthy volunteers and patients having different cardiac ailments such as myocardial infarction (MI), cardiomyopathy (CM), hypertrophy (HT), dysrhythmia (DT), myocartidis and bundle branch block (BBB) at the Department of Cardiology, University Clinic Benjamin Franklin in Berlin, Germany. A total number of 549 multilead ECG datasets from 290 subjects are given in the database. The subjects in different pathologies are- MI: 148; BBB: 17; CM: 14; HT: 7; valvular disease: 6; myocarditis: 4; miscellaneous: 4; and healthy control (HC): 52. Each multilead ECG data has 12 conventional leads (I, II, III, aVR, aVL, aVF, V1, V2, V3, V4, V5, V6) and 3 Frank leads (VX, VY, VZ). The sampling rate of each multilead ECG data is 1000Hz. CUDB database consists of $35$ ECG signals and each signal has $8$ minute duration. The ECG signals in the CUDB database have the annotations such as ventricular fibrillation (VF), sustained ventricular tachycardia (VT) and non VF rhythms. Similarly, the VFDB database consists of $22$ files of two channel ECG signals. Each lead ECG signal in VFDB database has 35 min duration. The annotations of ECG signals in VFDB database are normal sinus rhythm (NSR), ventricular flutter, VF, VT and other rhythms. The sampling frequency of the ECG signal in both CUDB and VFDB database is 250Hz. The MITDB database contains $40$ files of two lead ECG signals with sampling frequency of 360Hz. The annotations of the ECG signals in MITDB database are VF, ventricular flutter and VT.

## 2.2 Diagnostic Information from ECG

The Electrocardiogram (ECG) is used to assess the cardiac electrophysiological events and functions [3]. The spatial and the temporal view of the cardiac events are seen using multilead ECG. The ECG feature extraction is the important stage in ADS for detection of life-debilitating cardiac ailments. In

this stage, the diagnostic information of the cardiac activities are captured using features. Selecting relevant features is a challenging task for quantifying diagnostic information. The classifiers have been used to evaluate the performance of the diagnostic features of ECG. In this section, the feature extraction techniques for automated detection of various cardiac ailments such as MI, BBB, atrial arrhythmia, heart muscle diseases (HMD) and shockable ventricular arrhythmia (rapid VT and VF) are briefly discussed. The existing feature extraction methods for detection and localization of MI are discussed in first subsection. The second subsection describes the existing features for detection of different types of cardiac ailments such as BBB, supra-ventricular ectopic beats, ventricular ectopic beats and HMD. The existing methods for detection of shockable ventricular arrhythmia are discussed in third subsection.

### 2.2.1 Diagnostic Features for Detection of MI

Myocardial Infarction (MI) is a life-threatening cardiac ailment that can cause sudden death of a patient [1]. The pathological changes in ECG due to MI heart disease are the ST-segment elevation, the T-wave inversion and the abnormal Q-wave (as shown in Fig. 1.5 (b)-(d)) in different leads. Detection of acute MI from ECG and vectorcardiogram (VCG) signals is a challenging task in clinical practice. Number of methods have been proposed for detection of MI from ECG and VCG, using time domain features, frequency domain features and time-frequency features. The time domain features are the amplitude, the shape, the angle, the slope and the duration of the clinical components of ECG. Heden $et\ al.$ [70] have used ST-segment parameters such as ST-J amplitude, ST-slope and T-wave amplitude features of 12-lead ECG, and artificial neural network (ANN) for detection of acute MI. The sensitivity and the specificity values of 95% and 86.3% are found. Correa $et.\ al.$ [71] have evaluated ST-segment vector magnitude area, ST-T vector magnitude difference, spatial ventricular gradient, T-wave vector magnitude area features from VCG signal. These morphological features of VCG have been used for detection of acute myocardial ischemia. The sensitivity and the specificity values of 90.53% and 92.58% have been reported. Reddy $et\ al.$ [72] have used morphological features such as Q-wave amplitude, Q-wave duration, R-wave amplitude, S-wave amplitude and S-wave duration of 12-lead ECG, and ANN for detection of MI. The sensitivity and the specificity values of 82% and 93% are reported from their work. Ringborn $et\ al.$ [73] have used QRS-slope features

for evaluation of changes during depolarization in case of acute myocardial ischemia. The upward slope of R-wave, the downward slope of R-wave and the upward terminal slope of S-wave in lead V1, lead V2 and lead V3 are evaluated. Romero $et\ al.$ [74] have proposed a method for detection of myocardial ischemia from multilead ECG. This method uses QRS-angle to capture the pathological variations. The QRS-angles such as the R-wave angle, the upstroke angle and the down stroke angle are evaluated and these values have been used as diagnostic features. Arif $et\ al.$ [36] have evaluated Q-wave amplitude, T-wave amplitude and ST-segment features from multilead ECG signal. They have used KNN classifier for detection and localization of MI. The sensitivity and the specificity values of 99.97% and 99.9% are reported for MI detection. Fayn [75] has evaluated spatiotemporal features from lead I, lead II and lead V2 ECG signals. The decision tree classifier has been used for detection of myocardial ischemia from the spatiotemporal features of ECG. From their reported work, both sensitivity and specificity values of 98% are obtained.

Chang $et\ al.$ [76] have used hidden Markov model (HMM) model to evaluate diagnostic features from lead V1, lead V2, lead V3 and lead V4 ECG signals. The SVM and the Gaussian mixture model (GMM) have been used for detection of MI. The sensitivity and the specificity values of 85.71% and 79.82% are found using SVM classifier. Loewe $et\ al.$ [77] have proposed a new feature to quantify ST-segment deviation in ECG signal. This feature is defined as the mean of $25$ samples of ST-segment for a specific ECG lead. This new feature has been used for detection of MI. Arini $et\ al.$ [78] have evaluated the temporal indices of the ventricular repolarization dispersion and the spatial indices of ventricular repolarization dispersion features from ECG signal. These features have been used for detection of acute myocardial ischemia. Sun $et\ al.$ [2] have used polynomial curve fitting over ST-segments (approximately 200 samples) of each ECG lead. The polynomial coefficients and other morphological features of multilead ECG, and multi instance learning (MIL) classifier have been used for detection of MI. The sensitivity and the specificity values of 91.43% and 77.29% are reported. Lu $et\ al.$ [79] have evaluated ST-segment deviation and T-wave amplitude features from 12-lead ECG. These morphological features of multilead ECG and neuro-fuzzy classifier have been used for localization of MI. The sensitivity values for anterio-septal MI (ASMI), anterio-lateral MI (ALMI), extensive anterior MI, local anterior MI, inferior MI and inferio-lateral MI classes are 85.7%, 100%, 87.5%, 75%, 93.3% and 66.7%, respectively. The time domain features correctly capture the pathological

variations in ECG and VCG signals during MI, but the evaluation of these features require accurate detection of fiducial points (P, Q, R, S and T points). The automated evaluation of P, Q, R, S, T locations along each ECG lead using signal processing algorithms are not error free [43]. Therefore, the frequency domain features and the time-frequency based features are widely used for detection of MI.

In recent years, number of methods have been proposed for detection of MI based on the frequency domain and the wavelet based features of ECG. The frequency domain features are evaluated using the discrete Fourier transform (DFT) of ECG. The comparisons of high-frequency component of QRS-complex and the ST-segment depression are studied by Ringborn $et\ al.$ [80], for detection of acute myocardial ischemia. Song $et\ al.$ [81] have used QRS-slope features, spectral features of RR-time series and QRS-area features of ECG for detection of acute myocardial ischemia. The QRS-area features are evaluated using QR, RS and QS time intervals of ECG. Valverde and Arini [82] have studied the variations in the spectrum of T-wave during acute myocardial ischemia. The T-wave spectral variance feature has been evaluated using the DFT of T-wave and the spectral energy of ECG signal between 0.5 Hz to 50 Hz. The frequency domain features have limitations to capture pathological changes during MI [50]. Therefore, the time-frequency features have been used for detection of MI from ECG and VCG signals. The time-frequency features of the ECG signal are evaluated using wavelet transform [83]. Banerjee $et\ al.$ [49] have used discrete time continuous wavelet transform (CWT) for detection of MI from ECG signal. The discrete time CWT has been applied to both analyzed ECG and reference ECG for evaluation of wavelet cross spectrum (WCOS) and wavelet coherence (WCH) features. The KNN classifier is used for detection of MI from WCOS and WCH features. The sensitivity values of 97.40%, 98.83%, and 97.55% have been found using KNN classifier, and WCOS and WCOH features of lead II, lead III and lead aVF. Jayachandran $et\ al.$ [50] have used DWT of single lead ECG for evaluation of diagnostic features. The DWT based diagnostic features of ECG and the threshold based classifier are used for detection of MI. The accuracy value of 95% have been reported. Yang [14] has used multiscale recurrence quantification analysis (RQA) of vectorcardiogram (VCG) for detection of MI. The inverse DWT is used to evaluate the sub-band signals of VCG. The sub-band signals are subjected to RQA for evaluation of diagnostic features. The RQA based diagnostic features of VCG and the quadratic discriminant analysis (QDA)

classifier have been used for classification of MI and HC. The sensitivity and the specificity values of QDA classifier are 96.5% and 75%, respectively. The multiscale analysis has the advantage to divide the full spectrum of an ECG signal into multiple sub-bands [14]. The wavelet coefficients of these sub-bands capture the pathological variations in the clinical components of ECG during MI.

### 2.2.2 Diagnostic Features for Detection of Various Cardiac Ailments

The bundle branch block (BBB) and the HMD are life-debilitating cardiac abnormalities [1]. The wide QRS-complex, the wide S-wave and the loss of r-wave progression (as shown in Fig. 1.7) are the symptoms of BBB pathology. Similarly, the pathological variations in P-wave, T-wave and QRS-complex (as shown in Fig. 1.6) are the evidences for detection of HMD. In this subsection, the existing methods for detection of different groups of cardiac abnormalities (BBB, supra-ventricular ectopic beats (SVEB), ventricular ectopic beats (VEB) and HMD) from ECG are discussed. The reported methods for detection of BBB, HMD and other cardiac ailments have used morphological features and transformed domain features of ECG. Melgani $et\ al.$ [84] have used morphological features of ECG (QRS complex duration, RR interval, P-wave amplitude etc.) and SVM classifier for detection and classification of different cardiac abnormalities such as left BBB, right BBB, atrial premature complex (APC) beat, ventricular premature complex (VPC) beat and paced beat. The accuracy values for left BBB and right BBB classes are reported as 95.31% and 94.80%, respectively. Ebrahimzadeh $et\ al.$ [85] have used morphological features (RR-interval and RR-interval ratio) and HOS features of ECG, and radial basis function neural network (RBFNN) for classification of cardiac abnormalities such as left BBB, right BBB, APC and PVC. From their work, the sensitivity values for left BBB and right BBB are reported as 98.43% and 97.51%, respectively. Dogan $et\ al.$ [86] have used morphological features of ECG (QRS-height, QRS-width and RR-interval) and kernel fuzzy c-means clustering for classification of right BBB, APC, VPC and fusion beats. The sensitivity value of 93.76% has been reported. Ovreiu $et\ al.$ [15] have evaluated P-wave features of 5-lead ECG for detection of HMD. The P-wave diagnostic features of 5-lead ECG are the P-wave amplitude, the P-wave duration, the shape of P-wave and the ratio of right atrial excitation energy to total excitation energy, respectively. The performance of the P-wave diagnostic features is evaluated using neuro-fuzzy classifier. An overall accuracy value of 75% has been reported. Maji $et\ al.$ [87] have used Taguchi based feature optimiza-

tion approach for classification of left BBB, right BBB and PVC beats from ECG. The morphological features such as (QR-interval, RS-interval, ST-interval, R-wave angle etc.) are evaluated from ECG signal. The Bayes classifier has been used for classification of cardiac ailments (left BBB, right BBB and PVC beats) from the selected morphological features of ECG. The sensitivity values of 99.35% and 99.51% are reported for left BBB and right BBB classes. The morphological features of ECG are evaluated based on the detection of P, Q, R, S, T onset points along each lead. During pathology, the characteristics of ECG signal along each lead are different from the normal sinus rhythm (NSR). From signal processing prospective, it is a difficult task for accurate detection of P, Q, R, S, T points of ECG signal along each lead. Therefore, the transform domain features of multilead ECG have been used for detection of BBB, HMD and other cardiac abnormalities.

Khalaf $et\ al.$ [88] have used spectral correlation features of ECG and SVM for classification of left BBB, right BBB, normal beat, VPC beat and APC beat. The spectral correlation features are evaluated using the Fourier transform of the auto-correlation of ECG signal. An average accuracy value of 98.60% has been found using SVM classifier. Jen $et\ al.$ [89] have used cepstral coefficients of ECG as diagnostic features and SVM for classification of left BBB, right BBB and other cardiac ailments. An overall accuracy value of 97.5% has been reported. Linh $et\ al.$ [90] have used Hermite polynomial coefficients of QRS-complex as diagnostic features and neuro-fuzzy model for detection and classification of left BBB and right BBB ventricular escape beat, APC beat, VPC beat. From their work, the average accuracy value of 96% has been reported. Yu $et\ al.$ [91] have used ICA to evaluate diagnostic features of ECG signal. The RR-interval and the independent component (IC) features of ECG, and the Bayes classifier are used for classification of APC, PVC, left BBB and right BBB beats. The accuracy values of 93.63% and 94.93% have been reported for left BBB and right BBB classes. Chou $et\ al.$ [92] have evaluated features from the ICs of ECG signal. The IC features and the neural network have been used for classification of left BBB, right BBB, APC and PVC beats. For left BBB and right BBB classes, the sensitivity values of 96.25% and 99.15% have been reported. Pasoli $et\ al.$ [93] have used active learning methods for classification of left BBB, right BBB, VPC and APC beats from ECG. The sensitivity values of 98.81% and 98.68% have been reported for right BBB and left BBB classes. Lanata $et\ al.$ [94] have evaluated the mean and the variance of the bi-spectrum phase, the normalized bi-spectral entropy and the normalized bi-spectral

square entropy features from ECG signal. The bi-spectrum features of ECG and the KNN classifier have been used for classification of left BBB, right BBB, APC and VPC beats. The accuracy values for left BBB and right BBB classes are 82.37% and 94.44%, respectively. Thomas $et\ al.$ [51] have used DTCWT and artificial neural network (ANN) for classification of paced beat, left BBB, right BBB and PVC beats from ECG. They have evaluated the absolute value of the complex wavelet coefficients of QRS-complex and other diagnostic features from the QRS-complex of ECG. The ANN has been used to evaluate the performance of the QRS-complex features of ECG. The sensitivity values of 80.65% and 82.26% have been reported for left BBB and right BBB classes.

Although, the transform domain features have better performance for detection of BBB pathology from ECG, these methods are beat specific and uses only few ECG leads. In clinical standard, the cardiologists recommend serial recording of 12-lead ECG data for detection of BBB and HMD pathologies. A few methods have also been reported for detection of BBB and HMD using 12-lead ECG. Huang $et\ al.$ [58] have used tensor rank one discriminant analysis method for classification of NSR, left BBB, right BBB, sinus bradycardia and left ventricular hypertrophy. The accuracy values for right BBB and left BBB are reported as 96.80% and 97.65%, respectively. Rahman $et\ al.$ [39] have used morphological and temporal features of 12-lead ECG for detection of hypertrophic cardiomyopathy. The sensitivity and the specificity values of approximately 90% are reported using random forest classifier. Bogdanova $et.\ al$ [95] have used random projections of multilead ECG as diagnostic features for detection of different cardiac ailments. The binary sensing matrix based random projection technique has been applied to multilead ECG. The random projection features of multilead ECG and the neuro-fuzzy model are used for classification of NSR, MI and cardiomyopathy. An overall accuracy value of 90% has been reported using twenty random projection coefficients of multilead ECG and neuro-fuzzy classifier. The methods reported in [39] and [95] have less accuracy value for detection of HMD from multilead ECG. Therefore, new diagnostic features of 12-lead or multilead ECG are required for detection of HMD and BBB pathologies.

### 2.2.3 Diagnostic Features for Detection of Shockable Ventricular Arrhythmia

The shockable ventricular arrhythmia such as ventricular fibrillation (VF) and rapid ventricular tachycardia (VT) lead to sudden cardiac death, if the defibrillation is not done immediately [96] [97]. The

abnormal waves other than 'PQRST' morphologies are the pathological symptoms of rapid VT and VF (as shown in Fig. 1.8). Detection of shockable ventricular cardiac arrhythmia is the primary task in automated external defibrillator (AED) and implantable cardioverter defibrillator (ICD) devices. Number of methods have been proposed for detection of shockable ventricular arrhythmia from ECG. These methods are based on the evaluation of diagnostic features using time domain analysis, frequency domain analysis, time-frequency analysis, emperical mode decomposition (EMD) and variational mode decomposition (VMD) of ECG. Some of the methods have used multimodal features of ECG for detection of shockable ventricular arrhythmia. The performance of the diagnostic features of ECG for detection of shockable ventricular arrhythmia is shown in Table 2.1. Thakor $et\ al.$ [98] have proposed TCI features for detection of shockable ventricular arrhythmia episodes from ECG. The probability distributions of TCI feature for NSR and VF classes are evaluated. The VF and the NSR episodes in ECG are classified based on the overlapping in probability distributions. The sensitivity and specificity values are reported as 75.1% and 84.4%, respectively. Kuo $et\ al.$ [99] have proposed VF-filter leakage measure for detection of shockable ventricular arrhythmia from ECG. The VF-filter leakage measure has been evaluated using the original ECG and the shifted version of ECG. The sensitivity and the specificity values of 18.8% and 100% are found. Zhang $et\ al.$ [100] have proposed complexity measure for classification of NSR, VT and VF episodes from ECG. The complexity measure has been evaluated based on the non-linear analysis of ECG signal. The sensitivity and the specificity values of 59.2% and 92.0% are reported. Amman $et\ al.$ [53] have proposed time-delay features of ECG for detection of VF. The time-delay features are evaluated using the phase space representation of ECG signal. The time-delay features and the threshold based classifier have been used for detection of VF. The sensitivity and the specificity values of 79.0% and 97.8% have been reported. Ge $et\ al.$ [52] have used auto-regressive model coefficients of ECG as diagnostic features and generalized linear model (GLM) for classification of shockable ventricular arrhythmia, APC, VPC and NSR. Barro $et\ al.$ [101] have proposed spectral features of ECG for detection of VF and VT. The decision tree based diagnostic algorithm has been used to evaluate the performance of spectral features. From their work, the sensitivity and the specificity values of 29.1% and 99.9% are reported. Krasteva $et\ al.$ [102] have evaluated frequency domain features and morphological features from ECG signal. A threshold based classifier has been used for detection of shockable ventricular

**Table 2.1:** Comparison of the performance of existing methods for detection of shockable ventricular arrhythmia.

| Features | Classifier | Sensitivity | Specificity | Window |
|---|---|---|---|---|
| Threshold Crossing Interval (TCI) [98] | Overlapping of probability distributions | 75.10% | 84.4% | 8 sec |
| Complexity Measure [100] | Threshold based classifier | 59.2% | 92% | 8 sec |
| VF-filter leakage measure [99] | Threshold based classifier | 18.8% | 100% | 8 sec |
| Time-delay feature [53] | Threshold based classifier | 79.00% | 97.8% | 8 sec |
| Spectral features [101] | Decision tree algorithm | 29.1% | 99.9% | 8 sec |
| RCWT based ECG features [104] | Threshold based classifier | 91.7% | 83.3% | 2 sec |
| IMF angle features [105] | Bayes Classifier | 92.78% | 99.60% | 5 sec |
| Correlation of ECG with IMFs [106] | Threshold based classifier | 83.06% | 99.05% | 8 sec |
| Selected Multimodal Features [107] | SVM | 71.9% | 99.7% | 8 sec |
| Multimodal features [20] | SVM | 96.3% | 96.2% | 5 sec |

arrhythmia from these diagnostic features. Neurauter $et\ al.$ [103] have evaluated maximum power, peak frequency, centroid frequency and power at centroid frequency features from the spectrum of ECG signal. These features are evaluated in the frequency bands of $10 - 22$ Hz and $6 - 26$ Hz, respectively. The neural network classifier has been used for detection of VF. The area under ROC curve value of $0.863$ has been found. The time domain and the frequency domain features are not sufficient (less sensitivity values) to capture the pathological changes in ECG during shockable ventricular arrhythmia. Therefore, the time-frequency analysis based ECG diagnostic features have been used for detection of rapid VT and VF.

The time-frequency analysis describes the variation in the spectrum of an ECG signal with respect to time. The time-domain and the frequency-domain characteristics of ECG signal are different for shockable ventricular arrhythmia and NSR [3]. These pathological variations are effectively captured using time-frequency features of ECG. The time-frequency features of ECG signal are evaluated using Choi-williams distribution (CWD) and discrete time CWT. Roig $et\ al.$ [108] have used time-frequency analysis techniques such as CWD and cone kernel distribution (CKD) to evaluate the diagnostic features of ECG signal. The logistic regression model has been used to classify time-frequency analysis based features into shockable ventricular arrhythmia and NSR. The performance of time-frequency features is higher than both time-domain and frequency domain features. Khadra $et\ al.$ [104] have used raised cosine wavelet transform (RCWT) and threshold based classifier for classification of rapid VT and VF episodes from ECG. The sensitivity and the specificity values of 91.7% and 83.3% are reported. Balasundaram $et\ al.$ [48] have used discrete time CWT and singular

value decomposition (SVD) for detection of VT and VF episodes from ECG. The scalogram matrix of ECG is evaluated using discrete time CWT. Then, the scalogram matrix is decomposed into eigen matrices and diagonal matrix using singular value decomposition (SVD). The statistical features are evaluated from the columns of the eigen matrices. These statistical features and the GDA classifier have been used for classification. An overall accuracy (OA) value of 93.7% has been reported. The effectiveness of the wavelet based approach for detection of shockable ventricular arrhythmia is based on the selection of basis function (mother wavelet) which closely matches with the morphology of ECG signal. The abnormal waves other than NSR are appeared during shockable ventricular arrhythmia. Due to this reason, the sensitivity values of wavelet based methods are less for detection of shockable ventricular arrhythmia. Arafat $et\ al.$ [105] have used emperical mode decomposition (EMD) for detection of VF episodes from ECG. The Bayes classifier has been used to classify the intrinsic mode function (IMF) features of ECG into NSR and VF. The sensitivity and the specificity values of 92.78% and 99.60% are reported. Anas $et\ al.$ [106] have evaluated diagnostic features based on the similarity of the IMFs of ECG signal. A complex threshold decision parameter has been used for classification of VF and non-VF episodes. The sensitivity and the specificity values of 83.06% and 99.05% are found. The EMD for analysis of non-stationary signal has limitations such as the mode mixing, and if the amplitude of the high-frequency part of the signal is less than the low-frequency part, then the EMD can't separate the multi-component signal into the respective mono-components [109] [110]. In rapid VT, the QRS-complex spectral peaks are shifted slightly to low-frequencies [3]. Due to this reason, the EMD based methods for detection of shockable ventricular arrhythmia have less sensitivity values.

Number of methods have also been reported for detection of shockable ventricular arrhythmia using multimodal features of ECG. Li $et\ al.$ [20] have evaluated time-delay features, VF-filter leakage measure, complexity measure, spectral features, covariance, area and kurtosis features from ECG. They have used SVM to classify VF and non-VF episodes from the multimodal features of ECG. The sensitivity and specificity values of 96.3% and 96.2% are reported from their work. Atienza $et\ al.$ [19] have evaluated morphological features, spectral features and complexity features from ECG signal. The filter based feature selection and the SVM have been used for classification of shockable ventricular arrhythmia and non-shockable episodes. From their study, the sensitivity and the

specificity values of 95% and 99% are reported. Alwan $et\ al.$ [111] have evaluated VF-filter leakage measure, sample entropy, spectral parameters, phase space features and TCI features from ECG signal. The multiclass SVM has been used for classification of VT, VF and NSR from these diagnostic features. Jekova [112] has used spectral features, complexity features, VF-filter leakage features of ECG signal and GDA classifier for detection of shockable Ventricular arrhythmia. The sensitivity and the specificity values of 81.6% and 80% have been reported. Atienza $et\ al.$ [107] have evaluated time domain features, frequency domain features and time-frequency parameters of ECG signal. The feature selection technique based on bootstrap sampling and the SVM classifier have been used for detection of shockable ventricular arrhythmia. The sensitivity and the specificity values of 71.9% and 99.7% have been reported. Although, multimodal features have better performance for detection of shockable ventricular arrhythmia, the computational time required to evaluate these features is high. Therefore, the new diagnostic features of ECG are required to capture the pathological variations during shockable ventricular arrhythmia.

## 2.3 Wavelet Transform based ECG Signal Analysis

The wavelet transform (WT) has proven to be one of the effective technique for analysis of ECG signal [113]. This technique has been used for various ECG signal processing applications such as the denoising of ECG signal, the detection of QRS-complex, the detection of MI and the detection of shockable ventricular arrhythmia from ECG [114] [115] [49] [48]. The WT decomposes an ECG signal into wavelet coefficients using a series of basis functions [116]. These basis functions are obtained based on the dilation and the translation of mother wavelet. The WT can be evaluated for continuous time and discrete time signals [62]. The time-frequency localization of the ECG signal is observed using this transform. Ghaffari $et\ al.$ [115] have used discrete time CWT for detection of QRS-complex from ECG. They have magnified the QRS-peaks of ECG using dominant rescaled wavelet coefficients. A sensitivity value of 99.92% for QRS-complex detection has been reported. The CWT of an ECG signal, $\mathbf{x}(\bar{t})$ is given by

$$\mathbf{W}(a,b) = \int_{-\infty}^{\infty} \mathbf{x}(\bar{t})\psi_{a,b}(\bar{t})d\bar{t} \tag{2.1}$$

where, $\psi_{a,b}(\bar{t}) = \frac{1}{\sqrt{a}}\psi^*(\frac{\bar{t}-b}{a})$ and $\mathbf{W}(a,b)$ are the basis function for evaluation of wavelet coefficients and the scalogram matrix, respectively [116] [117]. '$a$' and '$b$' are the scaling and the translation parameters. The wavelet coefficients are the function of both scale and translation parameters. The mother wavelet basis is denoted as $\psi^*(\bar{t})$. The scale is inversely proportional to frequency. The large value of '$a$' identify the long term trends, whereas the short term behavior of the ECG signal is detected using the lower scales [117].

### 2.3.1 Discrete Wavelet Transform and ECG

The discrete wavelet transform (DWT) employs a dyadic grid to compute the wavelet coefficients of an ECG signal [118]. The diagnostic information of ECG is captured using the wavelet coefficients of different scales [29]. The multiscale analysis of ECG using DWT has been used for various ECG processing applications such as baseline wandering noise filtering, high-frequency noise filtering, data compression and feature extraction [60], [61], [62] [14] [50]. Sumathi $et\ al.$ [63] have used DWT for evaluation of diagnostic features from ECG signal. The adaptive neuro-fuzzy inference system (ANFIS) has been used to classify diagnostic features of ECG into NSR, PVC, atrial arrhythmia, MI and shockable ventricular arrhythmia. Martis $et\ al.$ [66] have used DWT and various machine learning techniques for classification of SVEB, VEB, fusion beats and non-ectopic beats from ECG. The diagnostic features are evaluated from the wavelet coefficients of ECG. Sharma $et\ al.$ [29] have used higher order statistics over wavelet sub-band for denoising of multilead ECG signal. They have shown that, the wavelet based denoising is effective to filter out high frequency noise from ECG and helps retaining the diagnostic information. The DWT has the advantage that it grossly segments the diagnostic information of ECG into different sub-bands. The basis functions in DWT are obtained by substituting the scaling and the translation parameters as $a = 2^l$ and $b = b_0 2^l k$ in equation 2.1. where $L$ is the number of decomposition levels of DWT and $l = 1, 2, ..., L$, $l \in Z$ and $b_0 = 1$. The scaling and the wavelet functions for DWT are given by [50]

$$\phi_{l,k}(n) = 2^{\frac{-l}{2}}\phi(2^{-l}n - k) \tag{2.2}$$

$$\psi_{l,k}(n) = 2^{\frac{-l}{2}}\psi(2^{-l}n - k) \tag{2.3}$$

The wavelet coefficients in approximation and detail sub-bands are evaluated using scaling and wavelet functions. The number of decomposition levels is selected based on the sampling frequency [119]. The decomposition levels for an ECG signal with sampling frequency of $F_s$ is given by

$$L = \log_2(F_s) - 2.96 \tag{2.4}$$

For an ECG signal $\mathbf{x}(n)$, the wavelet coefficients in the approximation and the $l^{\text{th}}$ detail sub-bands are evaluated as

$$cA_L(k) =< \mathbf{x}(n), \phi_{L,k}(n) > \tag{2.5}$$

$$cD_l(k) =< \mathbf{x}(n), \psi_{l,k}(n) > \tag{2.6}$$

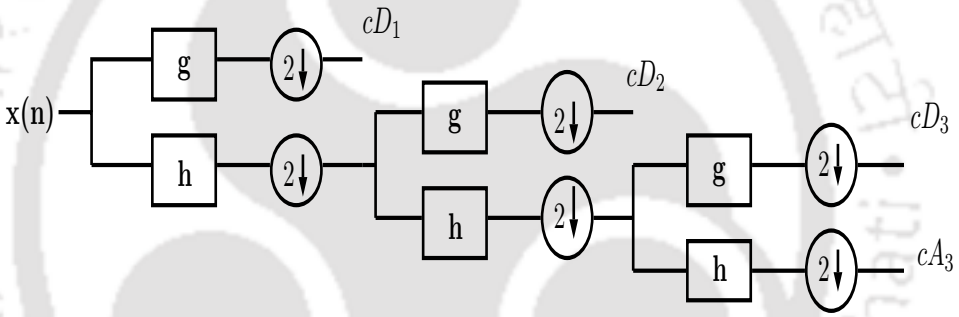


**Fig. 2.1:** Filter bank implementation of discrete wavelet transform.

where $cA_L(k)$ is the wavelet coefficients of the approximation sub-band or scale. The $cD_l(k)$ corresponds to the wavelet coefficients of the $l^{\text{th}}$ detail sub-band. The signal reconstructed from the wavelet coefficients is given as

$$\mathbf{x}(n) = \mathbf{x}_{A_L} + \sum_{l=1}^{L} \mathbf{x}_{D_l} \tag{2.7}$$

where $\mathbf{x}_{A_L}$ and $\mathbf{x}_{D_l}$ correspond to the reconstructed signals using approximation sub-band and $l^{th}$ detail sub-band wavelet coefficients. The approximation sub-band signal is given by

$$\mathbf{x}_{A_L}(n) = \sum_{k=-\infty}^{\infty} cA_L(k)\ \phi_{L,k}(n) \tag{2.8}$$

Similarly, the $l^{\text{th}}$ detail sub-band signal is evaluated as

$$\mathbf{x}_{D_l}(n) = \sum_{k=-\infty}^{\infty} cD_l(k)\ \psi_{l,k}(n) \tag{2.9}$$

In practice, the wavelet coefficients of the approximation sub-band and the detail sub-band are evaluated based on the filter-bank realization [120]. The filter bank implementation of DWT for an ECG signal with three decomposition levels is shown in Fig. 2.1. The '$\mathbf{g}$' and the '$\mathbf{h}$' are the impulse responses of high-pass and low-pass filters, respectively. The filter coefficients are chosen based on the type of mother wavelet. For ECG signal, the bi-orthogonal 6.8 low-pass and high-pass wavelet filters are typically used [121] [29].

### 2.3.2 Dual Tree Complex Wavelet Transform and ECG

The dual tree complex wavelet transform (DTCWT) uses two DWTs to produce complex wavelet coefficients of an ECG signal at different scales [122]. The first DWT evaluates the real part of the wavelet coefficients, whereas the imaginary part of the wavelet coefficients are computed using second DWT. The DTCWT has been used for various ECG processing applications such as the artifact detection and elimination from ECG, classification of cardiac abnormalities from ECG and removal of motion artifacts from photoplethysmographic (PPG) signals [122] [51] [123]. The DWT has the drawbacks such as the shift variant, the oscillatory characteristics of the wavelet coefficients and the aliasing effect of the wavelet coefficients [67]. The DTCWT has the properties such as the shift invariant, the non-oscillatory magnitude of the complex wavelet coefficients and the substantial reduction in the aliasing effect. The DTCWT provides phase information of the ECG signal in addition to the magnitude information. The complex wavelet coefficients at different scales are evaluated using the DTCWT of an ECG signal. The real part of the approximation sub-band and the $l^{\text{th}}$ detail sub-band wavelet coefficients for ECG signal are given by

$$\tilde{cA}_L(k) =< \mathbf{x}(n), \tilde{\phi}_{L,k}(n) > \tag{2.10}$$

$$\tilde{cD}_l(k) =< \mathbf{x}(n), \tilde{\psi}_{l,k}(n) > \tag{2.11}$$

where $l = 1, 2, 3, ..., L$ is the number of detail sub-bands. '$L$' is the decomposition levels of DTCWT. Similarly, the imaginary part of the approximation sub-band and the $l^{\text{th}}$ detail sub-band wavelet coefficients are evaluated as

$$\overline{cA}_L(k) =< \mathbf{x}(n), \overline{\phi}_{L,k}(n) > \tag{2.12}$$

$$\overline{cD}_l(k) =< \mathbf{x}(n), \overline{\psi}_{l,k}(n) > \tag{2.13}$$

where $\tilde{\phi}_{L,k}(n)$ and $\overline{\phi}_{L,k}(n)$ are the basis functions for evaluation of real and imaginary parts of approximation sub-band complex wavelet coefficients. The $\tilde{\psi}_{l,k}(n)$ and the $\overline{\psi}_{l,k}(n)$ are the basis functions for evaluation of real and imaginary parts of detail sub-band complex wavelet coefficients. The basis functions used to compute the real and the imaginary parts of the complex wavelet coefficients in different sub-bands are Hilbert pairs. The analytic form of the approximation sub-band and the $l^{\text{th}}$ detail sub-bands wavelet coefficients for ECG signal are defined by

$$cA_L(k) = \tilde{cA}_L(k) + j\ \overline{cA}_L(k) \tag{2.14}$$

$$cD_l(k) = \tilde{cD}_l(k) + j\ \overline{cD}_l(k) \tag{2.15}$$

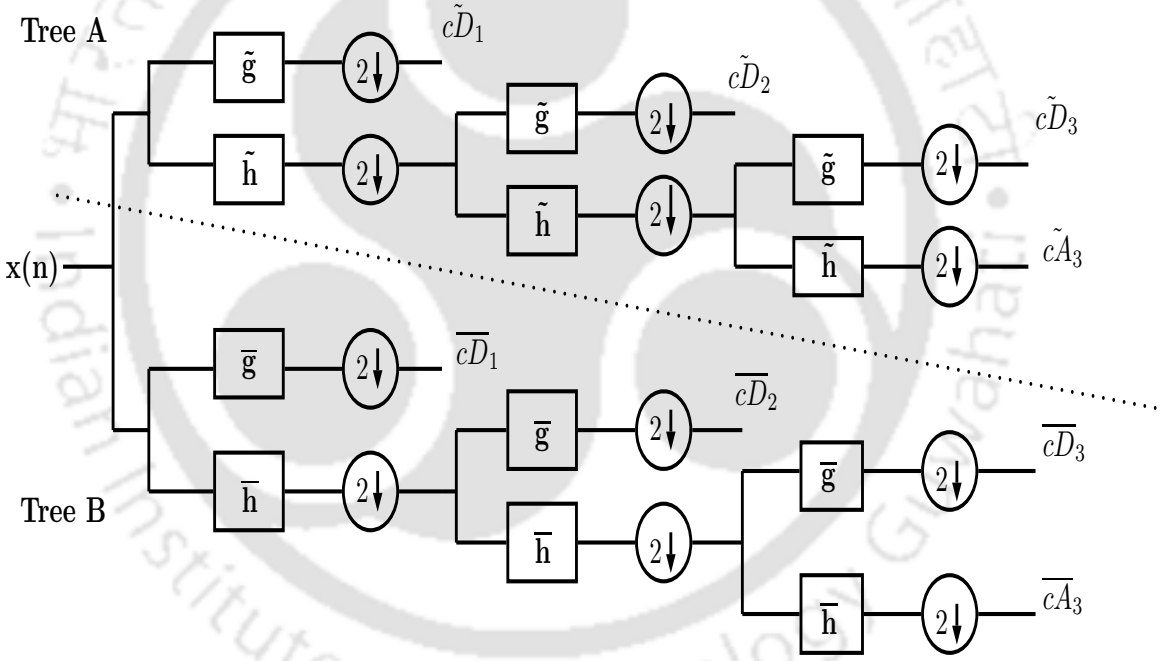


**Fig. 2.2:** Filter bank implementation of dual tree complex wavelet transform.

In practice, the complex wavelet coefficients of an ECG signal are evaluated based on a pair of filter banks. The three levels DTCWT based decomposition of an ECG signal, $\mathbf{x}(n)$ is shown in Fig. 2.2. The first filter bank (Tree A) generates the real wavelet coefficients. Similarly, the imaginary wavelet coefficients are obtained using second filter bank (Tree B). The impulse responses of the low-pass filters for tree A and tree B ($\tilde{\mathbf{h}}$ and $\overline{\mathbf{h}}$) are approximately Hilbert pairs and they are related as, $\overline{\mathbf{h}}(n) = \tilde{\mathbf{h}}(n - 0.5)$ [124]. Similarly, for tree A and tree B, the impulse responses for high pass filters ($\tilde{\mathbf{g}}$

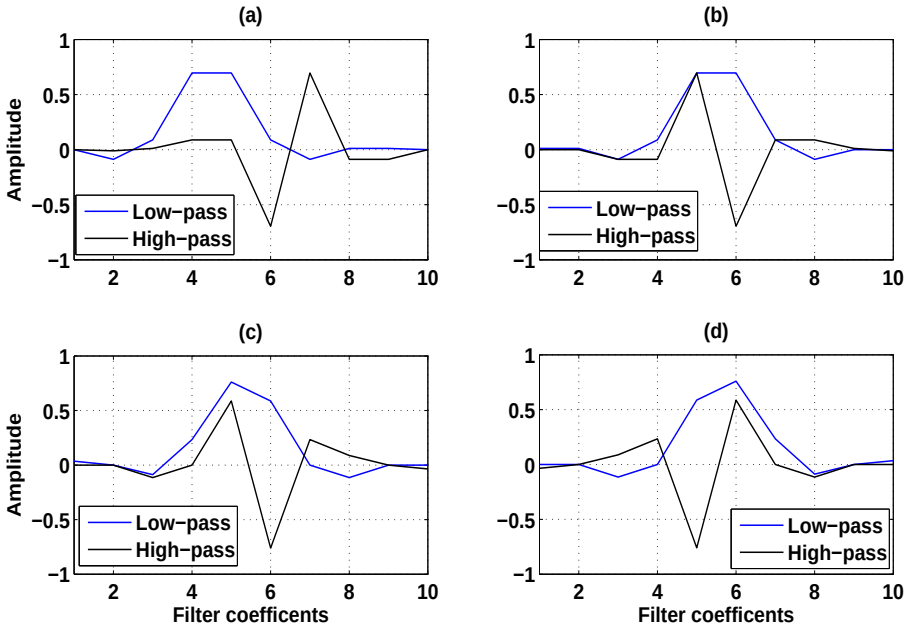


**Fig. 2.3:** (a) Impulse responses of low-pass and high-pass filters for tree A in level 1. (b) Impulse responses of low-pass and high-pass filters for tree B in level 1. (c) Impulse responses of low-pass and high-pass filters for tree A in other levels. (d) Impulse responses of low-pass and high-pass filters for tree B in other levels.

and $\overline{\mathbf{g}}$) are related by, $\overline{\mathbf{g}}(n) = \tilde{\mathbf{g}}(n-0.5)$. The filters for tree A and tree B are chosen based on the type of wavelet basis function. The selection of wavelet basis for ECG signal is a challenging task [125]. The bi-orthogonal wavelet basis has been used for DTCWT based analysis of ECG signal [122]. The morphology of QRS-complex of ECG signal is closely matched with bi-orthogonal basis function. For implementation of DTCWT of an ECG signal, two set of filters have been used. The first set of filters ($\tilde{\mathbf{g}}^1$, $\overline{\mathbf{g}}^1$, $\tilde{\mathbf{h}}^1$, $\overline{\mathbf{h}}^1$) are used in level 1, whereas for higher levels the second set of filters have been used [126] [51]. The impulse responses of the low-pass and the high-pass filters for tree A and tree B in first level and in other higher levels are shown in Fig. 2.3 (a)-(b) and Fig. 2.3 (c)-(d), respectively.

## 2.4 Variational Mode Decomposition and ECG

Variational mode decomposition (VMD) is a multi-resolution analysis technique to segregate the ECG signal into number of sub-signals or modes [68]. The VMD technique has been used for ECG de-noising and detection of various cardiac abnormalities from ECG. Lahmiri $et\ al.$ [28] have used VMD and DWT for denoising of ECG signal. From their study, it has been found that the combination of

VMD and DWT approach outperforms the EMD based method for denoising of ECG signal. Maji $et\ al.$ [69] have used VMD for detection and classification of ventricular flutter, rapid VT and atrial flutter. The center frequency, the maximum phase difference values of each mode of ECG are used as diagnostic features. The KNN classifier has been used to evaluate the performance of the center frequency, the maximum phase difference features of ECG. The VMD technique uses center frequency of each mode as prior for decomposition. The modes and the center frequencies for an ECG signal are extracted by solving the variational optimization problem [68]. The variational optimization problem for ECG signal is formulated in three steps. (i) The Hilbert transform is used to make each mode's frequency spectrum one sided or unilateral. (ii) Then, each mode frequency spectrum is shifted to base-band by a multiplying the factor $e^{-j\omega_t n}$, where $\omega_t$ is the center frequency of t$^{\text{th}}$ mode. (iii) The bandwidth of each mode is computed using the $L^2$-norm of the gradient of demodulated signal [68]. The original constrained optimization problem to evaluate number of modes and the center frequencies of an ECG signal, $\mathbf{x}(n)$ is given by

$$\min_{\{\mathbf{s}_t\},\{\omega_t\}} \left\{ \sum_{t=1}^{T} \left\| \frac{\partial}{\partial n} \left[ (\delta(n) + \frac{j}{\pi n}) * \mathbf{s}_t(n) \right] e^{-j\omega_t n} \right\|_2^2 \right\} \quad \text{subjected to} \sum_{t=1}^{T} \mathbf{s}_t(n) = \mathbf{x}(n) \tag{2.16}$$

where $\mathbf{s}_t(n)$ is a signal which corresponds to t$^{\text{th}}$ mode and $T$ is the total number of modes. The augmented Lagrangian ($\mathcal{L}$) is used for solving of the original constraint optimization problem. It is given by

$$\begin{aligned} \mathcal{L}(\{\mathbf{s}_t\},\{\omega_t\},\beta(n)) = \alpha \sum_{t=1}^{T} \left\| \frac{\partial}{\partial n} \left[ (\delta(n) + \frac{j}{\pi n}) * \mathbf{s}_t(n) \right] e^{-j\omega_t n} \right\|_2^2 \\ + \left\| \mathbf{x}(n) - \sum_{t=1}^{T} \mathbf{s}_t(n) \right\|_2^2 + \left\langle \beta(n), [\mathbf{x}(n) - \sum_{t=1}^{T} \mathbf{s}_t(n)] \right\rangle \end{aligned} \tag{2.17}$$

where, $\beta$ and $\alpha$ are the Lagrangian multiplier and the quadratic penalty factor, respectively. The modes and the center frequencies of the ECG signal are evaluated as

$$\begin{aligned} \tilde{\mathbf{s}}_t(n) = \underset{\{\mathbf{s}_t\}}{\text{argmin}} \left\{ \alpha \left\| \frac{\partial}{\partial n} \left[ (\delta(n) + \frac{j}{\pi n}) * \mathbf{s}_t(n) \right] e^{-j\omega_t n} \right\|_2^2 \right\} \\ + \left\| \mathbf{x}(n) - \sum_{t=1}^{T} \mathbf{s}_t(n) + \frac{\beta(n)}{2} \right\|_2^2 \end{aligned} \tag{2.18}$$

$$\tilde{\omega}_t = \underset{\{\omega_t\}}{\text{argmin}} \left\{ \left\| \frac{\partial}{\partial n} \left[ (\delta(n) + \frac{j}{\pi n}) * \mathbf{s}_t(n) \right] e^{-j\omega_t n} \right\|_2^2 \right\} \tag{2.19}$$

The equation 2.18 can be solved in spectral domain using Fourier isometry property and it is given by [68]

$$\begin{aligned} \tilde{\mathbf{s}}_t(\omega) = \underset{\{\mathbf{s}_t(w)\}}{\text{argmin}} \Big\{ \alpha \left\| j\omega \left[ (1 + sgn(\omega + \omega_t)) * \mathbf{s}_t(\omega + \omega_t) \right] \right\|_2^2 \Big\} \\ + \left\| \mathbf{x}(\omega) - \sum_{t=1}^{T} \mathbf{s}_t(\omega) + \frac{\beta(\omega)}{2} \right\|_2^2 \end{aligned} \tag{2.20}$$

The modes are obtained in an iterative manner by solving equation 2.20. The solution of equation 2.20 is given by

$$\tilde{\mathbf{s}}_{\tilde{t}}(\omega) = \frac{\mathbf{x}(\omega) - \sum_{t \neq \tilde{t}} \mathbf{s}_t(w) + \frac{\beta(\omega)}{2}}{1 + 2\alpha(\omega - \omega_{\tilde{t}})^2} \tag{2.21}$$

where, $\frac{1}{1+2\alpha(\omega-\omega_{\tilde{t}})^2}$ is the power spectrum prior for the residual signal, $\mathbf{x}(\omega) - \sum_{t \neq \tilde{t}} \mathbf{s}_t(w)$. The center frequency of each mode is updated as

$$\tilde{\omega}_t = \frac{\sum_w \omega \left| \mathbf{s}_t(w) \right|^2}{\sum_w \left| \mathbf{s}_t(w) \right|^2} \tag{2.22}$$

VMD uses several parameters to evaluate modes of an ECG signal. These parameters are the time-step of the dual ascent, the number of modes to be extracted ($T$), the balancing parameter of the data-fidelity constraint ($\alpha$), the tolerance of convergence criterion ($tol$), the initial Center frequencies ($\omega_t$) and the number of DC components [68]. In the following sections, the PCA, the HOS and the non-linear methods for analysis of ECG signal are briefly discussed.

## 2.5 Principal Component Analysis and ECG

Principal component analysis (PCA) is used as a dimension reduction technique in ECG processing applications [127]. The objective of PCA is to minimize the projection error and maximize the variance [44]. In the projected space, the first few principal components (PCs) capture significant diagnostic information. The first principal component (PC) provides the basis for direction of highest variability in data. Similarly, the second PC is orthogonal to the first PC and it provides the basis for direction of

next higher variability in data [45]. The PCA has been used for various ECG processing applications such as denoising, compression, feature extraction, quality assessment and dimension reduction [128], [129], [130], [43], [47]. The PCA can be used for single lead ECG and multilead ECG signals. The procedure for PCA of a multilead ECG data matrix ($\mathbf{X} \in R^{n \times m}$) is given below. The '$n$' and the '$m$' are the number of samples and the number of leads of multilead ECG.

(i) First, the covariance matrix is evaluated from the mean removed ECG data of each lead. This matrix is given as [131]

$$\mathbf{C} = \mathbf{X^T X} \tag{2.23}$$

(ii) The eigen matrix ($\mathbf{V}$) and the eigenvalue matrix, $\mathbf{\Lambda}$=$diag(\lambda_1, \lambda_2...., \lambda_n)$ are evaluated as

$$\mathbf{CV} = \mathbf{\Lambda V} \tag{2.24}$$

(iii) The eigenvectors in matrix $\mathbf{V}$ are sorted with respect to the descending order of the eigenvalues.

(iv) The projected data matrix evaluated using the PCA of multilead ECG is given by

$$\mathbf{Y} = \mathbf{XV} \tag{2.25}$$

The diagnostic information is captured using few PCs of multilead ECG. Selection of PCs of multilead ECG for measuring the diagnostic information is a challenging task. The method reported in [43] have used entropy ratio for selection of diagnostic relevant PCs of multilead ECG. The entropy ratio is evaluated using the probabilities of the eigenvalues of covariance matrix. Romero $et\ al.$ [55] have studied the depolarization changes in QRS-complex during acute myocardial ischemia. They have evaluated QRS-slope features from the first three PCs of multilead ECG. These slope features have been used for localization of MI. Tripathy $et\ al.$ [131] have proposed a method for detection of various cardiac ailments from multilead ECG. This method is based on the evaluation of principal component multivariate multiscale sample entropy (PMMSE) features of multilead ECG. The PCA has been used to reduce the dimension of multilead ECG. The multivariate multiscale sample entropy (MMSE) is evaluated over the projected matrix of multilead ECG. The PMMSE features and the least square-SVM classifier have been used for detection and classification of cardiac dysrhythmia, HMD and MI. Sharma $et\ al.$ [25] have used multiscale PCA for compression of multilead ECG data. The approximation sub-band and the detail sub-band wavelet coefficients of each ECG lead are eval-

uated using DWT. The sub-band matrices of multilead ECG have been formulated using the wavelet coefficients of each lead at different scales. The PCA has been applied to the sub-band matrices and the selected PCs are quantized and Huffman encoded for compression. Kalpana $et\ al.$ [132] have used PCA for detection of R-peaks in multilead ECG. The other morphological features of multilead ECG have been evaluated based of the detected R-peaks and the window based technique. These morphological features of multilead ECG are used for detection of diabetes.

The PCA of single lead ECG ($\mathbf{x} \in R^n$) is performed based on the evaluation of the covariance matrix. The covariance matrix is computed as, $\mathbf{C} = \mathbf{x}\mathbf{x}^\mathbf{T}$. The transformed domain signal (projected data) is obtained using the product of the eigen matrix ($\mathbf{V}$) of '$\mathbf{C}$' with the single lead ECG signal and it is given by $\mathbf{y} = \mathbf{x}\mathbf{V}$. Langley $et\ al.$ [133] have used PCA for analysis of beat-to-beat changes in ECG during respiration. The clinical components such as the P-wave, the QRS-complex and the T-wave of each ECG beat are segmented using R-peak detection and window based technique. The PCs of the P-wave, the QRS-complex and the T-wave are analyzed during respiration. Martis $et\ al.$ [59] have used discrete cosine transform (DCT) and PCA for classification of non-ectopic beats, SVEB, VEB and fusion beats from ECG. The DCT has been applied to the ECG beats and the coefficients are used as features. The PCA has been used to reduce the dimension of ECG feature vector (the DCT coefficients). The first twelve PCs are selected for classification.

## 2.6 Higher Order Spectra and ECG

Higher order spectra (HOS) are the spectral representation of the higher order moments of a signal [134]. The higher order spectral features of ECG has been used for detection of various cardiac ailments [57]. Martis $et\ al.$ [57] have used HOS features of ECG and least square SVM for classification of right BBB, left BBB, PVC and APC and NSR. The classification of atrial arrhythmia using the HOS of ECG has been proposed in [135]. The bi-spectrum of ECG signal is evaluated. The ICA has been used to reduce the dimension of the HOS feature vector of ECG. The classification and regression tree (CART) and the KNN classifier have been used for detection of atrial arrhythmia. Chua $et\ al.$ [136] have used higher order spectral features of ECG and SVM for classification of various cardiac ailments such as congestive heart failure, sick sinus syndrome, complete heart block and PVC. Khadra $et\ al.$ [137] have used higher order spectral features of ECG and threshold based classifier for

classification of supra-ventricular and ventricular tachyarrhythmia. Arief $et\ al.$ [138] have used linear and nonlinear features of ECG signal for classification of cardiac ailments. The non-linear features are evaluated using the HOS of ECG. The linear features of ECG is evaluated using PCA. The neural network has been used to classify the linear and the nonlinear features of ECG into SVEB, VEB, fusion beats and non-ectopic beats. The HOS measures the deviation from the Gaussianity, the phase correlation, the magnitude correlation and the non-linearity of an ECG [139]. The third order and the fourth order spectra are called as bi-spectrum and tri-spectrum, respectively. The bi-spectrum of an ECG signal is evaluated using the Fourier transform of the third order correlation [135]. Similarly, the tri-spectrum is defined as the Fourier transform of the fourth order correlation. The bi-spectrum and the tri-spectrum of an ECG signal, $\mathbf{x}(n)$ are given as

$$\mathbf{B}(f1, f2) = E[\mathbf{y}(f1)\mathbf{y}(f2)\mathbf{y}^*(f1 + f2)] \tag{2.26}$$

$$\mathbf{B}(f1, f2, f3) = E[\mathbf{y}(f1)\mathbf{y}(f2)\mathbf{y}^*(f3)\mathbf{y}^*(f1 + f2 + f3)] \tag{2.27}$$

where $\mathbf{y}(f)$ is the Fourier transform of the ECG signal, $\mathbf{x}(n)$ and $0 \leq f3 \leq f2 \leq f1 \leq f1 + f2 \leq 1$.

## 2.7 Non-linear Analysis and ECG

Non-linear analysis is widely used in biomedical signals to quantify irregularity and extract hidden information [140]. The non-linear features provide good performance during noisy conditions. The non-linear feature extraction methods such as fractal dimension (FD), Hurst exponent (HE), Lyapunov exponent (LE), detrend fluctuation analysis (DFA), correlation dimension (CD), approximate entropy (AE), sample entropy (SE), permutation entropy (PE), renyi entropy, recurrent quantification analysis (RQA) have been used for biomedical signals [37]. In ECG, the characteristics of P-wave, QRS-complex and T-wave are different during cardiac arrhythmia. The non-linear features are effective to capture these pathological variations [140] [141]. In recent years, number of methods have been proposed for detection of cardiac ailments using non-linear features of ECG and heart rate signals. Acharya $et\ al.$ [140] have used Poincare plot, RQA, SE, DFA, CD and EMD methods to evaluate features from heart rate signal. These non-linear features have been used for analysis of heart rate signals of normal and coronary artery disease (CAD) affected patients. Ubeyli $et\ al.$ [142] have used LE to evaluate diagnostic features from ECG signal. The LE based non-linear features and the adap-

tive neuro-fuzzy inference system (ANFIS) model have been used for classification of normal beat, congestive heart failure beat, ventricular tachyarrhythmia beat and atrial fibrillation beat from ECG. Acharya $et\ al.$ [54] have evaluated nonlinear features such as HE, DFA, AE, SE and CD from the wavelet coefficients of RR-time series. These non-linear features of the approximation sub-band and the detail sub-band, and SVM classifier have been used for prediction of sudden cardiac death. Owis $et\ al.$ [143] have used non-linear dynamical modeling of ECG for detection of ventricular arrhythmia episodes. The CD and the LE features are evaluated from ECG signal. The KNN classifier has been used to classify the nonlinear features of ECG into NSR and ventricular cardiac ailments such as ventricular couplet (VC), VT, VF and ventricular bigeminy (VB), respectively. Acharya $et\ al.$ [141] have evaluated FD features from HR signal. The FD features are evaluated using Higuchi's algorithm and Katz's algorithm. The FD features have been analyzed for NSR, PVC, atrial fibrillation, complete heart block and myocardial ischemia pathologies. Watanabe $et\ al.$ [144] have used multiscale sample entropy features of HR signal for prediction of ischemic stroke in patients with permanent atrial fibrillation. The multiscale sample entropy of the heart rate signal is found to be an effective diagnostic feature for analysis of permanent atrial fibrillation episodes. In [145], the SE features have been used to quantify irregularity or complexity of ECG signal. The threshold based classifier has been used to classify SE features of ECG into rapid VT and VF episodes. Chetan $et\ al.$ [146] have evaluated DFA and SE measures over the sub-band signals of multilead ECG. The neural network classifiers have been used for detection of MI and HMD from the non-linear features of multilead ECG. Taha $et\ al.$ [147] have evaluated spectral entropy features from the atrial activity signal. This atrial activity signal is derived from ECG using QRS-complex cancelation approach. The spectral entropy features and the threshold criteria have been used to classify atrial flutter, atrial fibrillation and other cardiac diseases. The permutation entropy (PE) is widely used to quantify irregularity or randomness of a physiological time-series data [148]. The higher value of PE indicates that the time series is irregular or more random. The PE of an ECG signal, $\mathbf{x}(n) = [x(1), x(2), ...., x(N)]$, $i = 1, 2..., N$ is evaluated using the embedding vector and the lag value. The embedding vector is evaluated as

$$\tilde{\mathbf{y}}(kk) = [x(kk), x(kk + \bar{l}), ....., x(kk + \bar{l} * (\bar{d} - 1))] \tag{2.28}$$

where $1 \leqslant kk \leqslant (N - \bar{l} * (\bar{d} - 1))$. $\bar{d}$ and $\bar{l}$ are the embedding dimension and the lag, respectively. For the embedding vector $\tilde{\mathbf{y}}(kk)$, a permutation pattern $\pi = (c_0, c_1, ..., c_{\bar{d}-1})$ is linked with respect to the following condition as

$$[x(kk + c_0) \leqslant x(kk + c_1), ....., \leqslant x(kk + c_{\bar{d}-2}) \leqslant x(kk + c_{\bar{d}-1})] \tag{2.29}$$

A probability distribution $P$, which consists of $\pi(i)$, $i = 1, 2, ...., \bar{d}!$ number of elements are considered as the $i^{\text{th}}$ permutation pattern [148]. The PE is given by

$$PE = -\sum_{i=1}^{\bar{d}!} \pi(i) log_2 \pi(i) \tag{2.30}$$

Taherkhani $et\ al.$ [149] have used PE to investigate the beat-by-beat fluctuations in the heart rates for congestive heart failure patients and HC. From their study, it has been found that the PE has a higher value for heart failure patients as compared to HC. The following sections briefly discuss different feature selection methods and the classifiers which have been used in ADS for choosing relevant diagnostic information and classification of cardiac abnormalities.

## 2.8 Feature Selection Methods

Feature selection is widely used in ADS for choosing relevant attributes from the high dimensional feature vector and reducing the computational complexity of classifier [150] [151]. In ECG, the diagnostic information is effectively captured based on the proper selection of features. Two kinds of feature selection methods are used in ADS for detection of cardiac abnormalities. These are filter based feature selection and wrapper based feature selection methods [152] [153]. In filter based feature selection, the features are ranked based on some statistical measure [154] [155]. The features which have higher rank are chosen for classification. The examples of filter based feature selection methods are correlation coefficient score, information gain, statistical dependency and Chi-square test [156] [155] [157]. The wrapper based feature selection divides the entire feature vector into feature subsets [107]. The classifier is used to evaluate the performance of each of the feature subset. Based on the performance of classifier, a score is assigned to the corresponding feature subset. The feature subset which has higher score are selected for classification. The genetic algorithm, the particle swarm optimization and the best-first search are the examples of wrapper based feature

selected methods [158]. The feature matrix ($\mathbf{Z} \in R^{p \times q}$) consists of '$p$' number of ECG instances and '$q$' number of diagnostic features. The feature vector for $i^{\text{th}}$ ECG instance is given by $\mathbf{z}_i \in R^q$. where $i = 1, 2, .., p$. The feature selection technique involves selection of few attributes from the '$q$' dimensional feature vector. The wrapper based methods require high computations than filter based techniques for feature selection. Therefore, the filter based feature selection methods have been widely used in ADS for detection of cardiac abnormalities [159]. In the following subsections, three different filter based feature selection methods (correlation based feature selection, mutual information based feature selection and symmetrical uncertainty) are briefly discussed.

### 2.8.1 Correlation based Feature Selection

The correlation based feature selection (CFS) is a simple method for evaluation of feature subset from the diagnostic feature vector of ECG. The CFS has been used as feature selection method for classification of sleep stages from ECG signal [156]. Mitra $et\ al.$ [160] have used CFS and ANN classifier for classification of various cardiac abnormalities from the diagnostic features of ECG. The CFS method uses the correlation between the feature and the class label, and the feature to feature inter-correlation for selecting few attributes from a high dimensional feature vector [161]. In CFS, the score of the feature subset is evaluated as

$$Score_A = \frac{\tilde{q}\,\overline{r}_{CF}}{\tilde{q} + (\tilde{q} - 1)\overline{r}_{FF}} \tag{2.31}$$

Where $Score_A$ is the score of the feature subset '$A$'. This feature subset contains $\tilde{q}$ number of attributes and $\tilde{q} < q$. $\overline{r}_{CF}$ and $\overline{r}_{FF}$ are the mean feature-class correlation and the mean feature-feature inter-correlation, respectively. The feature subsets which have higher correlation coefficient are eliminated from the $q$ dimensional feature vector. The new feature vector contains the attributes which have less feature to feature inter-correlation.

### 2.8.2 Mutual Information based Feature Selection

This feature selection approach is based on the evaluation of a score for each attribute in the feature vector of ECG. The score is computed using the marginal probability density function (PDF) of ECG feature instance vector, the marginal PDF of class label vector, and the joint PDF of class label vector

and feature instance vector, respectively [161] [154]. Doquire $et\ al.$ [155] have used morphological features and HOS features of ECG, and SVM classifier for classification of SVEB, VEB, normal beat and fusion beat. The mutual information based feature selection has been used for selection of relevant features. The mutual information score is the modification of statistical dependency (SD) sore for $d^{\text{th}}$ feature instance vector. The SD score of $d^{\text{th}}$ diagnostic feature of ECG is given by

$$SD^d = \sum_{\mathbf{z}^d} \sum_{\mathbf{y}} P(\mathbf{z}^d, \mathbf{y}) \frac{P(\mathbf{z}^d, \mathbf{y})}{P(\mathbf{y})P(\mathbf{z}^d)} \tag{2.32}$$

The mutual information score or information gain (IG) of $d^{\text{th}}$ attribute, $d = 1, 2, .., q$) in a '$q$' dimensional feature vector of ECG is given by

$$IG^d = \sum_{\mathbf{Z}^d} \sum_{\mathbf{y}} P(\mathbf{Z}^d, \mathbf{y}) log_2 \frac{P(\mathbf{Z}^d, \mathbf{y})}{P(\mathbf{Z}^d)P(\mathbf{y})} \tag{2.33}$$

where $P(\mathbf{Z}^d)$ and $P(\mathbf{y}_b)$ are the PDF of $d^{\text{th}}$ feature instance vector and the PDF of class label vector, respectively. $P(\mathbf{Z}_b^d, \mathbf{y}_b)$ is the joint occurrence frequencies of the $d^{\text{th}}$ feature instance vector and the output class label vector at a given lag. The PDF of feature instance vector is evaluated in two steps. First, the feature instance vector is quantized with a quantization label, Q=10. Then, the histogram or PDF is evaluated from the quantized feature instance vector. Similarly, the PDF of the class instance vector is evaluated using the probability of each class. For each attribute, the mutual information score is evaluated. The attribute having higher value of mutual information score is retained and other attributes are eliminated from the '$q$' dimensional feature vector.

### 2.8.3 Symmetrical Uncertainty based Feature Selection

The symmetrical uncertainty (SU) method uses the marginal entropy of the feature instance vector, the marginal entropy of the class label vector and the IG for selection of relevant features from a '$q$' dimensional feature vector [161]. Sasikala $et\ al.$ [157] have used SU based feature selection approach and various machine learning techniques for classification of biomedical datasets. The SU score of $d^{\text{th}}$ feature in a '$q$' dimensional feature vector is given as,

$$SU^d = \frac{2 \times IG^d}{H_{\mathbf{Z}^d} + H_{\mathbf{y}}} \tag{2.34}$$

where, $H_{\mathbf{Z}^d}$, $H_{\mathbf{y}}$ and $IG^d$ are the marginal entropy of $d^{\text{th}}$ feature instance vector, the marginal entropy of class label vector and the mutual information score. The IG of $i^{\text{th}}$ feature instance vector is evaluated using equation 2.33. The marginal entropy values of $d^{\text{th}}$ feature instance vector and the class label vector are evaluated as [161]

$$H_{\mathbf{Z}^d} = -\sum_{\mathbf{Z}^d} P(\mathbf{Z}^d) log_2 P(\mathbf{Z}^d) \tag{2.35}$$

$$H_{\mathbf{y}} = -\sum_{\mathbf{y}} P(\mathbf{y}) log_2 P(\mathbf{y}) \tag{2.36}$$

The features which have higher value of SU score are selected for classification. The new feature vector evaluated using SU based feature selection is used as input to the classifiers. The following section discusses a review on various classifiers for detection of cardiac abnormalities from the diagnostic features of ECG.

## 2.9 Classifiers and Performance Measures

The final stage of ADS is the classification of cardiac ailments from the diagnostic feature vector of ECG instance. In this stage, both supervised and unsupervised learning techniques are used. In this section, four supervised learning methods such as KNN, SVM, RF and ELM classifiers for detection of cardiac abnormalities from ECG features are briefly described. These classifiers have been used for detection of MI, shockable ventricular arrhythmia, BBB and HMD [49], [162] [20], [19], [163], [39]. The training and the test instances of these classifier are evaluated using hold-out cross validation and K-fold cross validation methods. The hold-out cross-validation method divides the feature matrix into training set and test set [44] [162]. In training phase, the parameters of the classifier are evaluated. The validation set is used to tune the model parameters [44]. The test data is evaluated using the optimal parameters of the training model. In K-fold cross-validation method, the feature matrix is divided into '$i$' number of subsets, $i = 1, 2...\tilde{K}$ ($\tilde{K}$ is number of folds) and the hold-out cross validation is repeated for '$i$' times [20]. Each time, the $i^{\text{th}}$ sub-set is used for testing and the remaining $i-1$ subsets of data are used for training of classifier. The overall performance of classifier has been evaluated based on the average of the accuracy values of folds.

### 2.9.1 K-nearest Neighbor Classifiers

K-nearest neighbor (KNN) is a simple classifier and it has been used for detection of cardiac ailments such as MI, shockable ventricular arrhythmia and atrial arrhythmia from ECG features [36] [164] [165]. The number of neighbors of a test ECG feature instance for KNN classifier is selected based on various distance measure [45]. For training of KNN classifier, the ECG feature instances are given by, $\mathbf{z}_1, \mathbf{z}_2, ...., \mathbf{z}_p$. where each $\mathbf{z}_i \in R^q$ and '$q$' is the number of diagnostic features. The class label of the $i^{\text{th}}$ ECG feature instance is given by, $y_i$. The test ECG feature instance is denoted as, $\mathbf{z}_{te}$. Three types of distance measures have been used for KNN classifier. These are Euclidean, Manhattan and Minkowski distances [22]. In KNN, the distances between the test ECG feature instance and all the training instances are evaluated. The Euclidean distance measure is given by

$$dist_i = \|\mathbf{z}_i - \mathbf{z}_{te}\|_2 \tag{2.37}$$

Similarly, the Manhattan distance metric is defined as

$$dist_i = \|\mathbf{z}_i - \mathbf{z}_{te}\|_1 \tag{2.38}$$

Likewise, the Minkowski distance measure is given as

$$dist_i = \|\mathbf{z}_i - \mathbf{z}_{te}\|_q \tag{2.39}$$

The distances of the required test ECG instance are arranged in ascending order. The $\tilde{k}$ number of minimum distances are selected for the require test instance. The training parameters of KNN classifier are the number of nearest neighbor ($\tilde{k}$) and the distance metric. Typically, the value of $\tilde{k}$ is selected from $3$ to $10$ [44]. The value of $\tilde{k}$ is evaluated using cross-validation method. The class labels of the test ECG instance in KNN classifier is obtained as the majority voting of the class labels of the $\tilde{k}$ nearest instances. The KNN classifier gives equal importance to the class labels of nearest neighbors for deciding the output of a test instance. The fuzzy KNN is the modifications of KNN classifier and it uses the membership to the output of each class [166]. The fuzzy KNN classifier has been used for detection of BBB and ventricular arrhythmia from ECG [162] [167].

### 2.9.2 Support Vector Machine Classifier

Support vector machine (SVM) is a binary classifier and it is based on the maximization of margin between two classes [168]. This classifier has been used for detection of various cardiac ailments from the diagnostic features of ECG signal [163]. Li $et\ al.$ [20] have used SVM classifier for detection of shockable ventricular arrhythmia from the diagnostic features of ECG. Atienza $et\ al.$ [107] have used SVM and feature selection methods for detection of life threatening ventricular arrhythmia from ECG. Tripathy $et\ al.$ [131] have used least square SVM for classification of HMD, MI and dysrhythmia pathologies. The objective of SVM is to find the decision boundary for which the margin between the two classes is maximized. The multiclass classification of cardiac ailments in SVM is based on various coding algorithms [169]. These are 'One vs One' and 'One vs All' [170]. The 'One vs One' and the 'One vs All' algorithms for multiclass classification create number of binary SVMs for the training data. The overall performance of multiclass SVM classifier is based on the majority voting or the maximum values of the class labels of the binary SVM classifiers for the test data. The formulation of SVM for a binary class is based on the primal-dual optimization problem [168]. The primal optimization problem of SVM for non-linear and non-separable data is given by

$$\begin{gathered}\mathbf{J}_{Primal} = \underset{\{\mathbf{w}\}}{\text{minimize}}\ \frac{\|\mathbf{w}\|^2}{2} + C\sum_{i=1}^{p}\epsilon_i \\ \text{subjected to}\ \ y_i(\mathbf{w}^T\phi(\mathbf{z}_i)+b) \geq 1-\epsilon_i, \epsilon_i \geq 0\end{gathered} \tag{2.40}$$

where $\epsilon_i$ is the error of the $i^{\text{th}}$ training ECG feature instance and, $i = 1, 2...p$. '$\mathbf{w}$' is the normal vector to the hyperplane. The $\mathbf{w}^T\phi(\mathbf{z}_i)+b) \geq 1$ and the $\mathbf{w}^T\phi(\mathbf{z}_i)+b) \leq -1$ are the hyperplanes for positive class (arrhythmia class) and negative class (HC class), respectively. The dual optimization problem of SVM is obtained using Lagrangian and it is given by [170]

$$\mathcal{L}(\mathbf{w}, b, \epsilon, \alpha, \beta) = \mathbf{J}_{primal} - \sum_{i=1}^{p}\alpha_i[y_i(\mathbf{w}^T\phi(\mathbf{z}_i)+b) - 1 + \epsilon_i] - \sum_{i=1}^{p}\beta_i\epsilon_i \tag{2.41}$$

where $\alpha_i > 0$ and $\beta_i > 0$ are the Lagrangian multipliers for $i^{\text{th}}$ training instance. The solution of equation 2.41 is obtained by the saddle point of Lagrangian as, $\max\limits_{\{\alpha,\beta\}}\ \min\limits_{\{\mathbf{w},b,\epsilon\}} \mathcal{L}(\mathbf{w}, b, \epsilon; \alpha, \beta)$. The dual

optimization problem of SVM is evaluated as

$$\mathbf{J}_{Dual} = \max_{\{\alpha\}} \sum_{i=1}^{p} \alpha_i - \frac{1}{2} \sum_{i=1}^{p} \sum_{r=1}^{p} \alpha_i \alpha_r y_i y_r K(\mathbf{z}_i, \mathbf{z}_r)$$
$$\text{such that } \sum_{i=1}^{p} \alpha_i y_i = 0 \tag{2.42}$$
$$0 \leq \alpha_i \leq C, i = 1, 2, ...., p$$

where $K(\mathbf{z}_i, \mathbf{z}_r)$ is the kernel function which maps the input feature vector into a higher dimensional space [171]. Various kernel functions are used for SVM. These are linear kernel, polynomial kernel and radial basis function (RBF) kernel, respectively. The linear kernel is given by

$$K(\mathbf{z}_i, \mathbf{z}_r) = \mathbf{z}_i^T \mathbf{z}_r \tag{2.43}$$

Similarly, the polynomial kernel is given as

$$K(\mathbf{z}_i, \mathbf{z}_r) = (1 + \mathbf{z}_i^T \mathbf{z}_r)^c \tag{2.44}$$

where $c$ is the degree of polynomial kernel. The RBF kernel is given by

$$K(\mathbf{z}_i, \mathbf{z}_r) = exp(\frac{- \|\mathbf{z}_i - \mathbf{z}_r\|_2^2}{\sigma^2}) \tag{2.45}$$

where $\sigma$ is the standard deviation of RBF kernel. The output of SVM for a test instance $\mathbf{z}_{te}$ is evaluated as

$$y_{te} = sign[\sum_{i=1}^{\neq SV} \alpha_i y_i K(\mathbf{z}_i, \mathbf{z}_{te}) + b] \tag{2.46}$$

where '$\neq SV$' is the number of support vectors of SVM. The training parameters of SVM classifier are the regularization term ($C$), the degree of polynomial kernel ($c$) and the standard deviation or width of Gaussian kernel ($\sigma$). In SVM, the parameter $C$ is used to maintain the trade-off between bias and variance [171]. A large value of $C$ corresponds to the model with low bias and higher variance, which can cause data over fitting. A small value of $C$ corresponds to the model with high bias and low variance, which causes data under fitting. The values of $C$ and $\sigma$ are selected from the validation set using grid-search [170]. The SVM classifier has several advantages for classification of cardiac ailments from ECG features. It uses kernel tricks to find the decision boundary for non-linear and non-separable data (ECG feature instance). Higher computation is required by transforming the

input ECG feature instance into a higher dimensional space. The kernel tricks help in computing the similarity score or dot product in original ECG feature space, without explicitly going in higher dimensional space [170]. If the regularization parameter is properly selected, the SVM classifier will have better performance for classification of cardiac ailments. The optimization problem in SVM is convex, so this classifier deliver a unique solution for evaluation of training parameters.

### 2.9.3 Random Forest Classifier

The random forest (RF) classifier consists of ensemble of trees in which the class label of a test instance is determined based on the individual decision [45]. This classifier has been used for detection of various cardiac abnormalities from the ECG features [172]. Rahman $et\ al.$ [39] have used RF classifier for detection of hypertrophic cardiomyopathy from the morphological features of ECG. The RF classifier has also been used for classification of ventricular ectopic beats, BBB from the features of ECG [173]. For training of RF classifier, the ECG feature matrix, $\mathbf{Z} \in R^{p \times q}$ is divided into $L$ number of sub datasets such as $\mathbf{Z}_1, \mathbf{Z}_2, \mathbf{Z}_3, ...., \mathbf{Z}_L$. The corresponding class label vectors for the sub-datasets are $\mathbf{y}_1, \mathbf{y}_2, \mathbf{y}_3, ...., \mathbf{y}_L$, respectively. The instances of the $L^{\text{th}}$ sub-dataset are randomly chosen from '$p$' number instances of the training feature matrix ($\mathbf{Z}$). For each sub dataset, one decision tree model is trained. The information gain measure is used to determine the split node of each decision tree [174]. The information gain measure is evaluated using the entropy impurity. The entropy impurity of the sub dataset ($\mathbf{Z}_L$) with class label vector ($\mathbf{y}_L$) is given by

$$Entropy(\mathbf{Z}_L) = -\sum_{i=1}^{\tilde{C}} P_i log_2 P_i \tag{2.47}$$

where, $P_i$ is the proportion of sub-dataset ($\mathbf{Z}_L$) belongs to class label $i$. where $i = 1, 2..., \tilde{C}$ and $\tilde{C}$ is the total number of classes. The information gain measure is given as

$$Gain(\mathbf{Z}_L, A) = Entropy(\mathbf{Z}_L) - \sum_{v \in A} \frac{|(\mathbf{Z}_L)_v|}{|\mathbf{Z}_L|} Entropy(\mathbf{Z}_L)_v \tag{2.48}$$

$(\mathbf{Z}_L)_v$ is the subset of $\mathbf{Z}_L$ for which the feature has a value '$v$'. The attribute having high information gain is selected for splitting. The splitting of the continuous valued attribute is based on a threshold value [44]. To select the threshold, the attributes are sorted in an increasing order. The threshold is obtained as the maximum information gain of the attribute. The splitting procedure is repeated until

the leaf node contain only class labels. The ECG test feature instance is evaluated over each of the decision trees. The class label of the test data is obtained as the majority voting of the decision tree outputs. The tuning parameters of RF classifier are the number of trees, the depth of each tree and the number of splits. The RF classifier has the advantage that, the error rate converges to certain value with increase in the number of trees [173]. The validation set is not required in RF classifier for evaluation of optimal training parameters.

### 2.9.4 Extreme learning Machine Classifier

Extreme learning machine (ELM) is a three layer feed forward network and it consists of input neurons, hidden neurons and output neurons [175]. The ELM classifier has been used for classification of cardiac arrhythmia from ECG [176] [163]. Kim $et\ al.$ [176] have used ELM for classification of right BBB, left BBB, PVC and APC beats from the diagnostic features of ECG. Karpagachelvi $et\ al.$ [163] have used ELM for classification of cardiac abnormalities such as VT, VF, left BBB, right BBB, PVC and APC from ECG features. For classification of cardiac ailments using ELM classifier, the weight and the bias values are randomly assigned at hidden layer. The weight value of the output layer $\tilde{W}$ is evaluated by solving the least square regularization problem and it is given by [177]

$$\underset{\tilde{W}\in R^{L\times r}}{\text{minimize}} \quad \frac{1}{2}\gamma \left\| F\tilde{W} - Y \right\|^2 + \frac{1}{2}\left\| \tilde{W} \right\|^2 \tag{2.49}$$

where, $Y \in R^{p\times r}$ and $\tilde{Y} \in R^{p\times r}$ are the actual output and the predicted output of ELM model. '$\gamma$' is the regularization parameter. The $\mathbf{F}$ corresponds to the hidden layer matrix of ELM. This matrix is given as

$$\mathbf{F} = \begin{bmatrix} f(\mathbf{w}_1, b_1, \mathbf{z}_1) & \cdots & f(\mathbf{w}_h, b_h, \mathbf{z}_1) \\ \vdots & \ddots & \vdots \\ f(\mathbf{w}_1, b_1, \mathbf{z}_p) & \cdots & f(\mathbf{w}_h, b_h, \mathbf{z}_p) \end{bmatrix}_{p\times h} \tag{2.50}$$

where '$\mathbf{w}_h$' is the weight vector of $h^{\text{th}}$ hidden neuron or mapping unit and '$b_h$' corresponds to the bias value. The $f(\mathbf{w}_h, b_h, \mathbf{z}_p)$ is the non-linear mapping or activation function. This activation function maps the input feature vector $\mathbf{z}_p$ to a new h-dimensional space (ELM feature space). Three activation functions such as 'sigmoid', 'Gaussian' and 'sine' are used [177]. These activation functions are given

as

$$f(\mathbf{w}_h, b_h, \mathbf{z}_p) = \frac{1}{1 + exp(-(\mathbf{w}_h.\mathbf{z}_p + b))} \tag{2.51}$$

$$f(\mathbf{w}_h, b_h, \mathbf{z}_p) = exp(-b \left\| \mathbf{w}_h - \mathbf{z}_p \right\|) \tag{2.52}$$

$$f(\mathbf{w}_h, b_h, \mathbf{z}_p) = sin(\mathbf{w}_h.\mathbf{z}_p + b) \tag{2.53}$$

The output weight matrix evaluated from equation 2.49 is given by

$$\tilde{W} = \mathbf{F}^T(\frac{I}{\gamma} + \mathbf{F}\mathbf{F}^T)^{-1}Y \tag{2.54}$$

The predicted output of ELM classifier is given by

$$\tilde{\mathbf{y}} = \mathbf{F}\tilde{W} \tag{2.55}$$

where $I$ is the identity matrix. $\tilde{W} \in R^{h \times r}$ is the weight between the hidden layer and the output layer of ELM network. The values of '$h$' and '$r$' correspond to the number of hidden layer neurons and the number of output neurons, respectively. The value of $\gamma$ varies from 0.1 to 1.0 [177]. The training parameters of ELM classifier are the activation function, the regularization parameters and the number of hidden layer neurons. The ELM has the advantage over other classifiers that it requires less computation for evaluation of training parameters.

### 2.9.5 Performance Measures of Classifier

The performance of classifier for detection of cardiac ailments is evaluated using various metrics such as accuracy, sensitivity, specificity and area under receiver operating characteristics (ROC) curve [44] [45]. For two class classification task (HC and cardiac ailment), the area under ROC (AROC) curve, the sensitivity, the specificity and the accuracy values are used. These performance measures are evaluated using the confusion matrix. This matrix is evaluated using the actual outputs of the test ECG feature instances and the predicted outputs. The confusion matrix for a binary classifier is shown in Table 2.2.

The TP, the TN, the FP and the FN are number of true positives, number of true negatives, number of false positives and number of false negatives, respectively [22]. True positives (TP) are the number of positive decisions (cardiac ailments or abnormal) that are predicted from the total number of ECG

**Table 2.2:** Confusion Matrix of binary Classifier.

| **Actual Output** | **Predicted Output** | |
|---|---|---|
| | Abnormal | Normal |
| Abnormal | TP | FP |
| Normal | FN | TN |

feature instances. True negatives (TN) are the number of negative decisions (HC or normal) that are predicted from the total number of ECG instances. The false positives (FP) are the instances that are detected as positive (cardiac ailments or abnormal) but these are not actual positive instances. Similarly, the false negatives (FN) are the instances that are detected as negative (HC or normal) but these are not actual negative instances. The sensitivity, the specificity and the accuracy measures are evaluated from the number of TP, TN, FP and FN, respectively. The sensitivity (SE) is defined as proportion of abnormal ECG episodes that are correctly classified as abnormal and it is given by

$$SE = \frac{TP}{TP + FN} \tag{2.56}$$

The specificity (SP) is defined as proportion of normal or HC ECG episodes that are correctly classified as normal and it is given by

$$SP = \frac{TN}{TN + FP} \tag{2.57}$$

The accuracy (Acc) is defined as the proportion of ECG episodes that are classified as normal (HC) and abnormal (cardiac ailments). It is given by

$$Acc = \frac{TP + TN}{TP + TN + FP + FN} \tag{2.58}$$

**Table 2.3:** Confusion matrix of multiclass classifier.

| | | Predicted Output | | | | |
|---|---|---|---|---|---|---|
| | | Class1 | Class2 | Class3 | Class4 | Class5 |
| Actual Output | Class1 | $u_{11}$ | $u_{12}$ | $u_{13}$ | $u_{14}$ | $u_{15}$ |
| | Class2 | $u_{21}$ | $u_{22}$ | $u_{23}$ | $u_{24}$ | $u_{25}$ |
| | Class3 | $u_{31}$ | $u_{32}$ | $u_{33}$ | $u_{34}$ | $u_{35}$ |
| | Class4 | $u_{41}$ | $u_{42}$ | $u_{43}$ | $u_{44}$ | $u_{45}$ |
| | Class5 | $u_{51}$ | $u_{52}$ | $u_{53}$ | $u_{54}$ | $u_{55}$ |

The ROC curve is a plot between the true positive rate (sensitivity) and false positive rate (1-

specificity) of classifier [22]. The area under ROC (AROC) curve is widely used as a performance measure for binary classifier [127]. The classifier with higher value of AROC has better performance. The performance measures for multiclass classifier are individual class accuracy and the overall accuracy. These measures are evaluated from the multiclass confusion matrix [44]. The individual class accuracy measures the sensitivity of each class in multiclass classifier. The overall accuracy is evaluated using the average of the sensitivity values. The confusion matrix of a five class classifier is shown in Table 2.3. The individual class accuracy (IA) value of $i^{\text{th}}$ class is given by

$$IA_i = \frac{u_{ii}}{\sum_{\tilde{j}=1}^{5} u_{i\tilde{j}}} \tag{2.59}$$

where $i, \tilde{j} = 1, 2...., 5$. The overall accuracy (OA) of the multiclass classifier is evaluated as

$$OA = \frac{\sum_{i=\tilde{j}=1}^{5} u_{i\tilde{j}}}{\sum_{i=1}^{5} \sum_{\tilde{j}=1}^{5} u_{i\tilde{j}}} \tag{2.60}$$

## 2.10 Motivation for This Thesis Work

The 12-lead or multilead ECG views the heart from distinct angles and it is useful in localizing various life-debilitating cardiac ailments. The life-debilitating cardiac ailments occur due to the obstruction in one of the coronary arteries (MI), the defect in conduction process (BBB) and the abnormal heart muscle (hypertrophic cardiomyopathy). Quantifying diagnostic information from ECG signal for detection of cardiac ailments is a challenging task in signal processing. The diagnostic information of ECG can be effectively captured using various features. The motivation of this thesis work is the use of various signal processing techniques to estimate the diagnostic features of ECG signal. These diagnostic features can be used for detection of various cardiac ailments.

The state-of-art methods use only few ECG leads for detection of MI. Instead of entire ECG segments, the methods are also based on the analysis of the clinical components such as the ST-segment, T-wave and QRS-complex. This demands for an accurate detection of fiducial points (P, Q, R, S and T) of ECG signal along each lead. The prior information about the presence of MI in selected ECG leads are also required for MI detection and localization. In recent years, the multiscale analysis using DWT is found to be an effective method for various ECG signal processing applica-

tions [62], [91] [14]. The 'PQRST' morphologies of ECG signal are grossly captured in different sub-bands using Multiscale analysis [14]. The multiscale analysis of all the channels of multilead ECG with identical mother wavelet and same decomposition level helps in formulating the multivariate multiscale matrices. These sub-band matrices capture the inter-sample and the inter-lead correlations of multilead ECG at different wavelet scales. The inter-lead correlation can be higher for multilead ECG at different scales. The multiscale analysis of multilead ECG for detection and localization of MI has not been used. It is expected that, the multiscale analysis of multilead ECG can provide discriminative diagnostic information, which are more sensitive to capture the pathological variations during MI. This motivates us to use the multiscale features of multilead ECG for detection and localization of MI.

The existing methods for detection and classification of various cardiac ailments such as BBB, MI, HMD and cardiac dysrhythmia are beat-specific and few ECG leads are used for evaluation of diagnostic features. In clinical setting, the serial recording of ECG data with multiple electrodes are used for accurate detection of MI, HMD and BBB pathologies [12]. Some of the reported methods have used various morphological features of multilead ECG. For evaluation of these features, it is required to detect the P, Q, R, S, T points of each ECG lead [41] [42]. The multiscale analysis using dual tree complex wavelet transform (DTCWT) has the advantage that, it provides both magnitude and phase information of the ECG signal in wavelet domain. The phase captures the temporal information of an ECG signal [178]. The duration parameters of ECG show significant variations during MI, BBB and HMD pathologies. It is expected that, the features evaluated from the phase of complex wavelet coefficients of multilead ECG at different scales will be helpful to capture pathological variations. The DTCWT also overcomes the drawbacks of DWT with its important properties such as the shift invariant, substantial reduction in aliasing effect and the non-oscillating characteristics of the wavelet coefficients [67]. The magnitude and the phase features of 12-lead or multilead ECG in wavelet domain have not been used for analysis of multilead ECG during various pathological cases. The complex wavelet magnitude and phase features of multilead ECG can be used for detection and classification of various cardiac ailments.

The existing diagnostic features are not sufficient to capture the pathological changes of ECG during shockable ventricular arrhythmia. The wavelet based methods for detection of shockable ventricular arrhythmia require proper selection of basis function with the morphology similar to that

of ECG signal. During VT and VF, the ECG signal doesn't have 'PQRST' morphologies. Therefore a data-dependent multiresolution analysis method for evaluation of the diagnostic features of ECG will be helpful for detection of shockable ventricular arrhythmia. The VMD is a data-dependent and iterative method to decompose ECG signal into modes or sub-signals. The center frequency and bandwidth of each mode are different. The pathological changes in the clinical components of ECG during shockable ventricular arrhythmia can be effectively captured using these modes. The non-linear analysis techniques such as the Renyi entropy (RE) and the permutation entropy (PE) provide a great opportunity to better understand the cardiac activities and explore the hidden patterns in ECG and heart rate (HR) signals [179] [149]. It is expected that, the time-domain features and the frequency-domain features evaluated from the modes of ECG will be helpful for detection and classification of shockable ventricular arrhythmia and non-shockable episodes.

The proposed investigations in this thesis are planned as follows

- To investigate the multiscale analysis of multilead ECG for detection and localization of MI. The multiscale analysis of ECG signal using DWT produces wavelet coefficients at different sub-bands. For multilead ECG, the wavelet coefficients of approximation sub-band and the detail sub-bands for each ECG lead can be evaluated. These sub-band wavelet coefficients of each ECG lead can be arranged to form the multivariate multiscale matrices. These multivariate multiscale matrices can capture the grossly segregated clinical components of each ECG lead. During MI, the T-wave inversion, ST-segment elevation, abnormal Q-wave and the loss of r-wave progression are observed in multilead ECG. These pathological variations may alter the characteristics of the multivariate multiscale matrices of multilead ECG. The features evaluated from these matrices will be useful for detection and localization of MI. The multiscale energy and eigenspace (MEES) features can be evaluated from the multivariate multiscale matrices of multilead ECG. The statistical significance of MEES features for detection and localization of MI can be analyzed. The MEES features and various classifiers can be used for detection and localization of MI.

- To investigate the complex wavelet magnitude and phase features of multilead ECG for detec-

tion and classification of cardiac ailments such as BBB, MI and HMD. The DTCWT of ECG signal produces complex wavelet coefficients at different scales. For multilead ECG, the complex wavelet coefficients of each ECG lead at different scales can be evaluated. The pathological changes in the multilead ECG due to MI, HMD and BBB pathologies can be captured using the complex wavelet coefficients. The features evaluated from the complex wavelet coefficients of multilead ECG will be useful for detection and classification of BBB, MI and HMD. The multiscale phase alternation (PA) features and the complex wavelet sub-band bi-spectrum (CWSB) magnitude and phase features can be evaluated from the complex wavelet coefficients of multilead ECG. The variations in the duration parameters of multilead ECG during BBB, HMD and MI can be captured using multiscale PA features. The higher order complex wavelet analysis can be used to evaluate the CWSB of each ECG lead. The statistical significance of complex wavelet magnitude and phase features can be investigated using one-way ANOVA method. The complex wavelet magnitude and phase features of multilead ECG, and various machine learning techniques can be used for detection and classification of BBB, MI and HMD pathologies.

- To investigate the variational mode energy and entropy (VMEE) features of ECG signal for detection and classification of shockable (VT/VF) ventricular arrhythmia and non-shockable episodes. The VMD of ECG produces modes or sub-signals. These modes can capture the grossly segmented clinical components of ECG signal. The abnormal patterns appear in ECG due to shockable ventricular arrhythmia. These abnormal patterns may alter the characteristics of the modes of ECG. It is expected that, the features evaluated from the variational modes of ECG will be useful for detection of ventricular arrhythmia. The energy, the PE and the RE features can be evaluated from the significant modes of ECG. The variational mode RE and permutation entropy features can capture the pathological changes in ECG signal during shockable ventricular arrhythmia. The statistical significance of the variational mode energy and entropy features can be investigated using t-test. The VMEE features, and the random forest classifier can be used for detection and classification of shockable ventricular arrhythmia and non-shockable episodes from ECG.

भारतीय प्रौद्योगिकी संस्थान गुवाहाटी
Indian Institute of Technology Guwahati

# 3

# Detection and Localization of Myocardial Infarction from Multilead ECG



## Contents

Myocardial infarction (MI) is a life-threatening cardiovascular disease and it occurs due to the impediment in one of the coronary arteries of the heart [9]. In clinical practice, it is a challenging task for detection and localization of MI from multilead ECG. The spatial and the temporal information of the heart electrical activity is captured using multilead ECG. Various categories of MI are diagnosed by observing the pathological changes in different ECG leads. So, monitoring ECG signal of each lead is advantageous for detection and localization of MI. In this Chapter, a new approach for detection and localization of MI from multilead ECG is proposed. This approach is based on the multiscale analysis of multilead ECG. The discrete wavelet transform (DWT) decomposes the ECG signal into approximation and detail coefficients at different scales or sub-bands. For multilead ECG, the approximation sub-band and the detail sub-band wavelet coefficients of each ECG lead are evaluated. These wavelet coefficients of each lead at different sub-bands are arranged to form multivariate multiscale matrices. The clinical components of multilead ECG are grossly divided in these multiscale multivariate matrices. In MI, the pathological symptoms (as shown in Fig. 1.5) such as the hyper-acute T-wave, the inversion in T-wave, the loss of r-wave progression, the abnormal Q-wave and the ST-segment elevation observe in multilead ECG. These pathological changes may alter the characteristics of the multivariate multiscale matrices of multilead ECG. The features evaluated from the multivariate multiscale sub-band matrices can be used for detection and localization of MI. The literature survey in Chapter 2 shows that, the multiscale analysis has been used for denoising and compression of multilead ECG data [29] [25]. The multiscale features of vectorcardiogram (VCG) and single lead ECG signals have been used for detection of MI [14] [50]. The multiscale analysis of multilead ECG for detection and localization of MI has not been addressed in the literature. The diagnostic features of multilead ECG evaluated using multiscale analysis have the potential to capture the pathological signatures of MI.

In this work, the multiscale energy and eigenspace (MEES) features of multilead ECG are evaluated. These MEES features are used for detection and localization of MI. For detection of MI, the MEES features and two classifiers such as k-nearest neighbor (KNN) and support vector machine (SVM) are used. Then, the MI detected multilead ECG frame is considered for localization. The MEES features of multilead ECG beat matrix and the multiclass SVM are used for localization of six categories of myocardial infarctions such as anterior MI, inferior MI, anterio-lateral MI, inferio-

posterio-lateral MI, inferio-lateral MI and anterio-septal MI. The rest of this chapter is organized as follows. The multiscale analysis of multilead ECG is described in Section 3.1. Section 3.2 describes the proposed method for detection and localization of MI from multilead ECG. The method for MI detection and localization is evaluated in Section 3.3. The summary of this chapter is written in Section 3.4.

## 3.1 Multiscale Analysis of Multilead ECG using DWT

The multiscale analysis of multilead ECG is performed using DWT [50]. The approximation coefficients and the detail coefficients at different scales are evaluated for each ECG lead. The DWT of an ECG signal $\mathbf{x}(n)$ with '$L$' number of decomposition levels result one approximation sub-band and $L$ number of detail sub-bands. The wavelet coefficients of the approximation sub-band, $cA_L(k)$ and the $l^{\text{th}}$ detail sub-band ($l = 1, 2...L$), $cD_l(k)$ are computed using equation 2.5 and equation 2.6, respectively. For a multilead ECG signal, $\mathbf{x}^m(n)$, the approximation sub-band and the $l^{th}$ detail sub-band wavelet coefficients are evaluated as $cA_L^m(k)$ and $cD_l^m(k)$, $l = 1, 2, ...L$, respectively. where, $m$ corresponds to the lead number. The multivariate sub-band matrices are formulated using the wavelet coefficients of each ECG lead [25]. The approximation sub-band matrix is evaluated as

$$\mathbf{A}_L = [cA_L^1(k), cA_L^2(k), ....., cA_L^m(k)] \tag{3.1}$$

For $l^{th}$ detail sub-band, the multivariate sub-band matrix is given by

$$\mathbf{D}_l = [cD_l^1(k), cD_l^2(k), ....., cD_l^m(k)] \tag{3.2}$$

The multivariate sub-band matrices grossly capture the clinical components (P-wave, QRS-complex and T-wave) of multilead ECG. In this study, the significant sub-bands of each ECG lead are selected based on the frequency content. The bandwidth of an ECG signal spans the frequency range between $0.5$ Hz to $50$ Hz [3]. The frequency contents of T-wave, P-wave and QRS-complex are [0.5-10 Hz], [5-30 Hz] and [8-50 Hz], respectively [180]. The $l^{\text{th}}$ detail sub-band of wavelet decomposition is associated with a frequency range of $\Delta f_{cD_l}$. The frequency range of the approximation sub-band is denoted as $\Delta f_{cA_L}$. The frequency ranges of the approximation sub-band and the $l^{\text{th}}$ detail sub-band

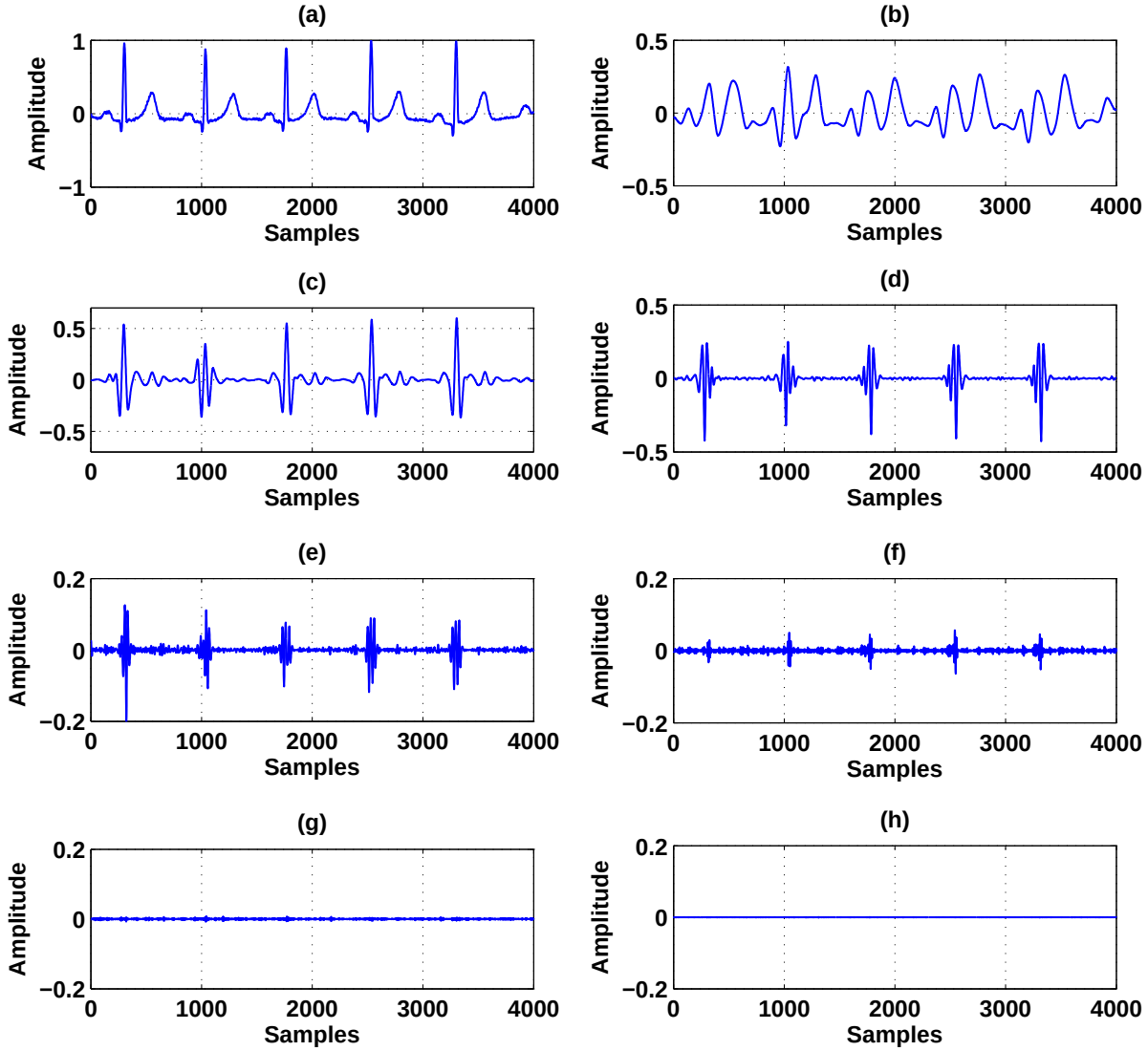


**Fig. 3.1:** (a) Lead I ECG Signal. The amplitude of ECG signal is in mV and the sampling frequency is 1000 Hz. (b) Signal reconstructed using the wavelet coefficients of approximation sub-band ($cA_6(k)$). (c) Signal reconstructed using the wavelet coefficients of $6^{th}$ detail sub-band ($cD_6(k)$). (d) Signal reconstructed using the wavelet coefficients of $5^{th}$ detail sub-band ($cD_5(k)$). (e) Signal reconstructed using the wavelet coefficients of $4^{th}$ detail sub-band ($cD_4(k)$). (f) Signal reconstructed using the wavelet coefficients of $3^{rd}$ detail sub-band ($cD_3(k)$). (g) Signal reconstructed using the wavelet coefficients of $2^{nd}$ detail sub-band ($cD_2(k)$) (h) Signal reconstructed using the wavelet coefficients of $1^{st}$ detail sub-band ($cD_1(k)$).

are given by [181]

$$0 \leq \Delta f_{cA_L} \leq 2^{-L-1} F_s \tag{3.3}$$

$$2^{-l-1} F_s \leq \Delta f_{cD_l} \leq 2^{-l} F_s \tag{3.4}$$

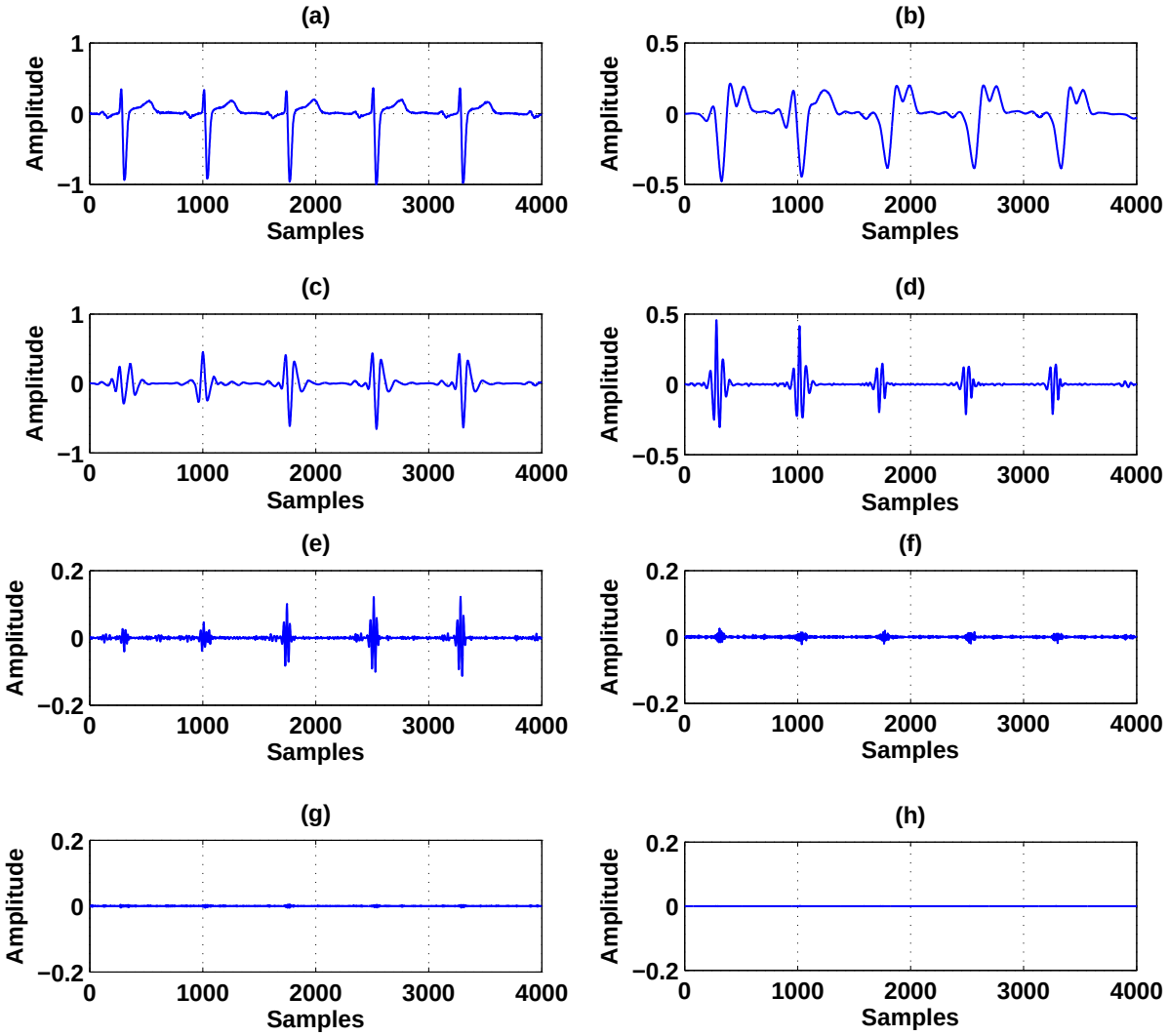


**Fig. 3.2:** (a) Lead V1 ECG Signal. The amplitude of ECG signal is in mV and the sampling frequency is 1000 Hz. (b) Signal reconstructed using the wavelet coefficients of approximation sub-band, $(cA_6(k))$. (c) Signal reconstructed using the wavelet coefficients of $6^{\text{th}}$ detail sub-band, $(cD_6(k))$. (d) Signal reconstructed using the wavelet coefficients of $5^{th}$ detail sub-band, $(cD_5(k))$. (e) Signal reconstructed using the wavelet coefficients of $4^{\text{th}}$ detail sub-band $(cD_4(k))$. (f) Signal reconstructed using the wavelet coefficients of $3^{\text{rd}}$ detail sub-band $(cD_3(k))$. (g) Signal reconstructed using the wavelet coefficients of $2^{\text{nd}}$ detail sub-band $(cD_2(k))$ (h) Signal reconstructed using the wavelet coefficients of $1^{\text{st}}$ detail sub-band $(cD_1(k))$.

where $F_s$ is the sampling frequency of the ECG signal and $l = 1, 2, ..., L$ are number of detail sub-bands. In this work, six decomposition levels for DWT of ECG signal along each ECG lead are used. The frequency range of $cD_1$, $cD_2$, $cD_3$, $cD_4$, $cD_5$ and $cD_6$ sub-band signals for each ECG lead are evaluated as [250 Hz, 500 Hz], [125 Hz, 250 Hz], [62.5 Hz, 125 Hz], [31.25 Hz, 62.5 Hz], [15.62 Hz, 31.25 Hz], [7.84 Hz, 15.62 Hz], respectively. The frequency range of approximation sub-band signal

is given as [0.5 Hz, 7.84 Hz].

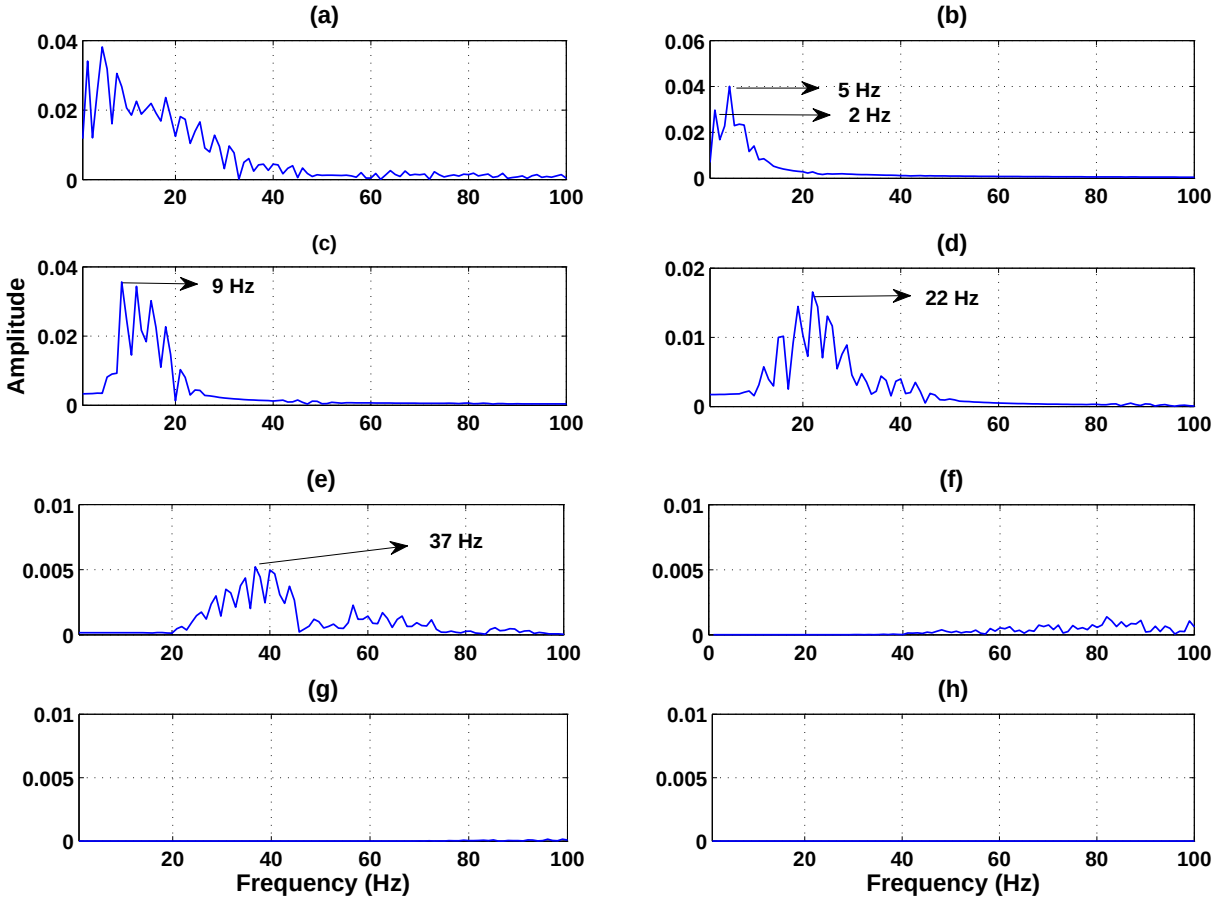


**Fig. 3.3:** (a) Spectrum of lead I ECG Signal. (b) Spectrum of $cA_6$ sub-band signal. (c) Spectrum of $cD_6$ sub-band signal. (d) Spectrum of $cD_5$ sub-band signal. (e) Spectrum of $cD_4$ sub-band signal. (f) Spectrum of $cD_3$ sub-band signal. (g) Spectrum of $cD_2$ sub-band signal. (h) Spectrum of $cD_1$ sub-band signal.

The lead I and the lead V1 ECG signals for healthy control (HC) are shown in Fig. 3.1 (a) and Fig. 3.2 (a), respectively. The sampling frequency of these signals is 1 kHz. It is observed that, the lead V1 ECG signal has r-wave progression and bi-phasic P-wave. The signals reconstructed using the wavelet coefficients of approximation sub-band and the $l^{\text{th}}$ detail sub-band for lead I and lead V1 ECG signals are depicted in Fig.3.1 (b)-(h) and Fig.3.2 (b)-(h), respectively. The spectra of the lead I ECG signal and the sub-band signals (signal reconstructed using the wavelet coefficients) are shown in Fig. 3.3. It is observed that, the diagnostic information of ECG is grossly divided in first four sub-band signals. The approximation sub-band signal captures the ST-segment, the T-wave and the low

frequency part of P-wave information with spectral peaks are at $2$ Hz and $5$ Hz, respectively. The $cD_6$ sub-band captures the high-frequency components of P-wave and the low-frequency components of QRS-complex information of ECG signal. The peaks obtained in the spectrum of $cD_6$ sub-band signal are $9$ Hz, $11$ Hz and $12.5$ Hz, respectively. Similarly, the QRS-complex information is captured using the $cD_5$ sub-band wavelet coefficients. The peak frequency of $cD_5$ sub-band signal is $22$ Hz. The $cD_4$ sub-band signal contains the high-frequency part of QRS-complex information. In frequency domain, the peak value of the $cD_5$ sub-band signal is at $37$ Hz. The above observations reveal that, the first four sub-bands ($cA_6$, $cD_6$, $cD_5$ and $cD_4$) capture the diagnostic components such as P-wave, QRS-complex and T-wave of ECG signal. The features evaluated from these sub-bands will be useful to capture the pathological variations in the clinical components of multilead ECG during MI. This motivates us to use $cA_6$, $cD_6$, $cD_5$ and $cD_4$ sub-bands of each ECG lead for evaluation of MEES features.

## 3.2 Proposed Method for Detection and Localization of MI

In this section, the proposed method for detection and localization of MI from multilead ECG is described. Fig. 3.4 (a) and Fig. 3.4 (b) show the block diagrams for detection and localization. The detection block comprises of preprocessing (noise filtering and frame based segmentation), evaluation of MEES features and classification. The detection block comprises of preprocessing (noise filtering and frame based segmentation), evaluation of MEES features and classification. In this block, the MI and the HC are classified using the MEES features of multilead ECG frame. The MI detected multilead ECG frame is used as input to the MI localization block which is shown in Fig. 3.4 (b). The localization block consists of multilead beat segmentation, evaluation of MEES features from the multilead ECG beat matrix and classification of different types of MI pathologies using multiclass SVM. The following sub-sections briefly describe each part of the block diagram.

### 3.2.1 Preprocessing

The preprocessing step consists of filtering and frame based segmentation of multilead ECG data. In the filtering part, the artifacts such as base line wandering or drift are eliminated using a moving average filter [22]. The high frequency noise is removed using the relative energies of wavelet sub-

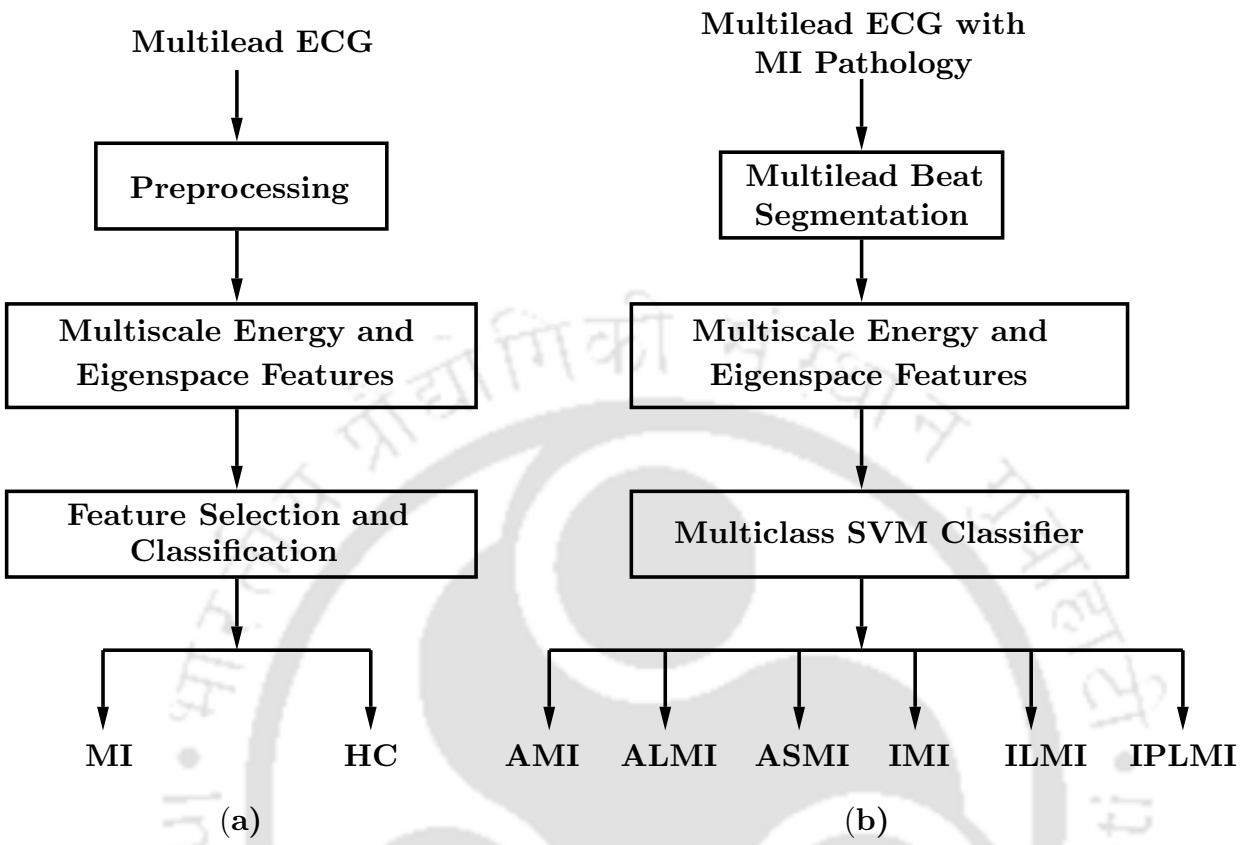


**Fig. 3.4:** Detection and localization of myocardial infarction from multilead ECG. Panel (a) Detection and (b) Localization.

bands and a noise variance based threshold [29]. The frame segmentation of multilead ECG is done using a window of size $4000 \times 12$. The multilead ECG frame consists of atleast four multilead ECG beats. For localization, the MI detected multilead ECG frame is divided into multilead ECG beat matrices. The beat-to-beat segmentation is done based on the detection of R-peaks using Pan and Tomkin's algorithm [32]. In this work, for localization, six types of myocardial infarctions such as anterior MI (AMI), anterio-lateral MI (ALMI), anterio-septal MI (ASMI), inferior MI (IMI), inferio-lateral MI (ILMI), inferio-posterio-lateral MI (IPLMI) are considered.

### 3.2.2 Multiscale Energy and Eigenspace Features

In this subsection, the proposed multiscale energy and eigenspace features of multilead ECG are evaluated. The $cA_6$, $cD_6$, $cD_5$ and $cD_4$ sub-bands of each ECG lead capture significant diagnostic information. The multiscale energy features are evaluated from the wavelet coefficients of these four

sub-bands. The multiscale energy has been used for selection of diagnostically relevant sub-bands in Multilead ECG compression and enhancement [25] [65]. Jayachandran $et\ al.$ [50] have shown that, the multiscale energy features are effective for detection of MI from single lead ECG. The multiscale energy of the approximation sub-band and the $l^{\text{th}}$ detail sub-band for $m^{\text{th}}$ ECG lead are defined as

$$E^m_{cA_L} = \frac{\sum_{k=1}^{N_{\mathbf{A}_L}} [cA^m_L(k)]^2}{N_L} \tag{3.5}$$

$$E^m_{cD_l} = \frac{\sum_{k=1}^{N_{\mathbf{D}_l}} [cD^m_l(k)]^2}{N_l} \tag{3.6}$$

where $N_{\mathbf{A}_L}$ and $N_{\mathbf{D}_l}$ are the length of approximation sub-band and $l^{\text{th}}$ detail sub-band, respectively. The multiscale energy features capture the inter-sample correlation of multilead ECG in wavelet domain. Sharma $et\ al.$ [25] have shown that, for a six level wavelet decomposition of multilead ECG (sampling frequency=1 kHz), the $cA_6$, $cD_6$, $cD_5$ and $cD_4$ sub-bands of each ECG lead have higher energy compared to $cD_3$, $cD_2$ and $cD_1$ sub-bands. In this work, the energy is evaluated for $cA_6$, $cD_6$, $cD_5$ and $cD_4$ sub-bands of each ECG lead.

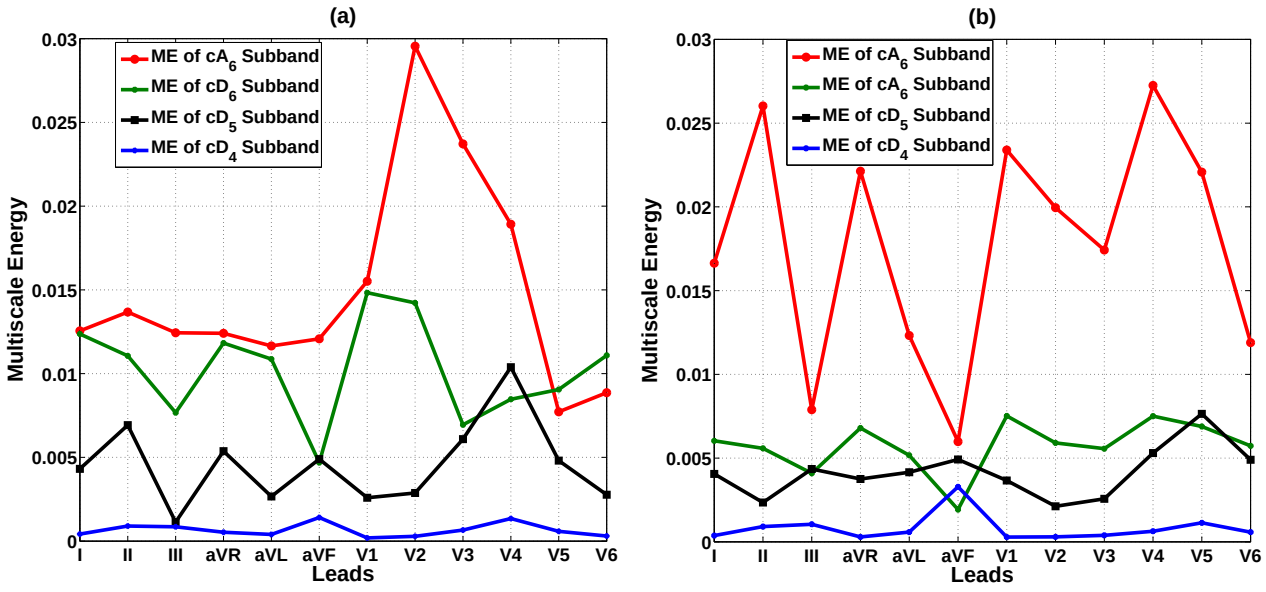


**Fig. 3.5:** (a) Multiscale energy values of each ECG lead for HC in $cA_6$, $cD_6$, $cD_5$ and $cD_4$ sub-bands. (b) Multiscale energy values of each ECG lead for MI in $cA_6$, $cD_6$, $cD_5$ and $cD_4$ sub-bands.

Fig. 3.5 (a) and Fig. 3.5 (b) show the variation of multiscale energy with ECG leads for HC and MI cases in $cA_6$, $cD_6$, $cD_5$ and $cD_4$ sub-bands. It is observed that, the multiscale energy values are

different for HC and MI cases at different ECG leads. These differences in the multiscale energy values can be used for detection and localization of MI pathology. In this work, $12$ multiscale energy features from each sub-band are evaluated. The multiscale energy feature vector is formulated by appending the energy features of each sub-band. This feature vector consists of $48$ attributes (12 $cA_6$, 12 $cD_6$, 12 $cD_5$ and 12 $cD_4$ sub-band energy features).

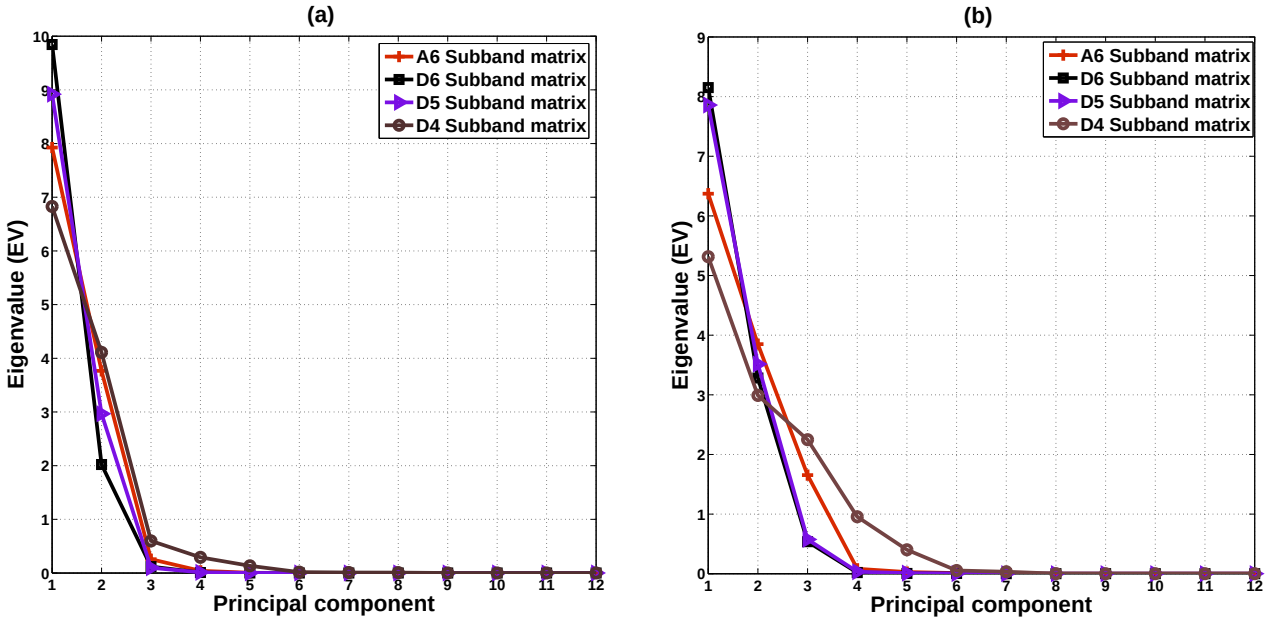


**Fig. 3.6:** (a) Multiscale eigenvalue plot for HC in $\mathbf{A}_6$, $\mathbf{D}_6$, $\mathbf{D}_5$ and $\mathbf{D}_4$ scales. (b) Multiscale eigenvalue plot for MI in $\mathbf{A}_6$, $\mathbf{D}_6$, $\mathbf{D}_5$ and $\mathbf{D}_4$ scales.

The multiscale eigenspace features are evaluated using the eigenvalues of the covariance matrices of multilead ECG. If the approximation sub-band matrix ($\mathbf{A}_L$) and the $l^{\text{th}}$ detail sub-band matrix ($\mathbf{D}_l$) are subjected to eigen analysis, the diagnostic information of multilead ECG can be captured using eigenvalues. The eigen analysis is performed based on the evaluation of covariance matrices for approximation scale and $l^{\text{th}}$ detail scale. The covariance matrices exploit the inter-lead correlation of multilead ECG in multiscale. The inter-lead correlation can't be perfectly captured, if the covariance matrix of multilead ECG is directly evaluated [25]. The multiscale analysis has the advantage to grossly segregate the clinical components of multilead ECG in sub-band matrices. If the covariance matrices are evaluated from the sub-band matrices of multilead ECG, then the inter-lead correlation can be effectively captured. The covariance matrices for approximation scale and $l^{\text{th}}$ detail scale are

given by [25]

$$\mathbf{C}_{\mathbf{A}_L} = \frac{1}{N_{\mathbf{A}_L} - 1}[\mathbf{A}_L]^T[\mathbf{A}_L] \tag{3.7}$$

$$\mathbf{C}_{\mathbf{D}_l} = \frac{1}{N_{\mathbf{D}_l} - 1}[\mathbf{D}_l]^T[\mathbf{D}_l] \tag{3.8}$$

The eigen analysis of the covariance matrices for approximation scale and $l^{th}$ detail scale are given as

$$\mathbf{C}_{\mathbf{A}_L}\mathbf{V}_{\mathbf{A}_L} = \mathbf{V}_{\mathbf{A}_L}\Lambda_{\mathbf{A}_L} \tag{3.9}$$

$$\mathbf{C}_{\mathbf{D}_l}\mathbf{V}_{\mathbf{D}_l} = \mathbf{V}_{\mathbf{D}_l}\Lambda_{\mathbf{D}_l} \tag{3.10}$$

where $\Lambda_{\mathbf{A}_L}$, $\Lambda_{\mathbf{D}_l}$ and $\mathbf{V}_{\mathbf{A}_L}$, $\mathbf{V}_{\mathbf{D}_l}$ are the eigenvalues and the eigenvectors of the approximation sub-band matrix ($\mathbf{A}_L$) and $l^{\text{th}}$ detail sub-band matrix ($\mathbf{D}_l$), respectively.

Fig. 3.6 (a) and Fig. 3.6 (b) depict the variation of multiscale eigenvalues with principal components (PCs) of multilead ECG for HC and MI cases at $\mathbf{A}_6$, $\mathbf{D}_6$, $\mathbf{D}_5$ and $\mathbf{D}_4$ scales. It is observed that, for each of the sub-band matrix the first six PCs have higher eigenvalue than other PCs. The eigenvalues of each of the sub-band matrix are different for MI and HC cases. The multiscale eigenvalue features have not been used for detection and localization of MI from multilead ECG. In this work, $6$ eigenvalue features from each sub-band matrix are evaluated as most of the energy are retained by them. For $\mathbf{A}_6$, $\mathbf{D}_6$, $\mathbf{D}_5$ and $\mathbf{D}_4$ sub-band matrices, a total of $24$ eigenvalue features are computed. The eigenvalue features of each sub-band matrix is appended to form multiscale eigenspace feature vector. The following subsection describes the selection of features from MEES feature vector and classification of different type of MI.

### 3.2.3 Feature Selection and Classification

In this work, for MI detection, $48$ multiscale energy features and $24$ multiscale eigenvalue features are evaluated from each multilead ECG frame. The MEES feature vector is formulated by combining $48$ multiscale energy features and $24$ multiscale eigenvalue features. This feature vector contains $72$ attributes. The $72$ dimensional feature vector is evaluated for each multilead ECG frame of both HC and MI classes. The multiscale feature matrix is denoted as $\mathbf{Z} \in R^{p \times q}$. where, $p$ and $q$ are the number

of instances or multilead ECG frames and number of MEES features, respectively. The multiscale feature matrix is used as input to the classifiers. In this study, the KNN and the SVM classifiers are used for MI detection. The class labels of both KNN and SVM classifiers for $i^{\text{th}}$ feature instance ($i = 1, 2, ..p$) is given as $y_i \in (0, 1)$. where, $0$ and $1$ are the class labels for HC and MI classes. The correlation based feature selection (CFS) approach is employed to reduce the dimension of the MEES feature vector [161]. The new feature matrix obtained using CFS is given as, $\tilde{\mathbf{Z}} \in R^{p \times \tilde{q}}$. where $\tilde{q} < q$ is the length of new feature vector. The training and the test instances of both KNN and SVM classifiers are selected using both hold-out cross-validation and 5-fold cross-validation approaches. In this work, for MI detection, the number of nearest neighbors and the distance metric for KNN classifier are selected as '$5$' and 'Euclidean', respectively. Similarly, for SVM classifier with linear kernel, the regularization parameter $C = 30$ is used. The regularization parameter $C = 30$ and the standard deviation $\sigma = 0.5$ are used for SVM classifier with RBF kernel function. The performance of both KNN and SVM classifiers on test data is evaluated using the metrics such as the sensitivity, the specificity and the accuracy. These metrics are computed using equation 2.56, equation 2.57 and equation 2.58, respectively.

For MI localization, the multiclass SVM classifier is used. The MEES feature vector is evaluated from the multilead ECG beat matrix. The feature matrix, $\mathbf{Z} \in R^{p \times q}$ for MI localization consists of $p$ number of multilead beats and $q$ number of MEES features. The class labels of $i^{\text{th}}$ multilead beat instance ($i = 1, 2, ..p$) is given as $y_i \in (1, 2, 3, 4, 5, 6)$. where, $1$, $2$, $3$, $4$, $5$ and $6$ are the class labels of AMI, ALMI, ASMI, IMI, ILMI and IPLMI. The CFS is also used for selection of few features from the $72$ dimensional MEES feature vector of multilead ECG beat. The hold-out cross-validation and the 5-fold cross-validation methods are also employed for selection of training and test instances of multiclass SVM classifier. The linear and the RBF kernel functions are used for multiclass SVM classifier. The 'one VS One' multiclass coding technique is also employed. The performance of multiclass SVM classifier on test data is evaluated using the overall accuracy (OA). The OA is computed using equation 2.60. The following section describes the evaluation of the proposed method.

## 3.3 Evaluation of the Proposed Method

In this work, the proposed method for MI detection and localization is evaluated using the multilead ECG signals from PTB (Physikalisch-Technische Bundesanstalt) diagnostic ECG database [4]. Here, the one hour recording of multilead ECG datasets from HC and MI are used. Each of these multilead ECG datasets are subjected to preprocessing for elimination of baseline wandering noise. After noise filtering, the multilead ECG frames for HC and MI classes are evaluated. For MI localization case, the detected multilead ECG frames are again segmented into multilead ECG beat matrices. The multilead data matrix contains the ECG samples as rows and $12$ ECG leads as columns. Then, the six levels wavelet decomposition of each multilead ECG frame is carried out using bi-orthogonal 6.8 wavelet filters [25]. The wavelet coefficients of $cA_6$, $cD_6$, $cD_5$ and $cD_4$ sub-bands of each ECG lead are computed. The multivariate multiscale matrices are evaluated from the wavelet coefficients of each ECG lead. The $48$ multiscale energy features and the $24$ multiscale eigenvalue features are evaluated from the multivariate multiscale matrices of multilead ECG. A $72$ dimensional feature vector is created by appending both multiscale energy and eigenspace features. Here, for MI detection $72$ dimensional feature vector is evaluated from $1074$ HC and $1074$ MI based multilead ECG frames. Similarly, for MI localization, the $72$ dimensional feature vector is evaluated from $726$ instances of each type of MI pathology. The following subsections describe the statistical analysis of multiscale energy and eigenspace features for MI detection and localization, the performance of KNN and SVM classifiers using MEES features for MI detection, and the performance of multiclass SVM classifier for MI localization.

**Table 3.1:** Mean and standard deviation values of multiscale Energy features for HC and MI in $cA_6$ sub-band.

| Classes | Param. | I | II | III | aVR | aVL | aVF | V1 | V2 | V3 | V4 | V5 | V6 |
|---|---|---|---|---|---|---|---|---|---|---|---|---|---|
| MI | $\mu$ | 0.200 | 0.149 | 0.162 | 0.136 | 0.210 | 0.116 | 0.120 | 0.205 | 0.162 | 0.082 | 0.054 | 0.061 |
| MI | $\sigma$ | 0.210 | 0.164 | 0.148 | 0.158 | 0.202 | 0.118 | 0.167 | 0.195 | 0.170 | 0.110 | 0.118 | 0.100 |
| HC | $\mu$ | 0.115 | 0.200 | 0.094 | 0.150 | 0.070 | 0.125 | 0.056 | 0.174 | 0.173 | 0.122 | 0.077 | 0.077 |
| HC | $\sigma$ | 0.089 | 0.179 | 0.152 | 0.110 | 0.077 | 0.158 | 0.055 | 0.187 | 0.134 | 0.084 | 0.084 | 0.118 |

### 3.3.1 Statistical Analysis of MEES Features for MI detection

In this subsection, the within-class variations and the statistical significance of multiscale energy and multiscale eigenspace features are investigated. The within-class variations of multiscale energy of

**Table 3.2:** Mean and standard deviation values of multiscale Energy features for HC and MI in $cD_6$ sub-band.

| Classes | Param. | I | II | III | aVR | aVL | aVF | V1 | V2 | V3 | V4 | V5 | V6 |
|---|---|---|---|---|---|---|---|---|---|---|---|---|---|
| MI | $\mu$ | 0.235 | 0.078 | 0.071 | 0.156 | 0.161 | 0.051 | 0.187 | 0.152 | 0.251 | 0.153 | 0.068 | 0.051 |
| MI | $\sigma$ | 0.207 | 0.089 | 0.100 | 0.134 | 0.176 | 0.077 | 0.170 | 0.122 | 0.190 | 0.138 | 0.089 | 0.077 |
| HC | $\mu$ | 0.117 | 0.142 | 0.064 | 0.177 | 0.065 | 0.088 | 0.185 | 0.182 | 0.311 | 0.224 | 0.098 | 0.077 |
| HC | $\sigma$ | 0.100 | 0.148 | 0.126 | 0.114 | 0.100 | 0.134 | 0.161 | 0.173 | 0.228 | 0.167 | 0.110 | 0.110 |

**Table 3.3:** Mean and standard deviation values of multiscale Energy features for HC and MI in $cD_5$ sub-band.

| Classes | Param. | I | II | III | aVR | aVL | aVF | V1 | V2 | V3 | V4 | V5 | V6 |
|---|---|---|---|---|---|---|---|---|---|---|---|---|---|
| MI | $\mu$ | 0.173 | 0.072 | 0.063 | 0.159 | 0.180 | 0.046 | 0.185 | 0.154 | 0.206 | 0.157 | 0.061 | 0.046 |
| MI | $\sigma$ | 0.167 | 0.071 | 0.095 | 0.141 | 0.192 | 0.071 | 0.167 | 0.141 | 0.141 | 0.148 | 0.071 | 0.063 |
| HC | $\mu$ | 0.108 | 0.157 | 0.072 | 0.217 | 0.093 | 0.097 | 0.243 | 0.206 | 0.283 | 0.275 | 0.116 | 0.095 |
| HC | $\sigma$ | 0.089 | 0.167 | 0.152 | 0.126 | 0.152 | 0.158 | 0.192 | 0.187 | 0.197 | 0.197 | 0.110 | 0.114 |

**Table 3.4:** Mean and standard deviation values of multiscale Energy features for HC and MI in $cD_4$ sub-band.

| Classes | Param. | I | II | III | aVR | aVL | aVF | V1 | V2 | V3 | V4 | V5 | V6 |
|---|---|---|---|---|---|---|---|---|---|---|---|---|---|
| MI | $\mu$ | 0.132 | 0.115 | 0.114 | 0.216 | 0.116 | 0.088 | 0.238 | 0.127 | 0.177 | 0.097 | 0.058 | 0.039 |
| MI | $\sigma$ | 0.170 | 0.134 | 0.170 | 0.224 | 0.173 | 0.134 | 0.195 | 0.118 | 0.173 | 0.118 | 0.071 | 0.045 |
| HC | $\mu$ | 0.064 | 0.157 | 0.108 | 0.201 | 0.061 | 0.119 | 0.251 | 0.147 | 0.209 | 0.160 | 0.108 | 0.079 |
| HC | $\sigma$ | 0.071 | 0.148 | 0.141 | 0.155 | 0.077 | 0.148 | 0.200 | 0.155 | 0.202 | 0.164 | 0.114 | 0.114 |

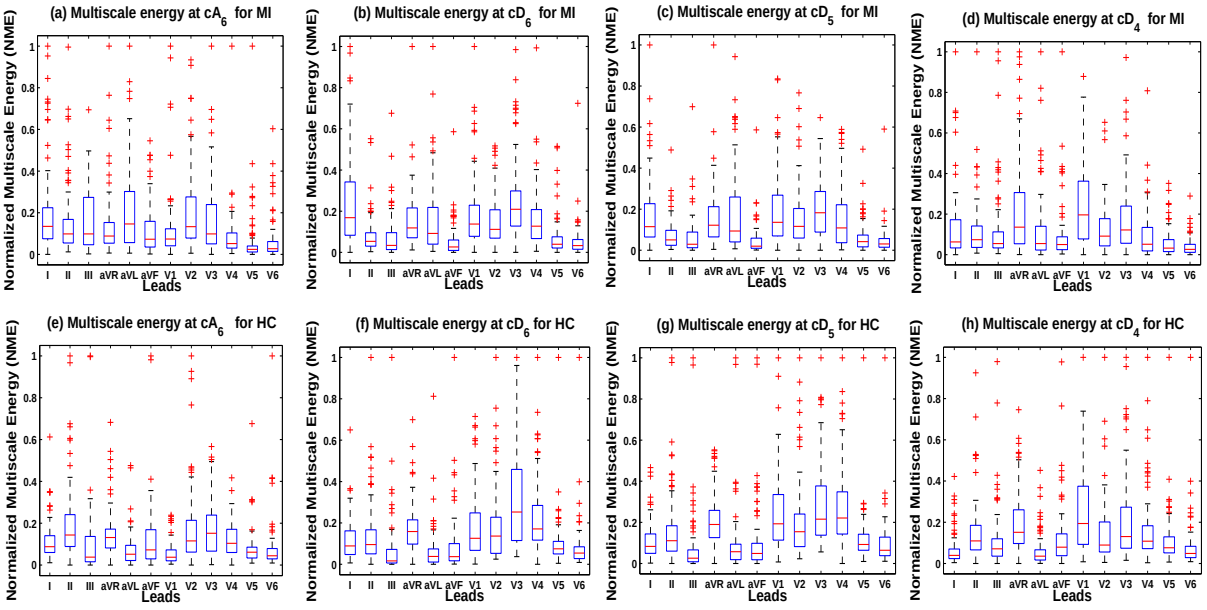


**Fig. 3.7:** Normalized multiscale energy for large data set which shows within-class variation. Panels (a) - (d) show variation of energy features of $cA_6$, $cD_6$, $cD_5$ and $cD_4$ sub-bands for all ECG leads of MI class. Panels (e) - (h) show variation of energy features of $cA_6$, $cD_6$, $cD_5$ and $cD_4$ sub-bands for all ECG leads of HC class.

all ECG leads for MI and HC class are shown as the box-plots in Fig. 3.7 (a)-(d) and Fig. 3.7 (e)-(h), respectively. The boxplots are shown by considering $1074$ HC and $1074$ MI cases. The mean ($\mu$) and the standard deviation ($\sigma$) values of multiscale energy for HC and MI in $cA_6$, $cD_6$, $cD_5$ and $cD_4$ subbands are shown in Table 3.1, Table 3.2, Table 3.3 and Table 3.4, respectively. It is observed that, for $cA_6$ sub-band of HC class, the mean values of multiscale energy in lead I and lead V1 are $0.115$ and $0.056$, respectively. Similarly, for MI class, the mean values of multiscale energy features are $0.200$ and $0.120$ in lead I and lead V1. The low-frequency diagnostic information of ECG (ST-segment and T-wave) are captured using the wavelet coefficients of $cA_6$ sub-band. The ST-segment and the T-wave shapes are different in MI pathology. This may be the reason for different mean values of multiscale energy in $cA_6$ sub-band of lead I and lead V1. For $cD_6$ sub-band of lead I, the mean and the standard deviation values of multiscale energy are $0.235$ and $0.207$, respectively, for MI, while for HC, the mean and the standard deviation values are $0.117$ and $0.100$, respectively. Differences in the mean and the standard deviation values are observed between MI class and HC class in other sub-bands and in all the leads. For $cA_6$ sub-band of lead I and lead aVF, the differences in the mean values of HC class and MI class are $0.085$ and $0.140$, respectively. Similar differences are observed for $cD_6$, $cD_5$ and $cD_4$ sub-bands of other ECG leads. These differences in the mean values of multiscale energy are due to the variations in the clinical components such as ST-segment elevation, abnormal Q-wave, T-wave inversion and loss of r-wave progression in MI.

The statistical significance of multiscale energy features is evaluated using paired t-test approach [182]. A feature is said to be 'statistically significant', if it has lower p-value and higher t-value. Here, t-test is conducted for $48$ multiscale energy features of HC class and MI class. The t-value and p-value of each multiscale energy feature is shown in Table 3.5. It is observed that, $37$ features out of $48$ multiscale energy features have p-value lower than $0.001$. It is also seen that, $10$ features out of $12$ multiscale energy features of $cA_6$ and $cD_6$ sub-bands have p-value less than $0.001$. The wavelet coefficients of $cA_6$ and the $cD_6$ sub-bands capture the ST-segment, the T-wave, the P-wave and low-frequency component of QRS-complex of ECG signal. These clinical components show significant variations during MI pathology. This may be the reason for which the maximum multiscale energy features in $cA_6$ and $cD_6$ sub-bands are statistically significant for MI detection.

The within-class variations of eigenspace features for MI and HC classes in $\mathbf{A}_6$, $\mathbf{D}_6$, $\mathbf{D}_5$ and $\mathbf{D}_4$

**Table 3.5:** t-value and p-value of multiscale energy features.

| cA6 subband | | | | | | | | | | | | |
|---|---|---|---|---|---|---|---|---|---|---|---|---|
| Leads | I | II | III | aVR | aVL | aVF | V1 | V2 | V3 | V4 | V5 | V6 |
| t-val | 6.75 | 15.18 | 5.00 | 10.55 | 6.49 | 11.49 | 2.51 | 5.01 | 2.57 | 5.82 | 13.23 | 11.73 |
| p-val | <0.001 | <0.001 | <0.001 | <0.001 | <0.001 | <0.001 | 0.011 | <0.001 | 0.010 | <0.001 | <0.001 | <0.001 |
| cD6 subband | | | | | | | | | | | | |
| Leads | I | II | III | aVR | aVL | aVF | V1 | V2 | V3 | V4 | V5 | V6 |
| t-val | 9.73 | 14.52 | 0.6435 | 8.43 | 11.72 | 10.01 | 4.24 | 2.44 | 2.91 | 5.39 | 12.11 | 10.62 |
| p-val | <0.001 | <0.001 | 0.519 | <0.001 | <0.001 | <0.001 | <0.001 | 0.014 | 0.003 | <0.001 | <0.001 | <0.001 |
| cD5 subband | | | | | | | | | | | | |
| Leads | I | II | III | aVR | aVL | aVF | V1 | V2 | V3 | V4 | V5 | V6 |
| t-val | 6.75 | 15.18 | 5.00 | 10.55 | 6.49 | 11.49 | 2.51 | 5.01 | 2.57 | 5.82 | 13.23 | 11.73 |
| p-val | <0.001 | <0.001 | <0.001 | <0.001 | <0.001 | <0.001 | 0.011 | <0.001 | 0.010 | <0.001 | <0.001 | <0.001 |
| cD4 subband | | | | | | | | | | | | |
| Leads | I | II | III | aVR | aVL | aVF | V1 | V2 | V3 | V4 | V5 | V6 |
| t-val | 7.84 | 6.75 | 4.16 | 0.57 | 3.06 | 6.71 | 3.76 | 1.08 | 2.54 | 4.69 | 11.16 | 8.29 |
| p-val | <0.001 | <0.001 | <0.001 | 0.562 | 0.002 | <0.001 | <0.001 | 0.279 | 0.010 | <0.001 | <0.001 | <0.001 |

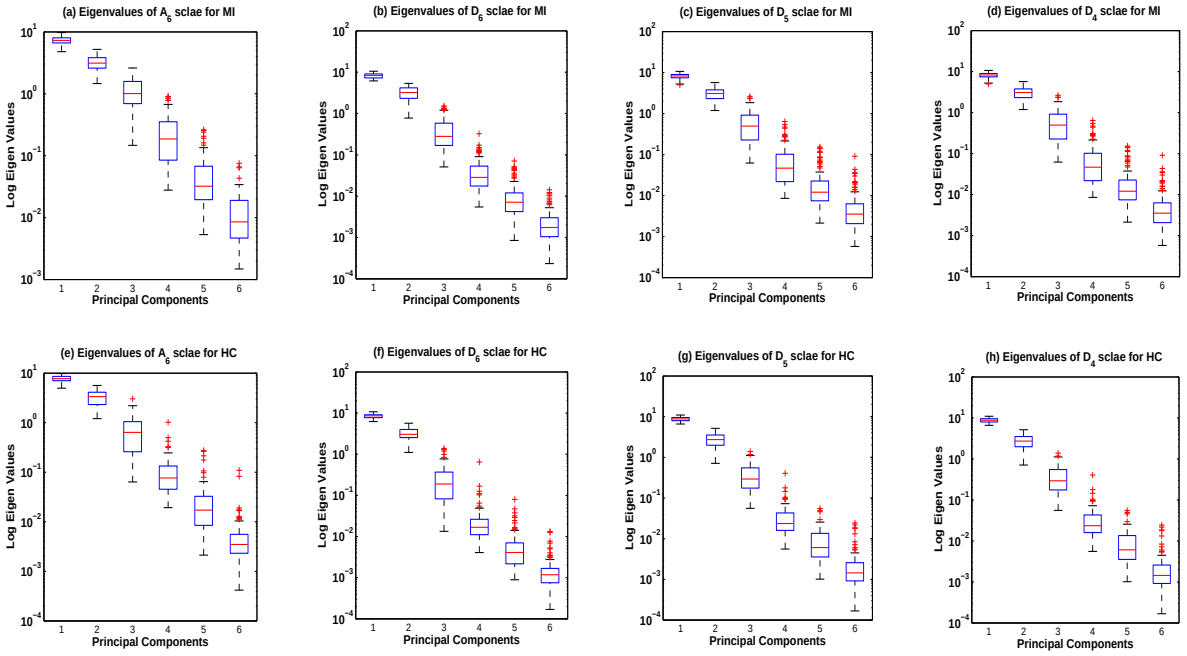


**Fig. 3.8:** (a), (b), (c) and (d) Shows the Box plot for variation of log-eigen values over 1074 MI multilead ECG frames at $\mathbf{A_6}$, $\mathbf{D_6}$, $\mathbf{D_5}$ and $\mathbf{D_4}$ scales respectively. (e), (f), (g) and (h) Shows the Box plot for variation of log-eigen values over 1074 HC multilead ECG frames at $\mathbf{A_6}$, $\mathbf{D_6}$, $\mathbf{D_5}$ and $\mathbf{D_4}$ scales respectively.

scales are depicted in Fig. 3.8 (a)-(d) and Fig. 3.8 (e)-(h), respectively. The eigenspace features are the eigenvalues of the first six PCs of $\mathbf{A}_6$, $\mathbf{D}_6$, $\mathbf{D}_5$ and $\mathbf{D}_4$ scales or sub-band matrices. The mean and the standard deviation values of multiscale eigenspace features for MI and HC are shown in Table 3.6. It is observed that, for MI class, the mean and the standard deviation values of first six eigenvalue

**Table 3.6:** Mean and standard deviation values of multiscale eigenvalue features in $\mathbf{A_6}$, $\mathbf{D_6}$, $\mathbf{D_5}$ and $\mathbf{D_4}$ scales for MI and HC.

| | Myocardial Infarction | | | | | | Healthy Control | | | | | |
|---|---|---|---|---|---|---|---|---|---|---|---|---|
| | $\mathbf{A_6}$ Scale | | | | | | $\mathbf{A_6}$ Scale | | | | | |
| PC | PC1 | PC2 | PC3 | PC4 | PC5 | PC6 | PC1 | PC2 | PC3 | PC4 | PC5 | PC6 |
| $\mu$ | 7.338 | 3.193 | 1.143 | 0.251 | 0.054 | 0.014 | 7.802 | 3.321 | 0.725 | 0.109 | 0.031 | 0.007 |
| $\sigma$ | 1.076 | 0.843 | 0.608 | 0.210 | 0.057 | 0.014 | 1.035 | 1.104 | 0.550 | 0.123 | 0.047 | 0.014 |
| | $\mathbf{D_6}$ Scale | | | | | | $\mathbf{D_6}$ Scale | | | | | |
| $\mu$ | 8.248 | 3.266 | 0.424 | 0.043 | 0.012 | 0.003 | 8.408 | 3.276 | 0.274 | 0.030 | 0.007 | 0.002 |
| $\sigma$ | 1.137 | 1.141 | 0.356 | 0.045 | 0.014 | 0.010 | 1.051 | 1.116 | 0.273 | 0.067 | 0.010 | 0.010 |
| | $\mathbf{D_5}$ Scale | | | | | | $\mathbf{D_5}$ Scale | | | | | |
| $\mu$ | 8.099 | 3.122 | 0.656 | 0.087 | 0.024 | 0.007 | 8.744 | 2.822 | 0.383 | 0.036 | 0.009 | 0.003 |
| $\sigma$ | 1.217 | 1.016 | 0.555 | 0.112 | 0.032 | 0.010 | 0.974 | 1.023 | 0.279 | 0.047 | 0.010 | 0.010 |
| | $\mathbf{D_4}$ Scale | | | | | | $\mathbf{D_4}$ Scale | | | | | |
| $\mu$ | 5.961 | 3.221 | 1.773 | 0.660 | 0.247 | 0.088 | 6.162 | 3.426 | 1.437 | 0.600 | 0.253 | 0.084 |
| $\sigma$ | 1.090 | 0.622 | 0.574 | 0.321 | 0.135 | 0.065 | 1.063 | 0.689 | 0.558 | 0.280 | 0.217 | 0.066 |

features for $\mathbf{A}_6$, $\mathbf{D}_6$, $\mathbf{D}_5$ and $\mathbf{D}_4$ scales are different than HC class. For $\mathbf{A}_6$ scale, the mean and the standard deviation values of eigenvalue features for MI class are $7.338$ and $1.076$, respectively, whereas the mean and the standard deviation values for HC class are $7.802$ and $1.035$. The difference between the mean values of first three eigenvalue features between HC and MI classes at $\mathbf{D}_5$ scale are $0.65$, $0.30$ and $0.26$, respectively. Similar differences are observed for eigenvalue features of $\mathbf{A}_6$, $\mathbf{D}_6$, $\mathbf{D}_4$ scales. These variations in the eigenvalue features at $\mathbf{A}_6$, $\mathbf{D}_6$, $\mathbf{D}_4$ and $\mathbf{D}_4$ scales are due to the differences in the structure of the covariance matrix. The inter-lead correlations of the clinical components of multilead ECG are effectively captured using the multiscale eigenspace features. The structure of the covariance matrix of multilead ECG is different for HC and MI cases in each wavelet scale. This may be the reason for which the mean and the standard deviation values of multiscale eigenspace features are different for HC and MI class.

The paired t-test is also used to evaluate the statistical significance of multiscale eigenspace features. The p-values and the t-values of eigenvalue features for $\mathbf{A}_6$, $\mathbf{D}_6$, $\mathbf{D}_5$ and $\mathbf{D}_4$ scales are shown in Table 3.7. It is observed that, out of $24$ multiscale eigenspace features, 15 features have p-value less than $0.001$. These $15$ features are statistically significant for detection of MI. The first three eigenspace features of $\mathbf{D}_4$ and $\mathbf{D}_5$ scales have lower p-value. The $\mathbf{D}_4$ and $\mathbf{D}_5$ scales capture the inter-lead correlations of the high frequency components (QRS-complex information) of multilead ECG. The covariance matrix structures of $\mathbf{D}_4$ and $\mathbf{D}_5$ scales are different for MI and HC cases. This

**Table 3.7:** t-value and p-value of multiscale eigenvalue features

| A6 scale | | | | | | |
|---|---|---|---|---|---|---|
| PC | PC1 | PC2 | PC3 | PC4 | PC5 | PC6 |
| t-value | 11.22 | 1.86 | 17.50 | 11.76 | 6.68 | 6.27 |
| p-Value | $<$0.001 | 0.062 | $<$0.001 | $<$0.001 | $<$0.001 | $<$0.001 |
| D6 scale | | | | | | |
| t-value | 7.63 | 4.35 | 10.64 | 0.37 | 0.49 | 0.22 |
| p-Value | $<$0.001 | $<$0.001 | $<$0.001 | 0.704 | 0.617 | 0.818 |
| D5 scale | | | | | | |
| t-value | 6.86 | 5.69 | 6.85 | 1.63 | 1.64 | 1.20 |
| p-Value | $<$0.001 | $<$0.001 | $<$0.001 | 0.103 | 0.102 | 0.22 |
| D4 scale | | | | | | |
| t-value | 6.67 | 3.40 | 12.71 | 8.72 | 0.20 | 0.403 |
| p-Value | $<$0.001 | $<$0.001 | $<$0.001 | $<$0.001 | 0.840 | 0.686 |

may be the reason for which the p-value of first three eigenvalue features of $\mathbf{D}_5$ and $\mathbf{D}_4$ scales are significant for detection of MI.

### 3.3.2 MI Detection Performance

In this subsection, the performance of KNN and SVM classifiers for MI detection are shown. The training and the test multilead ECG frames or instances of both KNN and SVM classifiers are selected using hold-out cross-validation and the 5-fold cross-validation methods. In this work, for hold-out cross-validation, $200$ instances, each from HC and MI classes are used for evaluation. Here, $100$ instances from MI and HC classes are used for training of both KNN and SVM classifiers. The other $100$ instances, each from MI and HC classes are used for testing. Table 3.8 shows the number of true positives, true negatives, false positives, false negatives, accuracy, sensitivity and specificity of KNN and SVM classifiers. It is observed that the SVM classifier with RBF kernel has an accuracy of 96%, sensitivity of 93% and specificity of 99%. The SVM with linear kernel function and the KNN classifiers have accuracy values of 89% and 81%, sensitivity values of 90.42% and 85% and specificity values of 87.69% and 77%. The performance of SVM with RBF kernel is better than KNN and SVM with linear kernel classifiers. The RBF kernel in SVM projects the feature vector to higher dimensional space [171]. This may be the reason for the better performance of SVM classifier with RBF kernel for MI detection. Fig.3.9 shows the ROC curves for KNN, SVM with linear kernel and SVM with RBF

kernel classifiers. It is noticed that, the area under the ROC curves for KNN, SVM with linear kernel and SVM with RBF kernel are $0.82895$, $0.88015$ and $0.96166$ respectively.

**Table 3.8:** Performance evaluation and confusion matrix for SVM and KNN classifiers

| Classifiers | TP | FN | TN | FP | Sensitivity(%) | Accuracy(%) | Specificity(%) |
|---|---|---|---|---|---|---|---|
| KNN | 85 | 15 | 77 | 23 | 85 | 81 | 77 |
| SVM Lin | 87 | 13 | 91 | 9 | 90.42 | 89 | 87.69 |
| SVM RBF | 93 | 7 | 99 | 1 | 93 | 96 | 99 |

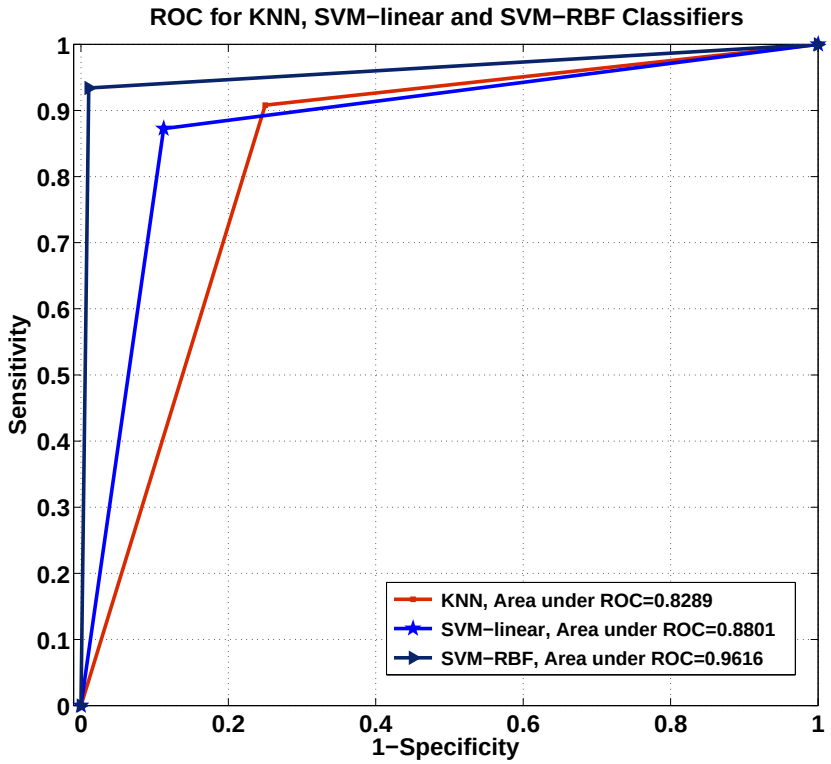


**Fig. 3.9:** ROC for KNN, SVM with linear kernel and SVM with RBF kernel classifiers

The 5-fold cross-validation technique for selection of training and test instances is performed for $2148$ multilead ECG instances. The performance of KNN and SVM classifier is shown using the multiscale energy features, the multiscale eigenspace features, the MEES features and with the feature subset derived using CFS. Table 3.9, Table 3.10, Table 3.11 and Table 3.12 show the performance of KNN and SVM classifiers along each fold using the aforementioned features. When multiscale energy features are used, the SVM classifier with RBF kernel produces an average accuracy of 90.14%, average sensitivity of 88.68% and average specificity of 91.62%, respectively. Similarly, when multi-

**Table 3.9:** Performance of KNN and SVM classifiers using multiscale energy features

| Classifiers | Parameters | Fold1 | Fold2 | Fold3 | Fold4 | Fold5 | Average |
|---|---|---|---|---|---|---|---|
| KNN | Accuracy(%) | 85.37 | 84.06 | 83.98 | 84.61 | 83.85 | 84.37 |
| | Sensitivity(%) | 86.08 | 83.77 | 85.05 | 84.58 | 85.14 | 84.92 |
| | Specificity(%) | 84.67 | 84.37 | 82.99 | 84.67 | 82.66 | 83.87 |
| SVM-Lin | Accuracy(%) | 86.62 | 83.00 | 87.75 | 86.62 | 86.12 | 86.02 |
| | Sensitivity(%) | 86.30 | 83.53 | 88.28 | 85.36 | 85.51 | 85.79 |
| | Specificity(%) | 86.97 | 82.47 | 87.22 | 87.90 | 86.79 | 86.27 |
| SVM-RBF | Accuracy(%) | 90.50 | 89.79 | 90.40 | 89.84 | 90.21 | 90.14 |
| | Sensitivity(%) | 89.91 | 89.8 | 88.66 | 87.97 | 87.09 | 88.68 |
| | Specificity(%) | 91.11 | 89.78 | 92.14 | 91.74 | 93.35 | 91.62 |

**Table 3.10:** Performance of KNN and SVM classifiers using multiscale eigenvalue features

| Classifiers | Parameters | Fold1 | Fold2 | Fold3 | Fold4 | Fold5 | Average |
|---|---|---|---|---|---|---|---|
| KNN | Accuracy(%) | 83.45 | 85.05 | 84.52 | 85.95 | 85.73 | 84.94 |
| | Sensitivity(%) | 85.11 | 86.87 | 85.68 | 88.33 | 87.64 | 86.72 |
| | Specificity(%) | 81.94 | 83.38 | 83.42 | 83.81 | 83.84 | 83.27 |
| SVM-Lin | Accuracy(%) | 74.62 | 76.75 | 76.62 | 72.12 | 74.87 | 74.99 |
| | Sensitivity(%) | 72.11 | 77.19 | 77.50 | 72.56 | 74.67 | 74.80 |
| | Specificity(%) | 77.39 | 76.34 | 76.12 | 71.93 | 75.14 | 75.38 |
| SVM-RBF | Accuracy(%) | 85.73 | 84.47 | 84.06 | 85.66 | 83.92 | 84.76 |
| | Sensitivity(%) | 84.07 | 81.87 | 83.93 | 84.53 | 84.01 | 83.68 |
| | Specificity(%) | 87.40 | 87.06 | 84.19 | 86.79 | 83.84 | 85.85 |

**Table 3.11:** Performance of KNN and SVM classifiers using all features

| Classifiers | Parameters | Fold1 | Fold2 | Fold3 | Fold4 | Fold5 | Average |
|---|---|---|---|---|---|---|---|
| KNN | Accuracy(%) | 83.37 | 82.15 | 82.62 | 81.25 | 81.75 | 82.28 |
| | Sensitivity(%) | 80.79 | 84.51 | 80.43 | 82.25 | 81.92 | 81.98 |
| | Specificity(%) | 86.13 | 80.37 | 82.50 | 80.36 | 82.25 | 82.32 |
| SVM-Lin | Accuracy(%) | 87.50 | 90.62 | 86.25 | 87.86 | 87.87 | 88.02 |
| | Sensitivity(%) | 85.08 | 89.93 | 86.32 | 86.08 | 88.75 | 87.23 |
| | Specificity(%) | 89.94 | 91.37 | 86.19 | 89.02 | 86.15 | 88.53 |
| SVM-RBF | Accuracy(%) | 96.03 | 96.68 | 96.42 | 95.14 | 96.50 | 96.15 |
| | Sensitivity(%) | 95.15 | 95.00 | 95.23 | 95.35 | 96.74 | 95.49 |
| | Specificity(%) | 96.92 | 98.37 | 97.62 | 94.94 | 96.26 | 96.82 |

scale eigenspace features are used, the SVM classifier with RBF kernel shows average accuracy of 84.76%, average sensitivity of 83.68% and average specificity of 85.85%, respectively. When all the features (MEES features) are used, the SVM classifier with RBF kernel shows an average accuracy of 96.15%, average sensitivity of 95.49% and average specificity of 96.82%. The SVM with linear

**Table 3.12:** Performance of KNN and SVM classifiers using selected features (CFS).

| Classifiers | Parameters | Fold1 | Fold2 | Fold3 | Fold4 | Fold5 | Average |
|---|---|---|---|---|---|---|---|
| KNN | Accuracy(%) | 85.06 | 85.24 | 85.72 | 85.60 | 85.57 | 85.23 |
| | Sensitivity(%) | 84.61 | 85.06 | 85.39 | 85.27 | 84.74 | 85.01 |
| | Specificity(%) | 86.63 | 84.49 | 87.12 | 85.95 | 84.65 | 85.76 |
| SVM-Lin | Accuracy(%) | 88.62 | 89.04 | 90.16 | 89.25 | 91.23 | 89.66 |
| | Sensitivity(%) | 88.31 | 88.43 | 90.59 | 90.83 | 90.29 | 89.69 |
| | Specificity(%) | 89.05 | 89.59 | 89.43 | 87.68 | 89.72 | 89.49 |
| SVM-RBF | Accuracy(%) | 97.80 | 96.85 | 96.09 | 96.30 | 97.12 | 96.83 |
| | Sensitivity(%) | 97.23 | 97.57 | 96.12 | 97.21 | 98.03 | 97.23 |
| | Specificity(%) | 96.67 | 96.56 | 97.16 | 95.41 | 96.21 | 96.40 |

**Table 3.13:** Comparison of proposed approach with existing MI detection methods.

| Methods | Sensitivity (%) | Specificity (%) | Accuracy (%) |
|---|---|---|---|
| Morphological features and Neural Network [72] | 79 | 97 | NA |
| Morphological features and Neuro-Fuzzy [79] | 84.6 | 90 | NA |
| ST-J amplitude, slope, T-amplitude and ANN [70] | 95 | 86.3 | NA |
| Polynomial coefficient features and MIL [2] | 91.43 | 77.29 | NA |
| Morphological Features and KNN [36] | NA | NA | 99 |
| Proposed Work | 93 | 99 | 96 |

kernel function and the KNN classifiers have average accuracy values of 88.02% and 82.28%, average sensitivity values of 87.23% and 81.98% and average specificity values of 88.53% and 82.32% respectively, for all the features. When the CFS method is employed, the average accuracy, average sensitivity and average specificity values are of 96.83%, 97.23% and 96.40%, respectively for SVM classifier with RBF kernel. It is observed that, the accuracy, the sensitivity and the specificity values of classifiers are improved with the CFS method. This may be due to the elimination of the correlated features from the $72$ dimensional feature vector. In this work, the features which are highly correlated to each other with correlation ratio of $0.9$ are eliminated. After removal of such redundant features, the 72 dimensional feature vector is reduced to a new feature vector containing 60 features. The above observations infer that, the MEES features of multilead ECG works well for detection of MI pathology.

The proposed MI detection approach is compared with the existing methods in Table 3.13. Most of the methods reported are beat-specific and they are based on neural network and other classifiers. The detection of MI using the ST-segment polynomial coefficients and the multi-instance learning model have been proposed in [2]. The sensitivity value value of 91.43% is found from this technique. In [183], the detection of MI from 12-lead ECG using morphological features and hermite expansion

coefficient features has been reported. An area under ROC curve value of 83.4% is found out using ANN. Detection of different cardiac abnormalities using the combinations of the PMMSE measure and the LS-SVM has been proposed in [131]. The accuracy value for MI class is found to be 93.95%. The performance of the MEES features is better than the methods reported in [131], [2], [183]. In [36], authors have used morphological features of multilead ECG. Evaluation of these features using signal processing methods is a tedious process. The performance of reported methods in literature depends on the accuracy of detection of ST-segment, ST-T complex and Q-wave. The proposed method does not require the prior segmentation ST-segment, QRS-complex and T-wave. The knowledge of presence of MI pathology is not necessary as the proposed method is based on 12-standard ECG leads. The accuracy value of proposed method is higher than the performance of the multiscale features of single lead ECG and VCG signals as reported in [50] [14]. In the following subsections, the statistical analysis of MEES features of multilead ECG beats and the performance of multiclass SVM classifier are shown for MI localization.

### 3.3.3 Statistical Analysis of MEES Features for MI localization

In this subsection, the statistical analysis of MEES features of multilead ECG is shown for MI localization. For each type of MI, the mean and the standard deviation values of MEES features are evaluated. The mean and the standard deviation values of multiscale energy features for anterior MI, anterio-lateral MI, anterio-septal MI, inferior MI, inferio-lateral MI and inferio-posterior-lateral MI are shown in Table 3.14, Table 3.15, Table 3.16, Table 3.17, Table 3.18 and Table 3.19, respectively. It is observed that, the mean values of multiscale energy features of $cA_6$ sub-band in (lead I, lead II, lead aVL, lead V2, lead V3, lead V4, lead V5 and lead V6) for anterior MI and anterio-lateral MI are ($0.043$, $0.034$, $0.040$, $0.160$, $0.096$, $0.071$, $0.036$ and $0.040$) and ($0.140$, $0.067$, $0.113$, $0.257$, $0.233$, $0.225$, $0.110$ and $0.112$), respectively. Similar mean and standard deviation values of multiscale energy features are observed for anterior MI and anterio-lateral MI in other sub-bands. Due to anterior MI, the T-wave inversions are observed in lead I, lead aVL, lead V2, lead V3, lead V4 and lead V5 [1]. The ST-segment elevations are also seen in lead I, lead V4 and lead V5.

For anterio-lateral MI, the T-wave inversion is observed in lead II, lead V3, lead V4, lead V5 and lead V6 [1]. The ST-segment elevations are also seen in lead I, lead aVL, lead V3 and lead V4. The

**Table 3.14:** Mean and standard deviation values of Multiscale energy features for Anterior MI at different ECG leads

| Sub-band | param. | I | II | III | aVR | aVL | aVF | V1 | V2 | V3 | V4 | V5 | V6 |
|---|---|---|---|---|---|---|---|---|---|---|---|---|---|
| $cA_6$ | $\mu$ | 0.043 | 0.034 | 0.042 | 0.048 | 0.040 | 0.035 | 0.060 | 0.160 | 0.096 | 0.071 | 0.036 | 0.040 |
| $cA_6$ | $\sigma$ | 0.022 | 0.032 | 0.046 | 0.030 | 0.029 | 0.039 | 0.047 | 0.127 | 0.075 | 0.050 | 0.030 | 0.037 |
| $cD_6$ | $\mu$ | 0.089 | 0.050 | 0.049 | 0.060 | 0.076 | 0.047 | 0.106 | 0.198 | 0.164 | 0.168 | 0.091 | 0.100 |
| $cD_6$ | $\sigma$ | 0.071 | 0.062 | 0.056 | 0.049 | 0.068 | 0.069 | 0.089 | 0.175 | 0.138 | 0.161 | 0.101 | 0.097 |
| $cD_5$ | $\mu$ | 0.123 | 0.041 | 0.044 | 0.105 | 0.100 | 0.028 | 0.129 | 0.188 | 0.202 | 0.095 | 0.083 | 0.089 |
| $cD_5$ | $\sigma$ | 0.108 | 0.050 | 0.043 | 0.087 | 0.096 | 0.034 | 0.137 | 0.228 | 0.212 | 0.123 | 0.106 | 0.091 |
| $cD_4$ | $\mu$ | 0.038 | 0.024 | 0.036 | 0.034 | 0.044 | 0.025 | 0.051 | 0.028 | 0.042 | 0.027 | 0.050 | 0.014 |
| $cD_4$ | $\sigma$ | 0.045 | 0.025 | 0.035 | 0.041 | 0.049 | 0.020 | 0.052 | 0.037 | 0.043 | 0.038 | 0.081 | 0.018 |

T-wave, the ST-segment and the low-frequency component of P-wave information are captured using $cA_6$ sub-band wavelet coefficients. This may be the reason for different mean and standard deviation values of multiscale energy features in lead I, lead II, lead aVL, lead V2, lead V3, lead V4, lead V5 and lead V6 in $cA_6$ sub-band. For anterio-septal MI, the mean values of multiscale energy features in $cD_5$ sub-band of lead V1 and lead V2 are $0.173$ and $0.093$, respectively. These values are lower than the mean value of multiscale energy features of anterio-lateral MI in $cD_5$ sub-band. The pathological symptoms for anterio-septal MI are loss of r-wave progression in lead V1 and lead V2 [1]. This may be the reason for different mean and standard deviation values of $cD_5$ sub-band energy features at lead V1 and lead V2 in anterior MI, anterio-lateral MI and anterio-septal MI.

**Table 3.15:** Mean and standard deviation values of Multiscale energy features for Anterio-lateral MI at different ECG leads

| Sub-band | param. | I | II | III | aVR | aVL | aVF | V1 | V2 | V3 | V4 | V5 | V6 |
|---|---|---|---|---|---|---|---|---|---|---|---|---|---|
| $cA_6$ | $\mu$ | 0.140 | 0.067 | 0.092 | 0.121 | 0.113 | 0.067 | 0.087 | 0.257 | 0.233 | 0.225 | 0.110 | 0.112 |
| $cA_6$ | $\sigma$ | 0.188 | 0.121 | 0.177 | 0.177 | 0.177 | 0.136 | 0.041 | 0.219 | 0.215 | 0.235 | 0.198 | 0.175 |
| $cD_6$ | $\mu$ | 0.128 | 0.114 | 0.095 | 0.107 | 0.113 | 0.113 | 0.158 | 0.264 | 0.227 | 0.176 | 0.121 | 0.128 |
| $cD_6$ | $\sigma$ | 0.191 | 0.167 | 0.155 | 0.169 | 0.169 | 0.170 | 0.103 | 0.216 | 0.196 | 0.137 | 0.149 | 0.117 |
| $cD_5$ | $\mu$ | 0.117 | 0.122 | 0.088 | 0.152 | 0.116 | 0.094 | 0.178 | 0.177 | 0.199 | 0.113 | 0.104 | 0.109 |
| $cD_5$ | $\sigma$ | 0.194 | 0.154 | 0.129 | 0.222 | 0.169 | 0.132 | 0.176 | 0.149 | 0.153 | 0.118 | 0.115 | 0.110 |
| $cD_4$ | $\mu$ | 0.063 | 0.122 | 0.113 | 0.092 | 0.090 | 0.116 | 0.131 | 0.079 | 0.127 | 0.135 | 0.161 | 0.096 |
| $cD_4$ | $\sigma$ | 0.131 | 0.181 | 0.186 | 0.151 | 0.160 | 0.184 | 0.191 | 0.130 | 0.181 | 0.206 | 0.227 | 0.182 |

The mean values of multiscale energy features of $cA_6$ sub-band in (lead I, lead II, lead III, lead aVL, lead aVF, lead V1, lead V2, lead V3, lead V5 and lead V6) for inferior MI, inferio-lateral MI, inferio-posterio-lateral MI classes are (0.098, 0.038, 0.055, 0.034, 0.027, 0.082, 0.077, 0.064, 0.069, 0.081), (0.072, 0.066, 0.025, 0.050, 0.030, 0.037, 0.061, 0.056, 0.050, 0.036) and (0.097, 0.020, 0.072, 0.041, 0.020, 0.052, 0.088, 0.060, 0.041, 0.046), respectively. For $cD_5$ sub-band, the mean

**Table 3.16:** Mean and standard deviation values of Multiscale energy features for Anterio-septal MI at different ECG leads

| Sub-band | param. | I | II | III | aVR | aVL | aVF | V1 | V2 | V3 | V4 | V5 | V6 |
|---|---|---|---|---|---|---|---|---|---|---|---|---|---|
| $cA_6$ | $\mu$ | 0.077 | 0.032 | 0.054 | 0.057 | 0.068 | 0.036 | 0.141 | 0.172 | 0.167 | 0.110 | 0.048 | 0.072 |
| $cA_6$ | $\sigma$ | 0.091 | 0.044 | 0.071 | 0.081 | 0.091 | 0.044 | 0.169 | 0.164 | 0.177 | 0.090 | 0.079 | 0.131 |
| $cD_6$ | $\mu$ | 0.080 | 0.042 | 0.075 | 0.041 | 0.096 | 0.062 | 0.180 | 0.144 | 0.156 | 0.140 | 0.121 | 0.123 |
| $cD_6$ | $\sigma$ | 0.100 | 0.040 | 0.097 | 0.033 | 0.136 | 0.067 | 0.156 | 0.117 | 0.158 | 0.131 | 0.106 | 0.123 |
| $cD_5$ | $\mu$ | 0.064 | 0.028 | 0.036 | 0.051 | 0.064 | 0.026 | 0.173 | 0.093 | 0.132 | 0.075 | 0.060 | 0.059 |
| $cD_5$ | $\sigma$ | 0.080 | 0.024 | 0.053 | 0.040 | 0.098 | 0.031 | 0.220 | 0.090 | 0.155 | 0.092 | 0.050 | 0.051 |
| $cD_4$ | $\mu$ | 0.019 | 0.024 | 0.019 | 0.026 | 0.020 | 0.019 | 0.061 | 0.028 | 0.058 | 0.036 | 0.037 | 0.014 |
| $cD_4$ | $\sigma$ | 0.024 | 0.023 | 0.020 | 0.028 | 0.026 | 0.015 | 0.063 | 0.029 | 0.077 | 0.055 | 0.036 | 0.015 |

values of multiscale energy features of (lead I, lead II, lead aVL, lead aVF, lead V1 and lead V6) are (0.086, 0.088, 0.086, 0.069, 0.149 and 0.157), (0.139, 0.044, 0.092, 0.017, 0.107 and 0.117) and (0.161, 0.057, 0.098, 0.019, 0.151 and 0.144) for inferior MI, inferio-lateral MI and inferio-posterio-lateral MI classes. Similar variations in the mean and the standard deviation values are also observed for $cD_6$ and $cD_4$ sub-bands. The pathological signatures of inferior MI are abnormal Q-waves in lead III and lead aVF, and ST-segment elevations in lead II, lead III and lead aVF, respectively. Similarly, for inferio-lateral MI, the abnormal Q-wave in lead aVF, ST-segment elevations in lead I and lead aVL, T-wave inversion in lead II and lead V6, and amplitude of r-waves are higher in lead V1, lead V2 and lead V3 [1]. For inferio-posterio-lateral MI, the ST-segment elevation and T-wave inversion in lead V5 and lead V6, reciprocal changes in lead V1 and lead V2, and abnormal Q-wave in lead III and lead aVF are observed. These pathological variations of multilead ECG are captured using the multiscale energy features of $cD_6$, $cD_5$ and $cD_4$ sub-bands. This may be the reason for different mean and standard deviation values of multiscale energy features for inferior MI, inferio-lateral MI, inferio-posterio-lateral MI cases along different ECG leads.

**Table 3.17:** Mean and standard deviation values of Multiscale energy features for Inferior MI at different ECG leads

| Sub-band | param. | I | II | III | aVR | aVL | aVF | V1 | V2 | V3 | V4 | V5 | V6 |
|---|---|---|---|---|---|---|---|---|---|---|---|---|---|
| $cA_6$ | $\mu$ | 0.098 | 0.038 | 0.034 | 0.089 | 0.055 | 0.027 | 0.082 | 0.077 | 0.064 | 0.075 | 0.069 | 0.081 |
| $cA_6$ | $\sigma$ | 0.111 | 0.057 | 0.057 | 0.102 | 0.070 | 0.052 | 0.157 | 0.098 | 0.067 | 0.077 | 0.071 | 0.096 |
| $cD_6$ | $\mu$ | 0.083 | 0.066 | 0.045 | 0.070 | 0.062 | 0.056 | 0.136 | 0.122 | 0.126 | 0.215 | 0.201 | 0.205 |
| $cD_6$ | $\sigma$ | 0.081 | 0.072 | 0.089 | 0.058 | 0.098 | 0.090 | 0.166 | 0.107 | 0.105 | 0.204 | 0.175 | 0.190 |
| $cD_5$ | $\mu$ | 0.086 | 0.088 | 0.065 | 0.110 | 0.086 | 0.069 | 0.149 | 0.122 | 0.193 | 0.178 | 0.175 | 0.157 |
| $cD_5$ | $\sigma$ | 0.081 | 0.124 | 0.163 | 0.097 | 0.161 | 0.157 | 0.162 | 0.137 | 0.178 | 0.200 | 0.146 | 0.127 |
| $cD_4$ | $\mu$ | 0.029 | 0.054 | 0.057 | 0.038 | 0.046 | 0.056 | 0.057 | 0.032 | 0.069 | 0.075 | 0.109 | 0.026 |
| $cD_4$ | $\sigma$ | 0.039 | 0.091 | 0.099 | 0.042 | 0.078 | 0.097 | 0.068 | 0.038 | 0.082 | 0.086 | 0.142 | 0.031 |

**Table 3.18:** Mean and standard deviation values of Multiscale energy features for Inferio-lateral MI at different ECG leads

| Sub-band | param. | I | II | III | aVR | aVL | aVF | V1 | V2 | V3 | V4 | V5 | V6 |
|---|---|---|---|---|---|---|---|---|---|---|---|---|---|
| $cA_6$ | $\mu$ | 0.072 | 0.025 | 0.050 | 0.047 | 0.066 | 0.030 | 0.037 | 0.061 | 0.056 | 0.084 | 0.050 | 0.036 |
| $cA_6$ | $\sigma$ | 0.035 | 0.091 | 0.081 | 0.089 | 0.042 | 0.091 | 0.033 | 0.046 | 0.043 | 0.068 | 0.064 | 0.067 |
| $cD_6$ | $\mu$ | 0.092 | 0.028 | 0.036 | 0.051 | 0.075 | 0.022 | 0.059 | 0.075 | 0.124 | 0.253 | 0.157 | 0.101 |
| $cD_6$ | $\sigma$ | 0.069 | 0.042 | 0.036 | 0.033 | 0.068 | 0.042 | 0.041 | 0.073 | 0.100 | 0.181 | 0.163 | 0.104 |
| $cD_5$ | $\mu$ | 0.139 | 0.044 | 0.030 | 0.131 | 0.092 | 0.017 | 0.107 | 0.093 | 0.239 | 0.205 | 0.151 | 0.117 |
| $cD_5$ | $\sigma$ | 0.141 | 0.035 | 0.035 | 0.103 | 0.111 | 0.016 | 0.074 | 0.093 | 0.180 | 0.146 | 0.150 | 0.123 |
| $cD_4$ | $\mu$ | 0.059 | 0.039 | 0.035 | 0.064 | 0.052 | 0.026 | 0.052 | 0.028 | 0.090 | 0.102 | 0.119 | 0.032 |
| $cD_4$ | $\sigma$ | 0.085 | 0.042 | 0.036 | 0.079 | 0.071 | 0.029 | 0.049 | 0.026 | 0.087 | 0.110 | 0.174 | 0.053 |

**Table 3.19:** Mean and standard deviation values of Multiscale energy features for Inferio-posterio-lateral MI at different ECG leads

| Sub-band | param. | I | II | III | aVR | aVL | aVF | V1 | V2 | V3 | V4 | V5 | V6 |
|---|---|---|---|---|---|---|---|---|---|---|---|---|---|
| $cA_6$ | $\mu$ | 0.097 | 0.020 | 0.041 | 0.059 | 0.072 | 0.020 | 0.052 | 0.088 | 0.060 | 0.073 | 0.041 | 0.046 |
| $cA_6$ | $\sigma$ | 0.090 | 0.018 | 0.039 | 0.059 | 0.063 | 0.020 | 0.042 | 0.066 | 0.053 | 0.072 | 0.052 | 0.060 |
| $cD_6$ | $\mu$ | 0.115 | 0.033 | 0.041 | 0.064 | 0.092 | 0.023 | 0.106 | 0.107 | 0.111 | 0.227 | 0.133 | 0.124 |
| $cD_6$ | $\sigma$ | 0.098 | 0.033 | 0.038 | 0.061 | 0.075 | 0.024 | 0.088 | 0.099 | 0.084 | 0.199 | 0.134 | 0.113 |
| $cD_5$ | $\mu$ | 0.161 | 0.057 | 0.029 | 0.163 | 0.098 | 0.019 | 0.151 | 0.123 | 0.243 | 0.225 | 0.158 | 0.144 |
| $cD_5$ | $\sigma$ | 0.119 | 0.051 | 0.026 | 0.129 | 0.075 | 0.018 | 0.113 | 0.106 | 0.221 | 0.193 | 0.165 | 0.145 |
| $cD_4$ | $\mu$ | 0.055 | 0.049 | 0.020 | 0.078 | 0.036 | 0.022 | 0.081 | 0.033 | 0.117 | 0.130 | 0.145 | 0.041 |
| $cD_4$ | $\sigma$ | 0.051 | 0.045 | 0.020 | 0.073 | 0.034 | 0.017 | 0.084 | 0.037 | 0.161 | 0.164 | 0.161 | 0.048 |

**Table 3.20:** p-value of multiscale energy features of different ECG leads for MI localization.

| SB | I | II | III | aVR | aVL | aVF | V1 | V2 | V3 | V4 | V5 | V6 |
|---|---|---|---|---|---|---|---|---|---|---|---|---|
| $cA_6$ | <0.001 | <0.001 | <0.001 | <0.001 | <0.001 | <0.001 | <0.001 | <0.001 | <0.001 | <0.001 | <0.001 | <0.001 |
| $cD_6$ | 0.003 | <0.001 | <0.001 | <0.001 | 0.005 | <0.001 | <0.001 | <0.001 | <0.001 | <0.001 | <0.001 | <0.001 |
| $cD_5$ | <0.001 | <0.001 | <0.001 | <0.001 | 0.037 | <0.001 | 0.003 | <0.001 | <0.001 | <0.001 | <0.001 | <0.001 |
| $cD_4$ | <0.001 | <0.001 | <0.001 | <0.001 | <0.001 | <0.001 | <0.001 | <0.001 | <0.001 | <0.001 | <0.001 | <0.001 |

The statistical significance of multiscale energy features for MI localization is evaluated using one-way ANOVA test [184]. The p-values of multiscale energy features for $cA_6$, $cD_6$, $cD_5$ and $cD_4$ sub-bands (SB) are shown in Table 3.20. It is observed that, all multiscale energy features of $cA_6$ and $cD_4$ sub-bands have p-value less than $0.001$. The T-wave and the ST-segment information of ECG are captured using $cA_6$ sub-band, and the $cD_4$ sub-band contains the high frequency information of QRS-complex. These clinical components show significant variations during different types of MI. This may be the reason for which the multiscale energy features of $cA_6$ and $cD_4$ sub-bands are highly significant. It is also seen that, out of $12$ features of both $cD_6$ and $cD_5$ sub-bands, $10$ features have p-value lower than $0.001$. These $10$ multiscale energy features of both $cD_6$ and $cD_5$ sub-bands are significant for localization of MI.

**Table 3.21:** Mean and standard deviation values of multiscale eigenvalue features for anterior MI and antero-lateral MI at different PCs.

| | Anterior MI | | | | | | Anterio-lateral MI | | | | | |
|---|---|---|---|---|---|---|---|---|---|---|---|---|
| | $\mathbf{A_6}$ Scale | | | | | | $\mathbf{A_6}$ Scale | | | | | |
| PC | PC1 | PC2 | PC3 | PC4 | PC5 | PC6 | PC1 | PC2 | PC3 | PC4 | PC5 | PC6 |
| $\mu$ | 7.724 | 3.224 | 0.895 | 0.124 | 0.014 | 0.003 | 7.405 | 3.187 | 1.162 | 0.180 | 0.038 | 0.010 |
| $\sigma$ | 1.035 | 0.993 | 0.490 | 0.105 | 0.015 | 0.003 | 1.050 | 0.962 | 0.575 | 0.166 | 0.055 | 0.019 |
| | $\mathbf{D_6}$ Scale | | | | | | $\mathbf{D_6}$ Scale | | | | | |
| $\mu$ | 7.887 | 3.513 | 0.535 | 0.038 | 0.010 | 0.002 | 8.553 | 2.794 | 0.454 | 0.118 | 0.043 | 0.015 |
| $\sigma$ | 1.096 | 1.101 | 0.506 | 0.088 | 0.031 | 0.007 | 1.420 | 1.113 | 0.437 | 0.204 | 0.094 | 0.036 |
| | $\mathbf{D_5}$ Scale | | | | | | $\mathbf{D_5}$ Scale | | | | | |
| $\mu$ | 8.033 | 3.122 | 0.648 | 0.116 | 0.039 | 0.014 | 8.029 | 2.816 | 0.750 | 0.218 | 0.096 | 0.047 |
| $\sigma$ | 1.205 | 0.827 | 0.639 | 0.283 | 0.113 | 0.045 | 1.512 | 1.174 | 0.517 | 0.296 | 0.175 | 0.096 |
| | $\mathbf{D_4}$ Scale | | | | | | $\mathbf{D_4}$ Scale | | | | | |
| $\mu$ | 6.463 | 3.008 | 1.651 | 0.554 | 0.202 | 0.068 | 6.074 | 2.752 | 1.620 | 0.818 | 0.381 | 0.197 |
| $\sigma$ | 1.186 | 0.547 | 0.516 | 0.397 | 0.148 | 0.066 | 1.104 | 0.505 | 0.428 | 0.320 | 0.209 | 0.176 |

**Table 3.22:** Mean and standard deviation values of multiscale eigenvalue features for anterio-septal MI and inferior MI at different PCs.

| | Anterio-septal MI | | | | | | Inferior MI | | | | | |
|---|---|---|---|---|---|---|---|---|---|---|---|---|
| | $\mathbf{A_6}$ Scale | | | | | | $\mathbf{A_6}$ Scale | | | | | |
| PC | PC1 | PC2 | PC3 | PC4 | PC5 | PC6 | PC1 | PC2 | PC3 | PC4 | PC5 | PC6 |
| $\mu$ | 7.377 | 3.215 | 1.108 | 0.231 | 0.044 | 0.008 | 8.178 | 3.037 | 0.664 | 0.085 | 0.016 | 0.004 |
| $\sigma$ | 1.231 | 0.773 | 0.681 | 0.230 | 0.052 | 0.016 | 1.177 | 1.020 | 0.502 | 0.088 | 0.015 | 0.004 |
| | $\mathbf{D_6}$ Scale | | | | | | $\mathbf{D_6}$ Scale | | | | | |
| $\mu$ | 8.310 | 3.084 | 0.505 | 0.063 | 0.017 | 0.005 | 8.143 | 3.548 | 0.250 | 0.033 | 0.008 | 0.002 |
| $\sigma$ | 1.204 | 1.146 | 0.466 | 0.137 | 0.049 | 0.019 | 0.984 | 1.013 | 0.331 | 0.079 | 0.021 | 0.008 |
| | $\mathbf{D_5}$ Scale | | | | | | $\mathbf{D_5}$ Scale | | | | | |
| $\mu$ | 8.273 | 2.863 | 0.657 | 0.141 | 0.035 | 0.011 | 8.745 | 2.825 | 0.314 | 0.069 | 0.021 | 0.007 |
| $\sigma$ | 1.312 | 1.021 | 0.445 | 0.177 | 0.056 | 0.021 | 1.255 | 1.110 | 0.412 | 0.127 | 0.055 | 0.024 |
| | $\mathbf{D_4}$ Scale | | | | | | $\mathbf{D_4}$ Scale | | | | | |
| $\mu$ | 5.795 | 3.244 | 1.797 | 0.711 | 0.279 | 0.102 | 6.288 | 3.333 | 1.534 | 0.537 | 0.187 | 0.066 |
| $\sigma$ | 1.036 | 0.609 | 0.527 | 0.302 | 0.130 | 0.064 | 1.219 | 0.658 | 0.637 | 0.247 | 0.112 | 0.051 |

The mean and the standard deviation values of multiscale eigenvalue features for anterior MI, anterio-lateral MI, anterio-septal MI, inferior MI, infero-lateral MI and inferio-posterior-lateral MI are shown in Table 3.21, Table 3.22 and Table 3.23, respectively. It is observed that, the mean and the standard deviation values of multiscale eigenvalue features are different for different principal components (PCs). For anterior MI, anterio-lateral MI and anterio-septal MI classes, the mean values of $\mathbf{A}_6$ scale eigenvalue features in PC1 are 7.72, 7.40 and 7.30, respectively. It is also seen that, for inferior MI, inferio-lateral MI and inferio-posterio-lateral MI classes, the mean values of the $\mathbf{D}_6$ scale eigenvalue features of (PC1, PC2, PC3) are (8.143, 3.548, 0.250), (8.757, 2.857, 0.333) and

**Table 3.23:** Mean and standard deviation values of multiscale eigenvalue features for Inferio-lateral MI and inferio-postero-lateral MI at different PCs.

| | Inferio-Lateral MI | | | | | | Inferio-posterio-lateral MI | | | | | |
|---|---|---|---|---|---|---|---|---|---|---|---|---|
| | $\mathbf{A_6}$ Scale | | | | | | $\mathbf{A_6}$ Scale | | | | | |
| PC | PC1 | PC2 | PC3 | PC4 | PC5 | PC6 | PC1 | PC2 | PC3 | PC4 | PC5 | PC6 |
| $\mu$ | 7.350 | 3.509 | 0.934 | 0.159 | 0.025 | 0.007 | 7.913 | 2.998 | 0.842 | 0.185 | 0.039 | 0.007 |
| $\sigma$ | 1.216 | 1.252 | 0.613 | 0.177 | 0.039 | 0.012 | 1.157 | 1.043 | 0.461 | 0.184 | 0.046 | 0.008 |
| | $\mathbf{D_6}$ Scale | | | | | | $\mathbf{D_6}$ Scale | | | | | |
| $\mu$ | 8.757 | 2.857 | 0.333 | 0.030 | 0.007 | 0.002 | 8.638 | 2.729 | 0.355 | 0.053 | 0.009 | 0.001 |
| $\sigma$ | 0.880 | 0.871 | 0.275 | 0.057 | 0.015 | 0.004 | 1.221 | 1.177 | 0.325 | 0.113 | 0.025 | 0.002 |
| | $\mathbf{D_5}$ Scale | | | | | | $\mathbf{D_5}$ Scale | | | | | |
| $\mu$ | 8.756 | 2.602 | 0.509 | 0.082 | 0.023 | 0.009 | 8.800 | 2.714 | 0.379 | 0.058 | 0.022 | 0.008 |
| $\sigma$ | 1.302 | 0.934 | 0.543 | 0.203 | 0.069 | 0.030 | 1.385 | 1.148 | 0.426 | 0.155 | 0.073 | 0.034 |
| | $\mathbf{D_4}$ Scale | | | | | | $\mathbf{D_4}$ Scale | | | | | |
| $\mu$ | 6.452 | 3.249 | 1.466 | 0.495 | 0.204 | 0.075 | 6.210 | 3.210 | 1.658 | 0.614 | 0.194 | 0.066 |
| $\sigma$ | 1.263 | 0.753 | 0.632 | 0.317 | 0.159 | 0.063 | 0.907 | 0.595 | 0.458 | 0.338 | 0.122 | 0.046 |

(8.638, 2.729, 0.355), respectively. Similar variations in the mean and standard deviation values are observed for multiscale eigenvalues in other PCs. The eigenvalues of $\mathbf{A}_6$ and $\mathbf{D}_6$ scales capture the inter-lead correlations of the low-frequency clinical components of multilead ECG. Similarly, the inter-lead correlations of high-frequency clinical components of multilead ECG are captured using the eigenvalues of $\mathbf{D}_5$ and $\mathbf{D}_4$ scales. The structure of covariance matrices are different for different types of MI cases. This may be the reason for different mean and standard deviation values of multiscale eigenvalue features for various types of MI.

**Table 3.24:** p-value of multiscale eigenspace features at different PCs for MI localization.

| Scale | PC1 | PC2 | PC3 | PC4 | PC5 | PC6 |
|---|---|---|---|---|---|---|
| $\mathbf{A}_6$ | $<$0.001 | 0.002 | $<$0.001 | $<$0.001 | $<$0.001 | $<$0.001 |
| $\mathbf{D}_6$ | $<$0.001 | $<$0.001 | $<$0.001 | $<$0.001 | $<$0.001 | $<$0.001 |
| $\mathbf{D}_5$ | $<$0.001 | 0.005 | $<$0.001 | $<$0.001 | $<$0.001 | $<$0.001 |
| $\mathbf{D}_4$ | $<$0.001 | $<$0.001 | $<$0.001 | $<$0.001 | $<$0.001 | $<$0.001 |

The statistical significance of multiscale eigenvalue features are evaluated using one-way ANOVA test [184]. The p-value of multiscale eigenvalue features are shown in Table 3.24. It is observed that, out of $24$ multiscale eigenvalue features, $22$ features have p-value less than 0.001. These $22$ multiscale eigenvalue features are statistically significant for MI localization. It is also seen that, all the eigenvalue features of $\mathbf{D}_6$ and $\mathbf{D}_4$ scales have p-value lower than 0.001. The QRS-complex characteristics of multilead ECG is different for different type of MI cases [1]. These pathological

changes may alter the structure of the covariance matrices of $\mathbf{D}_6$ and $\mathbf{D}_4$ scales. This may be the reason for which all the eigenvalue features of $\mathbf{D}_6$ and $\mathbf{D}_4$ scales are statistically significant for localization of MI.

**Table 3.25:** Confusion matrix of multiclass SVM with linear kernel for MI localization

| Actual | Predicted | | | | | |
|---|---|---|---|---|---|---|
| | AMI | ALMI | ASMI | IMI | ILMI | IPLMI |
| AMI | 111 | 1 | 3 | 0 | 0 | 6 |
| ALMI | 2 | 114 | 4 | 0 | 1 | 0 |
| ASMI | 3 | 9 | 105 | 1 | 2 | 1 |
| IMI | 2 | 0 | 0 | 115 | 3 | 1 |
| ILMI | 2 | 0 | 0 | 1 | 116 | 2 |
| IPLMI | 3 | 1 | 6 | 6 | 0 | 105 |

### 3.3.4 MI Localization Performance

In this subsection, the performance of multiclass SVM classifier is shown for MI localization. First, the hold-out cross-validation method is used for selection of training and test instances of multiclass SVM classifier. For training, $100$ instances from each class of MI are considered. A total of 726 unknown instances are evaluated in the testing phase. Table 3.25 and Table 3.26 show the confusion matrix for both linear and RBF kernel based multiclass SVM classifiers. It is observed that, the number of true positives are more in RBF kernel multiclass SVM than that of linear kernel multiclass SVM classifiers. The overall accuracy (OA) of RBF kernel multiclass SVM classifier is found to be 99.58%, which is more than that of linear kernel multiclass SVM classifier (OA=91.73%).

**Table 3.26:** Confusion matrix of multiclass SVM with RBF kernel for MI localization

| Actual | Predicted | | | | | |
|---|---|---|---|---|---|---|
| | AMI | ALMI | ASMI | IMI | ILMI | IPLMI |
| AMI | 121 | 0 | 0 | 0 | 0 | 0 |
| ALMI | 1 | 119 | 0 | 0 | 0 | 1 |
| ASMI | 0 | 0 | 121 | 0 | 0 | 0 |
| IMI | 0 | 0 | 0 | 121 | 0 | 0 |
| ILMI | 0 | 0 | 0 | 0 | 121 | 0 |
| IPLMI | 0 | 0 | 0 | 1 | 0 | 120 |

For 5-fold cross validation case, $726$ instances from each class of MI are used. Table 3.27 shows the MI localization accuracy of multiclass SVM classifier with linear and RBF kernel considering all

**Table 3.27:** Overall Accuracy (OA) value of multiclass SVM classifier over each Fold for MI Localization

| Features | Classifiers | Fold1 | Fold2 | Fold3 | Fold4 | Fold5 | Average OA (%) |
|---|---|---|---|---|---|---|---|
| Energy | SVM-RBF | 98.07% | 95.45% | 96.83% | 96.69% | 97.93% | 97.00% |
| Eigenspace | SVM-RBF | 92.56% | 94.07% | 94.62% | 92.97% | 93.80% | 93.60% |
| All Features | SVM-Lin | 90.86% | 92.53% | 92.71% | 89.56% | 91.28% | 91.38% |
| All Features | SVM-RBF | 98.67% | 99.23% | 99.45% | 99.28% | 99.74% | 99.27% |
| CFS | SVM-Lin | 92.17% | 93.24% | 93.79% | 93.84% | 93.58% | 93.32% |
| CFS | SVM-RBF | 99.54% | 99.78% | 99.62% | 99.57% | 99.81% | 99.66% |

features and feature subset using CFS along each fold. The highest average OA of $99.66\%$ is found using multiclass SVM with RBF kernel for feature set using CFS. For MI localization case, the SVM classifier with RBF kernel produces an average OA value of 97% for the multiscale energy features. When the multiscale eigenspace features are used, the SVM classifier shows an average OA of 93.60%. The average OA value for combined multiscale energy and eigenspace features is 99.27% which is higher than the performance of individual feature sets. The higher OA values obtained using CFS is due to the elimination of redundant features. The above observations infer that, the proposed MEES approach is effective to localize MI using 12 lead ECG.

## 3.4 Summary

In this chapter, the multiscale energy and eigenspace (MEES) approach is proposed for detection and localization of MI from multilead ECG. The existing methods for MI detection are based on few ECG leads, which are expected to have MI characteristics. The proposed MEES approach for detection and localization of MI doesn't require any prior information about the pathologies in multilead ECG. The proposed approach is based on the evaluation of multiscale energy and eigenspace features of multilead ECG. Analysis with number of multilead ECG data shows that the multiscale energy and eigenvalue features are capable of not only discriminating HC and MI, but also they can differentiate between different types of MI pathologies.

For MI detection, the multilead ECG frames are used. The performance of multiscale energy and eigenvalue features of multilead ECG frames are evaluated using KNN and SVM classifiers. The SVM classifier with RBF kernel function has an accuracy value of $96\%$ for MI detection using multiscale

energy and eigenvalue features. For localization, the MI detected multilead ECG frame is divided into multilead beat matrices. Various pathological MI cases such as anterior MI, anterio-lateral MI, anterio-septal MI, inferior MI, inferio-lateral MI and inferio-posterio-lateral MI are used for localization. The multiscale energy and eigenvalue features are evaluated from the multilead ECG beat matrix. A localization accuracy of $99.58\%$ is found using multiclass SVM classifier and MEES features. The proposed method is simpler compared to the existing methods for MI detection. This method does not require prior detection of ST-segment.

# 4

# Complex Wavelets for Detection of BBB, HMD and MI

## Contents

The life-debilitating cardiac ailments occur due to improper conduction (bundle branch block), obstruction in one of the coronary arteries (myocardial infarction), and abnormal heart muscle (hypertrophic cardiomyopathy) [1]. In clinical setting, the cardiologist uses serial recording with multiple number of electrodes for diagnosis of these pathologies [1] [12] [16]. This shows the importance of the 12-lead or multilead ECG for detection of myocardial infarction (MI), bundle branch block (BBB) and heart muscle diseases (HMD). In Chapter 3, the multiscale features of multilead ECG have been proposed for detection and localization of MI. The discrete wavelet transform (DWT) has been used for evaluation of the multiscale features of multilead ECG. The DWT has the limitations such as the shift variant, the oscillatory characteristics and the aliasing effect of the wavelet coefficients [67]. The dual tree complex wavelet transform (DTCWT) overcomes the limitations of DWT with its basis properties such as the non-oscillatory magnitude of the wavelet coefficients, the shift invariant and the substantial reduction of the aliasing effect [67]. The other advantage of DTCWT is that, in addition to magnitude information, an extra information (phase information) is obtained using the DTCWT of ECG signal. The phase captures the temporal information of a time-series [178]. The duration parameters of ECG show significant variations during cardiac arrhythmia [1]. It is expected that, the complex wavelet phase can capture the pathological variations in the clinical components of ECG during cardiac abnormalities. In this chapter, two new methods for detection and classification of BBB, MI and HMD from multilead ECG are proposed. These methods are based on the evaluation of diagnostic features from the complex wavelet coefficients of multilead ECG. The dual tree complex wavelet transform (DTCWT) decomposes the multilead ECG signal into complex wavelet coefficients at different sub-bands. The clinical components of multilead ECG can be captured using the complex wavelet coefficients of different scales. In BBB, the pathological variations (as shown in Fig. 1.7) such as the wide QRS-complex pattern, the depression in ST-segment and the T-wave inversion are observed in different ECG leads [1]. The pathological signatures of hypertrophic cardiomyopathy (as shown in Fig. 1.6) are the appearance of deep T-wave inversion and the depression of ST-segment in different leads [16]. These pathological variations may alter the characteristics of the complex wavelet coefficients of multilead ECG. The features evaluated from the complex wavelet coefficients of multilead ECG at different sub-bands can be used for detection and classification of BBB, MI and HMD pathologies. The literature survey in chapter 2 shows that, the absolute value of the complex

wavelet coefficients of QRS-complex has been used for detection of ventricular arrhythmia and BBB from single lead ECG [51]. The complex wavelet magnitude and phase features of multilead ECG have not been used for detection of BBB, HMD and MI pathologies. The magnitude and phase features of multilead ECG evaluated in DTCWT domain have the potential to capture the pathological variations. This motivates us to use the complex wavelet magnitude and phase features of multilead ECG for detection of various cardiac ailments.

In first method, the multiscale phase alternation (PA) features of multilead ECG are proposed for detection and classification of BBB, HMD and MI. These features are evaluated from the phase of the complex wavelet coefficients of multilead ECG at different scales. The performance of the multiscale PA features is evaluated using KNN and fuzzy KNN classifiers. In second method, the complex wavelet sub-band bi-spectrum (CWSB) features are proposed for detection and classification of BBB, HMD and MI pathologies. The higher order complex wavelet analysis (HOCWA) is used to evaluate the complex wavelet bi-spectrum of each ECG lead at different scales. The magnitude and the phase features are computed from the CWSB of multilead ECG. The symmetrical uncertainty (SU) based feature selection approach is used for choosing few attributes from the complex wavelet magnitude and phase features of multilead ECG. The SVM and the ELM classifiers are used for detection and classification of BBB, MI and HMD pathologies from the magnitude and phase features of CWSB. The rest of this chapter is organized as follows. In Section 4.1, the analysis of multilead ECG using DTCWT is described. The proposed methods for evaluation of the complex wavelet magnitude and phase features of multilead ECG and the detection of cardiac ailments are discussed in Section 4.2. The methods are evaluated using the multilead ECG signals in Section 4.3. The summary of this chapter is drawn in Section 4.4.

## 4.1 Analysis of Multilead ECG using DTCWT

The analysis of ECG signal using DTCWT produces complex wavelet coefficients in different sub-bands. For 'L' levels decomposition of ECG signal $\mathbf{x}(n)$, the complex wavelet coefficients in approximation sub-band, $cA_L(k)$ and $l^{\text{th}}$ detail sub-band, $cD_l(k)$ are computed using equation 2.10, equation 2.11, equation 2.12 and equation 2.13, respectively. For a multilead ECG signal, $\mathbf{x}^m(n)$ the complex

wavelet coefficients of the approximation sub-band and the $l^{\text{th}}$ detail sub-band are evaluated as

$$cA_L^m(k) = \tilde{cA}_L^m(k) + j\ \overline{cA}_L^m(k) \tag{4.1}$$

$$cD_l^m(k) = \tilde{cD}_l^m(k) + j\ \overline{cD}_l^m(k) \tag{4.2}$$

where $m$ corresponds to the lead number in multilead ECG and $l = 1, 2..., L$ is the number of detail sub-bands. The magnitude of the complex wavelet coefficients in approximation sub-band and $l^{\text{th}}$ detail sub-band are evaluated as

$$|cA_L^m(k)| = \sqrt{[\tilde{cA}_L^m(k)]^2 + [\overline{cA}_L^m(k)]^2} \tag{4.3}$$

$$|cD_l^m(k)| = \sqrt{[\tilde{cD}_l^m(k)]^2 + [\overline{cD}_l^m(k)]^2} \tag{4.4}$$

Similarly, the phase of the complex wavelet coefficients in approximation sub-band and $l^{\text{th}}$ detail sub-band are given by

$$\phi_{cA_L}^m(k) = tan^{-1}[\frac{\overline{cA}_L^m(k)}{\tilde{cA}_L^m(k)}] \tag{4.5}$$

$$\phi_{cD_l}^m(k) = tan^{-1}[\frac{\overline{cD}_l^m(k)}{\tilde{cD}_l^m(k)}] \tag{4.6}$$

The significant sub-bands of multilead ECG are selected using the complex wavelet energy values. The energy due to the complex wavelet coefficients of the approximation sub-band and the $l^{\text{th}}$ detail sub-band for $m^{\text{th}}$ ECG lead are given by

$$E_{cA_L}^m = \frac{1}{N_L}\sum_{k=1}^{N_L}[(\tilde{cA}_L^m(k))^2 + (\overline{cA}_L^m(k))^2] \tag{4.7}$$

$$E_{cD_l}^m = \frac{1}{N_l}\sum_{k=1}^{N_l}[(\tilde{cD}_l^m(k))^2 + (\overline{cD}_l^m(k))^2] \tag{4.8}$$

where $N_L$ and $N_l$, $l = 1, 2, 3, ...., L$ are the length of the approximation sub-band and the $l^{\text{th}}$ detail sub-band, respectively. The average complex wavelet energy of all ECG leads in different sub-bands for healthy control (HC), MI, BBB and HMD cases are shown in Fig. 4.1. In this work, six decomposition levels are considered for DTCWT based analysis of multilead ECG. It is observed that, the $cA_6$, $cD_6$, $cD_5$ and $cD_4$ sub-bands have higher energy values than $cD_3$, $cD_2$ and $cD_1$ sub-bands. The lead V5

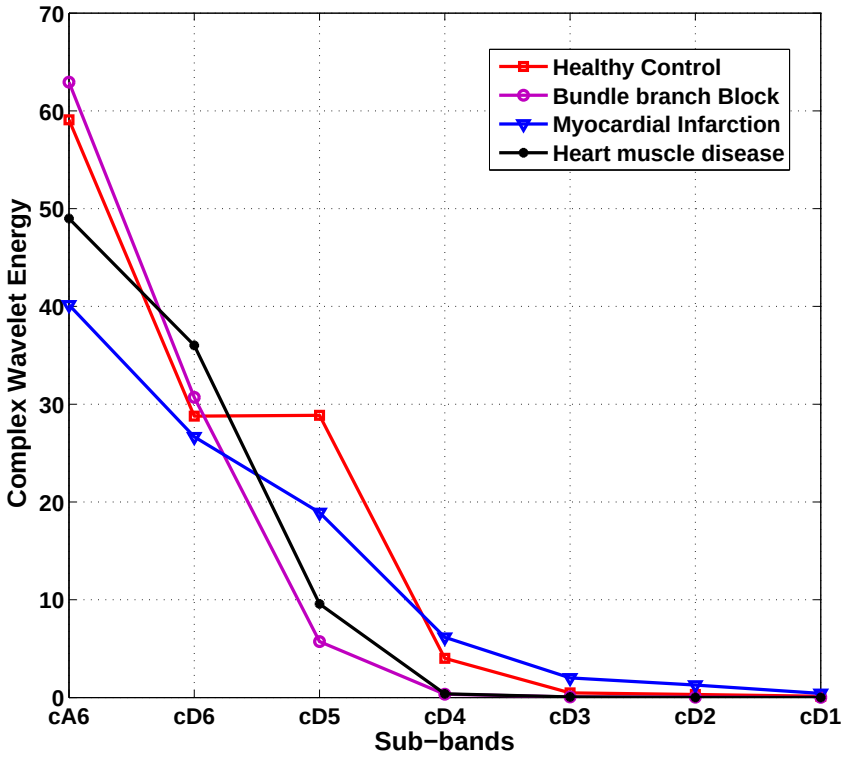


**Fig. 4.1:** Average energy of complex wavelet sub-band for all ECG leads.

ECG signal for HC is shown in Fig. 4.2 (a). The spectrum of this signal is shown in Fig. 4.2 (b). The signals reconstructed using the complex wavelet coefficients of $cA_6$, $cD_6$, $cD_5$ sub-bands are shown in Fig. 4.2 (c), Fig. 4.2 (e) and Fig. 4.2 (g), respectively. Fig. 4.2 (d), Fig. 4.2 (f) and Fig. 4.2 (h) show the spectra of $cA_6$, $cD_6$, $cD_5$ sub-band signals. Similarly, the $cD_4$, $cD_3$, $cD_2$ and $cD_1$ sub-band signals and their spectra are shown in Fig. 4.3. It is observed that, the morphological features of ECG signal are segregated in the first four sub-bands ($cA_6$, $cD_6$, $cD_5$ and $cD_4$) whereas, the other sub-bands (cD3, cD2 and cD1) don't contain significant information. The spectral content of T-wave of ECG signal is characterized within a frequency of 0.5 Hz to 10 Hz [180]. Similarly, the P-wave spectral information is grossly present in the frequency range from 5 Hz to 30 Hz [180]. Likewise, the frequency range from 8 Hz to 50 Hz contains the QRS-complex spectral information of ECG [180]. It is observed that, the cD6, cD5 and cD4 sub-band signals of ECG grossly capture the QRS-complex information. The information of ST-segment, the T-wave and the low-frequency components of P-

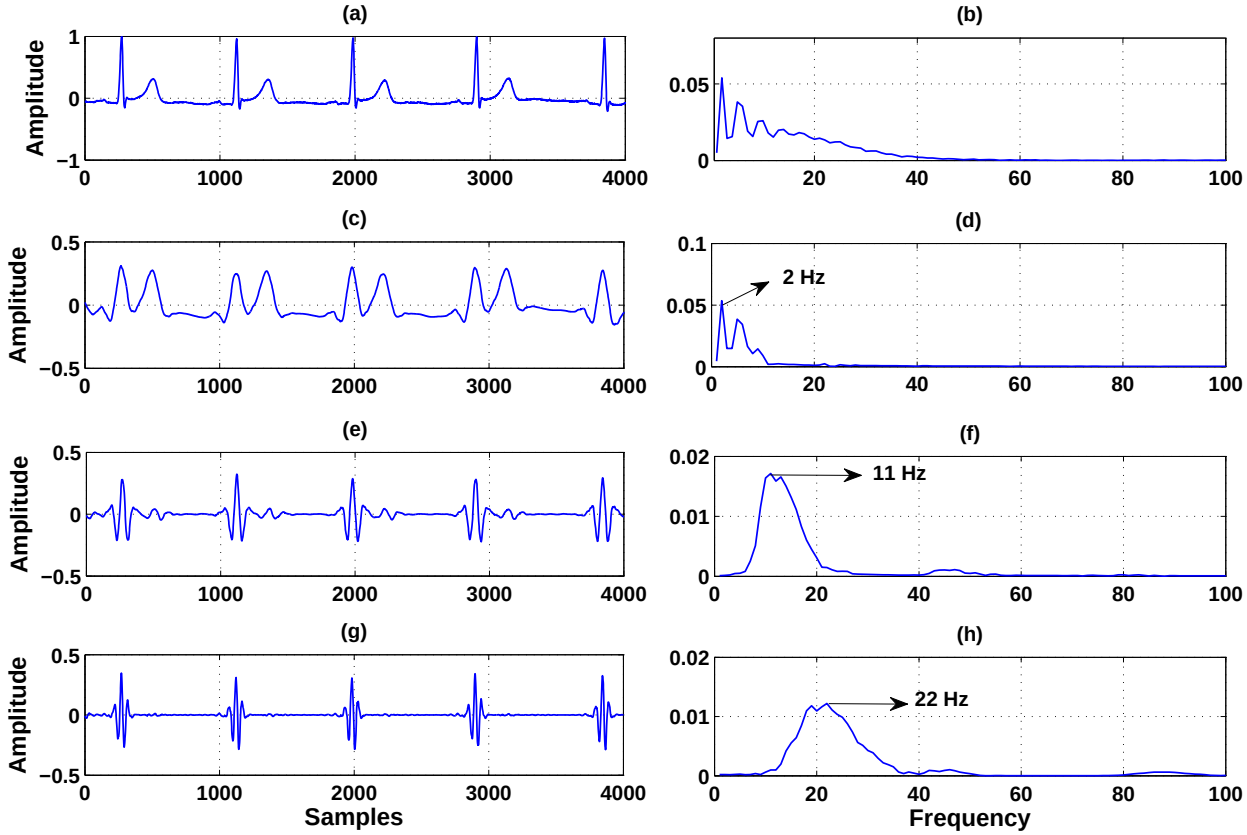


**Fig. 4.2:** (a) Lead V5 ECG signal for HC. The amplitude of the ECG signal is in mV and the sampling frequency is 1000 Hz. (b) Spectrum of lead V5 ECG signal. (c) Signal reconstructed using $cA_6$ sub-band complex wavelet coefficients. (d) Spectrum of $cA_6$ sub-band signal. (e) Signal reconstructed using $cD_6$ sub-band complex wavelet coefficients. (f) Spectrum of $cD_6$ sub-band signal. (g) Signal reconstructed using $cD_5$ sub-band complex wavelet coefficients. (g) Spectrum of $cD_5$ sub-band signal.

wave are observed in cA6 sub-band signal. Similarly, the high-frequency components of P-wave are captured using cD6 and cD5 sub-band signals. In this work, the wavelet coefficients of $cA_6$, $cD_6$, $cD_5$ and $cD_4$ sub-bands are considered for evaluation of complex wavelet magnitude and phase features.

In this study, the advantage of DTCWT based processing of ECG signal over DWT is investigated. The additive white Gaussian noises (AWGN) with different SNR values (16db, 6db and -3db) are added to the ECG signal. The synthetic ECG signal for lead I and the noisy ECG signal (ECG signal with AWGN of SNR=16 dB) are shown in Fig. 4.4 (a) and Fig. 4.4 (b), respectively. The DTCWT and the DWT are applied to the noisy ECG signals. Six levels of wavelet decomposition are considered for both DTCWT and DWT cases. The signals are reconstructed from the wavelet coefficients of $cA_6$, $cD_6$, $cD_5$ and $cD_4$ sub-bands using the inverse DWT (IDWT) and the inverse DTCWT (IDTCWT). The

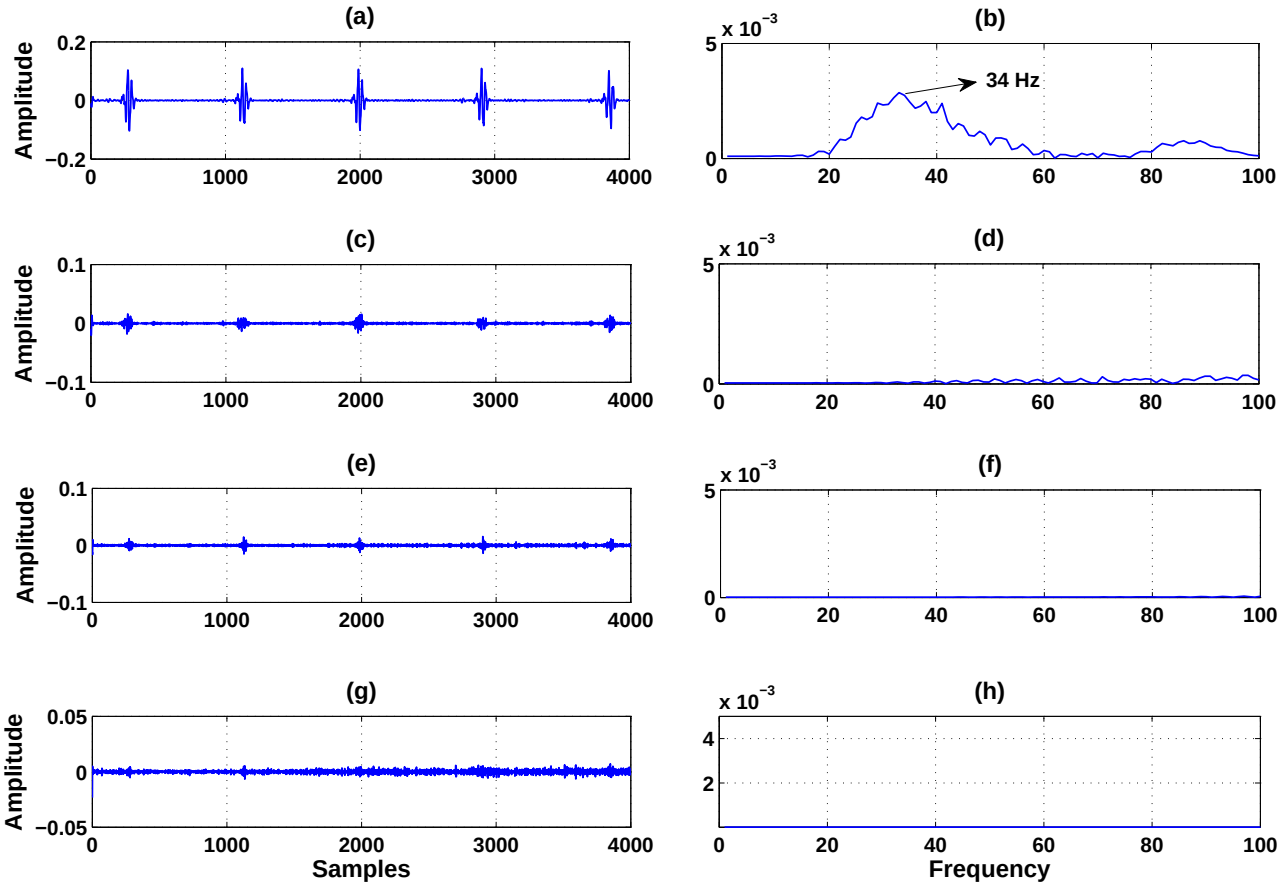


**Fig. 4.3:** (a) Signal reconstructed using $cD_4$ sub-band complex wavelet coefficients. (b) Spectrum of $cD_4$ sub-band signal. (c) Signal reconstructed using $cD_3$ sub-band complex wavelet coefficients. (d) Spectrum of $cD_3$ sub-band signal. (e) Signal reconstructed using $cD_2$ sub-band complex wavelet coefficients. (f) Spectrum of $cD_2$ sub-band signal. (g) Signal reconstructed using $cD_1$ sub-band complex wavelet coefficients. (h) Spectrum of $cD_1$ sub-band signal.

IDWT and the IDTCWT based reconstructed ECG signals are depicted in Fig. 4.4 (c) and Fig. 4.4 (d), respectively. The percentage root mean square difference (PRD) and the weighted diagnostic distortion (WDD) [8] values are evaluated for reconstructed ECG signals. It is observed that, for 6db SNR case, the PRD and the WDD values of the IDTCWT based reconstructed signal are 15.85% 2.33%, respectively. These values are less than the PRD and the WDD values (16.85% and 3.74%) of IDWT based reconstructed ECG signal. For other SNR cases, the PRD and the WDD values of IDTCWT based reconstructed ECG signal are less than the IDWT based reconstructed ECG. The lower WDD value implies that, the loss of clinical information in DTCWT based processing of ECG signal is lower than the DWT based processing of ECG. The DTCWT overcomes the shortcomings of

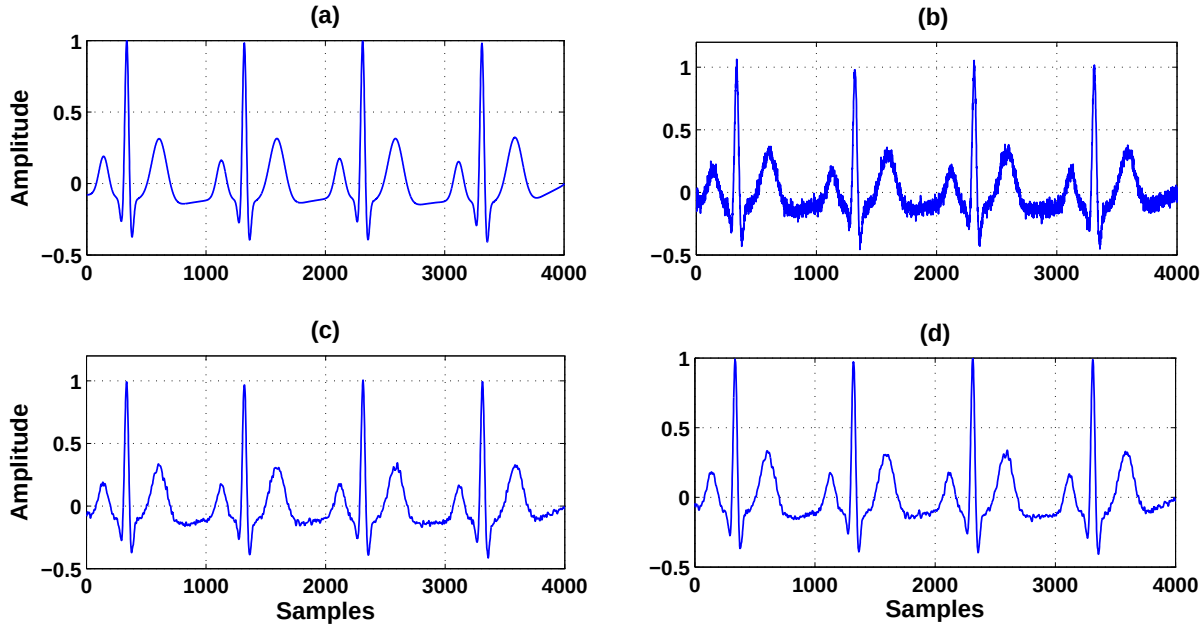


**Fig. 4.4:** (a) Synthetic ECG signal for lead I. The amplitude of the ECG signal is in mV and the sampling frequency is 1000 Hz. (b) ECG signal with AWGN noise. (c) Signal reconstructed using wavelet coefficients of $cA_6$, $cD_6$, $cD_5$ and $cD_4$ sub-bands. (d) Signal reconstructed using complex wavelet coefficients of $cA_6$, $cD_6$, $cD_5$ and $cD_4$ sub-bands.

DWT [67]. This may be the reason for which the PRD and the WDD values are less for IDTCWT based reconstructed ECG signal. The above observations motivate us to use DTCWT of multilead ECG for evaluation of complex wavelet magnitude and phase features. The following section describes the proposed methods for detection of MI, HMD and BBB pathologies from multilead ECG.

## 4.2 Proposed Methods for Detection of Cardiac Ailments

The block-diagrams of the proposed methods for detection of cardiac ailments such as BBB, HMD and MI are shown in Fig. 4.5 (a) and Fig. 4.5 (b), respectively. Each block-diagram consists of preprocessing, evaluation of diagnostic features from the complex wavelet coefficients of multilead ECG and classification of cardiac ailments. The preprocessing step consists of both filtering and segmentation of multilead ECG data. The baseline-wandering noise is eliminated using a zero phase Butterworth high-pass filter with a cutoff frequency of $0.5$Hz [25]. The high-frequency noise is filtered out based on the elimination of the complex wavelet coefficients from diagnostically irrelevant sub-bands ($cD_3$,

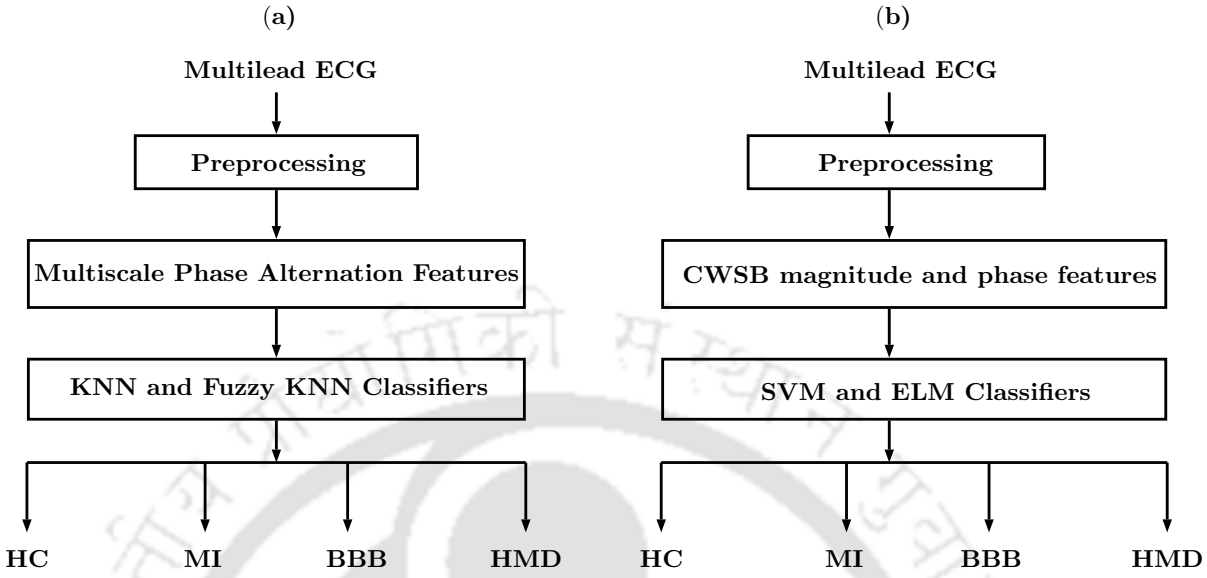


**Fig. 4.5:** (a) Block diagram of proposed method for detection of cardiac ailments using multiscale PA features. (b) Block diagram of proposed method for detection of cardiac abnormalities using CWSB magnitude and phase features.

$cD_2$ and $cD_1$ sub-bands). After filtering, the frame based segmentation of multilead ECG data is done using a window of size $4096 \times 12$. The frame based segmentation is used based on the following reasons. In clinical standard, cardiologist recommends serial recording of ECG data from 12-number of electrodes for detection of cardiac arrhythmia [12] [16]. The window used in this work for frame based segmentation contains at-least four cycles of multilead ECG. The intra-beat, inter-lead and inter-beat correlations are captured using the frame based processing of multilead ECG. After preprocessing, the complex wavelet coefficients of multilead ECG at different sub-bands are evaluated. The first method for detection of cardiac ailments is based on the evaluation of multiscale PA features from the complex wavelet coefficients of multilead ECG. In second method, the CWSB magnitude and phase features of multilead ECG are evaluated using HOCWA. The following subsections briefly describe the evaluation of the multiscale PA features and the CWSB features of multilead ECG.

### 4.2.1 Multiscale Phase Alternation Features

The complex wavelet coefficients of $cA_6$, $cD_6$, $cD_5$ and $cD_4$ sub-bands capture the significant diagnostic components of multilead ECG. In this work, the phases of $cA_6$, $cD_6$, $cD_5$ and $cD_4$ sub-bands of each ECG lead are considered for evaluation of multiscale PA features. Fig. 4.6 (a) and Fig. 4.6 (b)

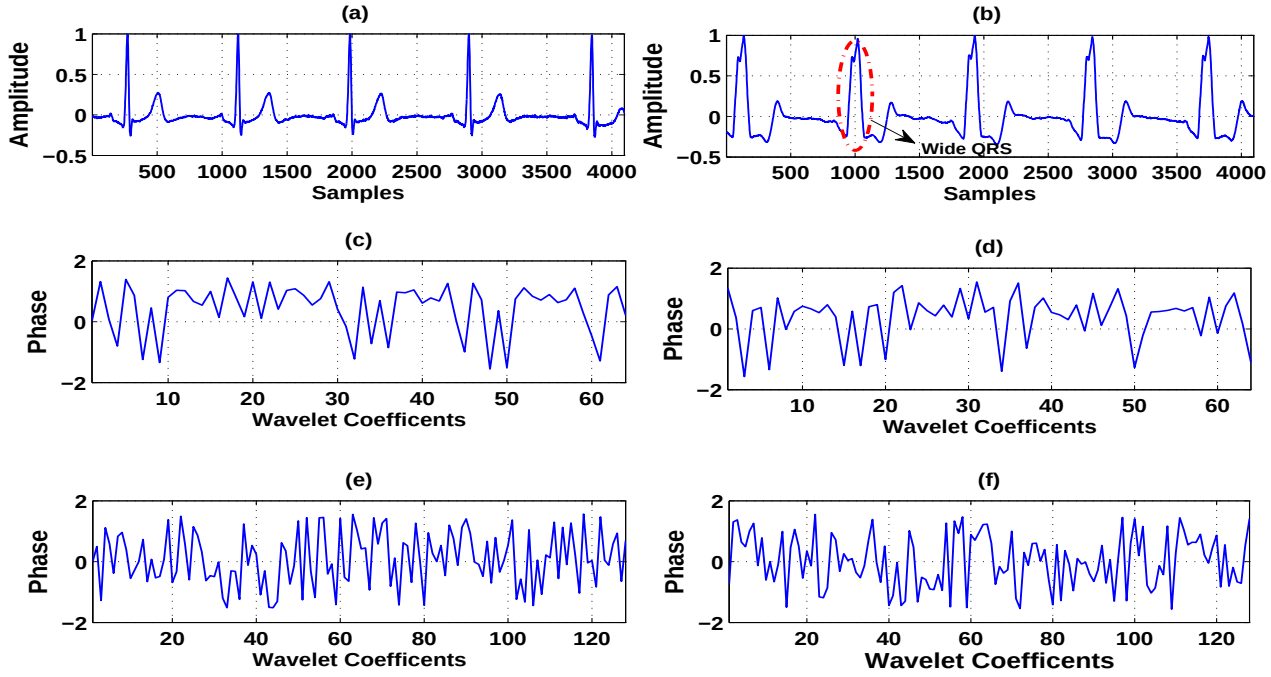


**Fig. 4.6:** (a) Lead V6 ECG signal for HC. (b) Lead V6 ECG signal for BBB. The amplitude of each ECG signal is in mV and the sampling frequency is 1000 Hz. (c) Phase of $cA_6$ sub-band for HC. (d) Phase of $cA_6$ sub-band for BBB. (e) Phase of $cD_5$ sub-band for HC. (f) Phase of $cD_5$ sub-band for BBB. The unit of phase is radian (rad).

depict the lead V6 ECG signals for HC and BBB cases. The wide QRS-complexes are observed for BBB case along each beat. The lead V6 ECG signals for HMD and MI cases are shown in Fig. 4.7 (a) and Fig. 4.7 (b), respectively. The T-wave inversion (Inv) and the ST-segment depression (Dep) are observed for HMD (cardiomyopathy) class. The ST-segment elevation (ELV) and the T-wave inversion in each beat are also seen for MI pathology. The phases of $cA_6$ and $cD_5$ sub-bands for HC and BBB are shown in Fig. 4.6 (c)-(d) and Fig. 4.6 (e)-(f), respectively. Similarly, for HMD and MI cases the phases of $cA_6$ and $cD_5$ sub-bands are depicted in Fig. 4.7 (c)-(d) and Fig. 4.7 (e)-(f), respectively. It is observed that, the phase characteristics of $cA_6$ and $cD_5$ sub-bands in lead V6 are different for pathological cases (HMD, BBB and MI) and HC. Similar variations in the phase characteristics are observed for $cD_6$ and $cD_4$ sub-bands of other leads. These variations in the multiscale phase can be used for classification of cardiac abnormalities. In this work, an algorithm for evaluation of multiscale PA features is proposed for ECG signal. This algorithm is presented as follows.

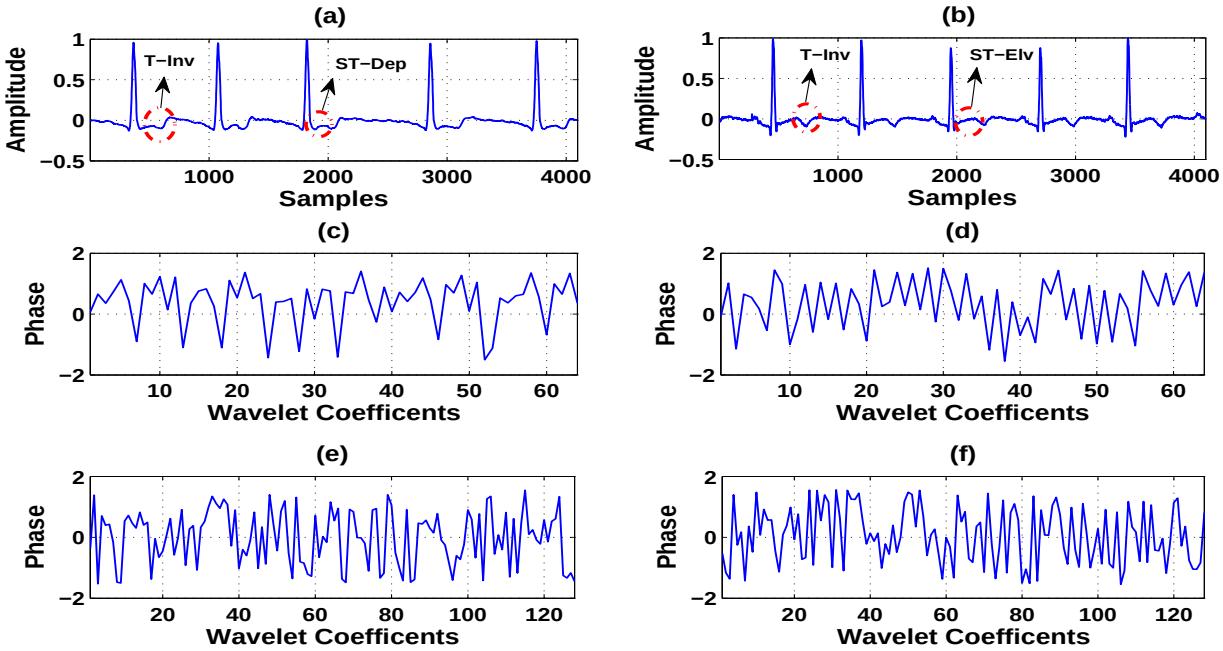


**Fig. 4.7:** (a) Lead V6 ECG signal for HMD (cardiomyopathy). (b) Lead V6 ECG signal for MI. The amplitude of each ECG signal is in mV and the sampling frequency is 1000 Hz. (c) Phase of $cA_6$ sub-band for HMD. (d) Phase of $cA_6$ sub-band for MI. (e) Phase of $cD_5$ sub-band for HMD. (f) Phase of $cD_5$ sub-band for MI. The unit of phase is radian (rad).

***Algorithm (Evaluation of multiscale PA features)***

***Input***: Phase of the complex wavelet sub-bands: $\phi_{\mathbf{d}}(k)$. where $\mathbf{d} \in (cA_6, cD_6, cD_5, cD_4)$ is the diagnostically significant sub-bands.

***Output***: phase alternation features of $\mathbf{d}^{\text{th}}$ sub-band: $PA_{\mathbf{d}}$.

***begin***

- Length (number of wavelet coefficients) of the $\mathbf{d}^{\text{th}}$ sub-band of each ECG lead is given as, $n_{\mathbf{d}}$=length($\phi_{\mathbf{d}}(k)$).
- Then, $\phi 1_{\mathbf{d}}(i)$ and $\phi 2_{\mathbf{d}}(i)$, $1 \leq i \leq n_{\mathbf{d}} - 1$ are evaluated as $\phi 1_{\mathbf{d}}(i) = \phi_{\mathbf{d}}(1 : n_{\mathbf{d}} - 1)$ and $\phi 2_{\mathbf{d}}(i) = \phi_{\mathbf{d}}(2 : n_{\mathbf{d}})$.
- Phase ratio (PR) of $\mathbf{d}^{\text{th}}$ sub-band, $PR_{\mathbf{d}}(i)$ is evaluated as

$$PR_{\mathbf{d}}(i) = \frac{\phi 1_{\mathbf{d}}(i)}{\phi 2_{\mathbf{d}}(i)} \tag{4.9}$$

- Then, the indices ($i$) of the $\mathbf{d}^{\text{th}}$ sub-band are found out using the condition, $PR_{\mathbf{d}}(i) < 0$.
- The total number of indices of the $\mathbf{d}^{\text{th}}$ sub-band is counted and it is denoted as, $g_{\mathbf{d}}$.
- PA feature of $\mathbf{d}^{\text{th}}$ sub-band is defined as the total number of indices, $PA_{\mathbf{d}} = g_{\mathbf{d}}$.

***end***

For $\mathbf{d}^{\text{th}}$ sub-band of $m^{\text{th}}$ ECG lead, the multiscale PA feature is denoted as, $PA^{m}_{\mathbf{d}}$. Here, the PA features of $cA_6$, $cD_6$, $cD_5$ and $cD_4$ sub-bands of each ECG lead are evaluated. The PA values of $cA6$ sub-band of lead V6 for HC, MI, HMD and BBB cases are $20$, $22$, $27$ and $37$, respectively. Similarly, for HC, MI, HMD and BBB cases, the PA values are $24$, $29$, $26$ and $28$ in $cD_6$ sub-band. For $cD_5$ and $cD_4$ sub-bands, similar changes in the PA features along each lead are observed for HC and cardiac abnormalities such as HMD, MI and BBB. The temporal information of a time series data is captured using phase [178]. The duration parameters (P-interval, PR-interval, QRS-interval, QT-interval, T-interval ) of the clinical components (P-wave, QRS-complex and T-wave) of multilead ECG are different for HC and pathological cases [1]. These pathological changes can be captured using multiscale PA features. This may be the reason for different PA values of HC, MI, HMD and BBB cases in $cA_6$, $cD_6$, $cD_5$ and $cD_4$ sub-bands of each ECG lead. In this work, $12$ PA features from the complex wavelet coefficients of each sub-band of multilead ECG are evaluated. The $12$ $cA_6$, $12$ $cD_6$, $12$ $cD_5$, $12$ $cD_4$ sub-bands PA features are combined to produce a $48$ dimensional multiscale PA feature vector. The $48$ dimensional multiscale PA feature vector is used for detection of cardiac abnormalities.

### 4.2.2 CWSB Magnitude and Phase Features

The complex wavelet sub-band bi-spectrum (CWSB) magnitude and phase features are evaluated using higher order complex wavelet analysis (HOCWA) of multilead ECG. The complex wavelet bi-spectrum of $\mathbf{d}^{\text{th}}$ sub-band, $\mathbf{d} \in (cA_6, cD_6, cD_5, cD_4)$ of $m^{\text{th}}$ ECG lead is defined as

$$\mathbf{B}^{m}_{\mathbf{d}}(k1, k2) = E[\mathbf{d}^{m}(k1)\mathbf{d}^{m}(k2)\mathbf{d}^{\star m}(k1 + k2)] \tag{4.10}$$

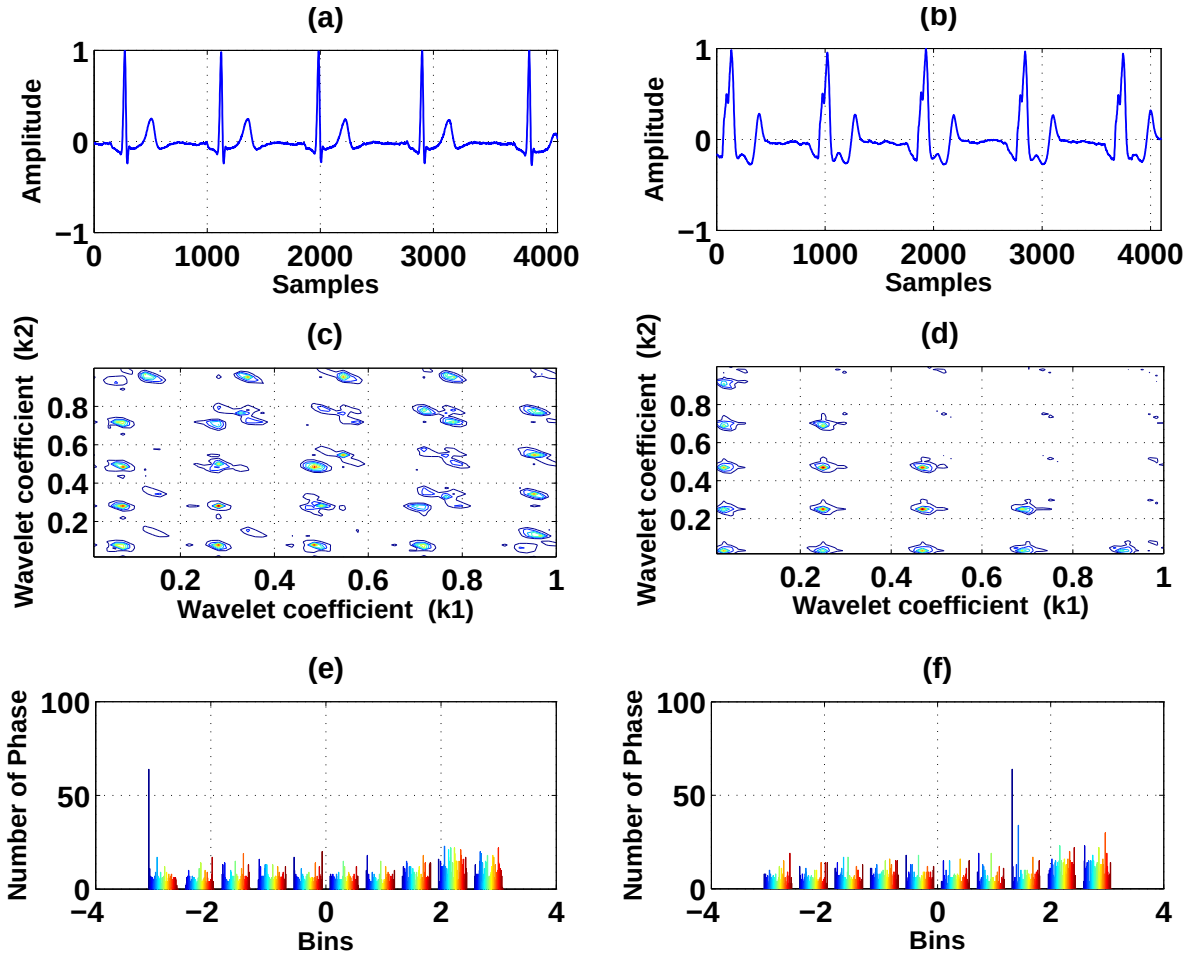


**Fig. 4.8:** (a) Lead V5 signal for HC. (b) Lead V5 signal for BBB pathogical case. The amplitude of each ECG signal is in mV and the sampling frequency is 1000 Hz. (c) Magnitude contour of the $cA_6$ sub-band bi-spectrum of HC. (d) Magnitude contour of the $cA_6$ sub-band bi-spectrum of BBB. (e) Histogram of the phase of $cA_6$ sub-band bi-spectrum for HC. (f) Histogram of the phase of $cA_6$ sub-band bi-spectrum for BBB.

where, '$E$' is the expectation operator and $1 \leq k1 \leq N_{\mathbf{d}}$, $1 \leq k2 \leq N_{\mathbf{d}}$. $N_{\mathbf{d}}$ is the number of wavelet coefficients of $\mathbf{d}^{\text{th}}$ sub-band. The analytic form of CWSB is given by

$$\mathbf{B}_{\mathbf{d}}^{m}(k1,k2) = \tilde{\mathbf{B}}_{\mathbf{d}}^{m}(k1,k2) + j\overline{\mathbf{B}}_{\mathbf{d}}^{m}(k1,k2) \tag{4.11}$$

The magnitude of the complex wavelet bi-spectrum of $\mathbf{d}^{\text{th}}$ sub-band of $m^{\text{th}}$ ECG lead is defined as

$$\mathbf{M}_{\mathbf{d}}^{m}(k1,k2) = \sqrt{[\tilde{\mathbf{B}}_{\mathbf{d}}^{m}(k1,k2)]^2 + [\overline{\mathbf{B}}_{\mathbf{d}}^{m}(k1,k2)]^2} \tag{4.12}$$

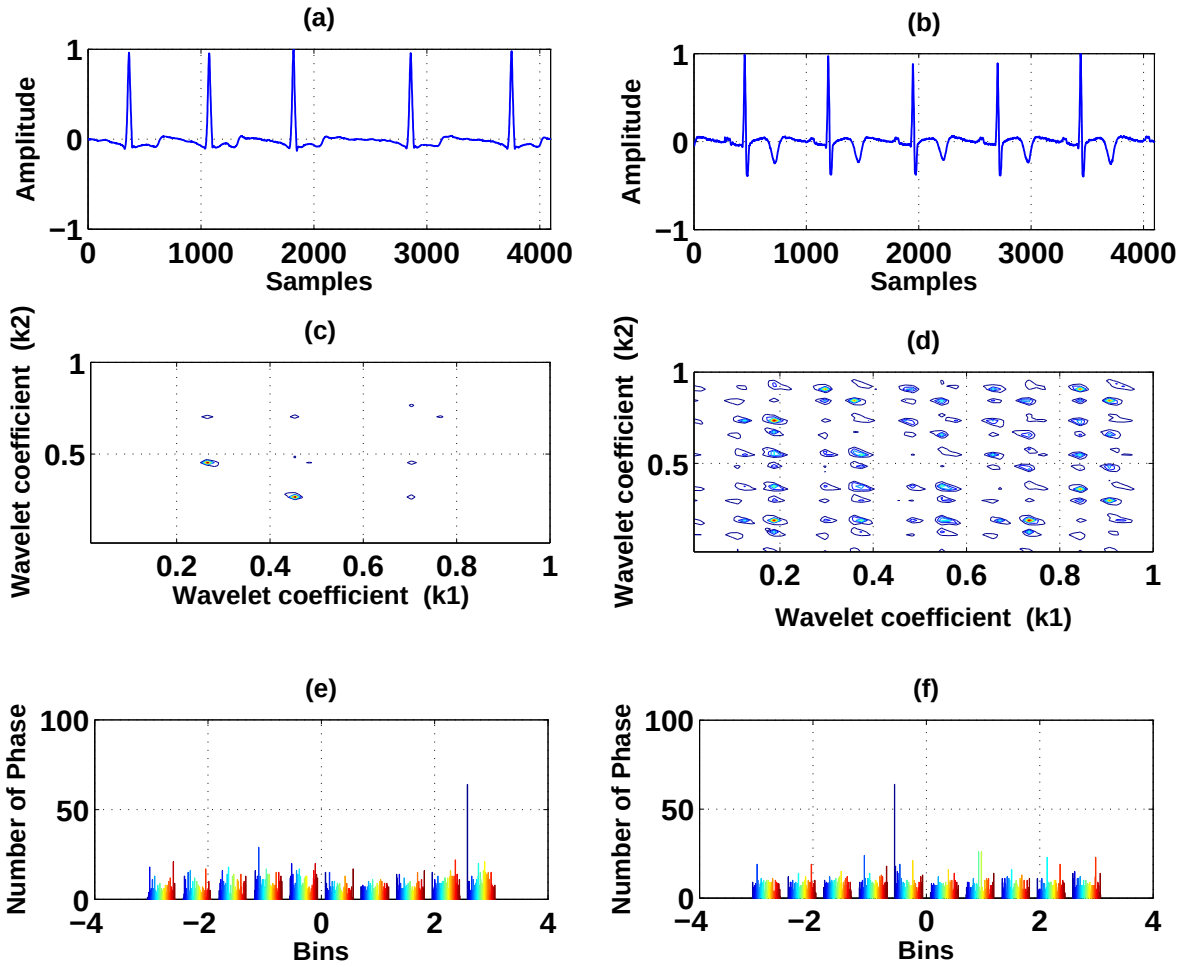


**Fig. 4.9:** (a) Lead V5 signal for HMD case. (b) Lead V5 signal for MI case. The amplitude of each ECG signal is in mV and the sampling frequency is 1000 Hz. (c) Magnitude contour of the $cA_6$ sub-band bi-spectrum of HMD. (d) Magnitude contour of the $cA_6$ sub-band bi-spectrum of MI. (e) Histogram of the phase of $cA_6$ sub-band bi-spectrum for HMD. (f) Histogram of the phase of $cA_6$ sub-band bi-spectrum for MI.

Similarly, the phase of the complex wavelet bi-spectrum in $\mathbf{d}^{\text{th}}$ sub-band of $m^{\text{th}}$ ECG lead is defined by

$$\phi^m_{\mathbf{d}}(k1,k2) = tan^{-1}[\frac{\overline{\mathbf{B}}^m_{\mathbf{d}}(k1,k2)}{\tilde{\mathbf{B}}^m_{\mathbf{d}}(k1,k2)}] \tag{4.13}$$

$\phi^m_{\mathbf{d}}(k1,k2)$ captures the phase correlation of the complex wavelet coefficients in $\mathbf{d}^{\text{th}}$ sub-band. In this work, the magnitude and the phase features from the complex wavelet bi-spectrum of each ECG lead at significant sub-bands are evaluated. The magnitude feature of complex wavelet bi-spectrum in $\mathbf{d}^{\text{th}}$

sub-band of $m^{\text{th}}$ ECG lead is defined as

$$BM_{\mathbf{d}}^{m} = \frac{1}{N_{\mathbf{d}}^{2}} \sum_{k1=1}^{N_{\mathbf{d}}} \sum_{k2=1}^{N_{\mathbf{d}}} \mathbf{M}_{\mathbf{d}}^{m}(k1, k2) \tag{4.14}$$

Where, $BM$ corresponds to the bi-spectrum magnitude. The phase features such as the number of negative phase angle (NNP) and the number of positive phase angle (NPP) of CWSB are evaluated. The NNP and the NPP correspond to the total number negative phase and positive phase components in the phase of CWSB. The algorithm for evaluation of NNP and NPP features of complex wavelet bi-spectrum in $\mathbf{d}^{\text{th}}$ sub-band is given by,

***Algorithm (Evaluation of CWSB Phase features)***

***Input***: Phase of the complex wavelet bi-spectrum of the $\mathbf{d}^{\text{th}}$ sub-band of $m^{\text{th}}$ lead: $\phi_{\mathbf{d}}^{m}(k1, k2)$, $1 \leq k1 \leq N_{\mathbf{d}}$ and $1 \leq k2 \leq N_{\mathbf{d}}$.

***Output***: NNP and NPP features of the $\mathbf{d}^{\text{th}}$ sub-band of $m^{\text{th}}$ lead: $NPP_{\mathbf{d}}^{m}$, $NNP_{\mathbf{d}}^{m}$.

***begin***

- The NNP angles of the $\mathbf{d}^{\text{th}}$ sub-band of $m^{\text{th}}$ lead is $NPP_{\mathbf{d}}^{m} = count(\phi_{\mathbf{d}}^{m}(k1, k2) > 0)$.
- The NNP phase angles of the $\mathbf{d}^{\text{th}}$ sub-band of $m^{\text{th}}$ lead is $NNP_{\mathbf{d}}^{m} = count(\phi_{\mathbf{d}}(k1, k2) < 0)$.

***end***

Fig. 4.8 (a) and Fig. 4.8 (b) depict the lead V5 ECG signals for HC and BBB pathology. The lead V5 ECG signals for HMD and MI cases are shown in Fig. 4.9 (a) and Fig. 4.9 (b), respectively. It is noticed that, the shape and the beat-to-beat variations of the ECG signals are different for different cardiac ailments and healthy control. Fig. 4.8 (c) and Fig. 4.8 (d) show the magnitude contours of the complex wavelet bi-spectrum of $cA_6$ sub-band for HC and BBB case. The magnitude contours of the complex wavelet bi-spectrum for MI and HMD cases in $cA_6$ sub-band are depicted in Fig. 4.9 (c) and Fig. 4.9 (d), respectively. In this work, the wavelet coefficient axes of CWSB are normalized based on the total number of complex wavelet coefficients in the respective sub-band. Significant differences in the morphology of magnitude contours are observed for both HC and pathological cases. The complex wavelet bi-spectrum captures the third-order magnitude and phase correlations of complex wavelet coefficients. The structure of complex wavelet bi-spectrum matrix at each scale is different for HC and cardiac ailments. The BM, the NNP and the NPP features capture the changes

in the complex wavelet bi-spectrum matrix of different sub-bands during pathology. The average of the complex wavelet bi-spectrum magnitude (BM) for HC, MI, BBB and HMD cases in $cA_6$ sub-band are $0.7772$, $0.2621$, $2.8800$ and $0.1905$, respectively. Similar changes in the values of BM features are observed for HC, MI, HMD and BBB cases in other sub-bands.

Fig. 4.8 (e) and Fig. 4.8 (f) depict the histograms of the phase of complex wavelet bi-spectrum in $cA_6$ sub-band for HC and BBB cases. The histograms of the phase of complex wavelet bi-spectrum for MI and HMD cases in $cA_6$ sub-band is shown in Fig. 4.9 (e) and Fig. 4.9 (f), respectively. It is observed that, the peaks of the histograms of the CWSB are different for cardiac ailments and HC. The NNP and NPP features capture the variations in the phase of CWSB during pathology. The NNP values of complex wavelet bi-spectrum of $cA_6$ sub-band for HC, MI, BBB and HMD cases are $2405$, $1895$, $2162$ and $2337$, respectively. Similarly, the NPP values are $1961$, $2201$, $1934$ and $1759$ for HC, MI, BBB and HMD cases in $cA_6$ sub-band. Similar changes in the NNP and NPP features of CWSB are also observed for $cD_6$, $cD_5$ and $cD_4$ sub-bands. These variations in the BM, NNP and NPP values of CWSB can be used for detection and classification of cardiac disorders. In this work, $48$ magnitude features and $96$ phase features are evaluated from the CWSB of multilead ECG. A $144$ dimensional CWSB feature vector is created by appending the magnitude and the phase features.

### 4.2.3 Feature Selection and Classification

In this subsection, the feature selection and the classification of cardiac ailments from the complex wavelet magnitude and phase features of multilead ECG are discussed. In first method, the SD score and the one-way ANOVA are used for selection of few features from the $48$ multiscale PA feature vector of multilead ECG. The new feature vectors obtained after the SD score and the one-way ANOVA based feature selection methods are used as input to both KNN and fuzzy KNN classifiers for detection of BBB, HMD and MI pathologies. The number of nearest neighbors for KNN and fuzzy KNN classifiers are selected as $\tilde{k} = 5$. Similarly, for second method, the $144$ dimensional CWSB feature vector is used as input to SVM and ELM classifiers. The SU based feature selection technique is employed for choosing relevant features from $144$ dimensional CWSB feature vector. The CWSB magnitude and phase features, and the selected features using SU score are used for classification. The feature matrix and the class label vector for multilead ECG frames are denoted

as, $\mathbf{Z} \in R^{p \times q}$ and $\mathbf{y} \in R^{p}$, respectively. Here, $p$ and $q$ are the number of multilead instances or frames. For first method, '$q$' is the number of multiscale PA features. Similarly, the $q$ is considered as number of CWSB features in second method. For $i^{\text{th}}$ multilead instance ($i = 1, 2, ...p$), the class label is given as $\mathbf{y}_i \in \{1, 2, 3, 4\}$. These integer values ($\{1, 2, 3, 4\}$) are the class labels for HC, BBB, HMD and MI classes. The training and the test instances of ELM and SVM classifiers are chosen using 5-fold cross-validation approach. The training parameters of SVM classifier are selected as the regularization factor ($C = 0.005$), the degree of the polynomial kernel ($c = 5$) and the standard deviation of the RBF kernel ($\sigma = 0.25$). Similarly, for ELM classifier, the regularization parameter ($\gamma = 0.9$) is used. The 'sigmoid', the 'sine' and the 'Gaussian' activation functions are considered for ELM. The individual class accuracy (IA) and the overall accuracy (OA) values of classifiers are evaluated. These measures are computed using equation 2.59 and equation 2.60, respectively. The following subsection describes the evaluation of proposed methods for detection of HMD, MI and BBB pathologies.

## 4.3 Evaluation of the Proposed Methods

The proposed methods are implemented using the flow-charts as shown in Fig. 4.5 (a) and Fig. 4.5 (b), respectively. The multilead ECG signals from PTB diagnostic database are used for testing of the proposed methods. In this work, one hour recording of $16$ HC, $16$ MI, $16$ BBB and $20$ HMD ($13$ cardiomyopathy and $7$ hypertrophy) mutilead ECG datasets are considered. The filtering and the segmentation are applied to each multilead ECG dataset. For HC, MI, HMD and BBB classes, $361$, $361$, $420$ and $361$ number of multilead ECG frames are evaluated. The DTCWT is applied to each of the multilead ECG frame. The complex wavelet coefficients from the diagnostically significant sub-bands ($cA_6$, $cD_6$, $cD_5$ and $cD_4$) of each ECG lead are evaluated. The PA features are computed from the phase of the complex wavelet coefficients of these four sub-bands. The complex wavelet bi-spectrum is evaluated for $cA_6$, $cD_6$, $cD_5$ and $cD_4$ sub-bands of each ECG lead using HOCWA. Then, the magnitude and the phase features are computed from the CWSB of multilead ECG. In the following sections, the statistical analysis of both multiscale PA features and CWBS magnitude and phase features, the performance of fuzzy KNN and KNN classifiers using multiscale PA features and the performance of ELM and SVM classifiers using CWSB features of multilead ECG are shown.

**Table 4.1:** Mean and standard deviation values of normalized phase alternation features of $cA_6$ sub-band in different ECG leads.

| Classes | Param. | I | II | aVR | aVL | V1 | V2 | V3 | V4 | V5 | V6 |
|---|---|---|---|---|---|---|---|---|---|---|---|
| HC | $\mu$ | 0.5482 | 0.5314 | 0.5242 | 0.5513 | 0.5107 | 0.5309 | 0.4507 | 0.4696 | 0.4039 | 0.4492 |
| HC | $\sigma$ | 0.1069 | 0.1215 | 0.1057 | 0.1225 | 0.0997 | 0.1269 | 0.0999 | 0.1071 | 0.0852 | 0.1007 |
| MI | $\mu$ | 0.6149 | 0.6047 | 0.6099 | 0.5921 | 0.5241 | 0.5475 | 0.5405 | 0.5797 | 0.5042 | 0.5368 |
| MI | $\sigma$ | 0.1274 | 0.1232 | 0.1050 | 0.1217 | 0.1217 | 0.1110 | 0.1127 | 0.1269 | 0.1129 | 0.1176 |
| HMD | $\mu$ | 0.5970 | 0.5678 | 0.6053 | 0.5460 | 0.5201 | 0.5609 | 0.5016 | 0.5311 | 0.4755 | 0.4664 |
| HMD | $\sigma$ | 0.1041 | 0.1050 | 0.1176 | 0.1257 | 0.1387 | 0.1253 | 0.1258 | 0.1284 | 0.1061 | 0.0994 |
| BBB | $\mu$ | 0.5603 | 0.5844 | 0.6011 | 0.5430 | 0.5573 | 0.5521 | 0.5337 | 0.5352 | 0.4764 | 0.4718 |
| BBB | $\sigma$ | 0.1340 | 0.1480 | 0.1505 | 0.1493 | 0.1425 | 0.1427 | 0.1048 | 0.1258 | 0.1285 | 0.1159 |

**Table 4.2:** Mean and standard deviation values of normalized phase alternation features of $cD_6$ sub-band in different ECG leads.

| Classes | Param. | I | II | aVR | aVL | V1 | V2 | V3 | V4 | V5 | V6 |
|---|---|---|---|---|---|---|---|---|---|---|---|
| HC | $\mu$ | 0.6754 | 0.6496 | 0.6582 | 0.6593 | 0.6613 | 0.6825 | 0.7071 | 0.6451 | 0.6433 | 0.6488 |
| HC | $\sigma$ | 0.1090 | 0.1041 | 0.1036 | 0.1042 | 0.0908 | 0.0968 | 0.1067 | 0.1040 | 0.0961 | 0.1002 |
| MI | $\mu$ | 0.6953 | 0.6729 | 0.6942 | 0.6726 | 0.6646 | 0.6187 | 0.6195 | 0.5864 | 0.6783 | 0.6951 |
| MI | $\sigma$ | 0.1039 | 0.0983 | 0.1022 | 0.1004 | 0.1135 | 0.1023 | 0.0999 | 0.1011 | 0.1086 | 0.1117 |
| HMD | $\mu$ | 0.6563 | 0.6232 | 0.6654 | 0.6367 | 0.6387 | 0.6423 | 0.6656 | 0.6108 | 0.6292 | 0.6470 |
| HMD | $\sigma$ | 0.1119 | 0.1151 | 0.1104 | 0.1097 | 0.1056 | 0.0958 | 0.1092 | 0.1060 | 0.1047 | 0.0999 |
| BBB | $\mu$ | 0.6459 | 0.6277 | 0.6553 | 0.6367 | 0.6183 | 0.6184 | 0.6333 | 0.6053 | 0.6431 | 0.6393 |
| BBB | $\sigma$ | 0.1206 | 0.1266 | 0.1161 | 0.1158 | 0.1240 | 0.1058 | 0.1266 | 0.1196 | 0.1167 | 0.1332 |

**Table 4.3:** Mean and standard deviation values of normalized phase alternation features of $cD_5$ sub-band in different ECG leads.

| Classes | Param. | I | II | aVR | aVL | V1 | V2 | V3 | V4 | V5 | V6 |
|---|---|---|---|---|---|---|---|---|---|---|---|
| HC | $\mu$ | 0.7677 | 0.7192 | 0.7557 | 0.7787 | 0.7567 | 0.7849 | 0.7348 | 0.7507 | 0.7441 | 0.7639 |
| HC | $\sigma$ | 0.0747 | 0.0692 | 0.0719 | 0.0753 | 0.0871 | 0.0854 | 0.0735 | 0.0724 | 0.0737 | 0.0734 |
| MI | $\mu$ | 0.7606 | 0.7491 | 0.7658 | 0.7441 | 0.7265 | 0.7513 | 0.7123 | 0.7430 | 0.7417 | 0.7558 |
| MI | $\sigma$ | 0.0789 | 0.0809 | 0.0800 | 0.0711 | 0.0844 | 0.0944 | 0.0847 | 0.0744 | 0.0761 | 0.0749 |
| HMD | $\mu$ | 0.7711 | 0.7435 | 0.7683 | 0.7621 | 0.7413 | 0.7539 | 0.7012 | 0.7294 | 0.7330 | 0.7562 |
| HMD | $\sigma$ | 0.0753 | 0.0722 | 0.0769 | 0.0743 | 0.0843 | 0.0892 | 0.0790 | 0.0768 | 0.0723 | 0.0785 |
| BBB | $\mu$ | 0.7358 | 0.7452 | 0.7672 | 0.7438 | 0.7556 | 0.7704 | 0.7206 | 0.7431 | 0.7347 | 0.7656 |
| BBB | $\sigma$ | 0.0897 | 0.0741 | 0.0823 | 0.0924 | 0.0879 | 0.0748 | 0.0801 | 0.0768 | 0.0719 | 0.0802 |

**Table 4.4:** Mean and standard deviation values of normalized phase alternation features of $cD_4$ sub-band in different ECG leads.

| Classes | Param. | I | II | aVR | aVL | V1 | V2 | V3 | V4 | V5 | V6 |
|---|---|---|---|---|---|---|---|---|---|---|---|
| HC | $\mu$ | 0.6223 | 0.6233 | 0.7104 | 0.6374 | 0.6482 | 0.6422 | 0.6521 | 0.6639 | 0.6573 | 0.6378 |
| HC | $\sigma$ | 0.0436 | 0.0432 | 0.0399 | 0.0499 | 0.0460 | 0.0455 | 0.0458 | 0.0669 | 0.0425 | 0.0411 |
| MI | $\mu$ | 0.6919 | 0.7703 | 0.7999 | 0.7935 | 0.7694 | 0.7609 | 0.7736 | 0.7808 | 0.7698 | 0.7666 |
| MI | $\sigma$ | 0.1083 | 0.1050 | 0.1059 | 0.0727 | 0.0963 | 0.0983 | 0.0949 | 0.1084 | 0.1124 | 0.1134 |
| HMD | $\mu$ | 0.6308 | 0.6252 | 0.6179 | 0.7182 | 0.6697 | 0.6378 | 0.6440 | 0.6409 | 0.6451 | 0.6290 |
| HMD | $\sigma$ | 0.0571 | 0.0542 | 0.0434 | 0.0692 | 0.0580 | 0.0542 | 0.0512 | 0.0429 | 0.0473 | 0.0479 |
| BBB | $\mu$ | 0.6351 | 0.6209 | 0.6120 | 0.7185 | 0.6589 | 0.6434 | 0.6459 | 0.6421 | 0.6530 | 0.6450 |
| BBB | $\sigma$ | 0.0544 | 0.0500 | 0.1327 | 0.0609 | 0.0467 | 0.0554 | 0.0509 | 0.0463 | 0.0456 | 0.0413 |

### 4.3.1 Statistical Analysis of Multiscale PA features

In this subsection, the statistical analysis of the proposed multiscale PA features of multilead ECG is performed. The mean and the standard deviations values of PA features for HC and various pathological cases in $cA_6$, $cD_6$, $cD_5$ and $cD_4$ sub-bands are shown in Table 4.1, Table 4.2, Table 4.3 and Table 4.4, respectively. It is observed that, the mean and the standard deviation values of the PA features are different for pathological and HC cases in each sub-band. Except at lead V1 and lead V2, the $cA_6$ sub-band PA features have higher mean values for MI class in all ECG leads. For BBB class, higher mean values of the PA features are observed in lead V1 and lead V2, respectively. The pathological symptoms of right BBB are the ST-segment depression and the T-wave inversion in lead V1 and lead V2 [1]. Similarly, different types of MI are diagnosed by observing the pathological changes in the low-frequency components (ST-segment and T-wave) of different ECG leads [1]. The low-frequency diagnostic components of ECG are captured using the complex wavelet coefficients of $cA_6$ sub-band. This may be the reason for which the PA features of $cA_6$ sub-band have different mean values for all leads.

Similar variations in the PA features of $cD_6$ and $cD_5$ sub-bands are also observed for different ECG leads. The PA features in $cD_4$ sub-band have higher mean values for MI class. The mean values of PA features in HMD class are lower than the HC class at lead V3, lead V4 and lead V5, respectively. The QRS-complex morphology is different in HMD, BBB and MI pathologies [1]. The high-frequency clinical components of ECG are captured using $cD_4$ sub-band complex wavelet coefficients. Due to this reason, the mean values of the PA features in $cD_4$ sub-band are different for HC, MI, HMD and BBB classes.

**Table 4.5:** SD scores and p-values of PA features in $cA_6$, $cD_6$, $cD_5$ and $cD_4$ sub-bands of all ECG leads.

| Metrics | I | II | III | aVR | aVL | aVF | V1 | V2 | V3 | V4 | V5 | V6 |
|---|---|---|---|---|---|---|---|---|---|---|---|---|
| $SD_{cA_6}$ | 0.103 | 0.094 | 0.081 | 0.135 | 0.083 | 0.050 | 0.082 | 0.051 | 0.125 | 0.118 | 0.171 | 0.119 |
| p-val | <0.001 | <0.001 | <0.001 | <0.001 | <0.001 | <0.001 | <0.001 | 0.1079 | <0.001 | <0.001 | <0.001 | <0.001 |
| $SD_{cD_6}$ | 0.043 | 0.053 | 0.084 | 0.048 | 0.035 | 0.071 | 0.069 | 0.097 | 0.112 | 0.054 | 0.048 | 0.072 |
| p-val | <0.001 | <0.001 | <0.001 | <0.001 | <0.001 | <0.001 | <0.001 | <0.001 | <0.001 | <0.001 | <0.001 | <0.001 |
| $SD_{cD_5}$ | 0.064 | 0.050 | 0.047 | 0.024 | 0.065 | 0.043 | 0.031 | 0.047 | 0.044 | 0.039 | 0.017 | 0.032 |
| p-val | <0.001 | <0.001 | <0.001 | <0.001 | <0.001 | <0.001 | <0.001 | <0.001 | <0.001 | 0.0053 | 0.1367 | 0.3202 |
| $SD_{cD_4}$ | 0.117 | 0.507 | 0.686 | 0.262 | 0.471 | 0.698 | 0.392 | 0.437 | 0.494 | 0.473 | 0.420 | 0.450 |
| p-val | <0.001 | <0.001 | <0.001 | <0.001 | <0.001 | <0.001 | <0.001 | <0.001 | <0.001 | <0.001 | <0.001 | <0.001 |

The statistical significance of the multiscale PA features is performed using the one-way ANOVA

and the SD score [182]. The p-values and the SD scores of the PA features in $cA_6$, $cD_6$, $cD_5$ and $cD_4$ sub-bands are shown in Table 4.5. It is observed that, the PA features of $cD_4$ sub-band have higher SD value than other sub-bands. It is also seen that, maximum PA features in $cA_6$, $cD_6$ and $cD_4$ sub-bands have p-value lower than 0.001. The high frequency diagnostic components of ECG show significant variations in MI and hypertrophic cardiomyopathy [83]. The morphologies of the ST-segment and the T-wave are different for cardiac abnormalities (BBB, HMD and MI) and HC. Due to these reasons, the PA features of $cA_6$, $cD_6$ and $cD_4$ sub-bands are highly significant for classification of different groups of cardiac disorders.

### 4.3.2 Performance of KNN and Fuzzy KNN classifiers

In this subsection, the performance of KNN and fuzzy KNN classifiers are shown using multiscale PA features and selected PA features. The multiscale PA features are ranked based on SD scores and the p-values. From Table 4.5, it is observed that, out of $48$ multiscale PA features $44$ features have SD score greater than $0.035$. These $44$ features are selected for classification. Similarly, only $4$ features have p-value higher than $0.001$ and these features are eliminated from the multiscale PA feature vector. The selected features using SD score and ANOVA are used as input to KNN and fuzzy KNN classifiers. Table 4.6 shows the IA and the OA values of KNN and fuzzy KNN classifiers using different feature combinations. It is observed that, the IA values of KNN classifier for MI, HMD and BBB classes using all multiscale PA features are 94.37%, 77.27% and 77.14%, respectively. The IA value of HMD class is improved to 81.82% using ANOVA based selected features. The IA values of fuzzy KNN classifier are 94.60%, 78.86% and 78.41% for MI, HMD and BBB classes. The OA value of fuzzy KNN classifier is improved using ANOVA based feature selection approach. The performance of KNN and fuzzy KNN classifiers using multiscale PA features is highest for MI class compared to BBB and HMD classes. The phase change occurs due to the variation in the temporal information of a signal [178]. The complex wavelet coefficients capture the time-frequency localization of multilead ECG. In MI, there are the variations in the shape and the duration of different clinical components along each lead. The PA features at different wavelet scales correctly capture the pathological changes and the performance (OA value) of these features is 95.17% using fuzzy KNN classifier. The above observations infer that, the proposed multiscale PA features and the fuzzy

KNN classifier are suitable to classify cardiac abnormalities from multilead ECG.

**Table 4.6:** Performance of fuzzy KNN and KNN classifiers using different feature combinations.

| Feature Selection | Classifiers | IA (HC) (%) | IA (MI)(%) | IA (HMD) (%) | IA (BBB) (%) | OA (%) |
|---|---|---|---|---|---|---|
| All Features | Fuzzy KNN | 89.46 | 94.60 | 78.86 | 78.41 | 84.96 |
| Selected Features using ANOVA | Fuzzy KNN | 92.33 | 94.31 | 80.90 | 78.12 | **86.09** |
| Selected Features using SD | Fuzzy KNN | 90.63 | **95.17** | 78.86 | 77.27 | 85.09 |
| All Features | KNN | 90 | 94.37 | 77.27 | 77.14 | 84.29 |
| Selected Features using ANOVA | KNN | 87.14 | 92.86 | **81.82** | 76.06 | 84.28 |
| Selected Features using SD | KNN | 95.71 | 91.55 | 77.27 | 75.71 | **84.61** |

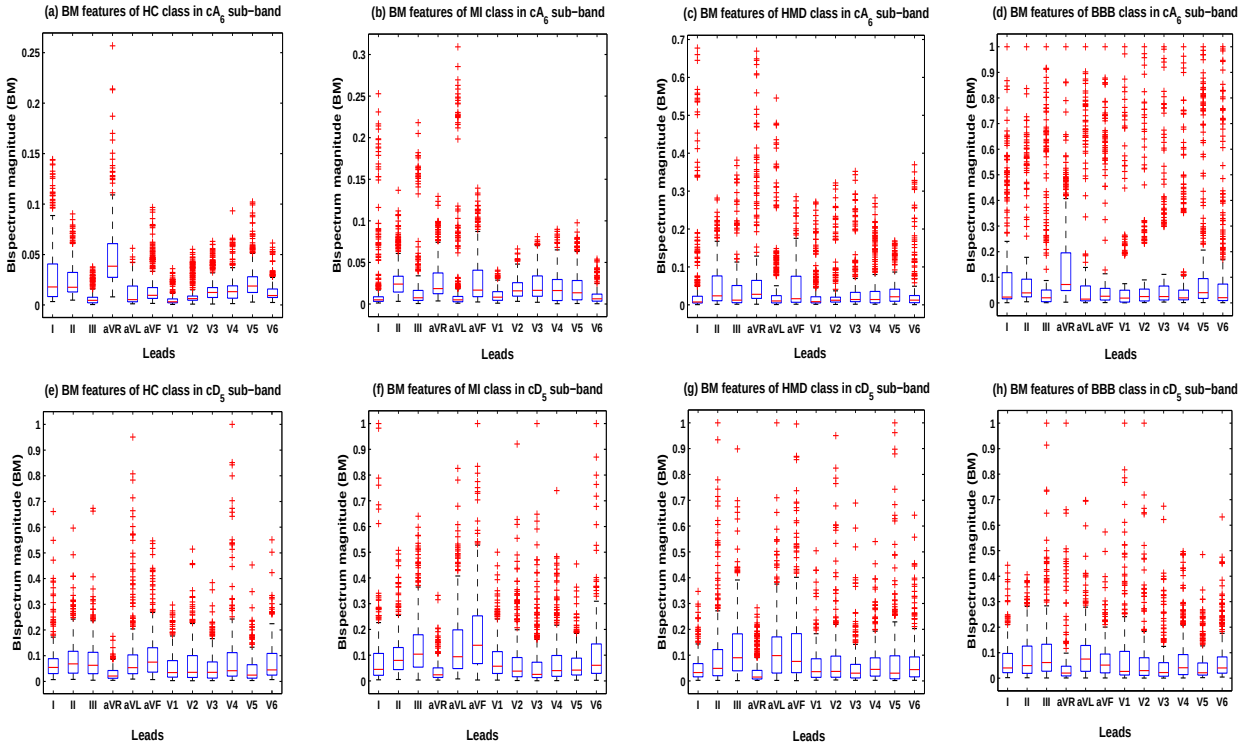


**Fig. 4.10:** (a) Box plot of BM features of HC class in $cA_6$ sub-band. (b) Box plot of BM features of MI class in $cA_6$ sub-band. (c) Box plot of BM features of HMD class in $cA_6$ sub-band. (d) Box plot of BM features of BBB class in $cA_6$ sub-band. (e) Box plot of BM features of HC class in $cD_5$ sub-band. (f) Box plot of BM features of MI class in $cD_5$ sub-band. (g) Box plot of BM features of HMD class in $cD_5$ sub-band. (h) Box plot of BM features of BBB class in $cD_5$ sub-band.

### 4.3.3 Statistical Analysis of CWSB magnitude and Phase features

In this subsection, the statistical analysis of CWSB magnitude and phase features is shown. Fig. 4.10 (a)-(d) and Fig. 4.10 (e)-(h) depict the within-class variations (Boxplots) of BM feature of all ECG leads in $cA_6$ and $cD_6$ sub-bands. For HC and pathological cases (HMD, BBB and MI), the median

**Table 4.7:** Mean and standard deviation values of BM features for HC class at different ECG leads.

| Sub-band | param. | I | II | III | aVR | aVL | aVF | V1 | V2 | V3 | V4 | V5 | V6 |
|---|---|---|---|---|---|---|---|---|---|---|---|---|---|
| $cA_6$ | $\mu$ | 0.030 | 0.025 | 0.007 | 0.048 | 0.011 | 0.016 | 0.005 | 0.011 | 0.016 | 0.016 | 0.023 | 0.013 |
| $cA_6$ | $\sigma$ | 0.312 | 0.018 | 0.008 | 0.034 | 0.011 | 0.018 | 0.008 | 0.012 | 0.013 | 0.014 | 0.017 | 0.009 |
| $cD_6$ | $\mu$ | 0.075 | 0.070 | 0.030 | 0.063 | 0.033 | 0.053 | 0.055 | 0.070 | 0.073 | 0.083 | 0.074 | 0.071 |
| $cD_6$ | $\sigma$ | 0.085 | 0.051 | 0.035 | 0.041 | 0.041 | 0.052 | 0.052 | 0.062 | 0.056 | 0.100 | 0.068 | 0.055 |
| $cD_5$ | $\mu$ | 0.076 | 0.091 | 0.085 | 0.030 | 0.098 | 0.103 | 0.057 | 0.071 | 0.056 | 0.095 | 0.045 | 0.077 |
| $cD_5$ | $\sigma$ | 0.081 | 0.082 | 0.082 | 0.025 | 0.133 | 0.098 | 0.058 | 0.082 | 0.059 | 0.141 | 0.053 | 0.078 |
| $cD_4$ | $\mu$ | 0.014 | 0.019 | 0.006 | 0.011 | 0.041 | 0.003 | 0.049 | 0.043 | 0.037 | 0.014 | 0.031 | 0.036 |
| $cD_4$ | $\sigma$ | 0.012 | 0.024 | 0.011 | 0.012 | 0.046 | 0.007 | 0.056 | 0.051 | 0.053 | 0.025 | 0.048 | 0.051 |

**Table 4.8:** Mean and standard deviation values of BM features for BBB class at different ECG leads.

| Sub-band | param. | I | II | III | aVR | aVL | aVF | V1 | V2 | V3 | V4 | V5 | V6 |
|---|---|---|---|---|---|---|---|---|---|---|---|---|---|
| $cA_6$ | $\mu$ | 0.113 | 0.114 | 0.121 | 0.152 | 0.114 | 0.109 | 0.076 | 0.085 | 0.094 | 0.093 | 0.135 | 0.107 |
| $cA_6$ | $\sigma$ | 0.189 | 0.187 | 0.233 | 0.173 | 0.233 | 0.217 | 0.173 | 0.182 | 0.187 | 0.191 | 0.238 | 0.212 |
| $cD_6$ | $\mu$ | 0.114 | 0.140 | 0.109 | 0.127 | 0.096 | 0.096 | 0.133 | 0.129 | 0.139 | 0.129 | 0.164 | 0.130 |
| $cD_6$ | $\sigma$ | 0.139 | 0.144 | 0.152 | 0.110 | 0.150 | 0.142 | 0.162 | 0.165 | 0.181 | 0.163 | 0.162 | 0.126 |
| $cD_5$ | $\mu$ | 0.067 | 0.084 | 0.105 | 0.051 | 0.086 | 0.071 | 0.084 | 0.070 | 0.055 | 0.076 | 0.050 | 0.069 |
| $cD_5$ | $\sigma$ | 0.073 | 0.083 | 0.132 | 0.106 | 0.100 | 0.075 | 0.140 | 0.116 | 0.086 | 0.097 | 0.067 | 0.089 |
| $cD_4$ | $\mu$ | 0.010 | 0.033 | 0.008 | 0.047 | 0.017 | 0.003 | 0.104 | 0.065 | 0.037 | 0.010 | 0.030 | 0.041 |
| $cD_4$ | $\sigma$ | 0.016 | 0.044 | 0.013 | 0.124 | 0.031 | 0.006 | 0.161 | 0.099 | 0.060 | 0.015 | 0.050 | 0.062 |

**Table 4.9:** Mean and standard deviation values of BM features for MI class at different ECG leads.

| Sub-band | param. | I | II | III | aVR | aVL | aVF | V1 | V2 | V3 | V4 | V5 | V6 |
|---|---|---|---|---|---|---|---|---|---|---|---|---|---|
| $cA_6$ | $\mu$ | 0.020 | 0.028 | 0.020 | 0.029 | 0.025 | 0.029 | 0.010 | 0.019 | 0.024 | 0.019 | 0.020 | 0.009 |
| $cA_6$ | $\sigma$ | 0.043 | 0.022 | 0.039 | 0.025 | 0.059 | 0.030 | 0.007 | 0.011 | 0.019 | 0.017 | 0.019 | 0.009 |
| $cD_6$ | $\mu$ | 0.042 | 0.083 | 0.049 | 0.059 | 0.046 | 0.065 | 0.117 | 0.115 | 0.106 | 0.084 | 0.099 | 0.087 |
| $cD_6$ | $\sigma$ | 0.032 | 0.088 | 0.037 | 0.039 | 0.035 | 0.048 | 0.089 | 0.085 | 0.085 | 0.062 | 0.072 | 0.060 |
| $cD_5$ | $\mu$ | 0.088 | 0.105 | 0.143 | 0.039 | 0.145 | 0.182 | 0.085 | 0.079 | 0.069 | 0.079 | 0.067 | 0.109 |
| $cD_5$ | $\sigma$ | 0.122 | 0.090 | 0.127 | 0.042 | 0.139 | 0.156 | 0.083 | 0.111 | 0.113 | 0.102 | 0.066 | 0.135 |
| $cD_4$ | $\mu$ | 0.046 | 0.190 | 0.066 | 0.029 | 0.093 | 0.083 | 0.066 | 0.049 | 0.075 | 0.031 | 0.086 | 0.115 |
| $cD_4$ | $\sigma$ | 0.103 | 0.183 | 0.198 | 0.037 | 0.200 | 0.183 | 0.065 | 0.067 | 0.121 | 0.066 | 0.099 | 0.151 |

**Table 4.10:** Mean and standard deviation values of BM features for HMD class at different ECG leads.

| Sub-band | param. | I | II | III | aVR | aVL | aVF | V1 | V2 | V3 | V4 | V5 | V6 |
|---|---|---|---|---|---|---|---|---|---|---|---|---|---|
| $cA_6$ | $\mu$ | 0.041 | 0.042 | 0.034 | 0.064 | 0.038 | 0.040 | 0.022 | 0.025 | 0.030 | 0.030 | 0.028 | 0.028 |
| $cA_6$ | $\sigma$ | 0.109 | 0.051 | 0.061 | 0.113 | 0.083 | 0.053 | 0.043 | 0.050 | 0.055 | 0.049 | 0.033 | 0.058 |
| $cD_6$ | $\mu$ | 0.055 | 0.106 | 0.058 | 0.096 | 0.056 | 0.088 | 0.108 | 0.103 | 0.098 | 0.092 | 0.142 | 0.105 |
| $cD_6$ | $\sigma$ | 0.034 | 0.123 | 0.048 | 0.149 | 0.050 | 0.097 | 0.098 | 0.080 | 0.070 | 0.081 | 0.168 | 0.092 |
| $cD_5$ | $\mu$ | 0.047 | 0.095 | 0.123 | 0.035 | 0.126 | 0.136 | 0.060 | 0.081 | 0.058 | 0.065 | 0.074 | 0.061 |
| $cD_5$ | $\sigma$ | 0.050 | 0.136 | 0.124 | 0.050 | 0.127 | 0.163 | 0.069 | 0.126 | 0.082 | 0.075 | 0.134 | 0.088 |
| $cD_4$ | $\mu$ | 0.007 | 0.035 | 0.006 | 0.012 | 0.025 | 0.005 | 0.052 | 0.051 | 0.046 | 0.010 | 0.040 | 0.025 |
| $cD_4$ | $\sigma$ | 0.013 | 0.060 | 0.009 | 0.020 | 0.032 | 0.012 | 0.096 | 0.106 | 0.077 | 0.014 | 0.082 | 0.472 |

value, the minimum value and the maximum value of the boxplot of each ECG lead at $cA_6$ and $cD_6$ sub-bands are different for each CWSB magnitude feature. The mean and the standard deviation values of CWSB magnitude features for HC, BBB, MI and BBB classes are shown in Table 4.7, Table

4.8, Table 4.9 and Table 4.10, respectively. It is observed that, the mean and the standard deviation values of BM features of $cA_6$, $cD_6$, $cD_5$ and $cD_4$ sub-bands are different for cardiac ailments and the HC in each lead. For lead I, the mean values of BM features for (HC, MI, HMD and BBB) in $cA_6$, $cD_6$, $cD_5$ and $cD_4$ sub-bands are (0.030, 0.020, 0.041, 0.113), (0.075, 0.042, 0.055, 0.114), (0.076, 0.088, 0.047, 0.067) and (0.014, 0.046, 0.007, 0.010), respectively. Similarly, for lead aVL, the mean values of BM for (HC, MI, HMD and BBB) are (0.011, 0.025, 0.038, 0.114), (0.033, 0.046, 0.056, 0.096), (0.098, 0.145, 0.126, 0.086) and (0.041, 0.093, 0.025, 0.017), respectively. Likewise, for lead V6, the mean values of BM features for (HC, MI, HMD and BBB) are (0.013, 0.009, 0.028, 0.107), (0.071, 0.087, 0.105, 0.130), (0.077, 0.109, 0.061, 0.069) and (0.036, 0.115, 0.025, 0.041) in $cA_6$, $cD_6$, $cD_5$ and $cD_4$ sub-bands. Similar variations in the mean and standard deviation values of the BM features in $cA_6$, $cD_6$, $cD_5$ and $cD_4$ sub-bands are observed for other leads. The morphological features such as T-wave shape, QRS-complex duration, QRS-complex shape and ST-segment slope show significant variations during BBB, MI and HMD pathologies. This may be the reason for different mean and standard deviation values of BM features for HC, MI, BBB and HMD classes in each sub-band.

**Table 4.11:** p-value of CWBS magnitude features.

| p-value | I | II | III | aVR | aVL | aVF | V1 | V2 | V3 | V4 | V5 | V6 |
|---|---|---|---|---|---|---|---|---|---|---|---|---|
| $cA_6$ BM | <0.001 | <0.001 | <0.001 | <0.001 | <0.001 | <0.001 | <0.001 | <0.001 | <0.001 | <0.001 | <0.001 | <0.001 |
| $cD_6$ BM | <0.001 | <0.001 | <0.001 | <0.001 | <0.001 | <0.001 | <0.001 | <0.001 | <0.001 | <0.001 | <0.001 | <0.001 |
| $cD_5$ BM | <0.001 | 0.010 | <0.001 | <0.001 | <0.001 | <0.001 | <0.001 | 0.294 | 0.084 | 0.017 | <0.001 | <0.001 |
| $cD_4$ BM | <0.001 | <0.001 | <0.001 | <0.001 | <0.001 | <0.001 | <0.001 | 0.007 | <0.001 | <0.001 | <0.001 | <0.001 |

The statistical significance of CWSB magnitude features is evaluated using one-way ANOVA test [182]. The p-values of BM features for each ECG lead at different sub-bands are shown in Table 4.11. It is observed that, all BM features of $cA_6$ and $cD_6$ sub-bands have p-value lower than 0.001. Except at lead V2, the BM features in $cD_4$ sub-band have less p-value and these features are statistically significant for classification MI, HMD and BBB pathologies. The low-frequency components of ECG signal such as ST-segment, T-wave show significant variations during MI and HMD cases. These low-frequency clinical components of multilead ECG is captured using the BM features of $cA_6$ sub-band. This may be the reason for which all BM features of $cA_6$ sub-band are statistically significant. The abnormal Q-wave, the wide QRS-complex and the increase in the amplitude of R-wave are the

symptoms for MI, BBB and HMD pathologies. The BM features of $cD_6$, $cD_5$ and $cD_4$ sub-bands capture the grossly divided QRS-complex information of multilead ECG. This may be the reason for which maximum number of BM features from these sub-bands are significant for classification of cardiac ailments. It is also seen that, out of $12$ BM features of $cD_5$ sub-band, $8$ features have p-value less than $0.001$ and these $8$ features are highly significant for detection of heart pathologies.

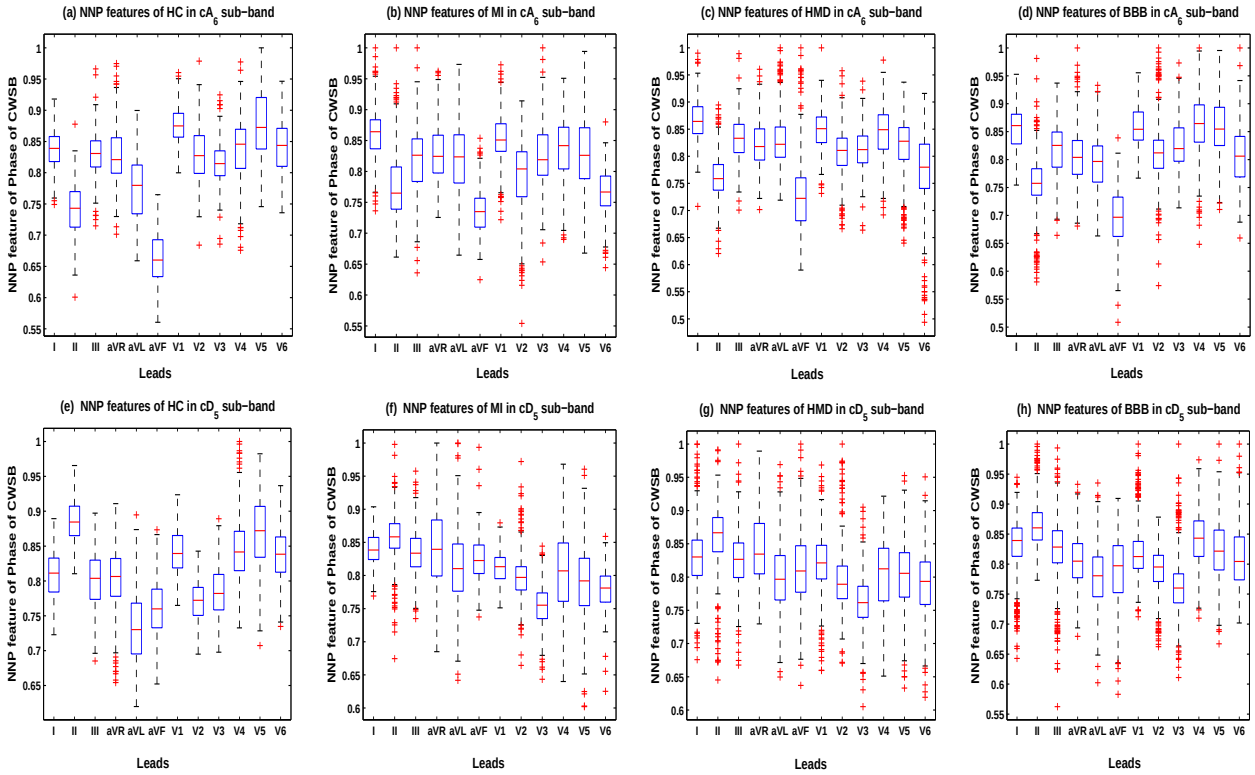


**Fig. 4.11:** (a) Box plot of NNP features of phase of CWSB of HC class in $cA_6$ sub-band. (b) Box plot of NNP features of phase of CWSB of MI class in $cA_6$ sub-band. (c) Box plot of NNP features of phase of CWSB of HMD class in $cA_6$ sub-band. (d) Box plot of NNP features of phase of CWSB of BBB class in $cA_6$ sub-band. (e) Box plot of NNP features of phase of CWSB of HC class in $cD_5$ sub-band. (f) Box plot of NNP features of phase of CWSB of MI class in $cD_5$ sub-band. (g) Box plot of NNP features of phase of CWSB of HMD class in $cD_5$ sub-band. (h) Box plot of NNP features of phase of CWSB of BBB class in $cD_5$ sub-band.

Fig. 4.11 (a)-(d) and Fig. 4.11 (e)-(h) show the within-class variation of NNP features of CWSB for HC, MI, HMD and BBB classes in $cA_6$ and $cD_5$ sub-bands. Significant differences in the median value, the minimum value and the maximum value are observed in each boxplot for all ECG leads. The mean and the standard deviation values of NNP features for lead I, lead II, lead V1, lead V2, lead V3, lead V4, lead V5 and lead V6 in $cA_6$ and $cD_5$ sub-bands of HC, MI, HMD and BBB classes are shown in Table 4.12, Table 4.13, Table 4.14, Table 4.15, respectively. It is observed that, the mean

**Table 4.12:** Mean and Standard deviation values of normalized NNP and NNP features for HC class in $cA_6$ and $cD_5$ sub-bands.

| Features | param. | Lead I | Lead II | Lead V1 | Lead V2 | Lead V3 | Lead V4 | Lead V5 | Lead V6 |
|---|---|---|---|---|---|---|---|---|---|
| $cA_6$ NNP | $\mu$ | 0.8370 | 0.7408 | 0.8768 | 0.8298 | 0.8153 | 0.8374 | 0.8777 | 0.8408 |
| $cA_6$ NNP | $\sigma$ | 0.0307 | 0.0393 | 0.0292 | 0.0418 | 0.0326 | 0.0501 | 0.0521 | 0.0429 |
| $cA_6$ NPP | $\mu$ | 0.7477 | 0.7407 | 0.7298 | 0.6269 | 0.7082 | 0.6234 | 0.6926 | 0.7022 |
| $cA_6$ NPP | $\sigma$ | 0.0336 | 0.0348 | 0.0332 | 0.0294 | 0.0308 | 0.0251 | 0.0247 | 0.0291 |
| $cD_5$ NNP | $\mu$ | 0.8091 | 0.8865 | 0.8414 | 0.7703 | 0.7840 | 0.8444 | 0.8685 | 0.8375 |
| $cD_5$ NNP | $\sigma$ | 0.0347 | 0.0309 | 0.0330 | 0.0294 | 0.0352 | 0.0469 | 0.0500 | 0.0377 |
| $cD_5$ NPP | $\mu$ | 0.7338 | 0.6128 | 0.6127 | 0.7421 | 0.6163 | 0.6734 | 0.6917 | 0.6244 |
| $cD_5$ NPP | $\sigma$ | 0.0345 | 0.0297 | 0.0292 | 0.0356 | 0.0284 | 0.0221 | 0.0266 | 0.0298 |

**Table 4.13:** Mean and Standard deviation values of NNP and NNP features for MI class in $cA_6$ and $cD_5$ sub-bands.

| Features | param. | Lead I | Lead II | Lead V1 | Lead V2 | Lead V3 | Lead V4 | Lead V5 | Lead V6 |
|---|---|---|---|---|---|---|---|---|---|
| $cA_6$ NNP | $\mu$ | 0.8616 | 0.7755 | 0.8535 | 0.7929 | 0.8278 | 0.8358 | 0.8285 | 0.7660 |
| $cA_6$ NNP | $\sigma$ | 0.0407 | 0.0567 | 0.0387 | 0.0603 | 0.0544 | 0.0526 | 0.0598 | 0.0363 |
| $cA_6$ NPP | $\mu$ | 0.7477 | 0.7424 | 0.7298 | 0.6255 | 0.7099 | 0.6237 | 0.6943 | 0.7029 |
| $cA_6$ NPP | $\sigma$ | 0.0504 | 0.0333 | 0.0499 | 0.0281 | 0.0384 | 0.0402 | 0.0449 | 0.0366 |
| $cD_5$ NNP | $\mu$ | 0.8403 | 0.8579 | 0.8117 | 0.7976 | 0.7542 | 0.8060 | 0.7897 | 0.7790 |
| $cD_5$ NNP | $\sigma$ | 0.0250 | 0.0380 | 0.0238 | 0.0361 | 0.0305 | 0.0624 | 0.0565 | 0.0296 |
| $cD_5$ NPP | $\mu$ | 0.7311 | 0.6129 | 0.6150 | 0.7421 | 0.6166 | 0.6751 | 0.6951 | 0.6252 |
| $cD_5$ NPP | $\sigma$ | 0.0323 | 0.0354 | 0.0273 | 0.0423 | 0.0282 | 0.0455 | 0.0414 | 0.0359 |

**Table 4.14:** Mean and Standard deviation values of NNP and NNP features for HMD class in $cA_6$ and $cD_5$ sub-bands.

| Features | param. | Lead I | Lead II | Lead V1 | Lead V2 | Lead V3 | Lead V4 | Lead V5 | Lead V6 |
|---|---|---|---|---|---|---|---|---|---|
| $cA_6$ NNP | $\mu$ | 0.8612 | 0.7649 | 0.8539 | 0.8041 | 0.8152 | 0.8449 | 0.8257 | 0.7815 |
| $cA_6$ NNP | $\sigma$ | 0.0400 | 0.0449 | 0.0380 | 0.0477 | 0.0433 | 0.0475 | 0.0529 | 0.0699 |
| $cA_6$ NPP | $\mu$ | 0.7429 | 0.7409 | 0.7345 | 0.6267 | 0.7120 | 0.6224 | 0.6952 | 0.7057 |
| $cA_6$ NPP | $\sigma$ | 0.0372 | 0.0447 | 0.0368 | 0.0378 | 0.0308 | 0.0324 | 0.0414 | 0.0408 |
| $cD_5$ NNP | $\mu$ | 0.8300 | 0.8629 | 0.8215 | 0.7928 | 0.7639 | 0.8083 | 0.8078 | 0.7937 |
| $cD_5$ NNP | $\sigma$ | 0.0453 | 0.0483 | 0.0432 | 0.0459 | 0.0391 | 0.0533 | 0.0565 | 0.0485 |
| $cD_5$ NPP | $\mu$ | 0.7301 | 0.6167 | 0.6159 | 0.7375 | 0.6184 | 0.6755 | 0.6955 | 0.6297 |
| $cD_5$ NPP | $\sigma$ | 0.0475 | 0.0425 | 0.0402 | 0.0508 | 0.0378 | 0.0378 | 0.0437 | 0.0381 |

and the standard deviation values of NNP features of complex wavelet bi-spectrum are different for HC and pathological cases in each sub-band. The mean values of NNP features for (HC, MI, HMD, BBB) in $cA_6$ of lead I, lead V1 and lead V6 are (0.8370, 0.8616, 0.8612, 0.8545), (0.8768, 0.8535, 0.8539, 0.8602) and (0.8408, 0.7660, 0.7815, 0.8095), respectively. Similar changes in the mean and the standard deviation values of NNP features of CWSB are observed for other ECG leads in $cD_6$ and $cD_4$ sub-bands. The $cA_6$ sub-band NNP features of CWSB capture the information of the

low-frequency components such as ST-segment and T-wave. During pathology, the characteristics of these clinical components are different than normal sinus rhythm (NSR). This may be the reason for different mean and standard deviation values of NNP features in $cA_6$ sub-band. For $cD_5$ sub-band, the mean values of NNP features of CWSB for (HC, MI, HMD, BBB) are (0.8091, 0.8403, 0.8300, 0.8302), (0.8414, 0.8117, 0.8215, 0.8213) and (0.8375, 0.7790, 0.7937, 0.8141) in lead I, lead V1 and lead V6, respectively.

**Table 4.15:** Mean and Standard deviation values of NNP and NNP features for BBB class in $cA_6$ and $cD_5$ sub-bands.

| Features | param. | Lead I | Lead II | Lead V1 | Lead V2 | Lead V3 | Lead V4 | Lead V5 | Lead V6 |
|---|---|---|---|---|---|---|---|---|---|
| $cA_6$ NNP | $\mu$ | 0.8545 | 0.7582 | 0.8602 | 0.8113 | 0.8280 | 0.8606 | 0.8581 | 0.8095 |
| $cA_6$ NNP | $\sigma$ | 0.0348 | 0.0563 | 0.0331 | 0.0599 | 0.0465 | 0.0557 | 0.0519 | 0.0551 |
| $cA_6$ NPP | $\mu$ | 0.7444 | 0.7451 | 0.7330 | 0.6232 | 0.7118 | 0.6199 | 0.6909 | 0.7046 |
| $cA_6$ NPP | $\sigma$ | 0.0370 | 0.0442 | 0.0366 | 0.0374 | 0.0368 | 0.0334 | 0.0432 | 0.0437 |
| $cD_5$ NNP | $\mu$ | 0.8302 | 0.8674 | 0.8213 | 0.7885 | 0.7658 | 0.8421 | 0.8247 | 0.8141 |
| $cD_5$ NNP | $\sigma$ | 0.0490 | 0.0399 | 0.0467 | 0.0380 | 0.0548 | 0.0463 | 0.0513 | 0.0528 |
| $cD_5$ NPP | $\mu$ | 0.7323 | 0.6133 | 0.6140 | 0.7415 | 0.6156 | 0.6728 | 0.6918 | 0.6280 |
| $cD_5$ NPP | $\sigma$ | 0.0489 | 0.0378 | 0.0413 | 0.0452 | 0.0418 | 0.0382 | 0.0418 | 0.0409 |

For $cA_6$ sub-band, the mean values of NPP features for HC, MI and BBB are $0.8091$, $0.8403$ and $0.8302$, respectively. The mean values of NNP features for HC, MI and HMD classes are $0.8414$, $0.8117$ and $0.8213$ in $cA_6$ sub-band. The elevation in ST-segment and the inversion of T-wave are the pathological characteristics during MI [1]. In hypertrophic cardiomyopathy, the ST-segment depression and the T-wave inversion are seen in ECG signal [16]. For ECG signal, the $cA_6$ sub-band complex wavelet coefficients capture the ST-segment and the T-wave information. This may be the reason for the different mean values of NPP and NNP features for HC, MI, BBB and HMD classes. Similar variations in the mean and the standard deviation values of NNP and NNP features are observed for other leads. The statistical significance of CWSB phase features are evaluated using one way ANOVA test [182]. It is observed that, only $24$ features out of $48$ NNP features of CWSB have p-value less than $0.001$ and these features are highly significant for detection of HMD, BBB and MI pathologies. The above observations infer that, the CWSB magnitude and phase features can capture the pathological changes in multilead ECG for detection of cardiac abnormalities.

**Table 4.16:** Overall Accuracy (OA) values of SVM classifier using different kernel functions

| Feature Selection | Classifiers | OA (%) |
|---|---|---|
| $cA_6$+$cD_6$ CWSB features | SVM Linear | 87.60 |
| $cA_6$+$cD_6$ CWSB features | SVM Poly | 61.78 |
| $cA_6$+$cD_6$ CWSB features | SVM RBF | 92.35 |
| $cD_5$+$cD_4$ CWSB features | SVM Linear | 84.77 |
| $cD_5$+$cD_4$ CWSB features | SVM Poly | 62.36 |
| $cD_5$+$cD_4$ CWSB features | SVM RBF | 94.34 |
| All features | SVM Linear | 94.54 |
| All features | SVM Poly | 82.78 |
| All features | SVM RBF | 97.10 |
| SU feature selection | SVM Linear | 95.82 |
| SU feature selection | SVM Poly | 85.86 |
| SU feature selection | SVM RBF | 97.75 |

**Table 4.17:** Overall Accuracy (OA) values of ELM classifier using different activation functions

| Feature Selection | Classifiers | OA (%) |
|---|---|---|
| $cA_6$+$cD_6$ CWSB features | ELM Sigmoid | 75.59 |
| $cA_6$+$cD_6$ CWSB features | ELM Radbas | 90.55 |
| $cA_6$+$cD_6$ CWSB features | ELM Sine | 91.71 |
| $cD_5$+$cD_4$ CWSB features | ELM Sigmoid | 74.63 |
| $cD_5$+$cD_4$ CWSB features | ELM Radbas | 84.71 |
| $cD_5$+$cD_4$ CWSB features | ELM Sine | 85.87 |
| All features | ELM Sigmoid | 88.11 |
| All features | ELM Radbas | 95.05 |
| All features | ELM Sine | 96.08 |
| SU feature selection | ELM Sigmoid | 88.18 |
| SU feature selection | ELM Radbas | 96.53 |
| SU feature selection | ELM Sine | 97.17 |

### 4.3.4 Performance of SVM and ELM classifiers

In this subsection, the performance of SVM and ELM classifiers is shown using the CWSB magnitude and phase features. The overall accuracy (OA) values of each fold for SVM and ELM classifiers are evaluated. Fig. 4.12 shows the variation of OA values of ELM and SVM classifiers with number of folds. The ELM classifier with 'sine' activation function shows higher OA value in each fold than the ELM classifier with 'sigmoid' activation function. Similarly, the OA value of SVM classifier with RBF kernel is higher than the SVM classifier with polynomial and linear kernel functions along each fold. The average OA values of SVM and ELM classifiers for different feature combinations are shown

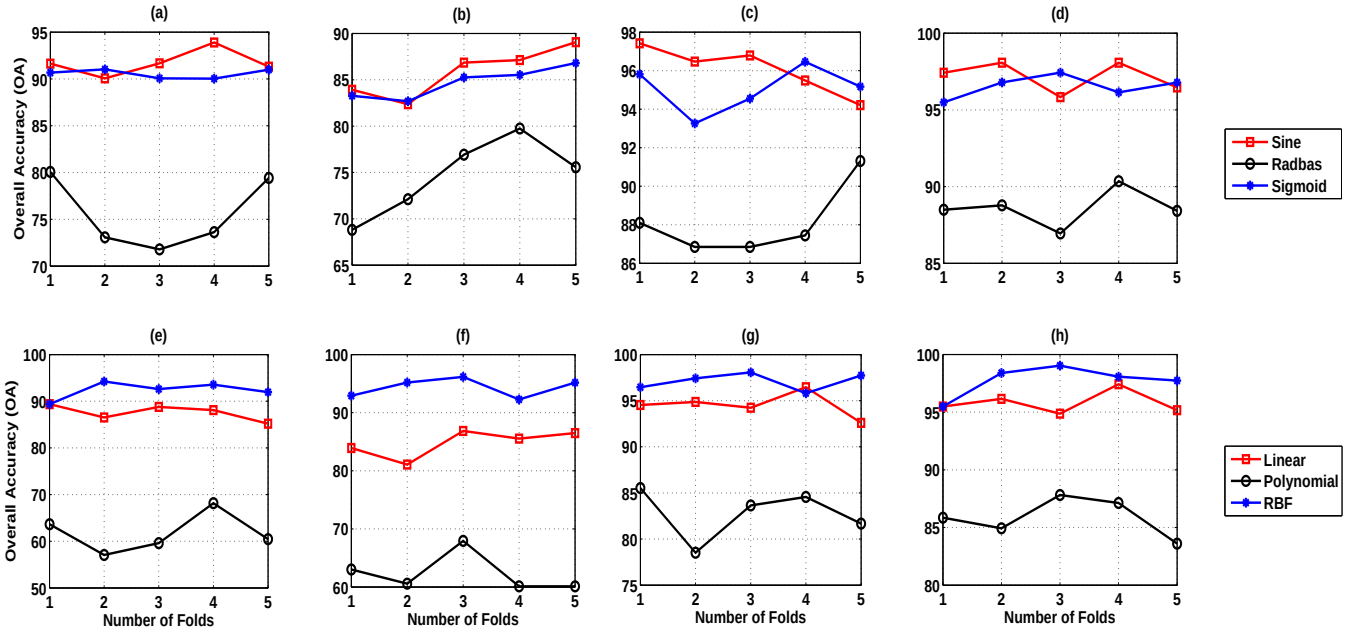


**Fig. 4.12:** (a) Accuracy of ELM classifier at each fold using $cA_6$ and $cD_6$ CWBS features. (b) Accuracy of ELM classifier at each fold using $cD_5$ and $cD_4$ CWBS features. (c) Accuracy of ELM classifier at each fold using all CWBS features. (d) Accuracy of ELM classifier at each fold using SU based selected CWBS features.(e) Accuracy of SVM classifier at each fold using $cA_6$ and $cD_6$ CWBS features. (f) Accuracy of SVM classifier at each fold using $cD_5$ and $cD_4$ CWBS features. (g) Accuracy of SVM classifier at each fold using all CWBS features. (h) Accuracy of SVM classifier at each fold using SU based selected CWBS features.

in Table 4.16 and Table 4.17, respectively. When $cA_6$ and $cD_6$ CWSB features are used, the SVM classifier produces an average OA value of 92.35%. Similarly, using $cD_5$ and $cD_4$ CWSB features, the average OA value of SVM classifier is found to be 94.35%. The $cD_5$ and $cD_4$ sub-bands complex wavelet coefficients capture the QRS-complex information of ECG signal. Due to pathology (MI, HMD and BBB), the shape and the duration of QRS-complex are different from NSR along each ECG lead [1]. This may be the reason for the better performance of SVM classier using $cD_5$ and $cD_4$ CWSB features. Using all the CWSB features, the RBF kernel based SVM classifier produces an average OA value of 97.10%, which is better than the linear and polynomial kernel based SVM. When all CWSB features are used, the average OA value of ELM classifier and 'sine' activation function is found to be 96.08%. This value is higher than the OA value of ELM classifier with 'radbas' and 'sigmoid' activation functions. The OA value of RBF kernel based SVM classifier is higher than the ELM classifier with 'sine' kernel. The SU scores of CWBS magnitude and phase features (BM,

NNP and NPP) are shown in Fig. 4.13. The CWSB features which have SU score values greater than 0.011 are considered and the remaining CWSB features are eliminated. The new feature vector obtained after SU based feature selection method contains 80 attributes. This 80 dimensional feature vector is used as input to both ELM and SVM classifiers. From Table 4.16, it is observed that the OA of SVM classifier is improved to 97.75% using SU based feature selection approach. Similarly, the performance of the ELM classifier is improved using the selected features. The redundant CWSB magnitude and phase features are eliminated using SU based feature selection approach. Due to this reason, the accuracy values of SVM and ELM classifiers for each class are improved.

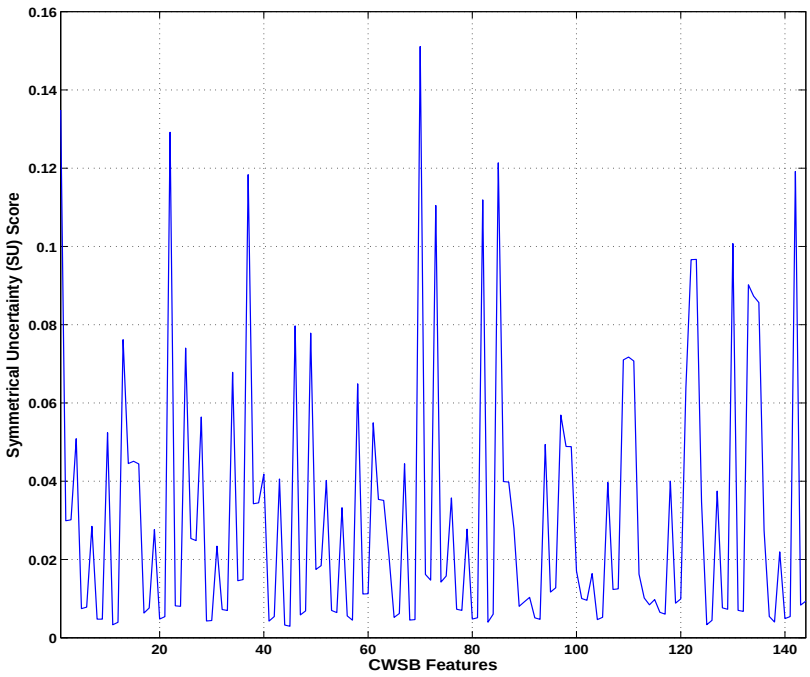


**Fig. 4.13:** Symmetrical uncertainty (SU) scores of each CWSB feature.

The individual class accuracy (IA) values of ELM and SVM classifiers are shown in Table 4.18. It is observed that, the SVM classifier have higher accuracy values for MI, HMD and BBB classes using $cA_6$ and $cD_6$ CWBS features. Using $cD_5$ and $cD_4$ CWBS features, the accuracy value of the ELM classifier is higher than the SVM classifier for BBB class. The performance of $cA_6$ and $cD_6$ CWSB features is higher than $cD_5$ and $cD_4$ CWSB features using ELM classifier. The features evaluated using $cA_6$ and $cD_6$ sub-band complex wavelet coefficients of multilead ECG capture the

**Table 4.18:** Individual Class Accuracy (IA) Values of ELM and SVM classifiers.

| Features | Classifiers | IA (HC) (%) | IA (MI) (%) | IA (HMD) (%) | IA (BBB) (%) |
|---|---|---|---|---|---|
| $cA_6$+$cD_6$ CWSB features | ELM | 94.02 | 96.47 | 91.30 | 88.08 |
| $cA_6$+$cD_6$ CWSB features | SVM | 92.10 | 94.56 | 91.52 | 91.41 |
| $cD_5$+$cD_4$ CWSB features | ELM | 86.15 | 93.76 | 95.00 | 68.17 |
| $cD_5$+$cD_4$ CWSB features | SVM | 94.56 | 96.19 | 94.13 | 92.51 |
| All CWSB features | ELM | 95.93 | 98.37 | 97.39 | 92.79 |
| All CWSB features | SVM | 97.55 | 98.37 | 96.52 | 96.12 |
| Selected CWSB features | ELM | 95.91 | 97.83 | 98.70 | 94.45 |
| Selected CWSB features | SVM | 98.90 | 98.37 | 97.39 | 96.40 |

**Table 4.19:** OA value of classifiers for hold-out cross-validation.

| Training/ Test data percentage | Classifiers | OA (%) |
|---|---|---|
| 80% training and 20% testing | ELM | 92.85 |
| | SVM | 98.39 |
| 70% training and 30% testing | ELM | 95.07 |
| | SVM | 97.43 |

clinical components such as the T-wave, the ST-segment, the P-wave and the low-frequency part of the QRS-complex. These clinical components show significant variations during MI, cardiomyopathy and BBB pathologies [1]. The SVM classifier shows better performance for each class using $cD_5$ and $cD_4$ CWSB features. The pathological variations in the clinical components such as the QRS-interval, the amplitude of QRS-complex and the shape of QRS-complex are used for diagnosis of MI, HMD and BBB diseases [1]. The QRS-complex information of multilead ECG is grossly divided in $cD_5$ and $cD_4$ sub-band. This may be the reason for the higher average accuracy value of the SVM classifier for each class of cardiac ailments using $cD_5$ and $cD_4$ CWSB features. The OA accuracy values of SVM and ELM classifiers for hold-out cross-validation is shown in Table 4.19. Here, two hold-out cross-validation methods are considered for selection of training and test instances of ELM and SVM classifiers. In first method, the 70% of CWSB feature instances are used for training and the rest of 30% are considered for testing of both classifiers. Similarly, 80% of CWSB feature instances are used for training in second method. It is observed that, the SVM classifier have a higher accuracy value using 20% of CWSB feature instances.

The confusion matrices for ELM and SVM classifiers using CWSB features are shown in Table 4.20 and Table 4.21, respectively. These matrices are evaluated based on the hold-out cross vali-

**Table 4.20:** Confusion matrix of ELM classifier with sine activation function using CWSB features.

| Actual | Predicted | | | |
|---|---|---|---|---|
| | HC | MI | HMD | BBB |
| HC | 93 | 0 | 9 | 1 |
| MI | 1 | 114 | 1 | 0 |
| HMD | 2 | 1 | 131 | 1 |
| BBB | 0 | 1 | 6 | 106 |

**Table 4.21:** Confusion matrix of SVM classifier with RBF kernel function using CWSB features.

| Actual | Predicted | | | |
|---|---|---|---|---|
| | HC | MI | HMD | BBB |
| HC | 97 | 1 | 5 | 0 |
| MI | 0 | 115 | 1 | 0 |
| HMD | 1 | 0 | 134 | 0 |
| BBB | 0 | 2 | 2 | 109 |

dation for 70% training and 30% test CWSB feature instances. It is evident that, the number of true positives for HC, MI, HMD and BBB classes are higher for SVM classifier compared to ELM classifier. In 12-lead ECG, eight ECG leads (I, II, V1-V6) are directly recorded from the patient, whereas the remaining four leads (III, aVR, aVL and aVF) are derived from lead I and lead II. It is natural to get correlations in 12-lead ECG and these correlations are reflected in the CSWB feature matrix. In this study, the performance of classifiers is compared using the CWSB features of both 12-lead and 8-lead ECG signals. The OA values of ELM and SVM classifiers for 12-lead ECG and 8-lead ECG CWSB features are shown in Table 4.22. It is observed that, the OA value of RBF kernel based SVM classifier is 97.75% using 12-lead ECG CWSB features. Similarly, using 8-lead ECG, the OA value of SVM classifier is 95.63%. The performance of ELM classifier for 12-lead ECG CWSB features is higher than the 8-lead ECG CWSB features. The characteristics of lead III and lead aVF ECG signals are different for inferior MI and NSR [1]. These pathological changes can affect the complex wavelet bi-spectrum matrices of lead III and lead aVF in different sub-bands for NSR and anterior MI. This may be the reason for higher OA values of ELM and SVM classifiers using the CWSB features of 12-lead ECG. The performance of ELM and SVM classifiers using different wavelet decomposition levels based CWSB features of 12-lead ECG is shown in Table 4.23. It is observed that, the IA and the OA values of ELM and SVM classifiers are highest for six levels DTCWT decomposition based CWSB

**Table 4.22:** OA values of ELM and SVM classifiers using CWSB features of 8-lead ECG and 12-lead ECG

| 8-lead ECG | | | 12-lead ECG | | |
|---|---|---|---|---|---|
| **Classifiers** | **Kernels** | **OA (%)** | **Classifiers** | **Kernels** | **OA (%)** |
| ELM | sigmoid | 84.51 | ELM | sigmoid | 88.11 |
| ELM | radbas | 92.67 | ELM | radbas | 95.05 |
| ELM | sine | 94.66 | ELM | sine | 96.08 |
| SVM | linear | 91.97 | SVM | linear | 94.54 |
| SVM | polynomial | 78.80 | SVM | polynomial | 85.86 |
| SVM | RBF | 95.63 | SVM | RBF | 97.75 |

features of multilead ECG. The $L = 6$ is found to be optimum decomposition levels for detection of cardiac ailments from the CWSB features of multilead ECG.

**Table 4.23:** IA and OA values of ELM and SVM classifiers using all CWSB features of different wavelet decomposition levels

| **Levels** | **Classifiers** | **IA (NSR) (%)** | **IA(MI) (%)** | **IA(HMD) (%)** | **IA(BBB) (%)** | **OA (%)** |
|---|---|---|---|---|---|---|
| 7 | ELM | 95.39 | 95.38 | 95.71 | 91.59 | 94.52 |
| 7 | SVM | 95.92 | 97.56 | 97.38 | 96.23 | 96.77 |
| 6 | ELM | 95.93 | 98.37 | 97.39 | 92.79 | 96.12 |
| 6 | SVM | 97.55 | 98.37 | 96.52 | 96.12 | 97.14 |

**Table 4.24:** Performance of ELM and SVM classifiers using with phase unwrapping CWSB features and without phase unwrapped CWSB features.

| **CWSB features with phase unwrapping** | | **CWSB features without phase unwrapping** | |
|---|---|---|---|
| Classifiers | OA (%) | Classifiers | OA (%) |
| ELM | 36.90 | ELM | 96.12 |
| SVM | 55.09 | SVM | 97.14 |

In this work, the phase unwrapping is not required for evaluation of CWSB phase features. The performance of ELM and SVM classifiers using with phase unwrapping based CWSB features and without phase unwrapping based CWSB features are compared. The comparison result is shown in Table 4.24. It is observed that, the OA values of both SVM and ELM classifiers are drastically reduced using the CWSB features with phase unwrapping. The performance of ELM and SVM classifiers using CWSB features of multilead ECG with biorthogonal6.8 ('biorth6.8') and 'db5' wavelet filters are shown in Table 4.25. It is observed that, the ELM and the SVM classifiers have higher IA values for HC, MI, HMD and BBB classes using the CWSB features with biorthogonal wavelet basis function.

**Table 4.25:** Individual Class Accuracy (IA) Values of ELM and SVM classifiers using CWSB features of multilead ECG with biorth6.8 and db5 basis functions.

| Basis function | Classifiers | IA (HC) | IA (MI) | IA (HMD) | IA (BBB) |
|---|---|---|---|---|---|
| biorth6.8 | ELM | 95.93% | 98.37% | 97.39% | 92.79% |
| db5 | ELM | 92.11% | 91.84% | 93.69% | 84.63% |
| biorth6.8 | SVM | 97.55% | 98.37% | 96.52% | 96.12% |
| db5 | SVM | 93.48% | 94.83% | 95.65% | 94.49% |

The biorthogonal wavelet basis is closely matched with the morphology of ECG signal [122]. Due to this reason, the performance of biorthogonal wavelet basis based CWSB features of multilead ECG is better than the db5 based wavelet basis function. The following subsection shows the comparison of the performance of proposed methods with existing approaches using multilead ECG.

**Table 4.26:** Comparison of proposed work with existing methods for multilead ECG signals. (NU-Not used)

| Methods | IA (MI) (%) | IA (HMD) (%) | IA (BBB) (%) |
|---|---|---|---|
| Morphological Features+ANN [70] | 95 | NU | NU |
| Polynomial coefficients+MIL [2] | 91 | NU | NU |
| Hermite coefficients+ANN [183] | 83.4 | NU | NU |
| PMMSE features+LS-SVM [131] | 93.95 | 89.16 | NU |
| Morphological features+RF [39] | NU | 90 | NU |
| MEES features+SVM | 96 | NU | NU |
| Proposed multiscale PA features+Fuzzy KNN | 94.31 | 80.90 | 78.12 |
| Proposed CWSB features+SVM | 98.37 | 97.39 | 96.40 |

### 4.3.5 Comparison with Existing Methods

The classes of cardiac ailments in the proposed method are different than the reported techniques. In this work, to verify the effectiveness of the proposed methods, we have compared only the IA values of MI and HMD classes with existing 12-lead ECG based cardiac arrhythmia detection approaches. The comparison result is shown in Table 4.26. In [70], the morphological features of multilead ECG has been used for detection of MI. An accuracy value of 95% is reported for MI class. The method in [2], have used the polynomial coefficients of ST-segment along each ECG lead as features for detection of MI. An accuracy value of 91% has been reported for MI class using multi instance learning model. In [183], the hermite coefficients of 12-lead ECG and the artificial neural network (ANN) are used for detection of MI. They have reported an accuracy value of 83.4% for MI class. In the previous

chapter, the accuracy value of MI class using the MEES features and SVM classifier is found to be 96%. The proposed method (CWSB features and SVM) has higher accuracy value for MI class than the methods reported in [70], [2], [183]. In [131], the PMMSE features and the least square SVM (LS-SVM) have been used for detection of MI, heart muscle disease (cardiomyopathy and hypertrophy). The detection of hypertrophic cardiomyopathy using the temporal and the morphological features of multilead ECG has been proposed in [39]. An accuracy value of 90% is reported for HMD class using random forest (RF) classifier. The accuracy values of the SVM classifier using proposed CWSB features for MI and HMD classes are higher than the performance of PMMSE features and the morphological features of multilead ECG. In [51], the absolute value of the complex wavelet coefficients of single lead ECG and other morphological features have been used for detection of BBB. The sensitivity values for right BBB and left BBB classes are 80.65% and 82.26%, respectively. The proposed method has advantage of using CWSB features of 12-lead ECG for detection of BBB pathology. For BBB class, the proposed method has a IA value of 96.40%. The above observations reveal that, the complex wavelet magnitude and phase features of multilead ECG are effective for detection of various cardiac abnormalities.

## 4.4 Summary

In this chapter, two new methods have been proposed for detection of cardiac ailments. These methods are based on the evaluation of diagnostic features from the complex wavelet coefficients of multilead ECG. The DTCWT has been used to decompose multilead ECG into complex wavelet coefficients at different sub-bands. In first method, the multiscale PA features are evaluated from the complex wavelet coefficients of multilead ECG. The statistical analysis of multiscale PA features are performed. The performance of multiscale PA features are evaluated using KNN and fuzzy KNN classifier for detection of BBB, HMD and MI pathologies. The accuracy values of 94.31% 80.90% 78.12% for MI, HMD and BBB classes are found using Fuzzy KNN classifier and selected multiscale PA features. In second method, the CWSB magnitude and phase features of multilead ECG are evaluated. The statistical significance of CWSB magnitude and phase features are shown using ANOVA test. The SU score has been used for selecting relevant features from the CWSB feature vector of multilead ECG. The SVM and the ELM classifiers have been used to evaluate the performance of

CWSB magnitude and phase features of multilead ECG. For MI, HMD and BBB classes, the accuracy values 98.37% 97.39% 96.40% are obtained using SVM classifier. The accuracy values for MI and HMD classes using proposed methods are higher than the existing techniques.

भारतीय प्रौद्योगिकी संस्थान गुवाहाटी
Indian Institute of Technology Guwahati

# 5

# Variational Mode Decomposition for Detection of Shockable Ventricular Arrhythmia



## Contents

The rapid ventricular tachycardia (VT) and the ventricular fibrillation (VF) are two types of shockable ventricular arrhythmia that can lead to sudden cardiac death; however, they can be stopped with a shock delivered by a defibrillator and regular cardiac activity could be restored [96] [97]. Detection of these cardiac abnormalities is one of the important steps in automated external defibrillator (AED) and implantable cardioverter defibrillator (ICD) therapy [20]. In Chapter 3 and Chapter 4, the multiscale features of multilead ECG have been used for detection of various heart pathologies. These multi-scale features are evaluated using discrete wavelet transform (DWT) and dual tree complex wavelet transform (DTCWT). The DWT and the DTCWT based processing of ECG require proper selection of basis function or wavelet filters. The bi-orthogonal wavelet basis function is typically used for wavelet based analysis of ECG [122]. The morphology of ECG signal is different during shockable ventricular arrhythmia. The wavelet based methods has the drawbacks to quantify diagnostic information from ECG during rapid VT and VF [106]. Therefore, a data-dependent method for estimating diagnostic features of ECG is required for detection of shockable ventricular arrhythmia. This chapter proposes a new method for detection of shockable ventricular cardiac arrhythmia from ECG. The method uses variational mode decomposition (VMD) to evaluate diagnostic features from ECG signal. The VMD is a non-linear and recursive method to decompose the ECG signal into number of sub-signals or modes [68]. These variational modes capture the grossly segregated clinical components such as the P-wave, the QRS-complex and the T-wave of ECG. In rapid VT and VF, the abnormal waves (as shown in Fig. 1.8) appear in the ECG signal. These pathological changes can be captured using the modes of ECG signal. The literature survey in chapter 2 shows that, the VMD has been used for filtering of various noises from ECG [28]. The center frequency and the phase difference features of the variational modes of ECG have been used for detection of ventricular flutter, atrial flutter and VF [69]. The variational mode energy and entropy (VMEE) features have not been used for detection of shockable ventricular arrhythmia. The energy and the entropy features of the variational mode have the potential to capture the pathological changes in ECG signal.

In this work, three features such as the energy, the Renyi entropy (RE) and the permutation entropy (PE) are evaluated from the modes of the ECG signal. The mutual information based feature scoring is used for selection of important attributes from the VMEE features. The random forest classifier is employed for classification of ECG features (RE, energy, PE and selected features) into

shockable ventricular arrhythmia and non-shockable episodes. The rest of this chapter is organized as follows. In Section 5.1, the diagnostic information captured using the modes of ECG is briefly discussed. Section 5.2 describes the proposed method for detection and classification of shockable ventricular arrhythmia and non-shockable episodes. The method is evaluated in Section 5.3. The statistical significance of VMEE features of is analyzed in the same section. The performance of the random forest classifier using RE features, PE features, energy features and selected VMEE features is shown. In Section 5.4, the summary of this chapter is written.

## 5.1 Diagnostic Information in Modes of ECG

In this section, the diagnostic information present in the modes of ECG is discussed. The major spectral energy of an ECG signal is observed in the frequency range between 0.5 Hz to 35 Hz [20]. The frequency information of the clinical components of ECG are grossly divided in this range. The VMD technique divides an ECG signal into number of modes. Each mode of ECG signal has different center frequency and bandwidth. The modes, $\mathbf{s}_t(n)$ and the center frequencies, $\omega_t$ of an ECG signal, $\mathbf{x}(n)$ are evaluated using the equation 2.21 and the equation 2.22, respectively. where $t = 1, 2, ..., T$ is the number of modes of the ECG signal. In VMD, the center frequencies can be either uniformly assigned or randomly selected. During shockable ventricular arrhythmia, the electrical activity of heart is due to the firing of multiple pacemaker cells in the ventricles at different locations [1]. It is expected that, the electrical activity of heart during shockable ventricular arrhythmia can be captured using the randomly assigned center frequencies prior in VMD based analysis of ECG. In this work, the initial center frequencies of the modes of ECG are randomly assigned. The initial values of other parameters are the number of modes as $T = 5$, the balancing parameter of the data-fidelity constraint as $\alpha = 30$ and the tolerance of convergence criterion as $tol = 10^{-7}$, respectively. The frequency range from 0.5 Hz to 15 Hz is typically considered for analysis of ECG signal during shockable ventricular arrhythmia [104]. In this study, the first three modes of ECG signal based on the ascending order of center frequencies are considered for analysis. Fig. 5.1 (a) and Fig. 5.1 (b) depict the ECG signal and its spectrum for non-shockable ECG episode. The modes of the ECG signal obtained from VMD are shown in Fig. 5.1 (c), Fig. 5.1 (e) and Fig. 5.1 (f), respectively. It is observed that, the diagnostic components such as the P-wave, the QRS-complex and the T-wave of ECG are grossly segmented

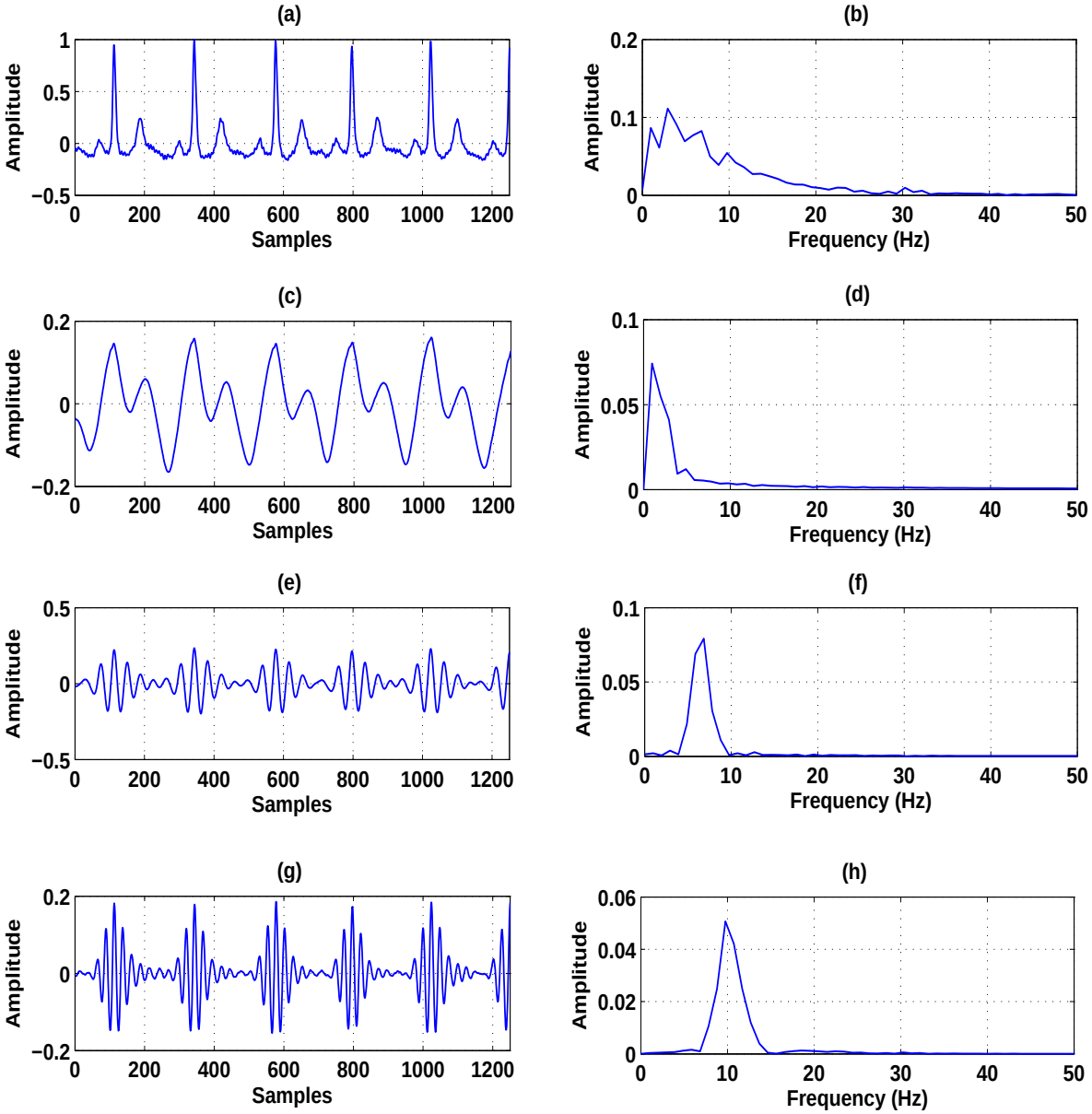


**Fig. 5.1:** (a) ECG signal for non-shockable episode (Normal sinus rhythm). (b) Spectrum of the ECG signal for non-shockable episode. (c) Mode1 Signal. (d) Spectrum of mode1 signal. (e) Mode2 Signal. (f) Spectrum of mode2 signal. (g) Mode3 Signal. (h) Spectrum of mode3 signal. The amplitude of the ECG signal is in mV and the sampling frequency is 250 Hz.

in first three modes. The center frequency and the bandwidth of mode1 signal are 0.97 Hz and 3.46 Hz, respectively. Similarly, for mode2, the center frequency and the bandwidth are evaluated as 6.83 Hz and 5.80 Hz. Likewise, the center frequency and the bandwidth of mode3 are 9.76 Hz and 8.80

Hz, respectively. The low-frequency information such as ST-segment, T-wave and P-wave appear in mode1. The mode2 and the mode3 signals grossly capture the QRS-Complex information of ECG.

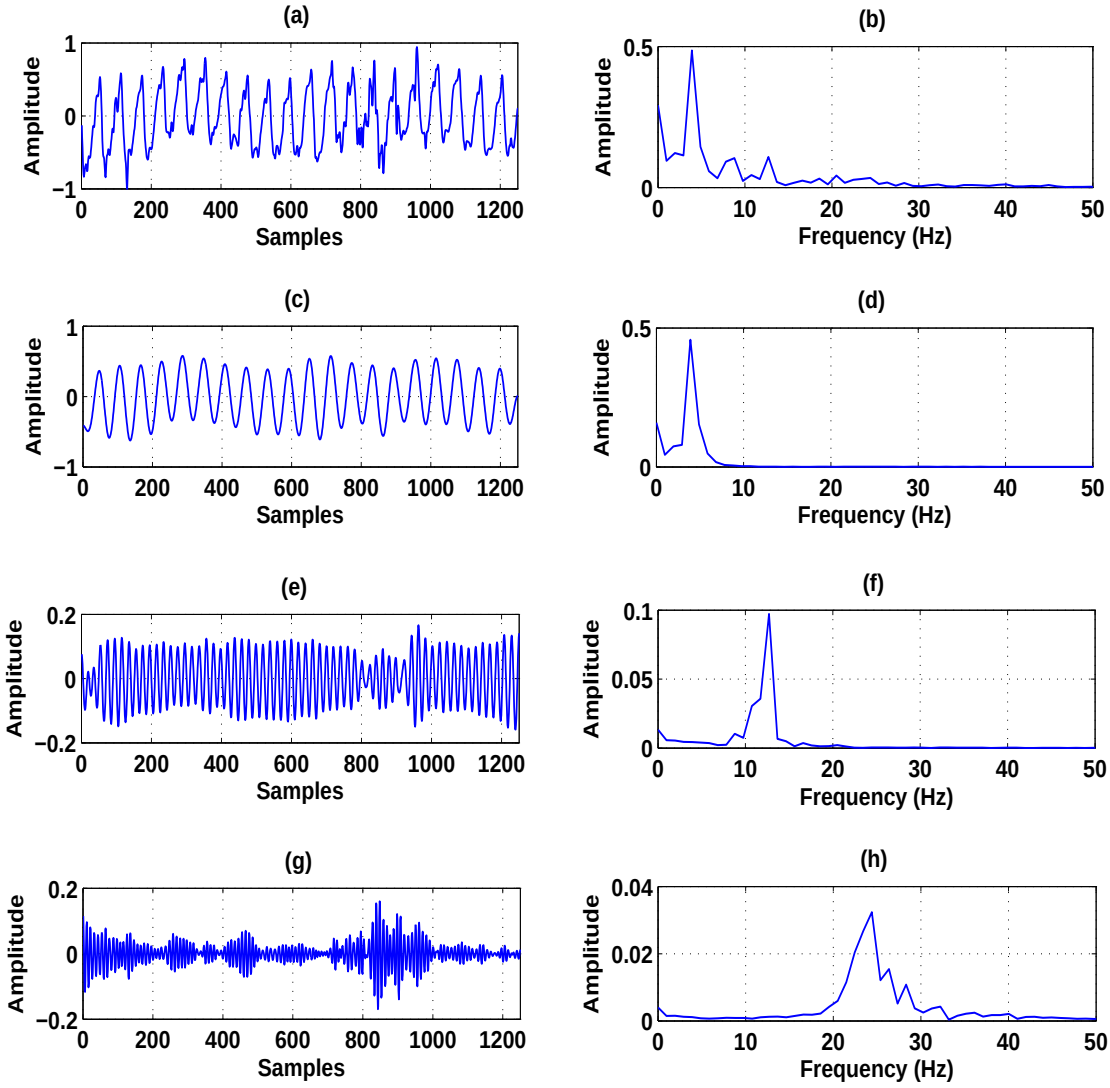


**Fig. 5.2:** (a) ECG signal for Shockable ventricular arrhythmia (rapid ventricular tachycardia) episode. (b) Spectrum of the ECG signal for shockable ventricular arrhythmia episode. (c) Mode1 Signal. (d) Spectrum of mode1 signal. (e) Mode2 Signal. (f) Spectrum of mode2 signal. (g) Mode3 Signal. (h) Spectrum of mode3 signal. The amplitude of the ECG signal is in mV and the sampling frequency is 250 Hz.

Fig. 5.2 (a) and Fig. 5.2 (b) show the ECG signal and its spectrum for shockable ventricular arrhythmia (rapid VT) episode. The modes of this ECG episode are depicted in Fig. 5.2 (c), Fig. 5.2 (e) and Fig. 5.2 (g), respectively. Fig. 5.2 (d), Fig. 5.2 (f) and Fig. 5.2 (h) show the frequency domain signals for mode1, mode2 and mode3. It is observed that, the rapid abnormal patterns due

to shockable ventricular arrhythmia are grossly captured in mode1, mode2 and mode3, respectively. The signal characteristics of mode1, mode2 and mode3 for shockable ventricular arrhythmia case are different than non-shockable case. The center frequency and the bandwidth of mode1 for shockable ventricular arrhythmia episode are 3.90 Hz and 5.86 Hz, respectively. Similarly, for mode2, the center frequency and the bandwidth are 12.70 Hz and 7.82 Hz, respectively. The center frequency and the bandwidth of mode3 are obtained as 24.41 Hz and 13.78 Hz, respectively. The spectral characteristics of each mode is different for shockable ventricular arrhythmia and non-shockable episodes. The center frequency values of mode1, mode2 and mode3 for shockable ventricular arrhythmia case are higher than the non-shockable case. The abnormal patterns other than 'PQRST' appear in ECG during shockable ventricular arrhythmia. These patterns are originated from the left ventricle and the right ventricle at a rate of 100 to 130 beats per minute [1]. The modes obtained using VMD capture the morphological features of ECG. This may be the reason for which the center frequency values of the modes of ECG show significant variation during shockable ventricular arrhythmia and non-shockable cases. The time domain and the frequency domain characteristics of the modes of ECG are different for shockable ventricular arrhythmia and non-shockable episodes. It is expected that, the time domain and the frequency domain features evaluated from the modes of ECG will be helpful for detection of shockable ventricular arrhythmia. In the following section, the proposed method for detection and classification of shockable ventricular arrhythmia and non-shockable episodes is described.

## 5.2 Proposed Method

The block diagram of the proposed method for detection and classification of shockable ventricular arrhythmia and non-shockable episodes from ECG is shown in Fig. 5.3. It consists of filtering and segmentation of ECG data, evaluation of VMEE features, feature selection using mutual information based scoring technique and classification using random forest classifier. In this work, the zero-phase Butterworth high pass filter with a cutoff frequency of 0.5 Hz is considered for elimination of low-frequency noise (baseline wandering) [22]. The high-frequency noise is removed using a zero-phase low pass filter with a cutoff frequency of 35 Hz [19]. The filtered ECG signal is segmented into non-overlapping episodes with the help of an analysis window. In literature, the 8 sec, the 6 sec

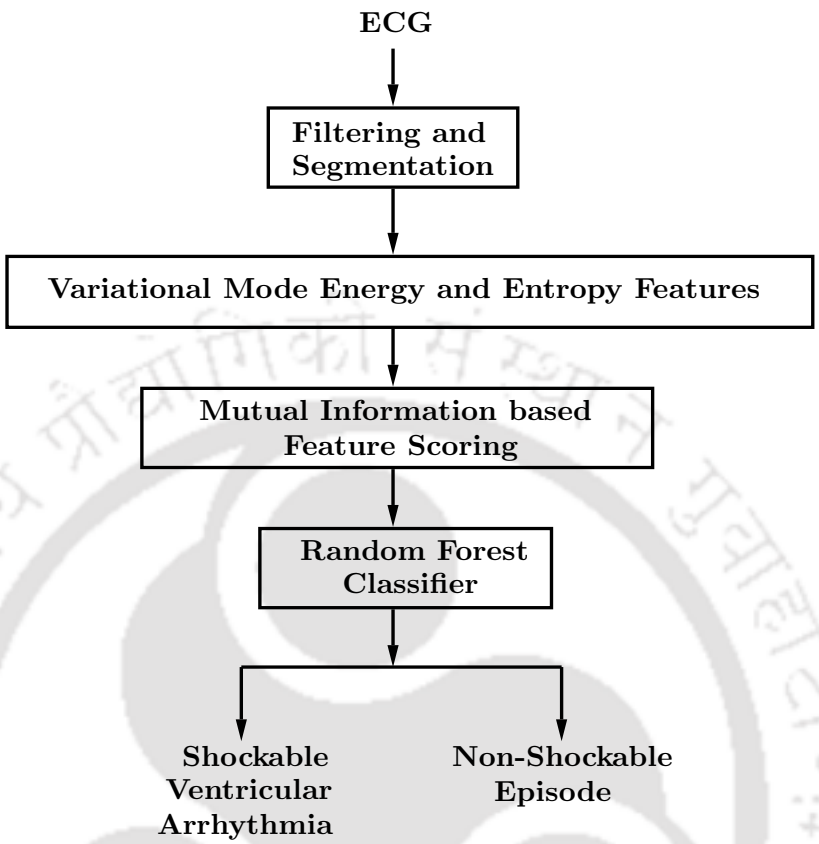


**Fig. 5.3:** Flow-chart of proposed method for detection and classification of shockable ventricular arrhythmia and non-shockable episodes from ECG.

and the 5 sec windows have been used to segment ECG data [19] [20]. In this study, both 8 sec and 5 sec windows are considered for segmentation. Here, the VF and the rapid VT ECG episodes are considered as shockable ventricular arrhythmia. The normal sinus rhythm (NSR), the ventricular bigeminy (VB), the ventricular ectopic beats (VEB) and the ventricular escape rhythms (VER) are considered as non-shockable ECG episodes.

### 5.2.1 Variational Mode Energy and Entropy Features

In this subsection, the time domain and the frequency domain features are evaluated from the modes of ECG signal. The modes evaluated using VMD of ECG capture the diagnostic information. For shockable ventricular arrhythmia and non-shockable cases, the characteristics of mode1, mode2 and mode3 are different. The energy measures the strength of each mode. The energy of the $t^{th}$ mode of

an ECG signal is defined by

$$E_t = \sum_{n=1}^{N} |\mathbf{s}_t(n)|^2 \tag{5.1}$$

where 'N' is the length of the ECG segment and $\mathbf{s}_t(n)$ corresponds to the time domain signal of t$^{th}$ mode. The PE captures the irregularity of each mode. Here, the PE features from the modes of ECG are evaluated. The PE of t$^{th}$ mode is evaluated using equation 2.28, equation 2.29 and equation 2.30, respectively. In this work, the values of embedding dimension and the lag of PE for each mode are considered as $\overline{d} = 5$ and $\overline{l} = 2$, respectively.

The RE has been used to quantify uncertainty in the frequency domain signal [185] [186]. The spectral characteristics of shockable ventricular arrhythmia and non-shockable ECG episodes (as shown in Fig. 5.1 and Fig. 5.2) are different for mode1, mode2 and mode3, respectively. These differences can be captured using the RE measure. The RE is evaluated using the probability of the Fourier coefficients of t$^{th}$ mode. The probability of t$^{th}$ mode is given by

$$P_t(w) = \frac{|s_t(w)|^2}{E_t} \tag{5.2}$$

where $s_t(w)$ is the frequency domain signal of t$^{th}$ mode. $E_t$ is the energy of the t$^{th}$ mode of ECG signal. The RE measure is evaluated as

$$RE_t = \frac{1}{1-\theta} log \sum_{w=1}^{BW_t} [P_t(w)]^{\theta} \tag{5.3}$$

where $BW_t$ corresponds to the bandwidth of t$^{th}$ mode and $\theta$ is the order of RE. The range of $\theta$ is given by $0 < \theta < 1$. Here, the value of $\theta = 0.5$ is considered for each mode.

### 5.2.2 Feature selection and Classification

In this work, the energy, the PE and the RE features are evaluated from the first three modes of ECG. Then, the mode energy, the mode RE and the mode PE feature vectors are formulated. Each of these feature vector contains three attributes. The total feature vector is created by combining the mode energy, the mode RE and the mode PE features. This feature vector contains nine attributes. The mutual information based feature selection is used for choosing the relevant attributes from the nine dimensional feature vector [155]. The mutual information score for each attribute is evaluated using equation 2.33. The features which have higher value of mutual information score are selected.

The mode energy feature vector, the mode RE feature vector, the mode PE feature vector, the total feature vector and the new feature vector derived using mutual information feature scoring are used as input to random forest (RF) classifier.

In this study, the RF classifier is considered to classify the diagnostic features of ECG into shockable ventricular arrhythmia and non-shockable episodes. The feature matrix for RF classifier is given by $\mathbf{Z} \in R^{p \times q}$. where $p$ and $q$ are the number of ECG episodes and number of features. The RF classifier is created using number of decision trees. The training and the testing instances of RF classifier is chosen using 5-fold cross-validation technique [44]. For training, the feature matrix or dataset $\mathbf{Z} \in R^{p \times q}$ is divided into $\tilde{L}$ number of sub datasets such as $\mathbf{Z}_1, \mathbf{Z}_2, \mathbf{Z}_3, ...., \mathbf{Z}_L$. The corresponding class label vectors for the sub datasets are $\mathbf{y}_1, \mathbf{y}_2, \mathbf{y}_3, ...., \mathbf{y}_L$. The instances of the $i^{\text{th}}$ sub-dataset ($i = 1, 2...\tilde{L}$) are randomly chosen from $p$ number instances of the feature matrix ($\mathbf{Z}$). The class label of a test feature instance in RF classifier is evaluated based on the output of each decision tree. In this study, the tuning parameters (number of trees, depth of each tree, number of splits) of RF classifier are selected based on the hit and trail method. First, the number of trees are varied from $1$ to $10$. Then, the number of splits and the depth of each tree vary from $1$ to $10$ and $2$ to $12$, respectively. The optimal parameters are selected based on the performance of RF classifier using VMEE features. The entropy impurity is considered to determine the split node of each decision tree in RF classifier. The performance of RF classifier for test data is evaluated using sensitivity, specificity and accuracy measures. These measures are evaluated using equation 2.56, equation 2.57 and equation 2.58, respectively. The sensitivity, the specificity and the accuracy values of RF classifier are evaluated for mode RE, mode PE and mode energy feature vectors of ECG.

## 5.3 Evaluation of the Proposed Method

The proposed method is evaluated using the ECG signals from CUDB, VFDB and MITDB databases [5], [6]. The sampling frequency of the ECG signals for CUDB and VFDB databases are 250 Hz. The sampling frequency of ECG signal for MITDB database is 360 Hz. The ECG signals of MITDB database are re-sampled to 250 Hz [107]. The ECG signals of CUDB, VFDB and MITDB databases are subjected to filtering and segmentation. In this work, the results are presented by considering both $5$ sec and $8$ sec ECG episodes. For shockable ventricular arrhythmia and non-shockable classes,

2605 and 6610 number of 5 sec ECG episodes are evaluated. Similarly, 2005 and 5018 number of 8 sec ECG episodes are also evaluated from shockable ventricular arrhythmia and non-shockable classes. The VMD is applied to the segmented ECG episodes of both shockable ventricular arrhythmia and non-shockable classes. The energy, the RE and the PE features are computed from the modes of ECG episodes. The mode RE feature vector, the mode PE feature vector and the mode energy feature vector are evaluated for each 8 sec and 5 sec ECG episodes. The RF classifier is employed to evaluate the performance of mode RE, mode PE and mode energy feature vectors of ECG. The following subsections describe the statistical significance of mode energy, mode RE and mode PE features of ECG, and the performance of RF classifier for different feature subsets.

### 5.3.1 Analysis of Mode Energy and Entropy Features

In this subsection, the statistical analysis of mode energy, mode PE and mode PE features is shown. The within-class variations (Box-plot) of energy feature for shockable ventricular arrhythmia and non-shockable classes at mode1, mode2 and mode3 are shown in Fig. 5.4 (a) and Fig. 5.4 (b), respectively. It is evident that, the minimum value, the median value and the maximum value of the box-plot are different for shockable ventricular arrhythmia and non-shockable classes at each mode. The mean and the standard deviation values of energy, RE and PE at mode1, mode2 and mode3 are shown in Table 5.1. The mean values of energy features for shockable ventricular arrhythmia and non-shockable classes in mode1, mode2 and mode3 are (33.54, 2.15), (6.94, 0.88) and (8.19, 0.38), respectively. Similar variations in the standard deviation values are also observed for mode1, mode2 and mode3, respectively. In VT, the QRS-complex duration is greater than 120 ms and these patterns are generated from the lower chambers of the heart at an intrinsic peaks of 100 to 130 beats per minute [17], [1]. The abnormal patterns other than normal heart rhythm are observed in ECG signal due to VF [1]. The mode energy features correctly captures these pathological variations with differences in the mean values of 31.39, 6.08 and 7.81 at mode1, mode2 and mode3, respectively. The statistical significance of energy feature for mode1, mode2 and mode3 is evaluated using two-tailed t-test method [140]. The t-value and the p-value of energy, RE and PE features for mode1, mode2 and mode3 are shown in Table 5.2. It is observed that, the t-value of energy feature in mode1, mode2 and mode3 are 28.10, 9.29 and 13.83, respectively. This high t-value and the low p-value ($p<0.001$)

reveal that, the energy features are significant to discriminate shockable ventricular arrhythmia and non-shockable episodes from ECG.

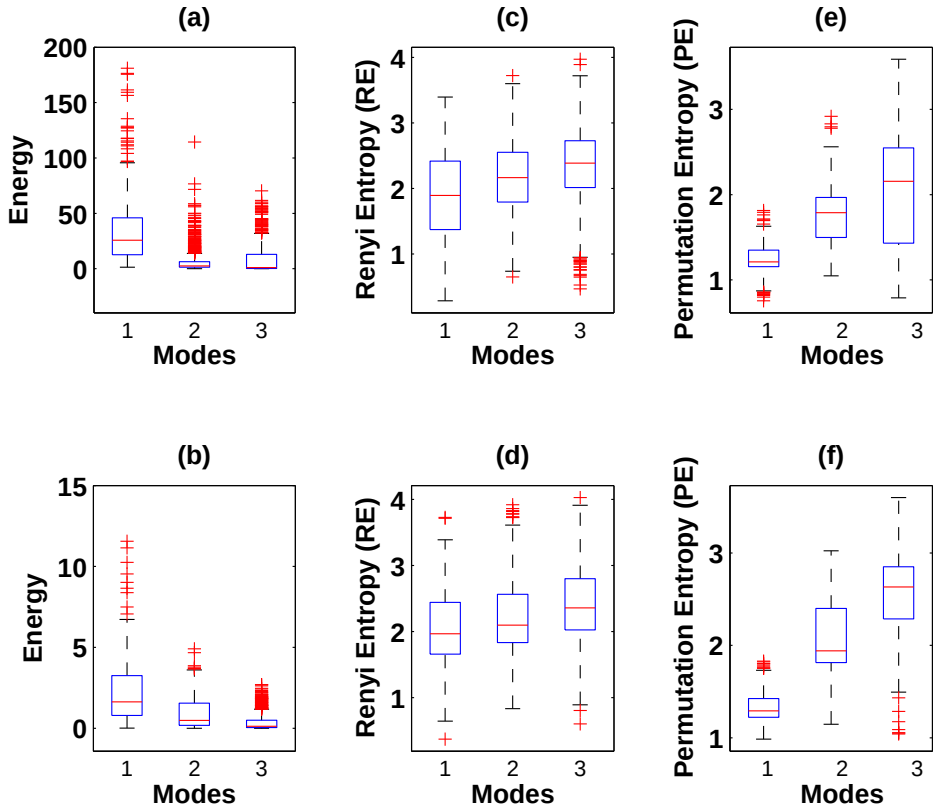


**Fig. 5.4:** (a) Within-class variation of energy for shockable ventricular arrhythmia class at mode1, mode2 and mode3. (b) Within-class variation of RE for non-shockable class at mode1, mode2 and mode3. (c) Within-class variation of PE for shockable ventricular arrhythmia class at mode1, mode2 and mode3. (d) Within-class variation of energy for non-shockable class at mode1, mode2 and mode3. (e) Within-class variation of RE for shockable ventricular arrhythmia at mode1, mode2 and mode3. (f) Within-class variation of PE for non-shockable class at mode1, mode2 and mode3.

Fig. 5.4 (c) and Fig. 5.4 (d) show the within-class variations of RE feature for shockable ventricular arrhythmia and non-shockable classes at mode1, mode2 and mode3. From Table 5.1, it is observed that the mean and the standard deviation values of RE are different for shockable ventricular arrhythmia and non-shockable classes. The non-shockable class has higher mean values of RE at mode1, mode2 and mode3 than the shockable ventricular arrhythmia class. As the RE feature captures the spectral variation of each mode, the mean and the standard deviation values are different for shockable ventricular arrhythmia and non-shockable classes. The t-values of RE feature at mode1, mode2 and mode3 are $6.82$, $2.53$ and $3.01$, respectively. From Fig. 5.2, it is ob-

**Table 5.1:** Mean ($\mu$) and Standard deviation ($\sigma$) values of energy, RE and PE at mode1, mode2 and mode3.

| | **Shockable Arrhythmia Class** | | **Non-shockable Class** | |
|---|---|---|---|---|
| **Features** | Mean ($\mu$) | Sigma ($\sigma$) | mean($\mu$) | Sigma ($\sigma$) |
| Energy Mode1 | 33.54 | 36.13 | 2.15 | 2.03 |
| Energy Mode2 | 6.94 | 21.11 | 0.88 | 0.87 |
| Energy Mode3 | 8.19 | 18.26 | 0.38 | 0.53 |
| RE Mode1 | 1.86 | 0.64 | 2.04 | 0.54 |
| RE Mode2 | 2.17 | 0.52 | 2.22 | 0.51 |
| RE Mode3 | 2.34 | 0.56 | 2.41 | 0.54 |
| PE Mode1 | 1.24 | 0.14 | 1.31 | 0.14 |
| PE Mode2 | 1.77 | 0.32 | 2.12 | 0.38 |
| PE Mode3 | 2.07 | 0.70 | 2.55 | 0.47 |

**Table 5.2:** The statistical significance of energy and entropy features.

| **Features** | **t-value** | **p-value** |
|---|---|---|
| Energy mode1 | 28.10 | $<$0.001 |
| Energy mode2 | 9.29 | $<$0.001 |
| Energy mode3 | 13.83 | $<$0.001 |
| RE mode1 | 6.82 | $<$0.001 |
| RE mode2 | 2.53 | 0.011 |
| RE mode3 | 3.01 | 0.002 |
| PE mode1 | 11.44 | $<$0.001 |
| PE mode2 | 22.57 | $<$0.001 |
| PE mode3 | 18.36 | $<$0.001 |

served that, the abnormal patterns other than QRS-complex are observed in mode1 of the shockable ventricular arrhythmia episode. The QRS spectral peaks are shifted slightly to low frequencies during rapid VT [3]. The mode1 captures the low-frequency components of ECG signal. The spectral characteristics of mode1 signal (as shown in Fig. 5.1 (d) and Fig. 5.2 (d)) is different for shockable ventricular arrhythmia and non-shockable episodes. This may be the reason for which the t-value of RE in mode1 is higher than the t-value of mode2 and mode3. It is also seen that, the p-value of RE at mode1 is less than $0.001$. The RE feature of mode1 is statistically significant for classification of shockable ventricular arrhythmia and non-shockable episodes from ECG. The within-class variations of PE for shockable ventricular arrhythmia and non-shockable classes at mode1, mode2 and mode3 are depicted in Fig. 5.4 (e) and Fig. 5.4(f), respectively. From Table 5.1, it is observed that for non-shockable class, the mean values of PE for mode1, mode2 and mode3 are higher than the shockable

ventricular arrhythmia class. The beat-to-beat variations of the clinical components of ECG are higher in normal sinus rhythm (NSR) compared to shockable ventricular arrhythmia (VT/VF) [50], [187]. This may be reason for different mean values of PE in mode1, mode2 and mode3 for shockable and non-shockable ventricular arrhythmia classes. The statistical significance of PE features of each mode is evaluated using t-test. From Table 5.2, it is observed that the t-value of PE at mode1, mode2 and mode3 are $11.44$, $22.57$ and $18.36$, respectively. These high values infer that, the mode PE features are statistically significant for detection and classification of shockable ventricular arrhythmia and non-shockable episodes from ECG. The following section discusses the performance of RF classifier using mode energy and entropy features.

### 5.3.2 Performance of Random Forest Classifier

In this subsection, the performance of RF classifier is shown using the mode energy feature vector, the mode PE feature vector, the mode RE feature vector and the feature vector derived using mutual information based feature selection approach. The optimal tuning parameters of RF classifier are evaluated as follows. First, the number of splits and depth of each tree in RF classifier is fixed. The variations of the average accuracy, the average sensitivity and the average specificity values with number of trees of RF classifier are shown in Table 5.3. It is observed that, the accuracy value of RF classifier is 97.09% for number of trees equal to $7$. By increasing the number of trees to $8$, the accuracy of RF classifier is reduced to 96.85%. So, number of trees equal to $7$ is found as the optimal value for classification performance of RF classifier. Table 5.4 shows the variations of the average accuracy, the average sensitivity and the average specificity values with depth of tree. Here, number of splits as 8 and number of tress as 7 are fixed. It is observed that, the accuracy of RF classifier increases by increasing the depth of each tree. When depth of tree is equal to $11$, the accuracy value of RF classifier is found to be 97.23%. The variations of the average accuracy, the average sensitivity and the average specificity values with number of splits are shown in Table 5.5. Here, the number of trees and the depth of each tree are fixed. It is seen that, the accuracy value of RF classifier is found to be 97.23% for the number of splits equal to 11. The above observations infer that, the number of trees as 7, the number of splits as 9 and the depth of tree as 11 are the optimal parameters of RF classifier for detection and classification of shockable ventricular arrhythmia and non-shockable

episodes from the VMEE features of ECG.

**Table 5.3:** Variation of Accuracy, Sensitivity and Specificity values with respect to number of trees (number of splits=8 and depth of each tree=10).

| Number of Trees | Accuracy(%) | Sensitivity (%) | Specificity (%) |
|---|---|---|---|
| 1 | 93.66 | 92.53 | 95.12 |
| 2 | 96.14 | 95.56 | 96.89 |
| 3 | 96.61 | 96.51 | 96.76 |
| 4 | 96.66 | 95.99 | 97.43 |
| 5 | 96.61 | 96.16 | 97.11 |
| 6 | 96.33 | 96.12 | 96.55 |
| 7 | 97.09 | 96.61 | 97.61 |
| 8 | 96.85 | 96.59 | 97.13 |
| 9 | 97.04 | 96.72 | 97.43 |
| 10 | 96.80 | 96.42 | 97.21 |

**Table 5.4:** Variation of Accuracy, Sensitivity and Specificity values with depth of tree (number of tress=7 and number of splits=8).

| Depth of Trees | Accuracy (%) | Sensitivity (%) | Specificity (%) |
|---|---|---|---|
| 2 | 91.28 | 89.34 | 94.85 |
| 3 | 93.76 | 95.31 | 92.46 |
| 4 | 93.38 | 93.22 | 94.06 |
| 5 | 95.33 | 95.56 | 95.37 |
| 6 | 95.85 | 95.22 | 96.54 |
| 7 | 96.23 | 96.46 | 96.05 |
| 8 | 96.57 | 96.16 | 97.06 |
| 9 | 96.66 | 95.89 | 97.49 |
| 10 | 96.76 | 95.76 | 97.86 |
| 11 | 97.23 | 97.06 | 97.42 |
| 12 | 97.04 | 96.17 | 97.97 |

Table 5.6 shows the average accuracy, the average sensitivity and the average specificity values of RF classifier using the VMEE features of 5 sec ECG episodes. It is observed that, the average accuracy, the average sensitivity and the average specificity values of RF classifier with mode energy features are higher than the mode RE and the mode PE features of ECG. The energy feature captures the strength of the signal along each mode. Due to shockable ventricular arrhythmia, the abnormal patterns are observed in ECG and the inter-beat variations in theses episodes are high [17], [1]. The mode energy features correctly quantify the pathological changes in ECG during shockable ventricular arrhythmia. This may be the reason for the performance of energy feature with RF classifier is

**Table 5.5:** Variation of Accuracy, Sensitivity and Specificity values with number of splits (number of tress=7, depth of tree=11).

| Number of Splits | Accuracy (%) | Sensitivity (%) | Specificity (%) |
|---|---|---|---|
| 1 | 93.19 | 92.11 | 94.64 |
| 2 | 95.23 | 95.77 | 94.73 |
| 3 | 95.47 | 95.55 | 95.57 |
| 4 | 95.95 | 96.55 | 95.68 |
| 5 | 96.90 | 96.61 | 97.24 |
| 6 | 96.80 | 96.26 | 97.40 |
| 7 | 96.85 | 96.27 | 97.50 |
| 8 | 97.19 | 96.63 | 97.79 |
| 9 | 97.23 | 96.54 | 97.97 |
| 10 | 97.23 | 96.45 | 98.08 |

**Table 5.6:** Accuracy, Sensitivity and Specificity of RF classifier using VMEE features of 5 sec ECG episodes.

| Features | Accuracy (%) | Sensitivity (%) | Specificity (%) |
|---|---|---|---|
| Mode Energy | 96.76 | 96.24 | 97.31 |
| Mode RE | 64.42 | 60.49 | 73.36 |
| Mode PE | 80.04 | 75.61 | 87.32 |
| All Features | 96.66 | 96.13 | 97.21 |
| Feature Selection | 97.23 | 96.54 | 97.97 |

**Table 5.7:** Accuracy, Sensitivity and Specificity of RF classifier using VMEE features of 8 sec ECG episodes.

| Features | Accuracy (%) | Sensitivity (%) | Specificity (%) |
|---|---|---|---|
| Mode Energy | 92.95 | 92.08 | 93.84 |
| Mode RE | 70.34 | 69.41 | 71.61 |
| Mode PE | 90.60 | 91.27 | 90.03 |
| All Features | 93.39 | 93.32 | 93.49 |
| Feature Selection | 94.07 | 94.37 | 94.73 |

higher than other features. Using all VMEE features, the average accuracy, average sensitivity and average specificity values of RF classifier are found to be $96.66\%$, $96.13\%$ and $97.21\%$, respectively. The weight value of each VMEE feature is shown in Fig. 5.5. These weights values are evaluated using the mutual information based feature scoring approach. It is observed that, the energy and the PE of mode1, mode2 and mode3 have higher weight values than those of RE features. Form t-test result, it is also seen that, the p-value of mode2 RE and mode3 RE are 0.011 and 0.022, respectively. These p-values are higher than 0.001 and the corresponding RE features of mode2 and mode3 are

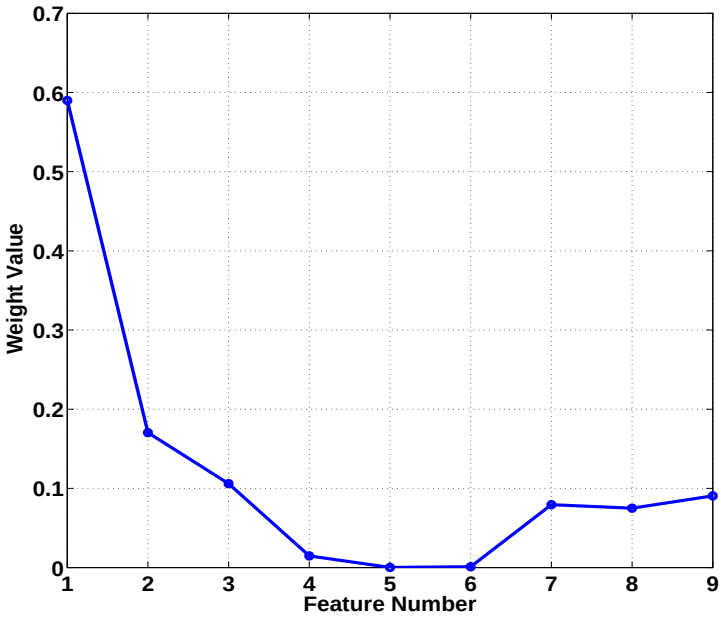


**Fig. 5.5:** Weight value of each feature using mutual information based feature scoring.

statistically insignificant. The mode2 RE and mode3 RE features are eliminated from the 9 dimensional VMEE feature vector. In this work, the energy and the PE of mode1, mode2, mode3, and the mode1 RE are used for deriving the new feature vector. It is observed that, the average accuracy, the average sensitivity and the average specificity values of RF classifier are improved to 97.19%, 96.63% and 97.79% using mutual information based feature scoring method.

Table 5.7 shows the average accuracy, the average sensitivity and the average specificity of RF classifier using the different feature combinations of 8 sec ECG episodes. It is observed that, the average accuracy and the average sensitivity of RF classifier using the mode RE and the mode PE features of 8 sec ECG episodes are higher than the features of 5 sec ECG episodes. The performance of RF classifier in terms of the average accuracy, the average sensitivity and the average specificity are 93.39%, 93.32% and 93.49%, respectively using all VMEE features. For 8 sec ECG episodes, the average accuracy, the average sensitivity and the average specificity of RF classifier using selected features are improved to 94.07%, 94.37% and 94.73%, respectively. The redundant features are eliminated using the mutual information based feature selection approach. This may be the reason for the better performance of RF classifier using selected VMEE features.

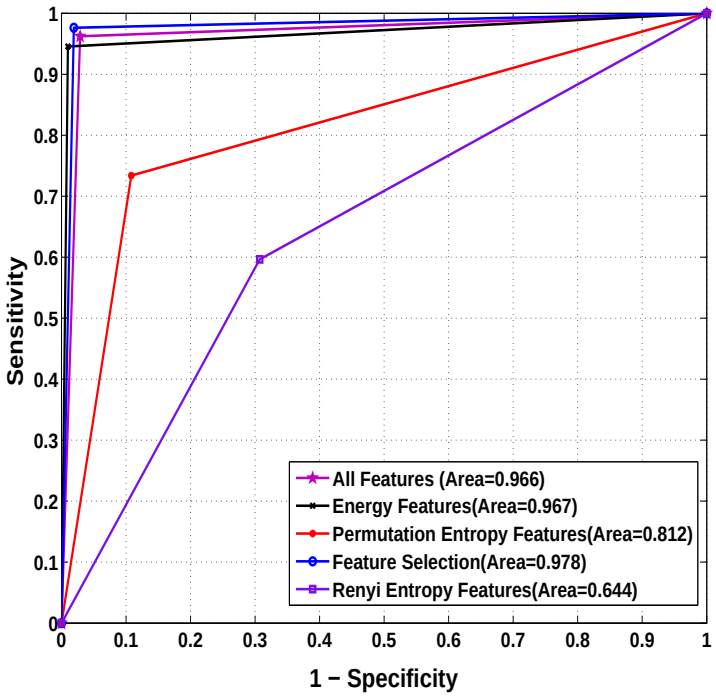


**Fig. 5.6:** ROC curves of RF classifier for different feature subsets of 5sec ECG episodes.

Fig. 5.6 and Fig. 5.7 depict the receiver operating characteristics (ROC) curves of RF classifier using different feature combinations of 5 sec and 8 sec ECG episodes. It is observed that, the RF classifier with mutual information based feature scoring approach has highest area under under ROC (AROC) values of 0.978 and 0.942 for 5 sec and 8 sec ECG episodes. The AROC value of RF classifier using the mode RE features of 8 sec ECG episodes is found to be 0.704. This value is higher than the AROC value of RF classifier and mode RE features of 5 sec ECG episodes. The RF classifier with mode energy features have higher AROC value for 5sec ECG episodes. The RF classifier and the mode PE features have higher AROC value of 0.913 for 8sec ECG episodes. This value is higher than the AROC value of RF classifier and the mode PE features of 5 sec ECG episodes. The mode PE features capture the irregularity of the clinical components of ECG. The beat-by-beat variations in non-shockable cases are higher than the shockable ventricular arrhythmia [50]. These pathological changes can be effectively captured using the modes of 8 sec ECG episode. This may be the reason for higher AROC value of RF classifier using the mode PE features of 8 sec ECG episodes.

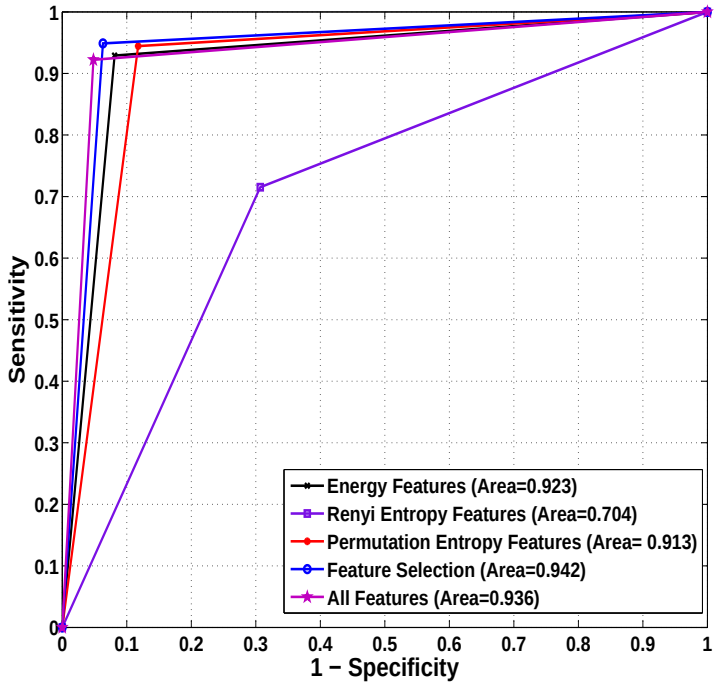


**Fig. 5.7:** ROC curves of RF classifier for different feature subsets of 8sec ECG episodes.

**Table 5.8:** Comparison of proposed approach with existing methods for detection of shockable VA, (Sensitivity-SE, Specificity-SP, Accuracy-Acc).

| Algorithm | SE(%) | SP(%) | Acc(%) | Window | Database | Features |
|---|---|---|---|---|---|---|
| Time-delay features [53] | 79 | 97.8 | 96.2 | 8Sec | CUDB, MITBIH, AHA | 5 |
| Signal Comparison Algorithm [188] | 71.2 | 98.5 | 96.2 | 8Sec | CUDB, MITBIH, AHA | 15 |
| Linear Discriminant Analysis [112] | 94.1 | 93.8 | NA | 10Sec | CUDB, VFDB, AHA | 10 |
| Filter and Count [189] | 94.4 | 95.9 | 94.7 | 10Sec | CUDB, VFDB, AHA | 3 |
| Improved filter and counts [190] | 97 | 98 | 98 | 6Sec | MITBIH, VFDB, CUDB | 10 |
| IMF angle and Bayes classifier [105] | 92.78 | 99.60 | NA | 5Sec | MITBIH | 3 |
| Correlations of ECG with IMFs [106] | 83.06 | 99.05 | NA | 8Sec | MITDB, VFDB, CUDB | 2 |
| Feature Selection and SVM [107] | 92 | 97 | NA | 8Sec | MITDB, VFDB, CUDB | 13 |
| Machine learning Approach [20] | 96.2 | 96.2 | 96.3 | 5Sec | CUDB, VFDB, AHA | 14 |
| Proposed Method | 96.54 | 97.97 | 97.23 | 5Sec | MITDB, VFDB, CUDB | 7 |
| Proposed Method | 94.37 | 94.73 | 94.07 | 8Sec | MITDB, VFDB, CUDB | 7 |

### 5.3.3 Comparison with the Existing Methods

The proposed method is compared with the existing techniques for detection of shockable ventricular arrhythmia. The comparison result is shown in Table 5.8. Amann $et\ al.$ [53] have evaluated five time delay features of ECG for detection of VF. A sensitivity value of $79\%$ is reported using 8sec ECG episodes. The method reported by Amann $et\ al.$ [188], is a signal comparison algorithm for

detection of shockable ventricular arrhythmia. The sensitivity value of 71% is obtained using 8 sec ECG episodes. Li $et\ al.$ [20] have used a machine learning approach for classification of shockable ventricular arrhythmia and non-shockable episodes from ECG. They have used VF-filter leakage measure, time-delay features, spectral features, auxiliary count features, kurtosis and area features. The sensitivity value is found to be 96.3% using SVM classifier and the diagnostic features of 5 sec ECG episodes. Atienza $et\ al.$ [107] have used morphological features, spectral features and complexity features of ECG and SVM classifier for detection of shockable ventricular arrhythmia. They have achieved a sensitivity value of $92\%$ using 8 sec ECG episodes. The proposed method outperforms the reported methods such as [53] [107], [20], [189] [53] in terms of accuracy, sensitivity and specificity values. However, the accuracy value reported in [190], is comparable with the proposed method. The average accuracy, the average sensitivity and the average sensitivity values of the proposed method are 94.37%, 94.73% and 94.07% using 8 sec ECG episodes. It is also observed that, for a window size of 8 sec, the performance of the proposed method (sensitivity value) is better than the existing techniques. The sensitivity and the specificity values of proposed method using 5 sec and 8 sec ECG episodes are better than the performance of EMD based techniques for detection of shockable ventricular arrhythmia [105] [106]. The proposed method has the advantage to capture the clinical components of ECG signal in different modes. The PE and the energy of each mode provide discriminative features for detection and classification shockable ventricular arrhythmia and non-shockable episodes from ECG. The method is implemented in MATLAB platform with a desktop computer of 4GB RAM. The simulation times for the evaluation of VMEE features of an ECG frame and the classification using RF classifier are found to be 0.941 sec and 0.012 sec, respectively. The proposed method can be implemented in real-time for detection of shockable ventricular arrhythmia.

## 5.4 Summary

In this chapter, a new method for detection and classification of shockable ventricular arrhythmia and non-shockable episodes from ECG signal is proposed. The method uses VMD to evaluate the modes of the ECG signal. The energy, the RE and the PE features of first three modes are computed. The mutual information based scoring method is used for selecting the optimal features. The RF classifier is used to evaluate the performance of different feature subsets. The proposed

method has an average accuracy, an average sensitivity and average specificity values of 96.54%, 97.97% and 97.23%, respectively using 5 sec ECG episodes. Similarly, by using 8 sec ECG episodes, the average accuracy, the average sensitivity and the average specificity values of proposed method were 94.37%, 94.73% and 94.07%, respectively. The accuracy value of proposed method is improved using the mutual information based feature scoring approach. Comparisons with the existing methods reveal the superiority of proposed method for detection of shockable ventricular arrhythmia.

# 6

# Conclusions


**Contents**

In this thesis, three new diagnostic information extraction methods are proposed for detection of various cardiac abnormalities from electrocardiogram (ECG). In order to design an automated diagnostic system (ADS), three most important components are preprocessing, diagnostic feature extraction and classification of cardiac ailments. The effectiveness of an ADS is based on the efficient quantification of the relevant diagnostic features. This research work attempted to develop new diagnostic features for ECG signal. The proposed diagnostic features are used for detection of various cardiac ailments such as myocardial infarction (MI), heart muscle diseases (HMD), bundle branch block (BBB) and shockable ventricular arrhythmia. For detection and localization of MI from multilead ECG, the multiscale energy and eigenspace (MEES) features is proposed. The complex wavelet magnitude and phase features of multilead ECG is introduced for detection of HMD, MI and BBB pathologies. The variational mode energy and entropy (VMEE) features of ECG are proposed for detection and classification of shockable ventricular arrhythmia and non-shockable episodes from ECG.

In **Chapter 1**, the morphological features of ECG signal, the cardiac ailments diagnosed using ECG and the ADS for detection of cardiac abnormalities are discussed. In the last section of the **Chapter 1**, the scope of the thesis work is written. In **Chapter 2**, a related review on the existing diagnostic feature extraction methods for detection of MI, BBB, shockable ventricular arrhythmia and other cardiac ailments are given. The advantages and the disadvantages of the existing diagnostic features of ECG are written. A related review on discrete wavelet transform (DWT), dual tree complex wavelet transform (DTCWT) and variational mode decomposition (VMD) based processing of ECG signal is also given. The principal component analysis (PCA), the higher order spectra (HOS), the non-linear analysis methods for quantifying diagnostic information from ECG are discussed. The mutual information based feature selection, the statistical uncertainty based feature selection and the correlation based feature selection techniques for ECG signal and other biomedical signals are discussed. A related reviews on k-nearest neighbors (KNN), support vector machine (SVM), random forest (RF) and extreme learning machine (ELM) classifiers for detection of cardiac ailments from the diagnostic features of ECG are given. It is felt that, the DWT and PCA, the DTCWT and HOS, and the VMD and non-linear analysis may be combined to quantify diagnostic information from ECG signal.

In **Chapter 3**, the multiscale approach for detection and localization of MI from multilead ECG has been proposed. The approach is based on the evaluation of MEES features from multilead ECG.

These MEES features of multilead ECG are used for detection and localization of MI. For MI detection, the MEES features from multilead ECG frames are evaluated. The statistical significance of MEES features is shown for both MI detection. The statistical test of MEES features for MI detection infer that, 37 multiscale energy features and 15 multiscale eigenvalue features are significant with p-values less than 0.001. The KNN and SVM classifiers are used for detection of MI from the MEES features of multilead ECG. The correlation based feature selection has been used for choosing relevant MEES features for MI detection and localization. The SVM classifier with RBF kernel has better performance with an accuracy, a sensitivity and a specificity values 96%, 93% and 99%, respectively. The performance of KNN and SVM classifiers are improved using the selected features. Comparison with existing techniques reveal that, the proposed method has advantage for detection and of MI from 12-lead or multilead ECG. The method doesn't require detection of ST-segment and T-wave of multilead ECG. For MI localization, the MEES features of multilead ECG beats are evaluated. The statistical significance of MEES features for MI localization is evaluated using ANOVA test. The 44 multiscale energy features and 22 multiscale eigenvalue features have p-values less than 0.001 and these 66 features are significant for MI localization. The multiclass SVM classifier is used to classify the MEES features of multilead ECG beat into anterior MI (AMI), anterio-lateral MI (ALMI), anterio-septal MI (ASMI), inferior MI (IMI), inferio-lateral MI (ILMI) and inferio-posterio-lateral MI (IPLMI). The multiclass SVM with RBF kernel has better performance for MI localization with an average accuracy value of 99.58%.

In **Chapter 4**, two new methods have been proposed for detection and classification of MI, HMD and BBB pathologies. The first method is based on the evaluation of multiscale PA features of multilead ECG. The multiscale PA features are evaluated from the phase of the complex wavelet coefficients of multilead ECG. The statistical significance of multiscale PA features of multilead ECG is shown. The $44$ features out of 48 multiscale PA features of multilead ECG are significant for classification of cardiac abnormalities. The KNN and the fuzzy KNN classifiers are used for classification of cardiac ailments from multiscale PA features. For MI, HMD and BBB classes, the accuracy values of 94.31%, 80.90% and 78.12% have been found. The second method evaluates the complex wavelet bi-spectrum of multilead ECG at different scales or sub-bands. The magnitude and the phase features of complex wavelet sub-band bi-spectrum (CWSB) are analyzed for healthy control and various

pathological cases such as MI, HMD and BBB. A feature selection technique based on symmetrical uncertainty score is used for choosing the relevant features of CWSB. The ELM and the SVM classifiers are used to evaluate the performance of CWSB features. The overall accuracy values of ELM and SVM classifiers are obtained as 97.17% and 97.55%, respectively. The individual class accuracy values of 98.37%, 97.39% and 96.40% are found for MI, HMD and BBB classes using selected CWSB features and SVM classifier. Comparison with existing 12-lead ECG based cardiac disease classification methods reveal the superiority of proposed approach.

In **Chapter 5**, a novel method has been proposed for detection and classification of shockable ventricular arrhythmia and non-shockable episodes from ECG. This method is based on the VMD of ECG signal. The modes of ECG are evaluated using VMD. The diagnostic information present in each mode has been investigated based on the frequency content. The energy, the permutation entropy (PE) and the Renyi entropy (RE) features from the modes of ECG are evaluated. The statistical significance and the within-class variations of VMEE features are investigated. The VMEE features of the ECG and the random forest classifiers are used for detection and classification of shockable ventricular cardiac ailments and non-shockable episodes. The proposed method has better performance with accuracy, sensitivity and specificity values of 97.23%, 96.54% and 97.97% using random forest classifier and selected VMEE features. The VMEE features correctly capture the diagnostic components of ECG for detection of shockable ventricular cardiac ailments.

The overall summary of the thesis work is given as follows. The research work mainly focused on the development of new diagnostic features of multilead ECG signal for detection of cardiac abnormalities. The first part of the work is based on the detection and localization of MI using MEES features. The proposed MEES features correctly capture the diagnostic information of multilead ECG during MI pathology. The proposed approach doesn't require any prior information about the presence of disease in the selected leads for MI detection and localization. In the second part of the work, the multiscale PA features and the CWSB magnitude and phase features are used for detection and classification of BBB, HMD and MI pathologies. The multiscale PA features correctly captures the pathological variations in MI. However, for BBB and HMD classes, the performance of multiscale PA features is less than that of MI class. The performance of CWSB features is higher than the morphological features for detection of HMD. The proposed CWSB features accurately capture the

pathological changes in multilead ECG during HMD, MI, BBB. The third part of the work based on the detection of shockable ventricular arrhythmia from the VMEE features of ECG signal. The important finding of this work is that, the energy and the permutation entropy of each mode are statistically significant for detection of shockable ventricular arrhythmia. The beat-to-beat variation in a normal sinus rhythm (healthy heart) is higher than that of shockable ventricular arrhythmia cases. The PE shows a lower mean value for shockable VA class. Similarly, the mean value of energy feature is higher for shockable ventricular arrhythmia class as compared to non-shockable class.

## 6.1 Scope for the Future Work

The following would be the directions for future work.

- The MEES features can be used for detection of atrial arrhythmia from multilead ECG. The multichannel recording of heart sound signals are effective for localization of valvular diseases. The MEES features can be used for detection of aortic stenosis, mitral stenosis, aortic regurgitation and mitral regurgitation from multichannel heart sound signals.
- The complex wavelet magnitude and phase features of multilead ECG can be used for localization of MI. The multiscale phase alternation features are not sufficient to capture pathological variations during BBB and HMD pathologies. Therefore, new features can be evaluated from the phase of the complex wavelet coefficients of multilead ECG.
- The VMEE features of ECG signal can be used for detection of other cardiac abnormalities such as atrial arrhythmia, BBB, MI and HMD. The sample entropy, the detrend fluctuation coefficients, the Hurst exponents and the distribution entropy features from the mode of ECG can be evaluated to capture the pathological variations. The VMEE features can be used for detection of valvular defects from the heart sound signals.
- The proposed diagnostic features can be used for detection of sleep apnea from ECG signal.
- The MEES features, the complex wavelet features and the VMEE features can be used for other biomedical signals.

भारतीय प्रौद्योगिकी संस्थान गुवाहाटी
Indian Institute of Technology Guwahati

# References


[1] A. L. Goldberger, *Clinical electrocardiography: a simplified approach*. Elsevier Health Sciences, 2012.

[2] L. Sun, Y. Lu, K. Yang, and S. Li, "Ecg analysis using multiple instance learning for myocardial infarction detection," *IEEE Transactions on Biomedical Engineering*, vol. 59, no. 12, pp. 3348–3356, 2012.

[3] G. D. Clifford, F. Azuaje, and P. McSharry, *Advanced methods and tools for ECG data analysis*. Artech House, Inc., 2006.

[4] M. Oeff, H. Koch, R. Bousseljot, and D. Kreiseler, "The ptb diagnostic ecg database," *National Metrology Institute of Germany, http://www. physionet. org/physiobank/database/ptbdb*, 2012.

[5] A. L. Goldberger, L. A. Amaral, L. Glass, J. M. Hausdorff, P. C. Ivanov, R. G. Mark, J. E. Mietus, G. B. Moody, C.-K. Peng, and H. E. Stanley, "Physiobank, physiotoolkit, and physionet components of a new research resource for complex physiologic signals," *Circulation*, vol. 101, no. 23, pp. e215–e220, 2000.

[6] G. B. Moody and R. G. Mark, "The impact of the mit-bih arrhythmia database," *Engineering in Medicine and Biology Magazine, IEEE*, vol. 20, no. 3, pp. 45–50, 2001.

[7] J. E. Hall, *Guyton and Hall textbook of medical physiology*. Elsevier Health Sciences, 2015.

[8] Y. Zigel, A. Cohen, and A. Katz, "The weighted diagnostic distortion (wdd) measure for ecg signal compression," *IEEE Transactions on Biomedical Engineering*, vol. 47, no. 11, pp. 1422–1430, 2000.

[9] M. S. Thaler, *The only EKG book you'll ever need*. Lippincott Williams & Wilkins, 2010.

[10] L. Sörnmo and P. Laguna, *Bioelectrical signal processing in cardiac and neurological applications*. Academic Press, 2005.

[11] C. Breen, T. Zhu, R. Bond, D. Finlay, and G. Clifford, "The evaluation of an open source online training system for teaching 12 lead electrocardiographic interpretation," *Journal of electrocardiology*, vol. 49, no. 3, pp. 454–461, 2016.

[12] K. Thygesen, J. S. Alpert, A. S. Jaffe, H. D. White, M. L. Simoons, B. R. Chaitman, H. A. Katus, F. S. Apple, B. Lindahl, D. A. Morrow *et al.*, "Third universal definition of myocardial infarction," *Journal of the American College of Cardiology*, vol. 60, no. 16, pp. 1581–1598, 2012.

[13] S. G. Goodman, P. G. Steg, K. A. Eagle, K. A. Fox, J. López-Sendón, G. Montalescot, A. Budaj, B. M. Kennelly, J. M. Gore, J. Allegrone *et al.*, "The diagnostic and prognostic impact of the redefinition of acute myocardial infarction: lessons from the global registry of acute coronary events (grace)," *American heart journal*, vol. 151, no. 3, pp. 654–660, 2006.

[14] H. Yang, "Multiscale recurrence quantification analysis of spatial cardiac vectorcardiogram signals," *IEEE Transactions on Biomedical Engineering*, vol. 58, no. 2, pp. 339–347, 2011.

[15] M. Ovreiu and D. J. Simon, "Cardiomyopathy detection from electrocardiogram features," 2012.

[16] J. A. Drezner, E. Ashley, A. L. Baggish, M. Börjesson, D. Corrado, D. S. Owens, A. Patel, A. Pelliccia, V. L. Vetter, M. J. Ackerman *et al.*, "Abnormal electrocardiographic findings in athletes: recognising changes suggestive of cardiomyopathy," *British Journal of Sports Medicine*, vol. 47, no. 3, pp. 137–152, 2013.

[17] D. P. Zipes, A. J. Camm, M. Borggrefe, A. E. Buxton, B. Chaitman, M. Fromer, G. Gregoratos, G. Klein, A. J. Moss, R. J. Myerburg *et al.*, "Acc/aha/esc 2006 guidelines for management of patients with ventricular arrhythmias and the prevention of sudden cardiac death: a report of the american college of cardiology/american heart association task force and the european society of cardiology committee for practice guidelines (writing committee to develop guidelines for management of patients with ventricular arrhythmias and the prevention of sudden cardiac death)," *Journal of the American College of Cardiology*, vol. 48, no. 5, pp. e247–e346, 2006.

[18] J. P. Daubert, W. Zareba, W. J. Hall, C. Schuger, A. Corsello, A. R. Leon, M. L. Andrews, S. McNitt, D. T. Huang, and A. J. Moss, "Predictive value of ventricular arrhythmia inducibility for subsequent ventricular tachycardia or ventricular fibrillation in multicenter automatic defibrillator implantation trial (madit) ii patients," *Journal of the American College of Cardiology*, vol. 47, no. 1, pp. 98–107, 2006.

[19] F. Alonso-Atienza, E. Morgado, L. Fernandez-Martinez, A. Garcia-Alberola, and J. L. Rojo-Alvarez, "Detection of life-threatening arrhythmias using feature selection and support vector machines," *IEEE Transactions on Biomedical Engineering*, vol. 61, no. 3, pp. 832–840, 2014.

[20] Q. Li, C. Rajagopalan, and G. D. Clifford, "Ventricular fibrillation and tachycardia classification using a machine learning approach," *IEEE Transactions on Biomedical Engineering*, vol. 61, no. 6, pp. 1607–1613, 2014.

[21] A. E. Johnson, M. M. Ghassemi, S. Nemati, K. E. Niehaus, D. Clifton, and G. D. Clifford, "Machine learning and decision support in critical care," *Proceedings of the IEEE*, vol. 104, no. 2, pp. 444–466, 2016.

[22] R. M. Rangayyan, *Biomedical signal analysis*. John Wiley & Sons, 2015, vol. 33.

[23] S. Luo and P. Johnston, "A review of electrocardiogram filtering," *Journal of electrocardiology*, vol. 43, no. 6, pp. 486–496, 2010.

[24] R. Sameni, M. B. Shamsollahi, C. Jutten, and G. D. Clifford, "A nonlinear bayesian filtering framework for ecg denoising," *IEEE Transactions on Biomedical Engineering*, vol. 54, no. 12, pp. 2172–2185, 2007.

[25] L. Sharma, S. Dandapat, and A. Mahanta, "Multichannel ecg data compression based on multiscale principal component analysis," *IEEE Transactions on Information Technology in Biomedicine*, vol. 16, no. 4, pp. 730–736, 2012.

[26] O. Sayadi and M. B. Shamsollahi, "Multiadaptive bionic wavelet transform: Application to ecg denoising and baseline wandering reduction," *EURASIP Journal on Advances in Signal Processing*, vol. 2007, no. 1, pp. 1–11, 2007.

[27] M. Blanco-Velasco, B. Weng, and K. E. Barner, "Ecg signal denoising and baseline wander correction based on the empirical mode decomposition," *Computers in biology and medicine*, vol. 38, no. 1, pp. 1–13, 2008.

[28] S. Lahmiri, "Comparative study of ecg signal denoising by wavelet thresholding in empirical and variational mode decomposition domains," *Healthcare technology letters*, vol. 1, no. 3, p. 104, 2014.

[29] L. Sharma, S. Dandapat, and A. Mahanta, "Ecg signal denoising using higher order statistics in wavelet subbands," *Biomedical Signal Processing and Control*, vol. 5, no. 3, pp. 214–222, 2010.

[30] J. C. Huhta and J. G. Webster, "60-hz interference in electrocardiography," *IEEE Transactions on Biomedical Engineering*, no. 2, pp. 91–101, 1973.

[31] N. V. Thakor and Y.-S. Zhu, "Applications of adaptive filtering to ecg analysis: noise cancellation and arrhythmia detection," *IEEE Transactions on Biomedical Engineering*, vol. 38, no. 8, pp. 785–794, 1991.

[32] J. Pan and W. J. Tompkins, "A real-time qrs detection algorithm," *IEEE Transactions on Biomedical Engineering*, no. 3, pp. 230–236, 1985.

[33] I. Jekova, G. Bortolan, and I. Christov, "Assessment and comparison of different methods for heartbeat classification," *Medical Engineering & Physics*, vol. 30, no. 2, pp. 248–257, 2008.

[34] M. S. Manikandan and S. Dandapat, "Wavelet-based electrocardiogram signal compression methods and their performances: a prospective review," *Biomedical Signal Processing and Control*, vol. 14, pp. 73–107, 2014.

[35] S. Padhy and S. Dandapat, "Exploiting multi-lead electrocardiogram correlations using robust third-order tensor decomposition," *Healthcare technology letters*, vol. 2, no. 5, pp. 112–117, 2015.

[36] M. Arif, I. A. Malagore, and F. A. Afsar, "Detection and localization of myocardial infarction using k-nearest neighbor classifier," *Journal of medical systems*, vol. 36, no. 1, pp. 279–289, 2012.

[37] R. Acharya, S. M. Krishnan, J. A. Spaan, and J. S. Suri, *Advances in cardiac signal processing*. Springer, 2007.

[38] S. Osowski and T. H. Linh, "Ecg beat recognition using fuzzy hybrid neural network," *IEEE Transactions on Biomedical Engineering*, vol. 48, no. 11, pp. 1265–1271, 2001.

[39] Q. A. Rahman, L. G. Tereshchenko, M. Kongkatong, T. Abraham, M. R. Abraham, and H. Shatkay, "Utilizing ecg-based heartbeat classification for hypertrophic cardiomyopathy identification," *IEEE Transactions on NanoBioscience*, vol. 14, no. 5, pp. 505–512, 2015.

[40] P. De Chazal, M. O. Dwyer, and R. B. Reilly, "Automatic classification of heartbeats using ecg morphology and heartbeat interval features," *IEEE Transactions on Biomedical Engineering*, vol. 51, no. 7, pp. 1196–1206, 2004.

[41] S. Mitra, M. Mitra, and B. B. Chaudhuri, "A rough-set-based inference engine for ecg classification," *IEEE Transactions on Instrumentation and Measurement*, vol. 55, no. 6, pp. 2198–2206, 2006.

[42] L. Biel, O. Pettersson, L. Philipson, and P. Wide, "Ecg analysis: a new approach in human identification," *IEEE Transactions on Instrumentation and Measurement*, vol. 50, no. 3, pp. 808–812, 2001.

[43] R. Tripathy, L. Sharma, and S. Dandapat, "Diagnostic measure to quantify loss of clinical components in multi-lead electrocardiogram," *Healthcare Technology Letters*, vol. 3, no. 1, pp. 61–66, 2016.

[44] R. O. Duda, P. E. Hart, and D. G. Stork, *Pattern classification*. John Wiley & Sons, 2012.

[45] C. Bishop, "Pattern recognition and machine learning (information science and statistics), 1st edn. 2006. corr. 2nd printing edn," 2007.

[46] H. Gothwal, S. Kedawat, R. Kumar *et al.*, "Cardiac arrhythmias detection in an ecg beat signal using fast fourier transform and artificial neural network," *Journal of Biomedical Science and Engineering*, vol. 4, no. 04, p. 289, 2011.

[47] R. J. Martis, U. R. Acharya, C. M. Lim, and J. S. Suri, "Characterization of ecg beats from cardiac arrhythmia using discrete cosine transform in pca framework," *Knowledge-Based Systems*, vol. 45, pp. 76–82, 2013.

[48] K. Balasundaram, S. Masse, K. Nair, and K. Umapathy, "A classification scheme for ventricular arrhythmias using wavelets analysis," *Medical & biological engineering & computing*, vol. 51, no. 1-2, pp. 153–164, 2013.

[49] S. Banerjee and M. Mitra, "Application of cross wavelet transform for ecg pattern analysis and classification," *IEEE Transactions on Instrumentation and Measurement*, vol. 63, no. 2, pp. 326–333, 2014.

[50] E. Jayachandran *et al.*, "Analysis of myocardial infarction using discrete wavelet transform," *Journal of medical systems*, vol. 34, no. 6, pp. 985–992, 2010.

[51] M. Thomas, M. K. Das, and S. Ari, "Automatic ecg arrhythmia classification using dual tree complex wavelet based features," *AEU-International Journal of Electronics and Communications*, vol. 69, no. 4, pp. 715–721, 2015.

[52] D. Ge, N. Srinivasan, and S. M. Krishnan, "Cardiac arrhythmia classification using autoregressive modeling," *Biomedical engineering online*, vol. 1, no. 1, p. 5, 2002.

[53] A. Amann, R. Tratnig, and K. Unterkofler, "Detecting ventricular fibrillation by time-delay methods," *IEEE Transactions on Biomedical Engineering*, vol. 54, no. 1, pp. 174–177, 2007.

[54] U. R. Acharya, H. Fujita, V. K. Sudarshan, V. S. Sree, L. W. J. Eugene, D. N. Ghista, and R. San Tan, "An integrated index for detection of sudden cardiac death using discrete wavelet transform and nonlinear features," *Knowledge-Based Systems*, vol. 83, pp. 149–158, 2015.

[55] D. Romero, M. Ringborn, P. Laguna, O. Pahlm, and E. Pueyo, "Depolarization changes during acute myocardial ischemia by evaluation of qrs slopes: standard lead and vectorial approach," *IEEE Transactions on Biomedical Engineering*, vol. 58, no. 1, pp. 110–120, 2011.

[56] S.-N. Yu and K.-T. Chou, "Selection of significant independent components for ecg beat classification," *Expert Systems with Applications*, vol. 36, no. 2, pp. 2088–2096, 2009.

[57] R. J. Martis, U. R. Acharya, H. Prasad, C. K. Chua, C. M. Lim, and J. S. Suri, "Application of higher order statistics for atrial arrhythmia classification," *Biomedical Signal Processing and Control*, vol. 8, no. 6, pp. 888–900, 2013.

[58] K. Huang and L. Zhang, "Cardiology knowledge free ecg feature extraction using generalized tensor rank one discriminant analysis," *EURASIP Journal on Advances in Signal Processing*, vol. 2014, no. 1, pp. 1–15, 2014.

[59] R. J. Martis, U. R. Acharya, K. Mandana, A. K. Ray, and C. Chakraborty, "Application of principal component analysis to ecg signals for automated diagnosis of cardiac health," *Expert Systems with Applications*, vol. 39, no. 14, pp. 11 792–11 800, 2012.

[60] E. Ercelebi, "Electrocardiogram signals de-noising using lifting-based discrete wavelet transform," *Computers in Biology and Medicine*, vol. 34, no. 6, pp. 479–493, 2004.

[61] B. A. Rajoub, "An efficient coding algorithm for the compression of ecg signals using the wavelet transform," *IEEE Transactions on Biomedical Engineering*, vol. 49, no. 4, pp. 355–362, 2002.

[62] P. S. Addison, "Wavelet transforms and the ecg: a review," *Physiological measurement*, vol. 26, no. 5, p. R155, 2005.

[63] S. Sumathi, H. L. Beaulah, and R. Vanithamani, "A wavelet transform based feature extraction and classification of cardiac disorder," *Journal of medical systems*, vol. 38, no. 9, pp. 1–11, 2014.

[64] S. Mallat, *A wavelet tour of signal processing*. Academic press, 1999.

[65] L. Sharma, S. Dandapat, and A. Mahanta, "Kurtosis-based noise estimation and multiscale energy to denoise ecg signal," *Signal, Image and Video Processing*, vol. 7, no. 2, pp. 235–245, 2013.

[66] R. J. Martis, U. R. Acharya, and L. C. Min, "Ecg beat classification using pca, lda, ica and discrete wavelet transform," *Biomedical Signal Processing and Control*, vol. 8, no. 5, pp. 437–448, 2013.

[67] I. W. Selesnick, R. G. Baraniuk, and N. G. Kingsbury, "The dual-tree complex wavelet transform," *IEEE Signal Processing Magazine*, vol. 22, no. 6, pp. 123–151, 2005.

[68] K. Dragomiretskiy and D. Zosso, "Variational mode decomposition," *IEEE Transactions on Signal Processing*, vol. 62, no. 3, pp. 531–544, 2014.

[69] U. Maji, S. Pal, and S. Majumder, "Estimation of arrhythmia episode using variational mode decomposition technique," in *Instrumentation and Measurement Technology Conference (I2MTC), 2015 IEEE International*. IEEE, 2015, pp. 767–772.

[70] B. Hedén, H. Öhlin, R. Rittner, and L. Edenbrandt, "Acute myocardial infarction detected in the 12-lead ecg by artificial neural networks," *Circulation*, vol. 96, no. 6, pp. 1798–1802, 1997.

[71] R. Correa, P. D. Arini, L. S. Correa, M. Valentinuzzi, and E. Laciar, "Novel technique for st-t interval characterization in patients with acute myocardial ischemia," *Computers in biology and medicine*, vol. 50, pp. 49–55, 2014.

[72] M. Reddy, L. Edenbrandt, J. Svensson, W. Haisty, and O. Pahlm, "Neural network versus electrocardiographer and conventional computer criteria in diagnosing anterior infarct from the ecg," in *Computers in Cardiology 1992, Proceedings of*. IEEE, 1992, pp. 667–670.

[73] M. Ringborn, D. Romero, E. Pueyo, O. Pahlm, G. S. Wagner, P. Laguna, and P. G. Platonov, "Evaluation of depolarization changes during acute myocardial ischemia by analysis of qrs slopes," *Journal of electrocardiology*, vol. 44, no. 4, pp. 416–424, 2011.

[74] D. Romero, M. Ringborn, P. Laguna, and E. Pueyo, "Detection and quantification of acute myocardial ischemia by morphologic evaluation of qrs changes by an angle-based method," *Journal of electrocardiology*, vol. 46, no. 3, pp. 204–214, 2013.

[75] J. Fayn, "A classification tree approach for cardiac ischemia detection using spatiotemporal information from three standard ecg leads," *IEEE Transactions on Biomedical Engineering*, vol. 58, no. 1, pp. 95–102, 2011.

[76] P.-C. Chang, J.-J. Lin, J.-C. Hsieh, and J. Weng, "Myocardial infarction classification with multi-lead ecg using hidden markov models and gaussian mixture models," *Applied Soft Computing*, vol. 12, no. 10, pp. 3165–3175, 2012.

[77] A. Loewe, W. H. Schulze, Y. Jiang, M. Wilhelms, A. Luik, O. Dössel, and G. Seemann, "Ecg-based detection of early myocardial ischemia in a computational model: impact of additional electrodes, optimal placement, and a new feature for st deviation," *BioMed research international*, vol. 2015, 2015.

[78] P. D. Arini, F. H. Baglivo, J. P. Martínez, and P. Laguna, "Evaluation of ventricular repolarization dispersion during acute myocardial ischemia: spatial and temporal ecg indices," *Medical & biological engineering & computing*, vol. 52, no. 4, pp. 375–391, 2014.

[79] H. Lu, K. Ong, and P. Chia, "An automated ecg classification system based on a neuro-fuzzy system," in *Computers in Cardiology 2000*. IEEE, 2000, pp. 387–390.

[80] M. Ringborn, J. Pettersson, E. Persson, S. G. Warren, P. Platonov, O. Pahlm, and G. S. Wagner, "Comparison of high-frequency qrs components and st-segment elevation to detect and quantify acute myocardial ischemia," *Journal of electrocardiology*, vol. 43, no. 2, pp. 113–120, 2010.

[81] J. Song, H. Yan, Z. Xu, X. Yu, and R. Zhu, "Myocardial ischemia analysis based on electrocardiogram qrs complex," *Australasian Physical & Engineering Sciences in Medicine*, vol. 34, no. 4, pp. 515–521, 2011.

[82] E. Valverde and P. D. Arini, "Study of t-wave spectral variance during acute myocardial ischemia," in *Computing in Cardiology (CinC), 2012*. IEEE, 2012, pp. 653–656.

[83] T. Tsutsumi, Y. Okamoto, N. Kubota-Takano, D. Wakatsuki, H. Suzuki, K. Sezaki, K. Iwasawa, and T. Nakajima, "Time–frequency analysis of the qrs complex in patients with ischemic cardiomyopathy and myocardial infarction," *IJC Heart & Vessels*, vol. 4, pp. 177–187, 2014.

[84] F. Melgani and Y. Bazi, "Classification of electrocardiogram signals with support vector machines and particle swarm optimization," *IEEE Transactions on Information Technology in Biomedicine*, vol. 12, no. 5, pp. 667–677, 2008.

[85] A. Ebrahimzadeh, B. Shakiba, and A. Khazaee, "Detection of electrocardiogram signals using an efficient method," *Applied Soft Computing*, vol. 22, pp. 108–117, 2014.

[86] B. DoğAn and M. Korürek, "A new ecg beat clustering method based on kernelized fuzzy c-means and hybrid ant colony optimization for continuous domains," *Applied Soft Computing*, vol. 12, no. 11, pp. 3442–3451, 2012.

[87] U. Maji, M. Mitra, and S. Pal, "Imposed target based modification of taguchi method for feature optimisation with application in arrhythmia beat detection," *Expert Systems with Applications*, vol. 56, pp. 268–281, 2016.

[88] A. F. Khalaf, M. I. Owis, and I. A. Yassine, "A novel technique for cardiac arrhythmia classification using spectral correlation and support vector machines," *Expert Systems with Applications*, vol. 42, no. 21, pp. 8361–8368, 2015.

[89] K. Jen and Y. Hwang, "Ecg feature extraction and classification using cepstrum and neural networks," *Journal of Medical and Biological Engineering*, vol. 28, no. 1, p. 31, 2008.

[90] T. Linh, S. Osowski, and M. Stodolski, "On-line heart beat recognition using hermite polynomials and neuro-fuzzy network," *IEEE Transactions on Instrumentation and Measurement*, vol. 52, no. 4, pp. 1224–1231, Aug 2003.

[91] S.-N. Yu and K.-T. Chou, "A switchable scheme for ecg beat classification based on independent component analysis," *Expert Systems with Applications*, vol. 33, no. 4, pp. 824–829, 2007.

[92] ——, "Integration of independent component analysis and neural networks for ecg beat classification," *Expert Systems with Applications*, vol. 34, no. 4, pp. 2841–2846, 2008.

[93] E. Pasolli and F. Melgani, "Active learning methods for electrocardiographic signal classification," *IEEE Transactions on Information Technology in Biomedicine*, vol. 14, no. 6, pp. 1405–1416, 2010.

[94] A. Lanata, G. Valenza, C. Mancuso, and E. P. Scilingo, "Robust multiple cardiac arrhythmia detection through bispectrum analysis," *Expert Systems with Applications*, vol. 38, no. 6, pp. 6798–6804, 2011.

[95] I. Bogdanova, F. Rincón, and D. Atienza, "A multi-lead ecg classification based on random projection features," in *Acoustics, Speech and Signal Processing (ICASSP), 2012 IEEE International Conference on*. IEEE, 2012, pp. 625–628.

[96] D. Pedersen, D. Zipes, P. Foster, and P. Troup, "Ventricular tachycardia and ventricular fibrillation in a young population." *Circulation*, vol. 60, no. 5, pp. 988–997, 1979.

[97] H. V. Huikuri, A. Castellanos, and R. J. Myerburg, "Sudden death due to cardiac arrhythmias," *New England Journal of Medicine*, vol. 345, no. 20, pp. 1473–1482, 2001.

[98] N. V. Thakor, Y.-S. Zhu, and K.-Y. Pan, "Ventricular tachycardia and fibrillation detection by a sequential hypothesis testing algorithm," *IEEE Transactions on Biomedical Engineering*, vol. 37, no. 9, pp. 837–843, 1990.

[99] S. Kuo and R. Dillman, "Computer detection of ventricular fibrillation," *Computers in cardiology*, pp. 347–349, 1978.

[100] X.-S. Zhang, Y.-S. Zhu, N. V. Thakor, and Z.-Z. Wang, "Detecting ventricular tachycardia and fibrillation by complexity measure," *IEEE Transactions on Biomedical Engineering*, vol. 46, no. 5, pp. 548–555, 1999.

[101] S. Barro, R. Ruiz, D. Cabello, and J. Mira, "Algorithmic sequential decision-making in the frequency domain for life threatening ventricular arrhythmias and imitative artefacts: a diagnostic system," *Journal of biomedical engineering*, vol. 11, no. 4, pp. 320–328, 1989.

[102] V. Krasteva and I. Jekova, "Assessment of ecg frequency and morphology parameters for automatic classification of life-threatening cardiac arrhythmias," *Physiological measurement*, vol. 26, no. 5, p. 707, 2005.

[103] A. Neurauter, T. Eftestøl, J. Kramer-Johansen, B. S. Abella, K. Sunde, V. Wenzel, K. H. Lindner, J. Eilevstjønn, H. Myklebust, P. A. Steen *et al.*, "Prediction of countershock success using single features from multiple ventricular fibrillation frequency bands and feature combinations using neural networks," *Resuscitation*, vol. 73, no. 2, pp. 253–263, 2007.

[104] L. Khadra, A. Al-Fahoum, and H. Al-Nashash, "Detection of life-threatening cardiac arrhythmias using the wavelet transformation," *Medical and Biological Engineering and Computing*, vol. 35, no. 6, pp. 626–632, 1997.

[105] M. A. Arafat, J. Sieed, and M. K. Hasan, "Detection of ventricular fibrillation using empirical mode decomposition and bayes decision theory," *Computers in Biology and Medicine*, vol. 39, no. 11, pp. 1051–1057, 2009.

[106] E. M. A. Anas, S. Y. Lee, and M. K. Hasan, "Exploiting correlation of ecg with certain emd functions for discrimination of ventricular fibrillation," *Computers in biology and medicine*, vol. 41, no. 2, pp. 110–114, 2011.

[107] F. Alonso-Atienza, J. L. Rojo-Álvarez, A. Rosado-Muñoz, J. J. Vinagre, A. García-Alberola, and G. Camps-Valls, "Feature selection using support vector machines and bootstrap methods for ventricular fibrillation detection," *Expert Systems with Applications*, vol. 39, no. 2, pp. 1956–1967, 2012.

[108] J. Millet-Roig, J. Rieta-Ibanez, E. Vilanova, A. Mocholi, and F. Chorro, "Time-frequency analysis of a single ecg: to discriminate between ventricular tachycardia and ventricular fibrillation," in *Computers in Cardiology, 1999*. IEEE, 1999, pp. 711–714.

[109] P. Flandrin, G. Rilling, and P. Goncalves, "Empirical mode decomposition as a filter bank," *IEEE Signal Processing Letters*, vol. 11, no. 2, pp. 112–114, 2004.

[110] P. Jain and R. B. Pachori, "An iterative approach for decomposition of multi-component non-stationary signals based on eigenvalue decomposition of the hankel matrix," *Journal of the Franklin Institute*, vol. 352, no. 10, pp. 4017–4044, 2015.

[111] Y. Alwan, Z. Cvetkovic, and M. Curtis, "Structured prediction for differentiating between normal rhythms, ventricular tachycardia, and ventricular fibrillation in the ecg," in *Engineering in Medicine and Biology Society (EMBC), 2015 37th Annual International Conference of the IEEE*. IEEE, 2015, pp. 310–314.

[112] I. Jekova, "Shock advisory tool: Detection of life-threatening cardiac arrhythmias and shock success prediction by means of a common parameter set," *Biomedical Signal Processing and Control*, vol. 2, no. 1, pp. 25–33, 2007.

[113] M. Moga, V. Moga, and G. I. Mihalas, "continuous wavelet transform in ecg analysis. a concept or clinical uses ," *Educational Technologies and Methodologies*, 2005.

[114] H. Zhu, "Method for signal denoising using continuous wavelet transform," Jul. 10 2008, uS Patent App. 12/216,719.

[115] A. Ghaffari, H. Golbayani, and M. Ghasemi, "A new mathematical based qrs detector using continuous wavelet transform," *Computers & Electrical Engineering*, vol. 34, no. 2, pp. 81–91, 2008.

[116] I. Daubechies, "The wavelet transform, time-frequency localization and signal analysis," *IEEE Transactions on Information Theory*, vol. 36, no. 5, pp. 961–1005, 1990.

[117] R. Polikar, "The wavelet tutorial part iv: Multiresolution analysis: The discrete wavelet transform," *Rowan University*, 2008.

[118] J. Kovacevic, V. K. Goyal, and M. Vetterli, "Fourier and wavelet signal processing," 2013.

[119] A. S. Al-Fahoum, "Quality assessment of ecg compression techniques using a wavelet-based diagnostic measure," *IEEE Transactions on Information Technology in Biomedicine*, vol. 10, no. 1, pp. 182–191, 2006.

[120] A. Bultheel, "Wavelets with applications in signal and image processing," 2006.

[121] B. N. Singh and A. K. Tiwari, "Optimal selection of wavelet basis function applied to ecg signal denoising," *Digital Signal Processing*, vol. 16, no. 3, pp. 275–287, 2006.

[122] G. Takla, K. A. Loparo, and B. Nair, "System for artifact detection and elimination in an electrocardiogram signal recorded from a patient monitor," May 7 2008, uS Patent App. 12/116,235.

[123] M. R. Ram, K. V. Madhav, E. H. Krishna, N. R. Komalla, K. Sivani, and K. A. Reddy, "Ica-based improved dtcwt technique for ma reduction in ppg signals with restored respiratory information," *IEEE Transactions on Instrumentation and Measurement*, vol. 62, no. 10, pp. 2639–2651, 2013.

[124] I. W. Selesnick, "Hilbert transform pairs of wavelet bases," *IEEE Signal Processing Letters*, vol. 8, no. 6, pp. 170–173, 2001.

[125] H. Yang, S. Bukkapatnam, and R. Komanduri, "Nonlinear adaptive wavelet analysis of electrocardiogram signals," *Physical Review E*, vol. 76, no. 2, p. 026214, 2007.

[126] N. Kingsbury, "A dual-tree complex wavelet transform with improved orthogonality and symmetry properties," in *Image Processing, 2000. Proceedings. 2000 International Conference on*, vol. 2. IEEE, 2000, pp. 375–378.

[127] R. Tripathy, S. Mahanta, and S. Paul, "Artificial intelligence-based classification of breast cancer using cellular images," *RSC Advances*, vol. 4, no. 18, pp. 9349–9355, 2014.

[128] I. Romero, "Principal component analysis or independent component analysis applied to ambulatory electrocardiogram signals," Mar. 21 2012, eP Patent App. EP20,110,181,173. [Online]. Available: http://www.google.com/patents/EP2430975A1?cl=3Den

[129] F. Castells, P. Laguna, L. Sörnmo, A. Bollmann, and J. M. Roig, "Principal component analysis in ecg signal processing," *EURASIP Journal on Applied Signal Processing*, vol. 2007, no. 1, pp. 98–98, 2007.

[130] R. Sameni, C. Jutten, and M. B. Shamsollahi, "Multichannel electrocardiogram decomposition using periodic component analysis," *IEEE Transactions on Biomedical Engineering*, vol. 55, no. 8, pp. 1935–1940, 2008.

[131] R. Tripathy, L. Sharma, and S. Dandapat, "A new way of quantifying diagnostic information from multilead electrocardiogram for cardiac disease classification," *Healthcare technology letters*, vol. 1, no. 4, p. 98, 2014.

[132] V. Kalpana, S. Hamde, and L. Waghmare, "Ecg feature extraction using principal component analysis for studying the effect of diabetes," *Journal of medical engineering & technology*, vol. 37, no. 2, pp. 116–126, 2013.

[133] P. Langley, E. J. Bowers, and A. Murray, "Principal component analysis as a tool for analyzing beat-to-beat changes in ecg features: application to ecg-derived respiration," *IEEE Transactions on Biomedical Engineering*, vol. 57, no. 4, pp. 821–829, 2010.

[134] C. L. Nikias and J. M. Mendel, "Signal processing with higher-order spectra," *IEEE Signal processing magazine*, vol. 10, no. 3, pp. 10–37, 1993.

[135] R. J. Martis, U. R. Acharya, C. M. Lim, K. Mandana, A. K. Ray, and C. Chakraborty, "Application of higher order cumulant features for cardiac health diagnosis using ecg signals," *International journal of neural systems*, vol. 23, no. 04, p. 1350014, 2013.

[136] C. K. Chua, V. Chandran, R. U. Acharya, and L. C. Min, "Cardiac health diagnosis using higher order spectra and support vector machine," *The open medical informatics journal*, vol. 3, p. 1, 2009.

[137] L. Khadra, A. S. Al-Fahoum, and S. Binajjaj, "A quantitative analysis approach for cardiac arrhythmia classification using higher order spectral techniques," *IEEE Transactions on Biomedical Engineering*, vol. 52, no. 11, pp. 1840–1845, 2005.

[138] F. A. Elhaj, N. Salim, A. R. Harris, T. T. Swee, and T. Ahmed, "Arrhythmia recognition and classification using combined linear and nonlinear features of ecg signals," *Computer Methods and Programs in Biomedicine*, 2016.

[139] D. Z. Li, W. Wang, and F. Ismail, "An enhanced bispectrum technique with auxiliary frequency injection for induction motor health condition monitoring," *IEEE Transactions on Instrumentation and Measurement*, vol. 64, no. 10, pp. 2679–2687, 2015.

[140] U. R. Acharya, O. Faust, V. Sree, G. Swapna, R. J. Martis, N. A. Kadri, and J. S. Suri, "Linear and nonlinear analysis of normal and cad-affected heart rate signals," *Computer methods and programs in biomedicine*, vol. 113, no. 1, pp. 55–68, 2014.

[141] R. Acharya, P. S. Bhat, N. Kannathal, A. Rao, and C. M. Lim, "Analysis of cardiac health using fractal dimension and wavelet transformation," *ITBM-RBM*, vol. 26, no. 2, pp. 133–139, 2005.

[142] E. D. Übeyli, "Adaptive neuro-fuzzy inference system for classification of ecg signals using lyapunov exponents," *Computer methods and programs in biomedicine*, vol. 93, no. 3, pp. 313–321, 2009.

[143] M. I. Owis, A. H. Abou-Zied, A.-B. M. Youssef, and Y. M. Kadah, "Study of features based on nonlinear dynamical modeling in ecg arrhythmia detection and classification," *IEEE Transactions on Biomedical Engineering*, vol. 49, no. 7, pp. 733–736, 2002.

[144] E. Watanabe, K. Kiyono, J. Hayano, Y. Yamamoto, J. Inamasu, M. Yamamoto, T. Ichikawa, Y. Sobue, M. Harada, and Y. Ozaki, "Multiscale entropy of the heart rate variability for the prediction of an ischemic stroke in patients with permanent atrial fibrillation," *PloS one*, vol. 10, no. 9, p. e0137144, 2015.

[145] D. Li, "Method and apparatus for cardiac arrhythmia classification using sample entropy," Sep. 2 2014, uS Patent 8,825,146.

[146] A. Chetan, R. Tripathy, and S. Dandapat, "Cardiac arrhythmia classification from multilead ecg using multiscale non-linear analysis," in *2015 IEEE UP Section Conference on Electrical Computer and Electronics (UPCON)*. IEEE, 2015, pp. 1–4.

[147] B. Taha, S. Reddy, and J. Xue, "Method of using spectral measures to distinguish among atrialfibrillation, atrial-flutter and other cardiac rhythms," Jul. 22 2003, uS Patent 6,597,943.

[148] X. Li, G. Ouyang, and D. A. Richards, "Predictability analysis of absence seizures with permutation entropy," *Epilepsy research*, vol. 77, no. 1, pp. 70–74, 2007.

[149] F. Taherkhani, M. Rahmani, F. Taherkhani, H. Akbarzadeh, and H. Abroshan, "Permutation entropy and detrend fluctuation analysis for the natural complexity of cardiac heart interbeat signals," *Physica A: Statistical Mechanics and its Applications*, vol. 392, no. 14, pp. 3106–3112, 2013.

[150] T. Mar, S. Zaunseder, J. P. Martínez, M. Llamedo, and R. Poll, "Optimization of ecg classification by means of feature selection," *IEEE Transactions on Biomedical Engineering*, vol. 58, no. 8, pp. 2168–2177, 2011.

[151] K. Ravichandran, D. Chiasson, and K. Oyedele, "Classification of electrocardiogram anomalies."

[152] S. Shilaskar and A. Ghatol, "Feature selection for medical diagnosis: Evaluation for cardiovascular diseases," *Expert Systems with Applications*, vol. 40, no. 10, pp. 4146–4153, 2013.

[153] C. Freeman, D. Kulić, and O. Basir, "An evaluation of classifier-specific filter measure performance for feature selection," *Pattern Recognition*, vol. 48, no. 5, pp. 1812–1826, 2015.

[154] J. Pohjalainen, O. Räsänen, and S. Kadioglu, "Feature selection methods and their combinations in high-dimensional classification of speaker likability, intelligibility and personality traits," *Computer Speech & Language*, vol. 29, no. 1, pp. 145–171, 2015.

[155] G. Doquire, G. De Lannoy, D. François, and M. Verleysen, "Feature selection for interpatient supervised heart beat classification," *Computational intelligence and neuroscience*, vol. 2011, p. 1, 2011.

[156] A. Noviyanto, S. M. Isa, I. Wasito, A. M. Arymurthy *et al.*, "Selecting features of single lead ecg signal for automatic sleep stages classification using correlation-based feature subset selection," *IJCSI International Journal of Computer Science Issues*, vol. 8, no. 5, 2011.

[157] S. Sasikala, S. A. alias Balamurugan, and S. Geetha, "Multi filtration feature selection (mffs) to improve discriminatory ability in clinical data set," *Applied Computing and Informatics*, 2014.

[158] P. Kora and S. R. Kalva, "Hybrid bacterial foraging and particle swarm optimization for detecting bundle branch block," *SpringerPlus*, vol. 4, no. 1, pp. 1–19, 2015.

[159] Y.-H. Chen and S.-N. Yu, "Selection of effective features for ecg beat recognition based on nonlinear correlations," *Artificial intelligence in medicine*, vol. 54, no. 1, pp. 43–52, 2012.

[160] M. Mitra and R. Samanta, "Cardiac arrhythmia classification using neural networks with selected features," *Procedia Technology*, vol. 10, pp. 76–84, 2013.

[161] C.-J. Huang, D.-X. Yang, and Y.-T. Chuang, "Application of wrapper approach and composite classifier to the stock trend prediction," *Expert Systems with Applications*, vol. 34, no. 4, pp. 2870–2878, 2008.

[162] M. Arif, M. U. Akram *et al.*, "Pruned fuzzy k-nearest neighbor classifier for beat classification," *Journal of Biomedical Science and Engineering*, vol. 3, no. 04, p. 380, 2010.

[163] S. Karpagachelvi, M. Arthanari, and M. Sivakumar, "Classification of electrocardiogram signals with support vector machines and extreme learning machine," *Neural Computing and Applications*, vol. 21, no. 6, pp. 1331–1339, 2012.

[164] I. Jekova and P. Mitev, "Detection of ventricular fibrillation and tachycardia from the surface ecg by a set of parameters acquired from four methods," *Physiological measurement*, vol. 23, no. 4, p. 629, 2002.

[165] H. Prasad, R. J. Martis, U. R. Acharya, L. C. Min, and J. S. Suri, "Application of higher order spectra for accurate delineation of atrial arrhythmia," in *Engineering in Medicine and Biology Society (EMBC), 2013 35th Annual International Conference of the IEEE*. IEEE, 2013, pp. 57–60.

[166] J. M. Keller, M. R. Gray, and J. A. Givens, "A fuzzy k-nearest neighbor algorithm," *IEEE Transactions on Systems, Man and Cybernetics*, no. 4, pp. 580–585, 1985.

[167] D. Cabello, S. Barro, J. Salceda, R. Ruiz, and J. Mira, "Fuzzy k-nearest neighbor classifiers for ventricular arrhythmia detection," *International journal of bio-medical computing*, vol. 27, no. 2, pp. 77–93, 1991.

[168] C. Cortes and V. Vapnik, "Support vector machine," *Machine learning*, vol. 20, no. 3, pp. 273–297, 1995.

[169] E. D. Übeyli, "Ecg beats classification using multiclass support vector machines with error correcting output codes," *Digital Signal Processing*, vol. 17, no. 3, pp. 675–684, 2007.

[170] J. A. Suykens, T. Van Gestel, J. De Brabanter, B. De Moor, J. Vandewalle, J. Suykens, and T. Van Gestel, *Least squares support vector machines*. World Scientific, 2002, vol. 4.

[171] N. Cristianini and J. Shawe-Taylor, *An introduction to support vector machines and other kernel-based learning methods*. Cambridge university press, 2000.

[172] C. Vimal and B. Sathish, "Random forest classifier based ecg arrhythmia classification," *International Journal of Healthcare Information Systems and Informatics (IJHISI)*, vol. 5, no. 2, pp. 1–10, 2010.

[173] N. Emanet, "Ecg beat classification by using discrete wavelet transform and random forest algorithm," in *Soft Computing, Computing with Words and Perceptions in System Analysis, Decision and Control, 2009. ICSCCW 2009. Fifth International Conference on*. IEEE, 2009, pp. 1–4.

[174] L. Breiman, "Random forests," *Machine learning*, vol. 45, no. 1, pp. 5–32, 2001.

[175] G.-B. Huang, Q.-Y. Zhu, and C.-K. Siew, "Extreme learning machine: theory and applications," *Neurocomputing*, vol. 70, no. 1, pp. 489–501, 2006.

[176] J. Kim, H. S. Shin, K. Shin, and M. Lee, "Robust algorithm for arrhythmia classification in ecg using extreme learning machine," *Biomed Eng Online*, vol. 8, no. 31, pp. 10–1186, 2009.

[177] G.-B. Huang, H. Zhou, X. Ding, and R. Zhang, "Extreme learning machine for regression and multiclass classification," *IEEE Transactions on Systems, Man, and Cybernetics, Part B: Cybernetics*, vol. 42, no. 2, pp. 513–529, 2012.

[178] A. V. Oppenheim and J. S. Lim, "The importance of phase in signals," *Proceedings of the IEEE*, vol. 69, no. 5, pp. 529–541, 1981.

[179] X. Yang, A. He, P. Liu, T. Sun, and X. Ning, "Complexity and characteristic frequency studies in ecg signals of mice based on multiple scale factors," *Science China Life Sciences*, vol. 54, no. 6, pp. 544–552, 2011.

[180] L. G. Tereshchenko and M. E. Josephson, "Frequency content and characteristics of ventricular conduction," *Journal of Electrocardiology*, vol. 48, no. 6, pp. 933–937, 2015.

[181] M. S. Manikandan and S. Dandapat, "Wavelet energy based diagnostic distortion measure for ecg," *Biomedical Signal Processing and Control*, vol. 2, no. 2, pp. 80–96, 2007.

[182] D. S. Fay and K. Gerow, "A biologist's guide to statistical thinking and analysis," *WormBook: the online review of C. elegans biology*, 2013.

[183] H. Haraldsson, L. Edenbrandt, and M. Ohlsson, "Detecting acute myocardial infarction in the 12-lead ecg using hermite expansions and neural networks," *Artificial Intelligence in Medicine*, vol. 32, no. 2, pp. 127–136, 2004.

[184] C. A. Mertler and R. A. Vannatta, "Advanced and multivariate statistical methods," *Los Angeles, CA: Pyrczak*, 2002.

[185] R. Sharma, R. B. Pachori, and U. R. Acharya, "Application of entropy measures on intrinsic mode functions for the automated identification of focal electroencephalogram signals," *Entropy*, vol. 17, no. 2, pp. 669–691, 2015.

[186] M. R. K. Mookiah, U. R. Acharya, J. E. Koh, C. K. Chua, J. H. Tan, V. Chandran, C. M. Lim, K. Noronha, A. Laude, and L. Tong, "Decision support system for age-related macular degeneration using discrete wavelet transform," *Medical & biological engineering & computing*, vol. 52, no. 9, pp. 781–796, 2014.

[187] Y. Baakek, Z. H. Slimane, and F. B. Reguig, "The quantification of the qt-rr interaction in ecg signal using the detrended fluctuationanalysis and ararx modelling," *Journal of medical systems*, vol. 38, no. 8, pp. 1–11, 2014.

[188] A. Amann, R. Tratnig, K. Unterkofler *et al.*, "Reliability of old and new ventricular fibrillation detection algorithms for automated external defibrillators," *Biomedical engineering online*, vol. 4, no. 1, p. 60, 2005.

[189] I. Jekova and V. Krasteva, "Real time detection of ventricular fibrillation and tachycardia," *Physiological measurement*, vol. 25, no. 5, p. 1167, 2004.

[190] S. Fokkenrood, P. Leijdekkers, and V. Gay, "Ventricular tachycardia/fibrillation detection algorithm for 24/7 personal wireless heart monitoring," in *Pervasive Computing for Quality of Life Enhancement*. Springer, 2007, pp. 110–120.

भारतीय प्रौद्योगिकी संस्थान गुवाहाटी
Indian Institute of Technology Guwahati

# LIST OF PUBLICATIONS

**Journal Papers:**

1. **R. K. Tripathy**, S. Dandapat, “Automated Detection of Heart Ailments from 12-lead ECG using Complex Wavelet Subband Bispectrum Features”, **IET Healthcare Technology Letters**, 2017 (Accepted).

2. **R. K. Tripathy**, S. Dandapat, “Detection of Cardiac Abnormalities using Multiscale Phase Alternation Features”, **Journal of Medical Systems, Springer**, 40(6):1-9, 2016. (Current IF-2.21)

3. **R. K. Tripathy**, L. N. Sharma, S. Dandapat, “Detection of Shockable Ventricular Arrhythmia using Variational Mode Decomposition”, **Journal of Medical Systems, Springer**, 40(4):1-13, 2016. (Current IF-2.21)

4. L. N. Sharma, **R. K. Tripathy**, S. Dandapat, “Multiscale Energy and Eigenspace Approach to Detection and Localization of Myocardial Infarction”, **IEEE Transactions on Biomedical Engineering**, 62(7):1827-1837, 2015. (Current IF-2.35)

5. **R. K. Tripathy**, L. N. Sharma, S. Dandapat, “A Novel Diagnostic measure to quantify loss of Clinical Components in Multilead Electrocardiogram”, **IET Healthcare Technology Letters**, 3(1): 107-112, 2016.

6. **R. K. Tripathy**, L. N. Sharma, S. Dandapat, “A New way of Quantifying Diagnostic Information from Multilead Electrocardiogram for Cardiac Disease Classification”, **IET Healthcare Technology Letters**, 1(4): 98-103, 2014.

**Book Chapters:**

1. **R. K. Tripathy** and S. Dandapat, “Quantifying Clinical Information in MECG using sample and channel convolution Matrices”, **Advances in communication and computing, Springer**, Ch-5, 73-80, 2015.

2. S. Dandapat, L. N. Sharma, **R. K. Tripathy**,"Quantification of Diagnostic Information from Electrocardiogram Signal: A Review", **Advances in communication and computing, Springer**, Ch-2, 17-39, 2015.

**Conference Papers:**

1. **R. K. Tripathy**, S. Dandapat, "Multiresolution Inter-sample and Inter-lead Eigen Error Features for Classification of Cardiac Ailments", **National Conference on Communication (NCC)**, IIT Guwahati, 2016.
2. A. Chetan, **R. K. Tripathy**, S. Dandapat, "Classification of Cardiac Arrhythmia from Multilead ECG using Multiscale Non-linear analysis", **IEEE Conference on Electrical, Computer and Electronics**, IIIT, Allahabad, 2015.
3. **R. K. Tripathy**, L. N. Sharma, S. Dandapat, "Detection of Cardiac Ailments from multilead ECG using Diagnostic Eigen Error Features", **IEEE Conference on Power, Communication and Information Technology**, SOA University, Bhubaneswar, 2015.

भारतीय प्रौद्योगिकी संस्थान गुवाहाटी
Indian Institute of Technology Guwahati